STRUCTURAL VARIATION AND ENZYMATIC SUSCEPTIBILITY OF COLLAGEN FIBRILS EXTRACTED FROM NATIVE AND OVERLOADED TAIL TENDONS

by

Samuel James Baldwin

Submitted in partial fulfilment of the requirements

for the degree of Doctor of Philosophy

at

Dalhousie University

Halifax, Nova Scotia

July 2019

Dedication

To my Mother and Father. For instilling in me an amazement of the natural world and a desire to comprehend it.

Table of Contents

List of Tables

List of Figures

Abstract

The mechanical overload of collagen based connective tissues is a common cause of injuries, resulting in the loss of locomotion. In the case of overloaded tendons, the transmission of forces between muscle and bone are affected, impeding the function associated with the localized musculoskeletal system. The result is a reduction in locomotion and quality of life of the injured person. Novel work performed in 2012 discovered a new damage motif along collagen fibrils sourced from tendon loaded until rupture *in vitro*. This damage motif, termed discrete plasticity, consists of characteristic, repetitive kink structures along the collagen fibril axis, and a fuzzy shell layer when imaged by SEM. Limitations of SEM to characterize discrete plasticity led to the development of a novel AFM technique to improve understanding of discrete plasticity.

This body of work describes the; development, physical basis of its function, and application to discrete plasticity, of such a technique. The unique aspect of the developed technique is the nano-scale mechanical characterization of hydrated collagen fibrils, and its increased sensitivity to structural variations. Four major studies were performed. The first analyzed sample collagen fibrils and explored the technique's ability to measure structural changes in fibrils following thermal treatments, as well as comprehend the physical mechanism that provides the increased sensitivity of the technique. The second, characterized the alteration of the collagen fibril associated with discrete plasticity. The third study revealed a connection between a natural, novel, variation along unloaded fibrils and the spacing of the kink structures along fibrils displaying discrete plasticity. The thesis culminates with a study of individual discrete plasticity and unloaded fibrils post and prior to incubation with either trypsin and MMP-9, a critical enzyme in initial stages of inflammation in injured tendon. In summary, this work encompasses the development and application of a novel technique which permits nano-scale studies of, biological, mechanical and thermal changes to collagen fibrils, in particular, fibrils displaying discrete plasticity. The development of such a technique should have far reaching application in understanding the fundamental response of protein aggregates to chemical, biological, and physical exposures.

List of Abbreviations Used

AFM	Atomic Force Microscopy
AGEs	Advanced Glycation End Products
ANOVA	Analysis of Variance
CD	Circular Dichroism
DIC	Differential Interference Contrast
ECM	Extracellular Matrix
EDC	1-ethyl-3-(3-dimethylaminopropyl)-carbodiimide
FD	Force Distance (maybe change to force distance curves… FDC)
FFT	Fast Fourier Transform
HRM	Hydrated Radial Modulus
LSD	Least Significant Difference
MMP	Matrix Metalloproteinase
MMP-1	Matrix Metalloproteinase-1
MMP-2	Matrix Metalloproteinase-2
MMP-9	Matrix Metalloproteinase-9
MMP-13	Matrix Metalloproteinase-13
PBS	Phosphate Buffered Saline
PF-QNM	Peak Force Quantitative Nanomechanical Mapping
PFSP	Peak Force Set Point
PMA	Phorbol 12-myristate
RMS	Root Mean Squared
SEM	Scanning Electron Microscopy
SHG	Second Harmonic Generation
SPIP	Scanning Probe Image Processor
STEM	scanning transmission electron microscopy
ZFH	Zero-Force Height

Acknowledgements

Here I would like to acknowledge a great many people who will likely never read this…. They have already heard about it enough times and I doubt they will want to have a go at it in written form. That being said, First and foremost I would like to thank my family for their support through the long years and hard times that coincided with my academic pursuit. It was instrumental to my being here now. I would also like to thank a number of friends, James, Chad, Cameron, Ryan, Dale, Rhys, Finn and others, who were always there to support me through this process and bring me back to sanity after long days…. weeks….. months…. In the lab. In particular I would like to acknowledge Tom and Justin. You are my brothers and have been there for me through thick and thin. Angela, you were my rock throughout the majority of this process and I will be forever grateful. I hope you find all that you desire in life as you continue your journey to art fame.

I would like to thank those who have assisted me in completing this degree. Dr. Sandi Suei, thank you for answering the million and one questions I had concerning the AFM in my early days. I was terrified of breaking it and you bore my pestering with grace. Andrew Quigley, Charlette Clegg, thank you for your help processing data back in the days prior to SPIP. I know it was a slog and I am so grateful for your help. Jasmin Astle, Adam Brown, Brandon Scott, and Khalid Hijazi, thank you for your help with sample preparations, dissections, and trips to the Abattoir. Especially thank you to Jasmin and Adam, who taught me how to perform tissue decellularization and mechanical loading experiments. With out this I would likely still be acquiring data. Also, I would like to quickly acknowledge Patrick Geeraert, Meghan Martin and Kamarie Perry for counting

kinks behind the scenes. A thank you to Dr.'s Manfred Jericho, Sam Veres, Andrew Rutenberg, and Kathy Gough, you have all played varying roles either in feed back for my research or by providing me with new experiences. Thank you for being there and enriching my career with your insight.

On the non-academic side of things, I want to acknowledge Jenn, Heather Anne and Valerie in the Physics office that have helped me through out the years. I want to especially thank Tanya Timmins for taking care of me, helping (doing) all the paper work that I despise with a passion, looking out for me for all these years, and for being a friend with a listening ear. You made this experience all the better.

Finally, I would like to thank my supervisors Dr.'s Laurent Kreplak and Mike Lee for the guidance, knowledge and wisdom they have shared with me throughout this process. You have brought me to the point where I am today and have shown great understanding and compassion for the difficult circumstance I found my self in for the majority of the years of this research. I doubt I would have reached this point with out you.

Chapter 1: Introduction

1.1 Motivation

Tendon and ligament injuries due to mechanical overload (strains and sprains) are a common occurrence which everyone is familiar. People are aware of the loss of locomotion associated with the injured tissue due to a change in mechanical properties. The mechanical properties characteristic of tendon are the result of its hierarchical collagenous structure. The fundamental unit of this hierarchical structure is the collagen fibril, a supermolecular aggregate of ECM proteins consisting primarily of collagen I molecules, which acts as the fundamental structural unit of tendon.[1-5] It is this fibril level of structure with which cells interact *in vivo*.[6-11] An understanding of collagen fibril alteration of injured tendon at the molecular level is needed to understand the fundamental loss of function of the tissue due to changes in its mechanical properties and the resulting cellular response.

In 2012, a novel damage motif was discovered at the fibril level following *in vitro* tendon overload. Termed discrete plasticity, this heterogeneous damage motif is characterized by sequential kink structures along individual fibrils.[12-14] The initial study utilized SEM for visualization of discrete plasticity in bulk tendon following mechanical overload.[12] Sample preparation for SEM prohibits sequential imaging of a sample as the process renders it biologically inert. This prevents before and after characterization of the sample when exposed to various enzymatic probes, cellular incubations, or hydration states.[12-14] Furthermore, probes for thermal stability such as DSC or HIT destroy the sample, preventing direct correlation between structural damage and thermal response.[12-14]

These technical issues prohibit multi-faceted characterization of a single sample and limit the ability to quantify the degradation of tendon at the molecular and fibril scale due to mechanical injury. The fundamental goal of this research was to develop a methodology capable of quantifying and discerning between molecular and fibril level damage in response to mechanical overload by combining multi-faceted analysis on a single isolated fibril basis. Being able to quantify collagen fibril damage at this scale is essential to understanding the precise alteration resulting from mechanical overload of connective tissues, and the physiological response to the damaged ECM.

1.2 Objective

The discovery of molecular and fibril scale alteration to mechanical overload of tendon opens new avenues for understanding the fundamental structure of collagen fibrils, their response to mechanical overload and the initial interaction of cells with tendon damage. The objective of this thesis was to characterize and discern the molecular and structural alteration of collagen fibrils displaying discrete plasticity and to investigate the susceptibility of individual damaged fibrils to enzymatic probes used in wound debridement or found in the initial stages of inflammation.

1.3 Collagen fibril structure

1.3.1 Collagen Protein Family

To understand molecular and fibril scale collagen failure mechanisms as a result of macroscopic tissue overload, it is necessary to understand the fibril-forming collagens as they are prior to damage. Fibril-forming collagens are one subset of a larger family of proteins, collagens, which is the most common family of proteins in the human body

(33% of total protein content).[1,15] The collagen family is very well conserved within the animal kingdom, making many mammalian animal models appropriate for initial studies into human collagen behavior.[15] Presently the collagen protein family consists of 29 members, classified by the supramolecular structures they form *in vivo*.[1,2,16] The collagen classifications are fibril-forming collagens (Types I, II, III,V,XI, XXIV, XXVII), network forming collagens (Type IV, VIII, X), beaded filament collagen (Type VI), transmembrane collagens (Types XIII, XVII, XXIII, XXV) and fibril associated collagens with interrupted triple helices (FACITs) (Types IX, XII, XIV, XVI, XIX, XX, XXI, XXII).[1,2,16] Fibril-forming collagens are of particular interest as they make up the collagen component of tendon. Fibril-forming collagens I, III, and V are the main constituents of the tendon hierarchical structure.[17-19] Collagen I, in particular, makes up 60%-97% of the collagen content of tendon.[19,20] Due to the prevalence of the collagen I molecule in tendon it will be the foundation for understanding collagen fibrils and molecules and the subject of the following sections.

1.3.2 Molecular structure of collagen I

The collagen family is defined by the unique triple helix quaternary structure and distinctive tripeptide Gly-X-Y amino acid repeat along the primary sequence.[1,2,15,21-23] The quaternary structure of collagen I is a heterotrimer composed of two types of primary sequence proteins, 2 α1(I) and 1 α2(I), called α-chains. Both α1(I) and α2(I) are 1058 amino acids in length and share a common secondary structure, a left handed polyproline II helix with short non-helical telopeptides.[24]. The polyproline II helix structure is necessary for the proper conformation of the 3-α-chain quaternary collagen I conformation and is the result of the high levels of proline and hydroxyproline in the X

and Y positions of the Gly-X-Y repeat.[4,5,24,25,] Each α-chain in the collagen I molecule is staggered length wise by a single amino acid, resulting in a glycine residue (single hydrogen) being present at each cross-sectional amino acid triplet of the collagen molecule.[4,5,24,25] In each of these triplets, the glycine residue is packed into the center of the triple-helix of the collagen molecule, allowing for tight coiling and inter α-chain hydrogen bonding.[1,2,16,21-25] The resulting collagen I molecule is a 300 nm long, 1.5 nm diameter rod-like object, with short non-helical telopeptides, which self-assembles into collagen fibrils.[5,26,27]

1.3.3 Fibrillogenesis and Fibril Structure

The primary component of tendon is its collagen based hierarchical structure, of which the collagen I fibril is the fundamental unit (Figure 1.1).[2-4] Collagen fibrils are supramolecular collagen aggregates whose formation is initiated by a hydrophobic/electrostatic driven process.[1,5] The resulting fibril has distinct intra-fibril structures, microfibrils and subfibrils.[5,26,27] The microfibril is a linear aggregate of collagen molecules, 5 molecules in cross-section, which are quarter staggered along the microfibril's length.[5,26-31] The quarter staggering of the molecules within the microfibril structure results in a 67 nm (234 residue) periodic fluctuation in its linear density.[5,26] This fluctuation is between 4 and 5 molecules with each region being 54% and 46% of the 67 nm period respectively.[5,26,28-32] Due to registered lateral aggregation of microfibrils within a fibril, this periodic behavior is observed as a 4/5's molecular density fluctuation along the length of a fibril and consists of a gap region (4/5) and an overlap region (5/5) and is referred to as the D-band.[1,4,5,21,25,26,28-32] This periodic fluctuation plays a key role in the thermal stability and physiological activity of

the fibril (Section 1.4.1). The resulting fibril is between 50-500 nm in diameter and of various lengths.[1,4,5,21,25,26,28-32] A second intra-fibril structure, the subfibril, is also apparent within the mature fibril. Subfibrils are thinner versions (20-50 nm diameter) of the mature fibril of which they are a part.[27,32]

1.3.4 Lateral Fibril Structure

Structural damage motifs at the fibril level depend upon the pre-existing structure of native collagen fibrils. Structural models developed from X-ray diffraction and negative staining EM demonstrate microfibrils are packed in a semi-crystalline, hexagonal order within the fibril and have their gap and overlap regions in register, giving rise to the D-band structure.[5,26-33] While the quasi-hexagonal packing of microfibrils is accepted, the intermediate lateral structure between the microfibril and the fibril, is still debated.[30,31,34-40] Presently there are two proposals of intermediate fibril structure: a tube-like model and a rope-like model based on structural data obtained from AFM and EM studies.[36-40] These models have implications for the proposed model of discrete plasticity formation discussed later (Section 1.8).

The tube-like model proposes a positive correlation between radial distance from the center of the fibril and the structural organization and molecular density of the collagen fibril.[34,36] Evidence for this model consists of: observed fibril bends reminiscent of the buckling found in hollow tubes (Figure 1.2, A), a vertical deflation of collagen fibrils adhered to a substrate upon dehydration, and a theoretical molecular packing model stating that the lowest energy state of microfibril organization in a collagen fibril is one with a less dense/organized core and a more dense/organized outer layer.[30,34-37]

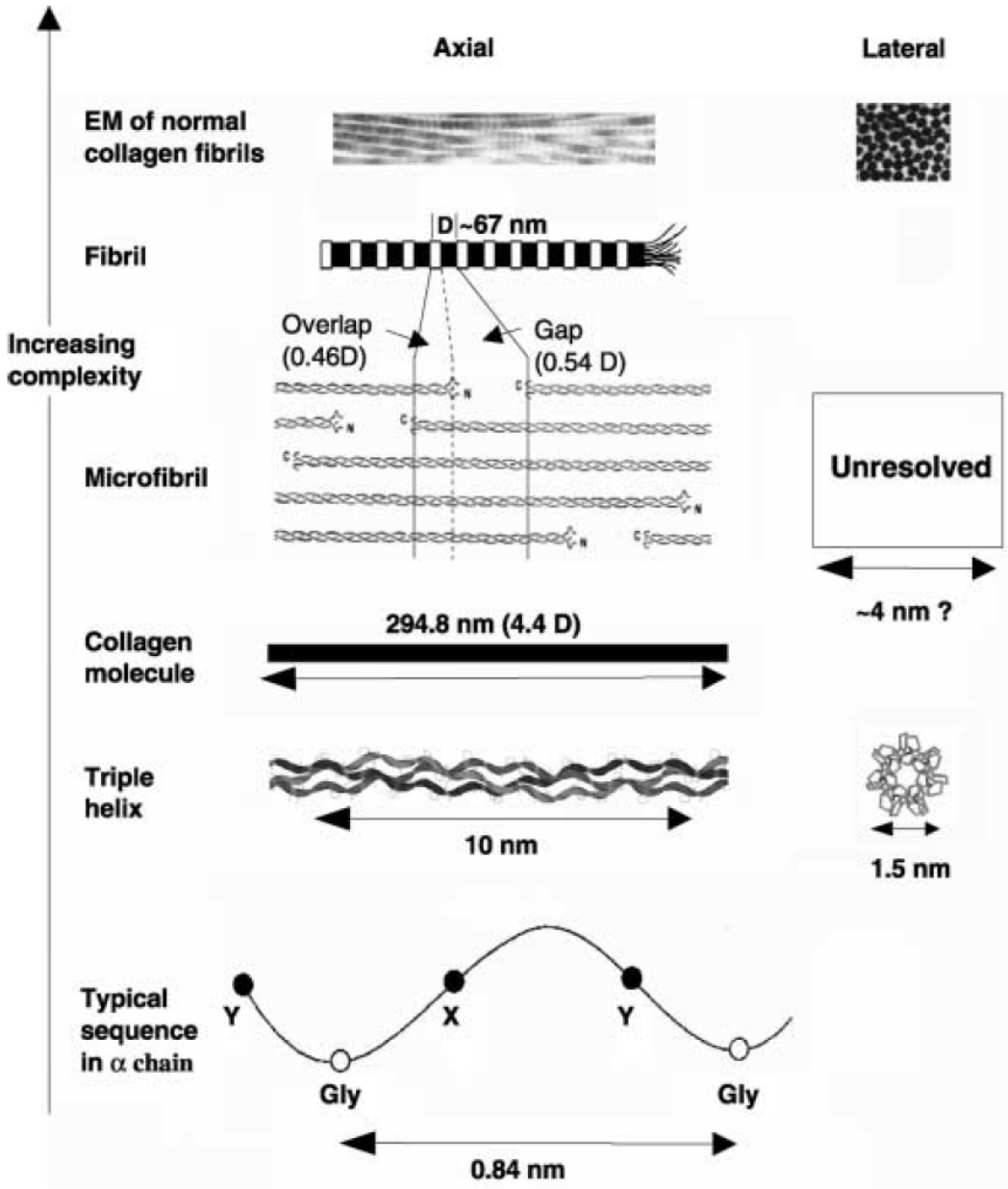

Figure 1.1: Structural levels of a collagen fibril from the individual alpha chain to complete fibril. Three alpha chains with the Gly-X-Y tripeptide repeat and staggered by 1 amino acid, assemble into a ~300nm triple-helical, collagen molecule. Collagen molecules then assemble into D-banded microfibrils that then form subfibrils or entire collagen fibrils while keeping their D-banded structures in register. Reproduced with permission from [30].

The rope like model proposes that the subcomponents of a collagen fibril are organized in a manner characteristic of a laid rope.[38] A laid rope is a hierarchical structure whose largest hierarchical tier is a laid rope strand comprised of many tiers of wound fibers.[41] When a laid rope is uniaxially compressed, the laid rope strands separate and bulge away from each other and a “bird cage” structure forms between the points of applied compression.[38,41] The primary evidence for this model are: a bird-cage damage motif observed by AFM (Figure 1.2, B), a 5° molecular pitch within tendon collagen fibrils as revealed by freeze etching, and the dissociation of collagen fibrils into their subfibril components following incubation with urea, a chaotropic agent disrupting non-covalent bonds, the NKISK pentapeptide which binds fibronectin, or Cathepsin G, a serine protease which cleaves fibronectin and not collagen I (Figure 1.3) .[36-40,42] The observed bird cage structures appear as bulges along the fibril’s axis where the subfibrils and their components have separated out into their individual strands and have a helical, rather than linear orientation with respect to the fibril’s axis.[38]

1.4 Thermal stability of collagen molecules and fibrils

The ability of the collagen molecule to remain in its native structure is of primary importance for the function of macroscopic tissue mechanics. While the pH, ionic strength, and temperature of the surrounding media all play a role in molecular conformation, here the focus is on the stabilizing factors of the collagen molecule with respect to temperature.[43-46] Temperature denaturation of collagen in solution results in a structural transition from the triple-helix to a random coil, increased hydration and increased molecular gyration. In this thesis, thermal denaturation serves as a standard for

molecular denaturation through which the mechanical based molecular and fibril damage will be framed.

1.4.1 Primary sequence and quaternary structure based thermal stability

The foundation of collagen thermal stability is its primary sequence and resulting quaternary structure.[21,25,38] The collagen I molecule is stabilized by, inter α-chain back bone and glycine residue hydrogen bonding, non-polar interactions between residues, such as glycine and proline, and by steric hinderance, hydrogen bonding and water-bridges from the residues of the X, and Y components of the Gly-X-Y tripeptide.[21,22,25,38,46-51] Mimetic protein studies have shown the thermal stability and rigidity of the collagen molecule is directly correlated to the X and Y components of the Gly-X-Y tripeptide.[1,25,38,47,52-54] The properties of thermal stability and molecular rigidity are coupled at the molecular level due to their joint dependence on steric hinderance and helical pitch, which are determined by the primary sequence of the molecule.[1,52-54] The Gly-Pro-Hyp tripeptide is the most thermally stable tripeptide followed by Gly-Pro-Pro. Regions devoid of Pro or Hyp in the Gly-X-Y tripeptide are associated with a decrease in thermal stability and rigidity of the α-chain and collagen molecule due to diminished steric hinderance of non-Pro or Hyp amino acid side chains.[25,38,47] Regions devoid of Hyp along the α1(I) and α2(I) chains have been reported as thermally labile domains.[54,55] The regions are described as flexible regions which undergo micro-unfolding events and function as initiation sites for a rate based,

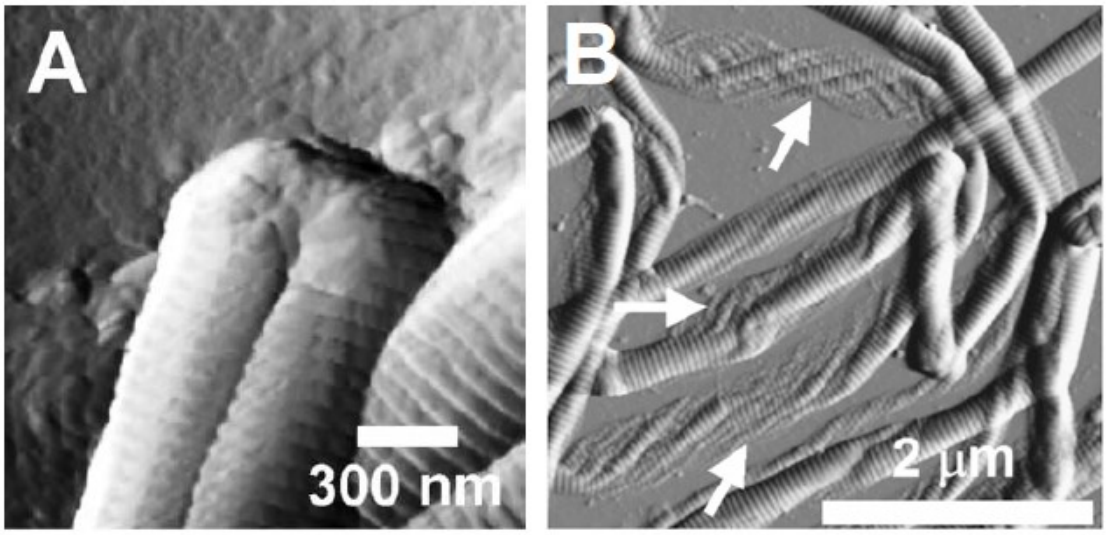

Figure 1.2: AFM evidence for the tube-like model (A) and the rope-like model (B). The sharp kink in (A) is similar to that found in the bending of hollow tubes, while the unwound, twisted structures seen in (B) are characteristic of bird-caging in ropes. (A) and (B) are reproduced with permission from [35,37], respectively.

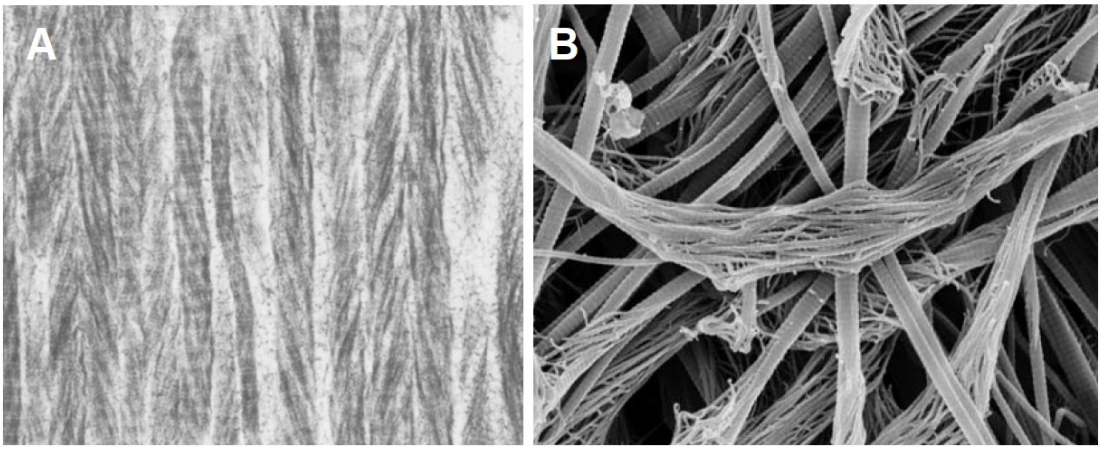

Figure 1.3: A TEM image of subfibrils revealed following incubation in 8M urea (A). A SEM image of collagen fibrils disassociating into their subfibril components following incubation with Cathepsin G. (A) and (B) are reproduced with permission from [39,40], respectively.

thermal denaturation process in which the molecule “unzips” into a random coil structure.[54,55] The three major thermally labile domains in the α1(I) (Gly85-Glu110, Gly169-Glu194, Gly877-Pro941) are all located within the gap region of the D-band of the collagen fibril.[55] This has implications for the thermal stability of collagen molecules within a fibril.

1.4.2 Fibril formation stabilizes the collagen molecule

In physiological solution at body temperature (37°C) individual collagen I molecules, sourced from rat tail tendon and human lung, have a preferred random coil structure, rather than a helical structure.[56] That is to say, the collagen I molecule is thermally unstable at physiological conditions and is denatured *in vitro*. Within a fibril, the thermal stability of a collagen I molecule drastically increases. Tiktopulo and Kajava demonstrated a 15°C increase in the thermal denaturation temperature of acid solubilized type I collagen from rat skin following fibril formation.[57] A proposed mechanism for this increase in thermal stability is based on changes in conformational entropy of the collagen molecule due to confinement by its neighbors within a collagen fibril. This “polymer-in-a-box” mechanism is supported by data demonstrating an increase in fibril denaturation temperature with dehydration.[58] Additionally, intermolecular crosslinks formed during fibrillogenesis, aging or chemical treatment *in vitro*, further increase the thermal stability of molecules within the collagen fibril by reducing molecular gyration and entropy.[59]

1.5 The onset of thermal denaturation of collagen molecules and fibrils

In sections 1.4.1 and 1.4.2, the mechanisms responsible for the thermal stability of the collagen molecule in solution and within a fibril were discussed. For collagen to become denatured, some of these stabilizing components must fail.[21,22,25,38,46-51] DSC was used to characterize the transition of soluble and fibrillar collagen to denatured, random coil structures via changes in the specific heat of collagen as a function of temperature.[53] The observed change in specific heat is the result of thermal energy being used in the phase transition (melting) of soluble molecules or fibrils from a native to a denatured state.[51,53,57] The phase transition is marked by the breaking of water-bridges and hydrogen bonds, which stabilize both the molecular and fibrillar structure. This is associated with increased molecular gyration, loss of triple helical structure, and increased interaction with water. It is important to note that this process does not result in the breakage of thermally stable covalent crosslinks.[21,22,38,46-51,53,57] The persistence of the covalent bonds prevents fibrillar collagen from transitioning into a fully denatured state.

The thermal denaturation of soluble and fibrillar collagen is rate dependent, with slower temperature ramps resulting in lower thermal denaturation temperatures. Denaturation temperatures for soluble collagen I molecules has been observed between 38-41°C depending on the applied heating rate (0.004°C/min, 2°C/min), while soluble molecules exposed to an isothermal temperature of 36°C for 3 hours resulted in molecular denaturation observable by CD.[56,57] For collagen fibrils, the denaturation temperature has been found to be between 50-84°C depending on heating rate, anatomic variation,

and crosslink density; with native fibrils from bovine tail tendon having a peak endotherm temperature of approximately 65°C at a rate of 5°C/min.[14,57,59,60]. In a single study, *in vitro* fibrillogenesis of acid solubilized collagen from rat skin was associated with an increase in endotherm peak temperature (denaturation temperature) of 10°C to 50°C at rate of 1°C/min.[57] The increase in endotherm peak temperature after fibrillogenesis is due to the addition of the attractive, hydrophobic, interaction between neighboring collagen molecules on top of the hydrogen bonds and water bridges found in the soluble molecule.[46-50,53-57]

A microthermal analysis study of rat tail tendon collagen fibrils found an onset temperature of denaturation of 58°C suggesting native rat tail tendon fibril melting begins at temperatures below 60°C [61]. This is independently supported by a separate study demonstrating progressive loss of second harmonic generation signal and shrinkage of tail tendons, from a Wistar rat, incubated at 58°C from 0-9 minutes.[62] Neither study provided further information on their tissue sources. The previously mentioned increase in endotherm peak temperature, associated with the *in vitro* fibrillogenesis of acid solubilized collagen from rat skin, was also associated with a ~90% increase in full width at half maximum of the endotherm compared to soluble collagen. This demonstrates that the thermal denaturation of fibrillar collagen is slower than soluble molecules and that there is a variation in the thermal stability of individual molecules within the fibril.[57] Taken together, these studies provide strong evidence that thermal denaturation of fibrillar collagen begins at temperatures below 60°C if enough time is sufficient for the process to occur.[56,57,61,62]

1.5.1 Collagen crosslinking as part of fibrillogenesis and aging

As mentioned previously, crosslinks increase the thermal stability of molecules within a collagen fibril, but also affect their enzymolysis and mechanical properties.[59,60,63-65] Although these are interesting topics on their own, the research presented in this thesis only discusses how possible variations in crosslinking density may explain the formation of the discrete plasticity damage motif. (Section 1.8). An overview of crosslink types and formation is presented here, but the actual implications of their existence are discussed intermittently throughout the rest of this chapter.

Primarily, there are two major natural crosslinking motifs between collagen molecules, enzymatically generated crosslinks and advanced glycation end products (AGE's). Enzymatic crosslinks form between helical and telopeptide lysine and hydroxylysine residues during fibril formation and are regulated by the extracellular enzyme lysyl-oxidase.[29,60,63,66,67] Advanced glycation end products form when a sugar molecule is covalently bonded between lysine and arginine residues of two collagen molecules.[60,63,64,66-69]

Enzymatic crosslinks are two tiered, starting as immature divalent crosslinks between two neighboring molecules.[63] Immature crosslinks are precursors to mature trivalent crosslink formation between an existing divalent bond and a histidine residue or by the combination of two immature crosslinks.[63] The formation of mature trivalent crosslinks is tissue type dependent and a much slower process than divalent crosslink formation, typically occurring between two microfibrils, stabilizing the collagen fibril.[63]

Advanced glycation end products (AGEs) are crosslinks that form when proteins or lipids are exposed to sugars.[68,69] In total there are 41 active sites along a collagen molecule available for AGE formation, 14 of which (6 intramolecular and 8 intermolecular) are readily available due to their location, conformation, and proximity of lysine and arginine residues (within 5Å) .[70,71] Through the formation of AGEs, collagen can become highly crosslinked, altering collagen fibril thermal stability, mechanics, and enzyme susceptibility.[70,71]

1.6 Collagenous hierarchical structure of tendon and mechanical properties

The hierarchical structure of tendon is based on collagenous material and results in mechanical properties distinct from those of its hierarchical components (Figure 1.4).[72-74] The tendon collagenous hierarchy consists of multiple levels spanning 7 orders of magnitude from individual molecules (1.5nm) to entire tendon (10mm) (Figure 1.4).[75] The general behavior of any tier of tendon tissue mechanics in response to uniaxial tensile loading can be broken down into three physical actions: recruitment and alignment of the intra-hierarchical structures to bear load, sliding of the intra-hierarchical structures and direct loading of intra-hierarchical structures resulting in elongation, rather than relative movement.[72-74,76-80] These processes become less complex as the level of structure moves from full tendon to individual fibril.[73,74,76]

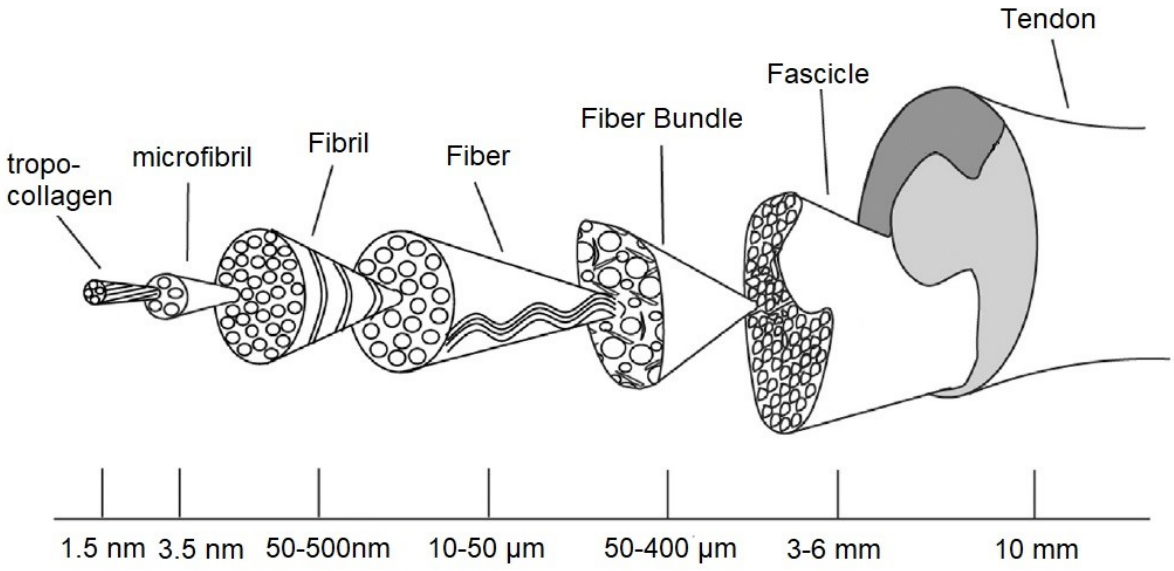

Figure 1.4: Tendon hierarchical structure with dimensional ranges for each level of structure. The fundamental unit of the hierarchical structure is the collagen fibril. Multiple collagen fibrils assemble into collagen fibers which then assemble into various stages of fiber bundles leading to complete tendon. Reproduced with permission from [75].

1.6.1 Uniaxial loading behavior of tendon

Uniaxial tensile testing of whole tendon has routinely revealed a characteristic stress/strain curve classified into 4 regions (Toe, Heel, Linear/elastic, Plastic) based upon observed macroscale mechanical behavior, derived from a series of unique, fundamental, mechanisms (Figure 1.5). Initially (Toe), mechanical behavior at low strain (~4%) is dominated by the alignment of microscopic crimp structures found at the fiber level of tendon, resulting in a region of relatively low tensile modulus.[72-74,76] The following region (heel) marks a transition from macroscale crimp alignment to the straightening of the thermally labile regions located in the gap region of the D-banded collagen fibrils.[73,77] Molecular segments in the gap region have more lateral mobility than the overlap due to a 20% decrease in molecular density and the limited amount of Pro and Hyp residues found in the thermally labile regions.[73,77,78] The increase in tensile modulus in the heel region is due to increasing entropic force associated with a decrease in conformational entropy from load based alignment of molecules in the gap region.[73,78]

Following the heel region, the strain induced molecular alignment in fibrils transitions to the direct loading of covalent bonds along the molecular backbone and crosslinks, resulting in molecular stretching and intermolecular slippage respectively (linear/elastic region). X-ray scattering analysis of molecular and fibril strain during whole tendon loading show a linear stress-strain relationship at both levels of structure and the onset of non-entropic loading of fibrils begins at ~4-5% bulk tendon strain (Figure 1.6). [72,73,79] Covalent bond loading at the fibril scale results in changes in the period of the D-band. An increase in D-period from 67nm to 67.6nm has been associated with

stretching of collagen molecules while further increases are the result of molecular sliding within fibrils.[80,81] Individual fibril and molecular loading experiments have demonstrated similar linear behavior, following a region associated with entropic alignment of the collagen molecules as observed in the heel region in whole tendon loading.[82-87] Fibril strain has been shown to only be 40% that of whole tendon strain in whole tendon loading, suggesting that interfibrillar sliding also plays a dominant role in tendon mechanics.[73] The final region of the stress/strain curve (plastic) is characterized by the loss of the linear stress/strain relationship observed in the elastic region, and large increases in strain with minimal increase in applied stress. It is at this point that tensile load begins to permanently alter the tendon structure at the molecular level. This is discussed further in its own section (Section 1.7). [74]

1.6.2 Loading parameters and tissue variations alter general mechanical response of tendon

The general tensile loading behavior described in section 1.6.1 is a simplification of a wide spectrum of tendon and fibril mechanical properties dependent on crosslinking, anatomical location, loading history and age, which is further complicated by the viscoelastic nature of tendon.[87-101] It is also important to note that tendon tissues are classified as extensor or flexor depending on their mechanical role in opening or closing a joint. The implications of this on tendon mechanics and fibril structure and behavior are numerous but outside the scope of this thesis.[102-116]

1.7 Fibril and molecular damage from tensile overload

The discussion of alteration and damage to tendon under uniaxial load has been avoided until now. Section 1.6 provides the basic understanding of the mechanical behavior of tendon under uniaxial load via a typical loading curve (Figure 1.5), and making note of the variability and normal range of function of the tissue prior to discussing damage. A single, or a low number of cyclic loadings into the plastic region of the typical loading curve of whole tendon is associated with permanent damage as the tendon approaches rupture (Figure 1.5).[73] High cyclic loading into the elastic region of the typical loading curve has been shown to result in tendon structure alteration, but will not be discussed in this thesis. Loading into the plastic region results in alteration to the entire tendon hierarchy, such as the loss of tendon crimp, but it is fibril and molecular level damage that are the prime substrates for cellular interaction during wound healing and the focus of this thesis.[76,117]

1.7.1 Fibril Level damage

Fibril level damage has been demonstrated via time resolved X-ray diffraction spectra from low strain rate (0.13% s^{-1}) tensile loading of 24 month old rat tail tendon.[118] Within the linear regime of the tendon loading curve, fibril loading is dominated by intra-fibril sliding and molecular stretching, resulting in an increase in D-band period from 67nm to 69 nm.[72,73,80,81,118] The increase in D-period in response to loading is a reversible process up to 68.4nm. Further stretching results in permanent alteration of the fibril.[80] Once a D-period of 69nm has been reached, further fiber elongation occurs via interfibrillar sliding resulting in the quick elongation of whole tendon, the cessation of

fibril strain and non-uniform intra fibril relaxation as seen by 20ms resolved X-ray diffraction during tendon rupture.[118] The non-uniform intra fibril relaxation is correlated with the sequential dissociation of fibrils into their sub-components and the formation of kink structures along the length of a fibril.[12-14,117,118] Interestingly, molecular slippage and backbone stretching is preserved at strain rates up to 5000% s^{-1} but interfibrillar slippage decreases and results in less fibril level damage.[118]

1.7.2 Molecular level damage

Decoupling molecular damage from fibrillar damage is difficult. Enzymatic analysis of ruptured human hand extensor tendon, bovine tail tendon and rat tail tendon, have all demonstrated an increase in proteolysis of collagen by trypsin, a serine protease which preferentially cleaves denatured collagen.[119-122]. Furthermore, DSC measurements have revealed a shift in the thermal stability of collagen molecules following bovine tail tendon rupture.[123] The study indicates that this is not due to molecular denaturation but changes in fibril structure such as that described in section 1.7.1.[123] A recent comprehensive study by Zitnay et. al. demonstrated that rat tail tendons loaded past 8% strain (into the plastic regime), at a rate of 0.5 $\%s^{-1}$, contained permanently denatured molecules via binding of a fluorescently labeled collagen hybridizing peptide (CHP). [121,124] Comparison of peptide binding with paired trypsin enzymolysis showed that both fluorescence intensity of the CHP and collagen digestion were linearly correlated and increased with increasing maximum strain.[121]

Two models of mechanical collagen denaturation were proposed that would result in available binding sites for CHP, covalent bond rupture along one or more α-chain

backbones from direct loading or the extraction of a single α-chain from a collagen molecule due to tensile forces associated with a crosslink during molecular sliding.[121,125,126] Simulation of a 10 Gly-Pro-Hyp peptide revealed that crosslink mediated α-chain extraction was the most likely scenario. The energy required for this mode of failure was $1/10^{th}$ that of covalent bond rupture, and physiologically possible when compared with experiment. [121] Further modeling studies have shown that α-chain extraction was associated with hydrogen bond failure and that both enzymatic and AGE crosslinks are capable of this mechanical denaturation mechanism.[127-129]

Both fibril and molecular damage, resulting from tensile overload of tendon hierarchical structures are negatively correlated with strain rate suggesting that fibril damage and molecular damage are viscoelastic damage motifs resulting from inter-fibrillar sliding pre and post rupture.[118-122] Recent support for this comes from multiple studies by Veres et al., demonstrating molecular and fibril damage in bovine tail tendon pulled to rupture at various strain rates and assessed by trypsin enzymolysis, thermal denaturation, and SEM imaging.[12-14,130] The results of these studies showed that molecular denaturation and fibril damage was negatively correlated with strain rate and occur simultaneously in discrete, repeating, kink structures along individual fibrils. This damage motif has been termed discrete plasticity.[12]

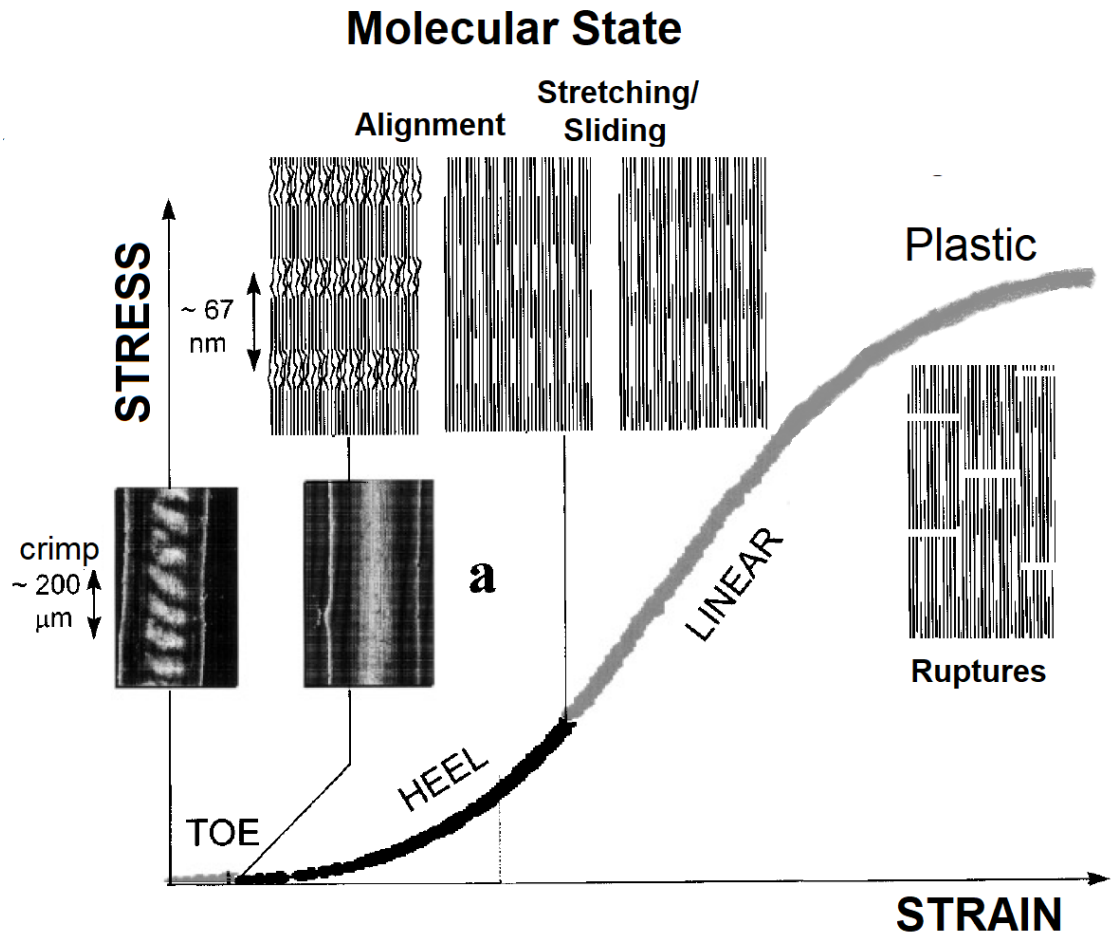

Figure 1.5: A typical stress-strain curve of a tendon under increasing tensile load. The stress-strain curve is comprised of 4 regions, the toe region, the heel region, the linear elastic region, and the non-linear plastic region. Each of these regions is dominated by specific loading processes within the tendon. The toe region is associated with the straightening of tendon crimp, the heel region is the alignment of the collagen fibrils and straightening of molecules within the collagen fibrils, the elastic region is dominated by direct loading of the collagen fibrils within the tendon leading to molecular stretching and sliding, and the plastic region is associated with the failure of the collagen fibrils, leading to their rupture and mechanical denaturation. Reproduced with permission from [73].

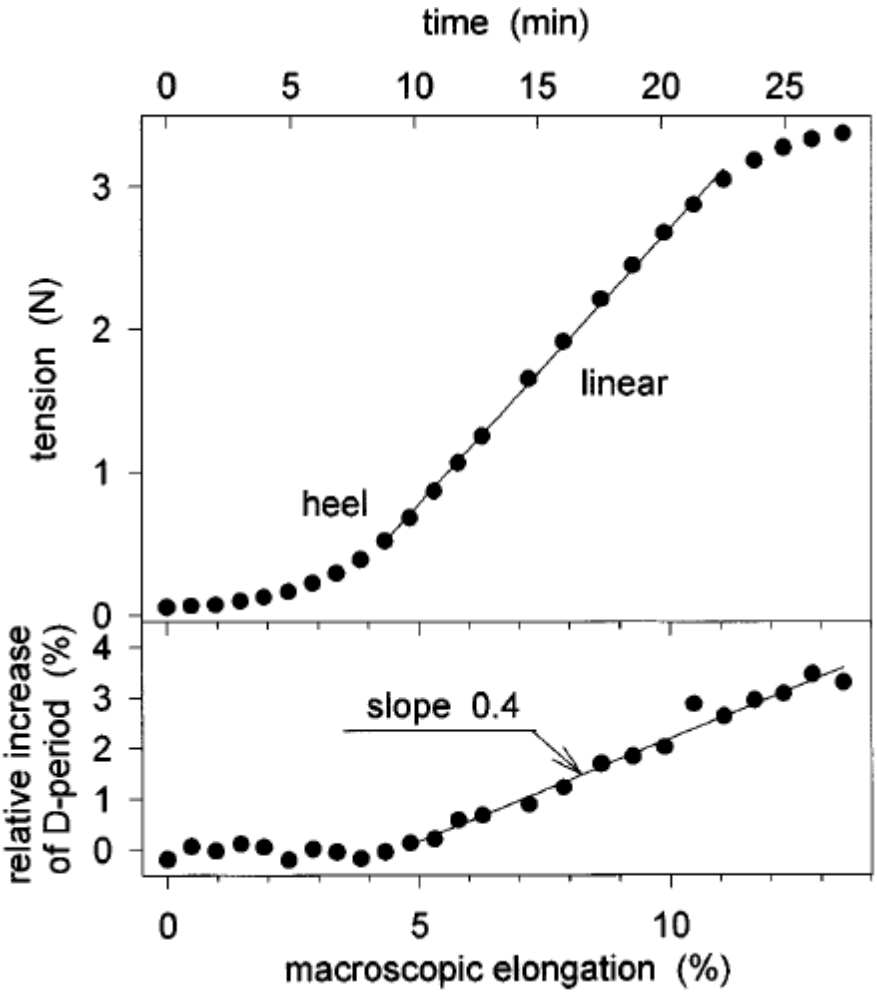

Figure 1.6: The stress-strain response of whole tendon (top) and fibril (bottom) during whole tendon loading. The onset of non-entropic loading of individual fibrils in bulk tendon initiates at 5% bulk tendon elongation. Reproduced with permission from [73].

1.8 Discrete Plasticity

Discrete plasticity is a damage motif first observed by SEM imaging and is characterized by discrete, repeating, kink structures spanned by non-kink, D-banded regions (Figure1.7).[12] Discrete plasticity is generated by the tensile overload of tendon into the

plastic regime of the stress-strain curve of tendon and is associated with the dissociation of fibril structure and molecular denaturation.[12-14] Some fibrils displaying discrete plasticity are accompanied by a distinctive shell layer.[12-14] Discrete plasticity damage increases with repetitive overloading into the plastic regime, decreased strain rate, and with lower concentrations of mature crosslinks in functionally distinct tendons.[13,130]

1.8.1 Thermal assessment of Discrete Plasticity

Thermal studies of tendon displaying discrete plasticity have shown that the mechanically denatured molecules are in a thermally stable state, suggesting that the molecular damage is distinct from that of thermally denatured collagen.[14,131] DSC measurements have shown decreases in onset thermal denaturation temperature of ~5°C and peak thermal denaturation temperature of ~ 2°C associated with overloaded tendons exhibiting discrete plasticity when compared to their paired control samples.[14] This is coupled with a two fold decrease in specific denaturation enthalpy and doubling of the full width at half maximum when compared to paired controlled samples (Figure 1.8).[14] Taken together, this represents an overall decrease in thermal stability of the fibrillar collagen and an increase in the heterogeneity of molecular thermal stability of discrete plasticity fibrillar collagen molecules.

The change in denaturation enthalpy is inversely correlated to the number of overload cycles performed on the tendon. [14] A similar result was observed in HIT experiments.[13] HIT is a technique that measures the change in generated force during a heating protocol of a collagenous tissue held at constant length.[132] Performing HIT on cyclically overloaded tendon demonstrated a decrease in initial and final denaturation

temperatures with respect to cumulative post-yield dissipated energy, an additive measure of the area between loading and relaxation curves defined by the termination of the elastic regime in a single overload cycle.[13] This is coupled with an increasing in kink density demonstrating that the decrease in thermal stability of the tendon is tied to progressive damage at the fibril level.

1.8.2 Enzymatic assessment of discrete plasticity by trypsin

The use of serine proteases as enzymatic probes of collagen conformation has been in practice nearly 40 years.[133] The serine protease trypsin is capable of cleaving both intact and denatured collagen, but demonstrates increased solubilization of thermally denatured collagen compared to unheated samples.[134,135] The rate of enzymolysis of collagen by trypsin is directly related to the availability of cleavage sites along the collagen molecule. These sites, arginine and lysine residues, are available in soluble collagen molecules both above and below their thermal denaturation temperature due to micro-unfolding events in the thermally labile region.[133-136] At temperatures below 25°C, micro-unfolding events are quenched, restricting trypsin denaturation sites along the collagen molecule.[133-136] A similar effect is achieved within the collagen fibril due to associated increases in molecular thermal stability.[58] Due to the sensitivity of trypsin to denatured collagen and altered collagen structures, it has found use in tendon mechanical overload studies and osteoarthritic cartilage studies, among others, as a metric of degraded or denatured collagen compared to control, or healthy tissues.[12-14,120,137]

The enzymatic susceptibility of fibrils displaying discrete plasticity is heterogenous in nature. Incubation of overloaded tendon with trypsin, and subsequent SEM imaging, has qualitatively demonstrated the increased enzymatic susceptibility of kink sites along fibrils displaying discrete plasticity compared to the inter-kink regions (Figure 1.7).[12] Tendons overloaded with the necessary parameters to generate discrete plasticity were incubated with trypsin at 30°C, 20°C and 4°C to quench micro-unfolding events as a source of solubilization.[12] Tendons incubated at all three temperatures demonstrated increased solubilization of collagen compared to paired, control, samples. This confirms that mechanically overloaded tendons result in structural alterations, discrete plasticity, which are more susceptible to digestion by trypsin than unloaded tendon.[12]

1.9 Cellular response to mechanical tendon damage in vivo

In vivo tendon injury is classified into acute injuries, involving singular mechanical overload or laceration, and chronic injuries, a degenerative process which can eventually lead to tendon rupture at normal physiological loads.[137,139] There are two modes of cellular response to tendon damage, the intrinsic mode and the extrinsic mode.[6-11] The intrinsic mode involves native tenocytes found within bulk tendon and fibroblast recruitment from the endotenon and epitenon. The intrinsic mode is associated with all tendon damage motifs, and is thought to be the sole mechanism of cellular response in the majority of tendinopathies.[6-11] The extrinsic mode is characteristic of standard inflammation where cells are recruited from the surface of the tendon.[10] This mode is typically associated with acute, traumatic, tendon injuries.[10] Rather than discussing the tendinopathic case, the acute injury model is the focus of this section as the *in vitro*

overloading of tendon resulting in discrete plasticity models this form of tendon injury.[140]

Reparative measures following acute tendon injury commonly involve surgical intervention to reconnect severed tissue components.[141] The cellular response to the traumatic acute injury involves both extrinsic and intrinsic modes of cellular response to the site of damage.[8] Both native tenocytes within bulk tendon and inflammatory cells, such as macrophages, from endotenon and paratenon tissues participate in the wound healing response, due to the macroscopic pathway between the tendon hierarchy characteristic of the injury.[10,137,141-144,]. The cells primary response to the damage tissue is upregulation of collagen and various proteins to debride and remodel the damaged ECM.[145] Matrix metalloproteinases (MMP's) are a key component of that response.[145-150]

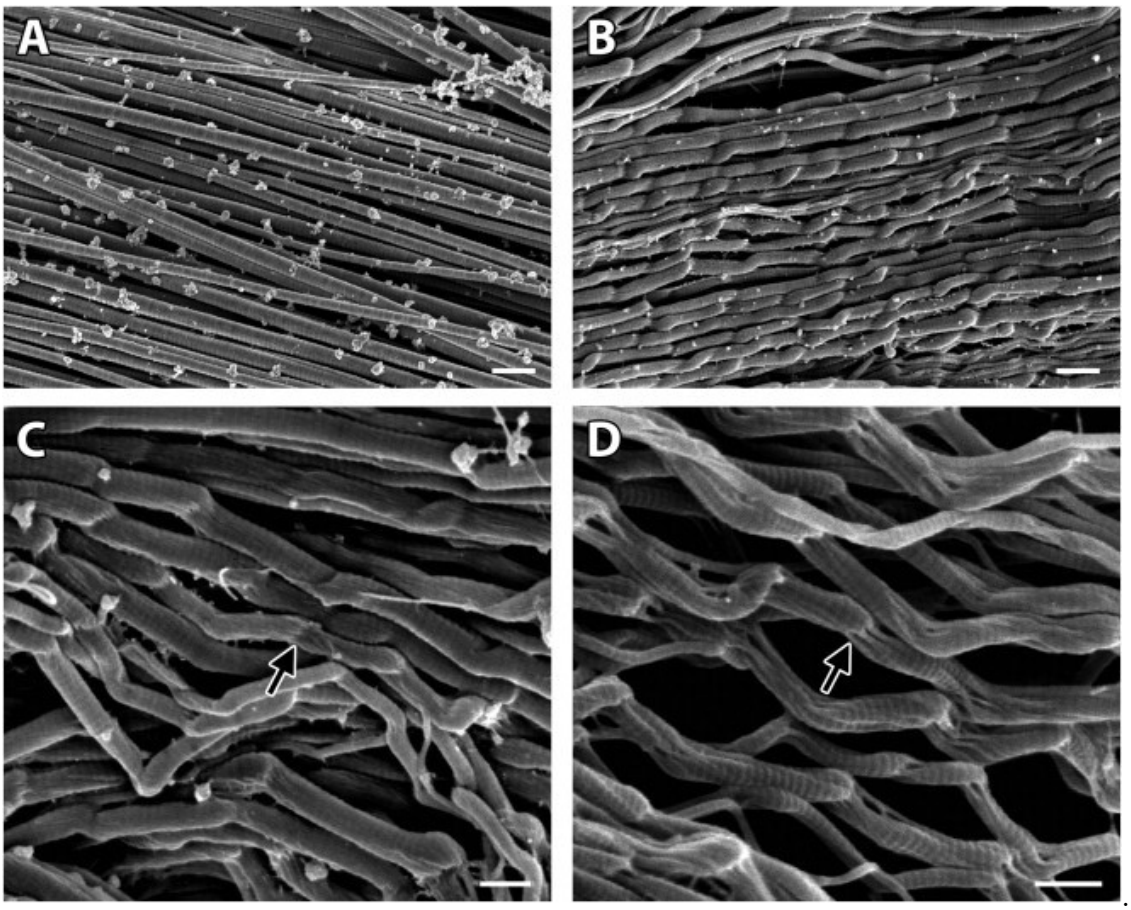

Figure 1.7: Scanning electron microscopy images of unloaded tendon (A), overloaded tendon displaying discrete plasticity (B,C) and fibrils displaying discrete plasticity following incubation with trypsin (D). The repetitive kink structures along the fibrils from mechanically overloaded tendon are quite clear when contrasted with unloaded tendon. The heterogeneous susceptibility of these fibrils to trypsin reveals their discrete nature is associated with localized denaturation of their comprising collagen (Arrows, C,D). Reproduced with permission from [12].

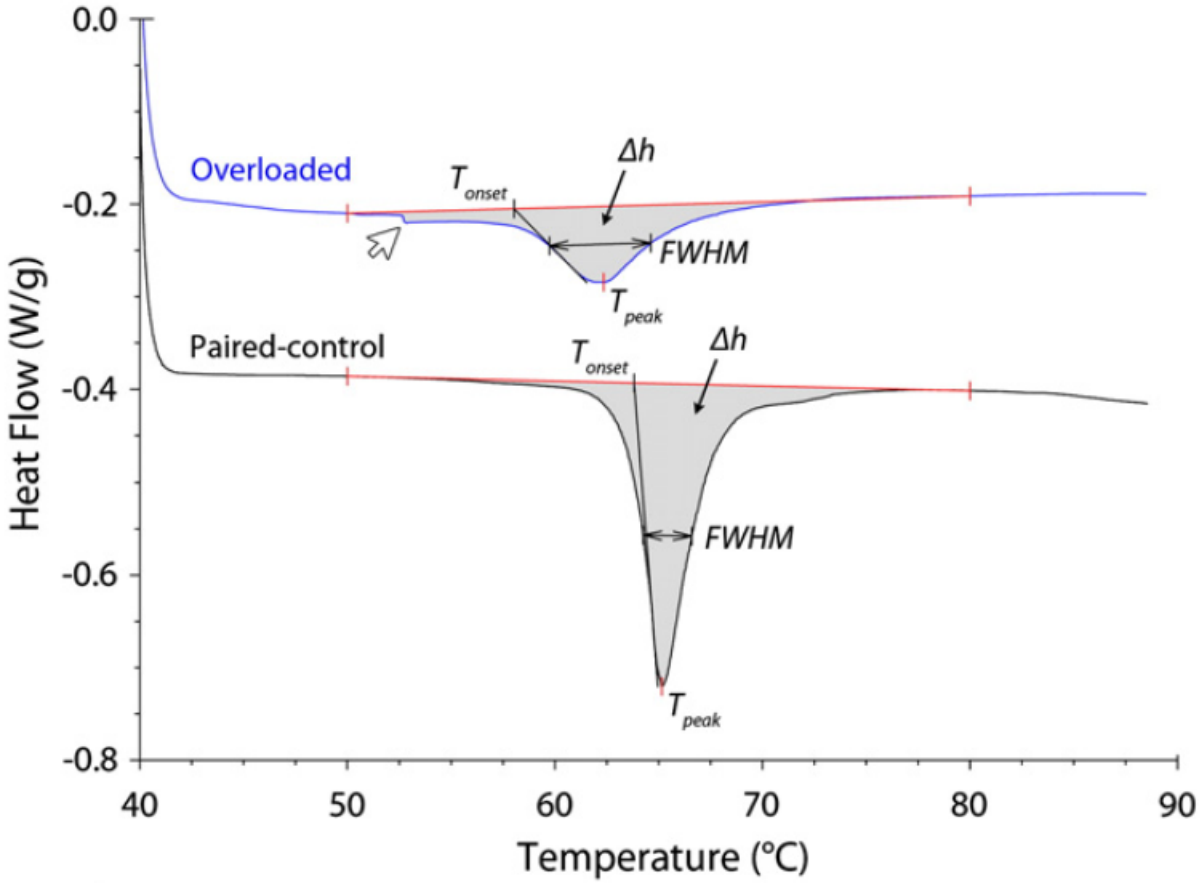

Figure 1.8: DSC endotherms of overloaded and paired control tendon samples demonstrating a decrease in onset temperature (T_{onset}), peak temperature (T_{peak}), and specific entropy of denaturation (Δh) following tendon overload. This is accompanied by a doubling of the full width at half maximum (FWHM) of the endotherm upon mechanical overload. The overload tendon endotherm has been shifted upwards on the y-axis to provide comparison with the control tendon endotherm. Reproduced with permission from [14].

1.9.1 Matrix metalloproteinases (MMP's) role in wound healing

Matrix Metalloproteinases (MMPs) are a family of 28 zinc dependent enzymes produced by cells to cleave specific components of the ECM to facilitate cell mobility and wound healing.[151-152] MMP activity is regulated in three ways: up or down regulation of enzyme production within cells, activation of pro-MMPs in the ECM, and binding of tissue inhibitors of matrix metalloproteinases (TIMPs) in the ECM.[151-152] Of distinct interest during wound healing are the Collagenases (MMP-1,-8,-13,-18) and gelatinases (MMP-2,-9).[145-147] In tendon biopsies, sourced from patients undergoing corrective surgery within 48 hours of tendon rupture, mRNA expression was increased for MMP-1 and MMP-9.[147] In a time interval *in vivo* rat tendon laceration model, it was shown that the up-regulation of MMP-9 and MMP-13 is contained to the initial debridement and remodeling stages of tendon healing.[148] It is this initial time frame during tendon wound healing that is of distinct interest in this thesis, as it focuses on the cellular response to fibrillar and molecular ECM damage motifs.

1.9.2 In vitro cellular response to discrete plasticity

The physiological response to the discrete plasticity damage motif is presently in question. Repetitive loading of tendon into the plastic regime of the stress strain curve results in an increase in fibril and molecular damage and the appearance of a fuzzy surface layer obscuring D-band features as viewed by SEM.[12] As cells interact with fibril surfaces, this fuzzy layer is likely to act as a strong signal of damage. Macrophage like U937 cells are able to recognize discrete plasticity damage from bovine tail tendons

following 15 cycles of subrupture mechanical overload at 1% strain rate and a decellularization process, also used in this thesis.[153] Cellular recognition was characterized by increased cellular contact with the damaged substrate and decreased MMP-9 releasate compared to cells incubated with native tissue.[153] It is important to note that future studies exploring the response of native tenocytes to discrete plasticity are needed as their pre-existence in bulk tendon ensures that they are the "first responders" to tendon damage.[6-11] The tendon overload protocol used to generate discrete plasticity in this thesis did not result in macroscopic ruptures, thus it is quite possible that the intrinsic mode of cellular recruitment could be the sole mechanism of the cellular response to the discrete plasticity damage motif following sub-rupture overload.[6-11]

1.10 New methods for studying discrete plasticity

The primary tool for studying discrete plasticity in this thesis is the atomic force microscope (AFM). Prior to this work, the molecular and fibrillar alteration associated with discrete plasticity had been characterized thermodynamically by DSC and HIT, enzymatically by incubation with trypsin, and visualized by SEM as discussed in section 1.8.[12-14] As mentioned in section 1.1, the motivation for this thesis was to discern between fibrillar and molecular level damage on collagen fibrils. To this end similar thermal and enzymatic treatments are coupled with AFM imaging. The AFM provides comparable visualization to SEM with the improvement of sample purity, hydration with buffer solution, mechanical analysis, and direct comparison of fibrils before and after thermal and enzymatic incubations. The study of isolated fibrils by AFM permits direct correlation between discrete plasticity damage and changes in structure and enzymolysis

without the variation of fibril states which exist in bulk tendon. This is exhibited throughout the main studies comprising this thesis.

1.10.1 Atomic force microscopy (AFM)

The atomic force microscope, first developed in 1986, has been extensively applied to biological processes and in biomedical applications by measuring molecular, cellular, viral and bacterial mechanical properties, and responses to specific incubations or drug treatments.[154-162] The functioning principles of the AFM are quite simple. A cantilever is deflected by interaction of a sharp tip and a sample material. The cantilever's behavior is measured by reflection of a laser and modeled as a spring.[154-157,163] By varying the vertical position of the cantilever, mechanical information of a sample may be acquired. The behavior of a single indentation of the sharp tip into a sample is described by the Sneddon model of contact mechanics. The Sneddon model relates the amount of force required to indent an infinite half-space of a given modulus, with a conical tip and is described by equation 1,

$$F = \frac{2E}{\pi(1-\nu^2)}(\tan\alpha)(\delta^2) \qquad (1)$$

where ν is the Poisson ratio taken to be 0.5, α is the indenter cone's half angle (18), δ is the depth of indentation into the sample (variable), F is the applied force by the tip (10nN), and E is the elastic modulus of the fibril.[164] A single indentation is capable of measuring, sample deformation, indentation modulus, sample-tip adhesion and energy dissipation. When multiple indentations are performed, in a raster scanning procedure, topographic and mechanical property maps of the sample can be generated.[154-157]

1.10.2 Previous AFM application to collagen fibrils

The state of AFM analysis of collagen fibrils up to the beginning of this thesis is quite varied. Other than being able to resolve fibril D-band on dehydrated collagen fibrils, topological AFM studies on fibril growth *in vitro* revealed: single collagen molecules acting as fibril nucleation sites, fibril growth resulting in the lateral alignment of gap and overlap structures, and the mitigation of fibril diameter and spacing by the proteoglycans lumican and decorin.[165,166] Time lapse topological AFM imaging of *in vitro* reconstituted fibril degradation by bacteria collagenases demonstrated AFM's ability to observe enzymatic processes on unaltered fibril structures.[167]

Indentation studies on dehydrated collagen fibrils revealed radial moduli of 9.4±1.8 GPa and 5-11.5 GPa for murine fibrils and fibrils reconstituted from bovine Achilles tendon collagen.[168,169] Comparing the dehydrated radial modulus of the gap and overlap structures on collagen fibrils from rat tail tendon and bovine Achilles tendon revealed a gap/overlap ratio of 0.62 and 0.55 indicating that in the dehydrated state, radial modulus does not correlate to molecular density.[170,171] Upon hydration, a 3-fold decrease in average radial modulus was observed, 1.9±0.5 GPa to 1.2±0.1 MPa, in fibrils sourced from bovine Achilles tendon.[172] A follow up study demonstrated that the hydrated radial indentation modulus increased with ionic strength of the buffer but decreased with increasing pH. Changes in the fibril radial indentation modulus were negatively correlated with changes in fibril diameter due to hydration level.[173] In summation, at the beginning of this work dehydrated imaging and analysis of collagen fibrils was the norm and hydrated analysis was only capable of average fibril mechanical quantification.

1.10.3 Needed improvements to AFM for fibril analysis

The dehydrated morphological studies discussed in section 1.10.1 exemplify the ability of the AFM to produce high resolution imaging of collagen fibrils, comparable to SEM. The hydrated mechanical studies demonstrate the high sensitivity of fibril structural response to various hydrated environments [165-173]. Due to the nature of discrete plasticity, neither the pre-existing dehydrated or hydrated AFM modalities were adequate for fully quantifying the damage motif. Dehydrated imaging is capable of revealing morphological structures similar to SEM, but the inability of dehydrated mechanical measurements to reproduce 4/5's gap/overlap ratio suggested that any mechanical quantification would be systematically skewed.[170,171] Hydrated imaging and mechanical analysis techniques were able to measure average fibril radial indentation modulus but lacked the resolution necessary for quantifying mechanical variations such as the D-band structure and were associated with long acquisition times. The development and application of a technique addressing the lack of resolution in hydrated AFM and substantial data acquisition time is the first step of this thesis (Chapter 2).

1.10.4 Enzymolysis of collagen by MMP's

The use of trypsin as a probe of collagen denaturation was previously discussed in section 1.8.2. MMP's function similar to trypsin, as their ability to cleave collagen is directly dependent upon availability of the active cleavage sites depending on: molecular conformation, fibril formation and applied tension which stabilizes collagen against MMP cleavage.[174-177] Recently it has been shown that the gelatinases, MMP-2 and MMP-9 are functional collagenases, cleaving α1 and α2 chains in soluble collagen at

37°C. Cleavage occurs at the characteristic Gly^{775}-$Ileu^{776}$ site of MMP's, resulting in the ¼, ¾ fragments as seen with MMP collagenases.[152,178-180]. The ability for MMP-2 and MMP-9 to cleave fibrillar collagen has not been demonstrated.

1.11 Thesis Justification and Outlook

Discerning between fibrillar and molecular damage in collagen fibrils is necessary for understanding the alteration of collagen fibrils to mechanical overload. Discrete plasticity is an established fibril level alteration following the mechanical overload of tendon.[13,130] The damage motif has been examined via SEM, HIT, DSC, and enzymolysis by trypsin.[12-14,131,] The results of this work reveal discrete plasticity to be repeating dissociation along a collagen fibril, coupled with decreased thermal stability and increased susceptibility to enzymolysis by trypsin.[12-14,131,145-150] The combination of these techniques for studying discrete plasticity is useful, but limited by sample coating, sample alteration by thermal denaturation, the non-specific cleavage of trypsin, and the lack of specificity associated with bulk tissue studies. These limitations prevent sequential, multi-faceted analysis of individual samples, and are further complicated due the dilution of the discrete plasticity signal in these measures due to the non-pervasive nature of discrete plasticity in overloaded tendon.

Alternatively, AFM has demonstrated a high capacity for studying collagen fibril structure with minimal alteration in both dehydrated and hydrated states and during enzymolysis.[165-173] By removing sample alteration from the analysis process and by focusing solely on isolated collagen fibrils, it is possible to combine multiple analytical techniques on an individual sample while removing signal dampening of each technique,

associated with bulk tendon measurement. This thesis represents a sequential series of experiments using AFM on isolated fibrils to determine the structural and molecular alteration of collagen fibrils sourced from mechanically overloaded tendon, specifically those displaying discrete plasticity (Chapters 2-5).

The first study (Chapter 2) focuses on the development of a novel AFM technique based upon high-speed indentation hydrated radial modulus (HRM) and its sensitivity to mechanical and thermal damage of individual collagen fibrils. The second study (Chapters 3 and 4) revolves around the application of this novel technique to isolated native and discrete plasticity collagen fibrils and the quantification of longitudinal and radial structures and damage in both fibril types. Chapter 4 lacks any defined objective/hypothesis structure as the results presented in the chapter were not the primary focus of the study, but discovered by post hoc analysis of the large data set acquired in chapter 3, based on previous findings in chapter 2. The culminating study (Chapter 5) couples AFM analysis of isolated native fibrils and those displaying discrete plasticity before and after incubation with the trypsin and MMP-9. This single fibril enzymatic assay isolates the susceptibility of individual fibrils to enzyme digestion by dimensional analysis while studying a selective avenue for discrete plasticity debridement.

Chapter 2: Nanomechanical Mapping of Hydrated Rat Tail Tendon Collagen I Fibrils

This chapter has been reproduced from the article “Nanomechanical mapping of hydrated rat tail tendon collagen I fibrils”, with permission from Biophysical Journal (Appendix F). The authors of the article are as follows “Baldwin, S.J., Quigley, A.S., Clegg, C. and Kreplak, L.”. As first author I was responsible for experimental design, data acquisition, the majority of data analysis, and writing of the first draft of the document as well as participating in the subsequent edits.

2.1 Motivation and Hypotheses

The motivation for this study was founded on the chance observation of increased structural sensitivity along a collagen fibril following AFM mechanical mapping of collagen fibrils at high indentation speed. The study was designed to quantify the relationship between indentation speed and the hydrated radial modulus (HRM) of a collagen fibril, test the technique's sensitivity to changes in fibril structure associated with thermal treatments and acquire preliminary data about the variable structure of a collagen fibril. The following hypotheses were tested.

Hypothesis 2.1: The HRM of collagen fibrils will increase with increasing AFM tip indentation speeds used in mechanical measurements.

Hypothesis 2.2: Increases in fibril radius associated with water uptake following thermal treatments of collagen fibrils will decrease as fibril HRM increases.

Hypothesis 2.3: High-speed indentation HRM of collagen fibrils is increased with higher molecular density and decreased with lower molecular density.

2.2 Introduction

Collagen is the primary protein component that provides structural integrity to mammalian tissues. Of the 28 varieties of collagen, types I, II, III, V, XI, XXIV, and XXVII form fibrils that provide mechanical strength to tissues such as bone, tendon, ligament, and skin.[4,15,181]) There is a vast body of literature describing the architecture and macroscopic mechanical properties of these tissues and how they are influenced by age, anatomical location, damage, exercise, and disease.[76,87-116,182-188] In contrast, the relationship between structure and mechanical properties at the single collagen fibril level is much less understood despite some recent advances.[181]

Collagen fibrils are linear aggregates of 300 nm long collagen molecules that have a diameter of 1.5nm and a distinctive triple-helical structure.[21,181] Tens to hundreds of thousands of collagen molecules are covalently bound to each other by cross-links and packed radially in a semi-crystalline fashion to form 50 to 500nm wide fibrils spanning microns to millimeters in length.[29] There are two intermediate stages of organization between individual molecules and the fibril, the microfibril and the subfibril. The microfibril consists of five strands of laterally organized collagen molecules with a diameter of 4-8nm, the subfibril has a diameter of around 25 nm but is not as well described in the literature as the microfibril.[37,40] Both the individual molecules and the intermediate structures run almost parallel to the fibril axis while the molecules are staggered with respect to each other giving rise to 67 nm wide bands also named D-periods. The current molecular model of the D-period involves two regions one where all the molecules overlap and one where 20% of the molecules are missing due to an axial gap. The relative length of these regions is 0.46 and 0.54 of the 67nm D-period

respectively. This model was proposed on the basis of electron microscopy images of negatively stained collagen fibrils and further refined with small angle X-ray scattering data of rat tail tendon.[5,30]

Mechanical measurements of single collagen fibrils are typically performed under tension using micro-electro-mechanical devices (MEMS) or nano-tensile testers, in bending where a microcantilever is used to apply loads on suspended fibrils, and via atomic force microscopy (AFM) based nano-indentation.[115,169,189-192] These studies acknowledge that collagen fibrils are heterogeneous yet only provide a single value for their mechanical properties. Previous nano-indentation measurements on dried collagen I fibrils demonstrated a factor of two in elastic modulus between the overlap and the gap region of the D-period.[171] Another strong indication that mechanical properties are not homogeneous along a collagen fibril is the occurrence of discrete plastic deformations observed along fibrils inside overloaded bovine tail tendons.[12] Both results are strong incentives to develop a method capable of mapping mechanical properties of an entire fibril at high spatial resolution while in a hydrated state

The technique of choice that combines mechanical measurements and high spatial resolution is an AFM mode named force-distance (FD) curves based imaging.[193] In this mode, an FD curve is measured at each pixel of the image. The resulting data is then used to generate maps of the mechanical properties of the sample, such as the radial elastic modulus, the deformation of the sample under an applied load, the adhesion force between tip and sample and the amount of mechanical energy dissipated during indentation. In this study we take advantage of the high-throughput capabilities of the technique to generate radial modulus maps of single collagen fibrils in water at a spatial

resolution around 10 nm and at indentation speeds around 10^5 nm/s. We demonstrate that this hydrated radial modulus (HRM) of collagen fibrils stiffens by a factor of five when varying the indentation speed from 10^2 to 10^6 nm/s. This effect allows us to observe the D-period in the Sneddon modulus channel. We report a 20% decrease in the HRM from the overlap to the gap region of the D-period as well as long range fluctuations in along the length of the fibrils that have not been reported so far. Furthermore, collagen fibrils exposed to temperatures between 50 and 62°C and cooled back to room temperature show a sharp decrease in HRM and a swelling of the fibril. This is also associated with a disappearance of the D-period and the appearance of twisted subfibrils in the Sneddon modulus channel of the image that persists upon dehydration of the collagen fibril.

2.3 Materials and Methods

2.3.1 Sample Preparation

Rat tails from 2-year-old, male Sprague Dawley rats were dissected to extract tendon fascicles for use as a sample source with approval by the Health Sciences Research Ethics Board of Dalhousie University (I18-15c). First the dermal layers were removed from the tail exposing the skeletal frame and tendons of the tail. To prevent tensile loading during tendon extraction, a scalpel blade was inserted between the skeletal structure and the tendon and was used to sever connecting material. Tendons were then lifted from the skeletal structure and stored in 20ml PBS with 500µl of antibacterial cocktail (Sigma-Aldrich, USA) for no longer than 1 week. Collagen fibrils were dissected from tail fascicles in phosphate buffer saline. To minimize fibril damage, a thin glass rod was used as the main dissection tool. Fascicles were held at one end with tweezers while the glass

rod was inserted in the fascicle and moved along its longitudinal axis to allow gentle separation of the hierarchical subcomponents. Great care was taken to keep the fascicles hydrated at all times during this process. The phosphate buffer saline solution containing the dissected fibrils was transferred to glass bottom petri dishes with a pipet and left for 30 minutes allowing the fibrils to physically adhere to the glass substrate. The dishes were then rinsed three times with de-ionized water to remove unattached material and residual salts. The samples were either used immediately or kept at 4°C until AFM measurement for no longer than 1 week.

2.3.2 Atomic force microscopy (AFM)

All the experiments were performed with a Bioscope Catalyst atomic force microscope (Bruker, USA) mounted on an IX71 inverted microscope (Olympus, Japan) with a differential interference contrast module and a 100X, 1.3NA, oil immersion objective. This set-up allowed the optical visualization of single collagen fibrils in water prior to AFM imaging. Samples were imaged in peak force quantitative nanomechanical mapping mode (PF-QNM) using ScanAsyst liquid+ (Bruker, USA) cantilevers with a nominal spring constant of 0.7 N/m, a nominal tip radius of 2 nm and an equivalent cone half angle of 18°. Prior to each experiment the cantilever spring constant was calibrated with the thermal noise method.[194] Images were acquired at a cantilever oscillation frequency of 1 kHz, a scanning frequency of 0.5 Hz and at an indentation speed between 400 and 1200 μm/s. The longitudinal axis of the collagen fibrils measured in this work was perpendicular to the fast scan axis unless otherwise mentioned. All indentation speed and heating images were taken at an imaging speed of 5μm/s while the 20μm, 40μm, and 80μm maps were acquired at 2μm/s, 5μm/s, 10μm/s respectively. The peak force was

kept between 1 and 10 nN depending on the scan size. The total number of pixels per image was kept constant at 65536.

We also used the heating stage of the Bioscope Catalyst to expose single collagen fibrils to different temperatures. The temperatures reported in this work are solution temperatures calibrated by thermal couple for 3ml of water within an AFM sample dish. Due to condensation issues it was not possible to continuously image the fibrils while increasing the temperature. For each AFM measurement the fibril was first kept at the target temperature for 15 or 30 min then cooled down to room temperature (~25°C) and imaged at that temperature. During each heating and cooling cycle, the sample was covered to limit evaporation. The heating rate was 10°C per minute and cooling rate was 2°C per minute. The total amount of water was fixed to 3ml to ensure a constant temperature profile between samples. Mechanical maps were acquired by PF-QNM once the sample had cooled to 25°C. Each fibril was either exposed to 62°C for 30 min or treated to subsequent temperatures of 50, 55, 58, 60, and 62°C, in that order, each time for 15 min. After the final heating and cooling cycle, the samples were dehydrated and imaged once more to reveal topological structures not visible in the hydrated state.

2.3.3 Data analysis

Force curves were selected from an area ±10% of the fibril's diameter from the apex of the collagen fibril by a simple filtering methodology (Appendix A Figure 1-5). Based on the shape of our tips and the typical indentation depth that was in the order of 30 nm we used the Sneddon model including adhesion to fit each force curve and extract the hydrated radial modulus (HRM).[164,195] The Poisson ratio of a collagen fibril was

assumed to be 0.5 as accepted in the literature for an incompressible material.[173] The point of tip-fibril contact was determined by least square fitting of the force curve.[196] The influence of the underlying glass substrate was minimized by only fitting the force curves to an indentation depth of 10% of the zero-force height (ZFH) of the fibril, according to Bueckle's rule.[197,198] The ZFH of the fibril was estimated by adding the height and deformation channels, extracting the values along the apex of the fibril and averaging; this value was typically around 200 nm. The deformation of the fibril at any given point was estimated using the distance between the indentation at maximum applied force and extension curve at a given force value. We used 15% of the peak force value to estimate the deformation and saw no significant difference when varying the peak force percentage to values as low as 5% of the peak force. Below this threshold the measurement of the deformation was unreliable.

In some cases, we imaged fibrils over their entire length. Mechanical maps of each section of a given fibril were stitched manually. HRMs profiles were extracted along the entire fibrils and Fourier transformed to reveal periodic fluctuations. We used adjacent averaging to remove long wavelength fluctuations from the data to determine the amplitude of the short wavelength fluctuations observed.

2.4 Results

2.4.1 Influence of indentation speed on HRM

Typically, AFM based indentation measurements on collagen fibrils are performed at indentation speeds in the μm/s range.[173] To investigate the viscoelastic response of

collagen fibrils in water we measure the dependency of the HRM with indentation speed over 4 decades from 100 nm/s to 1 mm/s (Figure 2.1).

To average out spatial variations and fibril-to-fibril variations we use 3 different fibrils and a 5 μm long segment for each fibril. The order in which we measure the FD curves for the different indentation speeds is different for each fibril to avoid bias due to indentation history. The HRM is weakly dependent on the logarithm of the indentation speed below roughly 70 μm/s and then increases five to ten-fold in one decade (Figure 2.1). The same behavior is observed for each fibril individually but the range of HRM is large in the high-speed regime. When acquiring HRM maps we are in the regime where the collagen fibril appears to stiffen significantly compared to previously published radial modulus data that are typically obtained at an indentation speed of 1 μm/s.[173] Interestingly the indentation speed dependence observed in this study is very similar to the one observed for a model cross-linked polymer network below the glass to rubber transition.[199] In the glass state the mobility of the chains within the network is constrained in comparison to the rubber state, yielding an apparent stiffening of the network for indentation speeds well above the mobility of the chains. This means that in our case we are acquiring HRM maps in a regime where some characteristic relaxation mechanism of the molecules within a fibril is suppressed giving rise to an elastic contrast that should depend mainly on the molecular density.

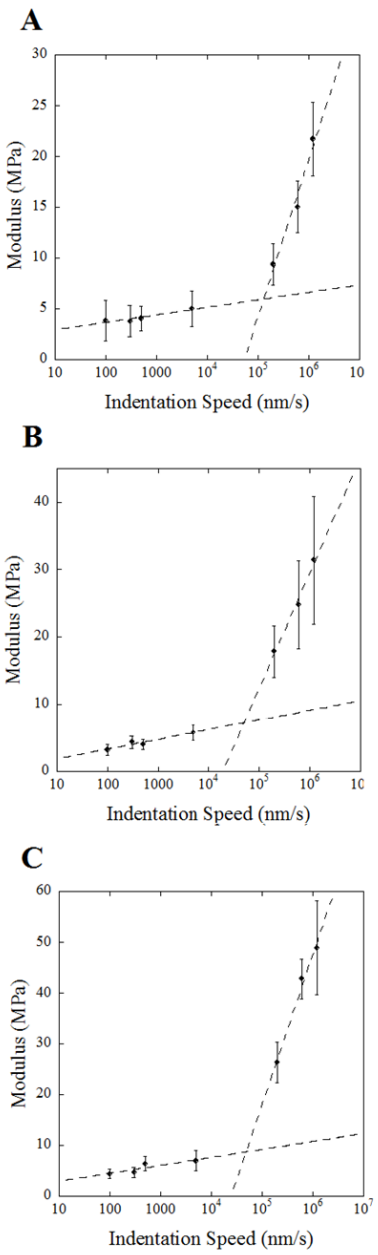

Figure 2.1: The HRM of 3 different collagen fibril segments 5 μm in length as a function of indentation speed. Logarithmic least square fits through the data are shown as dashed lines, highlighting the presence of two distinct regimes. Error bars are the standard deviation of each measurement.

2.4.2 HRM variations along a single fibril

A first demonstration of the capabilities of our approach is the observation of the D-period in the HRM maps of single collagen fibrils in room temperature water at an indentation speed of 600μm/s. At a scan size of 2 by 2 μm the D-period is visible in the height, the Sneddon modulus and the deformation channels (Figure 2.2). The variation between gap and overlap regions in each channel is small, 2-3 nm for the height and deformation, and several MPa for the HRM. However, the three channels are correlated with the overlap region being higher, stiffer and less deformable than the gap region as expected (Figure 2.2, B-D). Over a two micron range the HRM maps are quite uniform except for the D-period, but it is not true at length scales of tens of microns. Imaging fibril segments of 80 μm, 40 μm, and 20 μm at 45 nm, 20 nm, and 8 nm pixel resolution respectively reveals long-range variations in HRM that are on the micron-scale and fluctuations associated with structural anomalies (Figure 2.3, A-C).

Two interesting features are fibril ends and sharp bends that exhibit lower HRM than their surroundings. The HRM behavior of these defects appear as, at least, a four-fold decrease in HRM at the defect site with a linear gradient towards the mean HRM of the fibril spanning ~5μm (Figure 2.3, arrows). From the Fourier transforms of the HRM profiles extracted from the 40 μm and 20 μm maps, we can accurately measure the D-period at 66.4±0.2 nm and 67.6±0.2 nm, respectively (Figure 2.4 A and B).

To estimate the mean contrast in HRM between the gap and overlap regions of the D-period, we use both maps, (Figure 2.3 B and C) excluding the 5 μm segments surrounding the sharp bend and fibril ends, respectively (Table 2.1). Calculating the

moduli of the gap and overlap regions from the mean moduli of the fibril and the root mean-square of the D-period reveals a gap/overlap ratio of 0.80±0.04 and 0.82±0.04 for the 20 μm and 40 μm maps respectively. This is in excellent agreement with the molecular density ratio between the two regions as proposed by Hodge and Petruska.[5] This in turn indicates that the HRM scales locally with the molecular density as mentioned above.

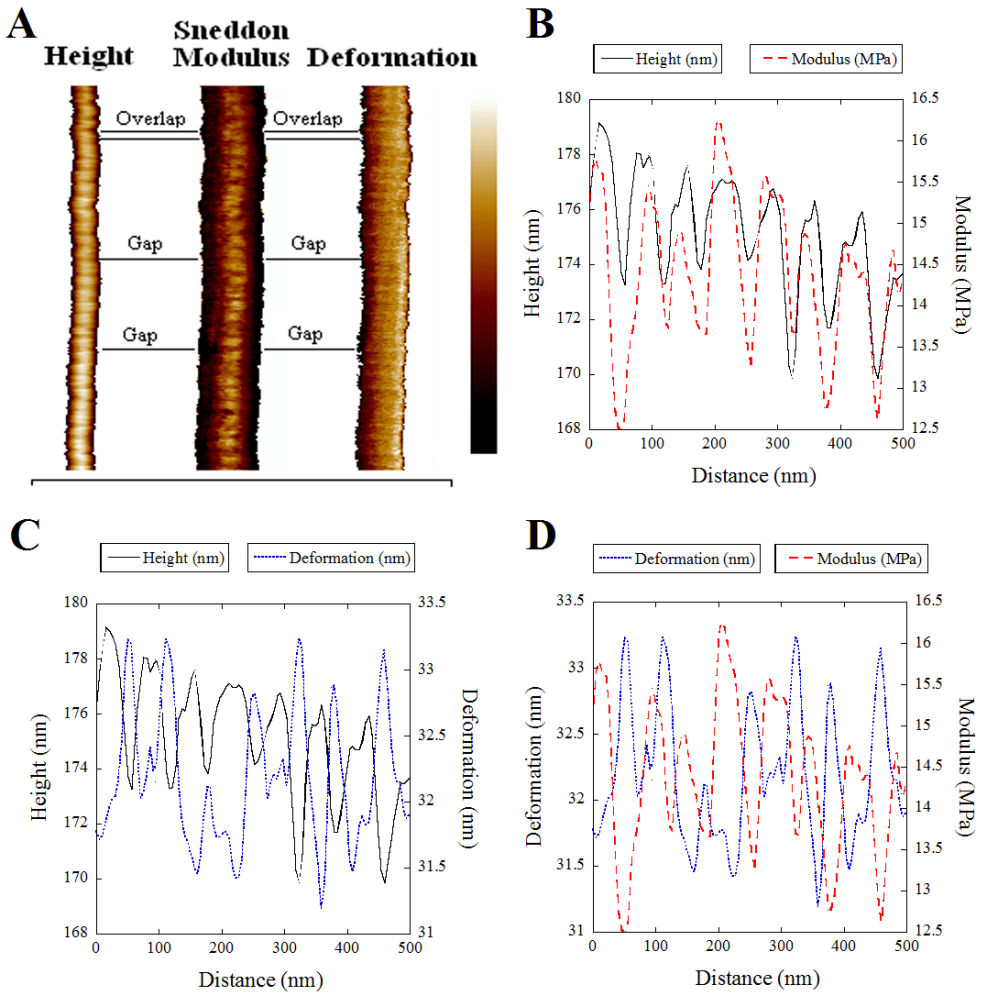

Figure 2.2: Observation of the D-period along a hydrated fibril. A) Height, Sneddon modulus (HRM) and deformation channel of a single collagen fibril. The differences in apparent diameter of the fibril are due to the choice of scale bar range used for each channel to visualize the D-period. Scale Bar: Height 140-190 nm; Sneddon modulus 0-30 MPa; Deformation 20-40 nm. The length of the fibril is 2μm. B-D) Comparison of the height, HRM and deformation channels are shown for 500 nm segments demonstrating the alignment of the HRM and height of the fibril and the 180° phase shift between the HRM and deformation of the fibril. The D-period is visible in all three channels. The overlap region appears higher, stiffer and less deformable than the gap region.

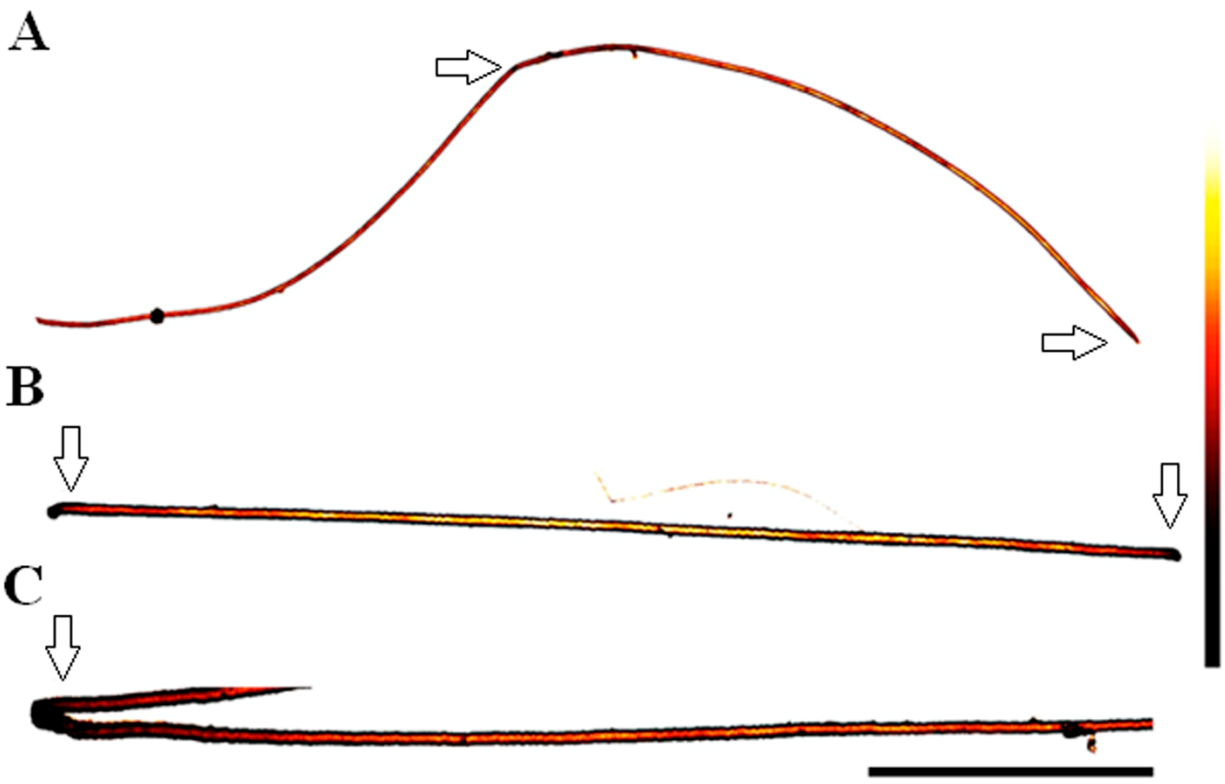

Figure 2.3: HRM maps of collagen fibrils. A) 80 μm long segment of fibril at 45 nm pixel resolution with fibril bend (center arrow) and fibril end (right arrow). B) 40 μm long fibril at 20 nm pixel resolution, the HRM decays from the center to the ends (Arrows). C) 20 μm long segment of fibril at 8 nm pixel resolution, a sharp bend appears softer than its surrounding (Arrow). Structural variations not associated with structural anomalies were also observed in all three fibril maps. Color Scale Bar: 0-30 MPa (A, C); 0-50 MPa (B). Length scale bar: (A) 20 μm, (B) 10 μm, (C) 5 μm.

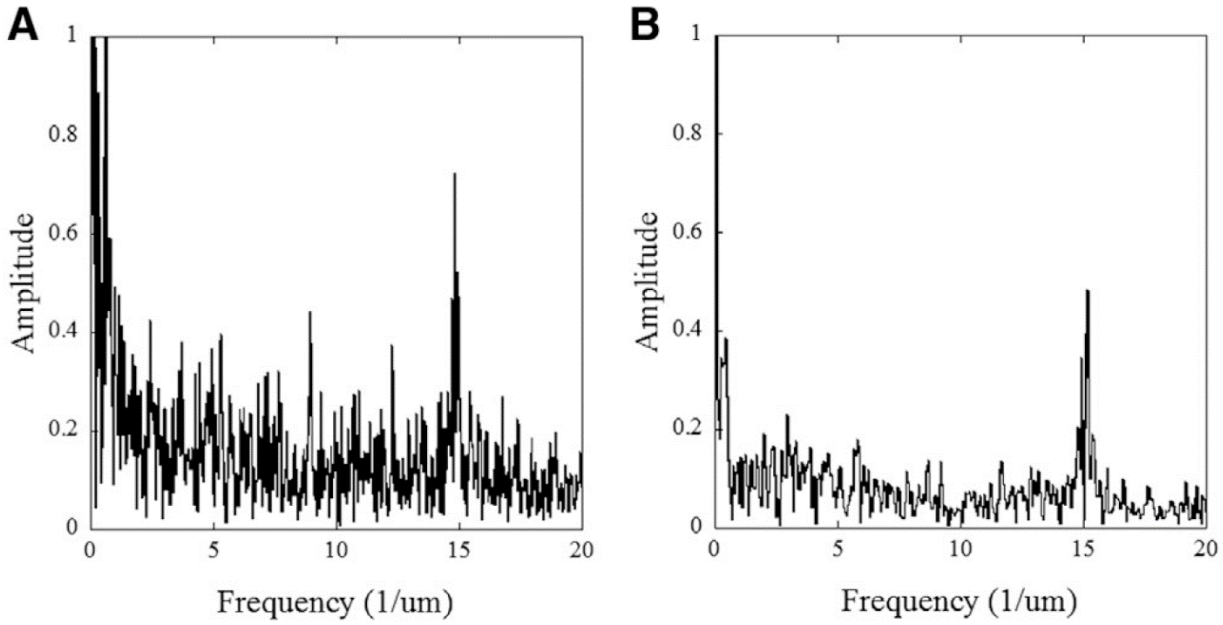

Figure 2.4: Fourier transforms of HRM profiles extracted from the apex of two fibrils in Figure 12. A) 40 μm long fibril at 20 nm pixel resolution. B) 20 μm long segment of fibril at 8 nm pixel resolution. The peak corresponding to the D-period is clearly visible in both cases.

Table 2.1: Summary of D-band HRM variation and period with standard deviation (HRM data) and pixilation (D-period) as error.

Fibril Length (μm)	Mean HRM (MPa)	Gap HRM (MPa)	Overlap HRM (MPa)	Gap/Overlap	D-period (nm)
20	16±3	14.5±0.6	18.1±0.6	0.80±0.04	67.6±.2
40	33±6	30±1	37±1	0.82±0.04	66.4±.2
80	16±4	NA	NA	NA	NA

2.4.3 Structural and mechanical alterations due to temperature exposure

As a next step we measure the HRM of 5 μm long segments of two collagen fibrils exposed to temperature ranging from 25°C to 62°C in water (Figure 2.5). We use a softer cantilever than stated previously with a spring constant of 0.3 N/m and an indentation velocity of 1.2 mm/s. At 25°C the two fibrils show a HRM and ZFH of 12.7±0.3 MPa and 250nm (Figure 2.5 A and B), and 9.8±0.2 MPa and 350nm (Figure 2.5 D and E), respectively. These HRM values are below the 20-40 MPa range mentioned above for the same indentation speed. This is due to the use of a different cantilever (MSNL, Bruker, USA) with a lower spring constant of 0.25 N/m compared to previous measurements (Figure 2.1). The lower spring constant had a maximum measurable value of ~15MPa. This was selected to provide higher contrast at the lower elastic moduli observed after fibrils were exposed to a temperature greater than 50°C. The behavior of the fibril between 25°C and 50°C was checked with a ScanAsyst cantilever and showed the same behavior as the MSNL cantilever. To compare results from both fibrils, we normalize all HRM values to the ones obtained prior to any temperature exposure. After exposure to temperatures above 50°C, fibrils exhibited a sharp decrease in HRM when measured at room temperature (Figure 2.5). This decrease in HRM progressed with exposure to temperatures as high as 62°C at which point the HRM was found to be around 1MPa, or 10% of its original value. This decrease in HRM was found to persist up to 36 hours after temperature exposure, suggesting a permanent alteration to the fibrillar structure. The softening of the fibrils for temperatures above 50°C is accompanied by two structural

changes. The ZFH of the fibrils increases by 15% and 30% (Figure 2.5 B and E) and the D-period disappears completely from the HRM maps (Figure 2.5 C and F).

To quantify this disappearance, we compute the FFT of the HRM profile extracted from the apex of each fibril after each temperature exposure. The amplitude of the D-period peak in the FFT is a measure of its visibility in the HRM maps. This quantity is presented in Figure 2.5 and shows that the D-period has completely disappeared after exposure to 60°C. The disappearance of the D-period is associated with the appearance of subfibrillar structures that are only barely visible in the peak force error channel when the fibril is perpendicular to the fast scan axis (Figure 2.6, A). However, they appear clearly on the HRM maps when the fibril is tilted 45° from the fast scan axis (Figure 2.6, C) or when the fibril is dried (Figure 2.6, E). The subfibrillar structures were determined to be subfibrils as their diameter (~20-40 nm), was far larger than that of microfibrils, 4-8nm.[40] Our best HRM map image showing subfibrils with a pitch in the micron range was obtained after directly exposing a fibril to 62°C for 30 min and then cooling it back to 25°C (Figure 2.6, C). These structures were not observed on the fibril at 25°C prior to heating (Fig. 2.6B) or after dehydration (Figure 2.6, D). All the fibrils exposed to a temperature of 62°C, stepwise (Figure 2.6, A) or directly (Figure 2.6, C) show both a D-period and prominent subfibrils with a minimum diameter of 20 nm when dehydrated (Figure 2.6, E).

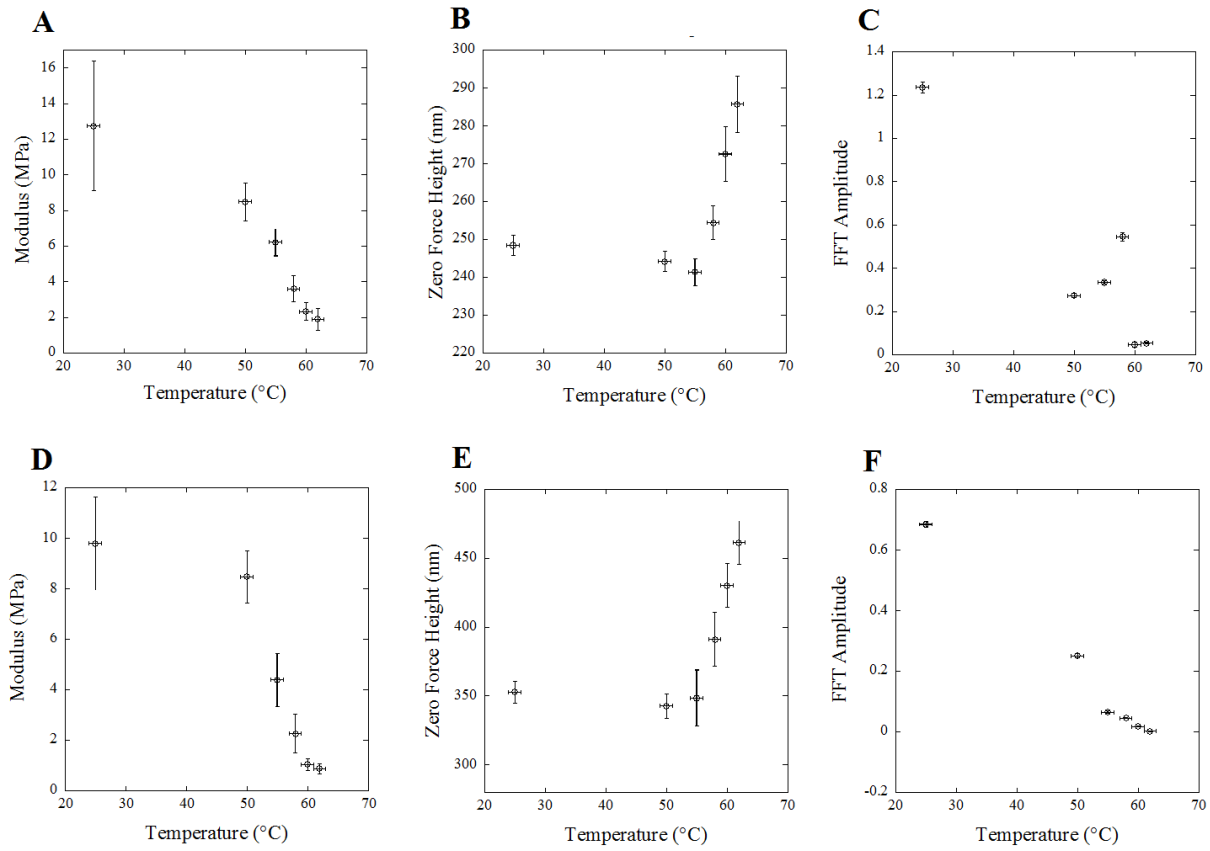

Figure 2.5: The HRM (A, D), ZFH (B,E) and FFT amplitude of the HRM profile at the D-period wavelength (C,F) for two 5µm segments acquired from two collagen fibrils as a function of applied temperature. The indentation speed was 1.2 mm/s. Vertical error bars are the standard deviation of each measurement.

No alteration to the D-period was observed between dehydrated control fibrils, 67.6 ± 2.7 nm and fibrils dehydrated after being exposed to 62°C, 66.1 ± 1.5 nm (Table 2.1). However, the height difference between the overlap and gap regions decreases from 5.6 ± 0.3 nm to 2.8 ± 0.3 nm after exposure to 62°C. This decrease in D-band contrast is coupled with a decrease in the relative length of the gap region from 44 ± 2% (n=2) of the D-period to 34 ± 2% of the D-period. These two values are different from the relative length of the gap region, 54% of the D-period, measured by X-ray scattering for hydrated fibrils at room temperature.[30] The discrepancy between the X-ray value and the AFM value of control fibrils can be attributed to a combination of drying and AFM imaging artifacts due to the tip shape.[200] Admittedly, the sample sizes used in this study (n=2) are insufficient for statistical statements, but should be taken as a preliminary look at fibril structures response to temperature and measurement with a novel technique.

2.5 Discussion

2.5.1 A rat tail collagen fibril behaves as a polymer network in a glassy state

In solution, the triple helix motif characteristic of the collagen molecule becomes unstable around body temperature.[56] Within a fibril the same structural motif shows an increased thermal stability due to the proximity of neighboring chains. The decrease in mobility of the molecules in the crowded fibril environment compared to a dilute solution is associated with a decrease in conformational entropy at a given temperature. This is the so-called polymer in a box model of collagen fibril denaturation. In other words, below the denaturation temperature, typically 65°C, the molecules within a collagen fibril are

less mobile than above that threshold.[58] This is comparable to polymer networks where the relaxation time characteristic of chain motion increases significantly below the glass transition temperature.

As mentioned above, the relationship between indentation modulus and indentation speed of polymer networks below the glass transition temperature is very similar to the one observed for collagen I fibrils at room temperature (Figure 2.1).[199] Based on this comparison we found that collagen I fibrils display a characteristic relaxation time of 0.1 ms, estimated using a typical deformation of 20 nm and a critical indentation speed around 70 μm/s (Figure 2.1). When the experimental time is smaller than the relaxation time the collagen fibril stiffens by nearly sevenfold within the accessible range of indentation speeds (Figure 2.1). In that regime the collagen molecules have no time to rearrange locally and should deform cooperatively. The resulting deformation should be similar to the one observed after permanently indenting dried collagen fibrils.[169] Using a 20 nm radius tip, Wenger and coworkers achieved an imprint depth of 30 nm that extended along the fibril axis over two D-periods.[169] If this picture holds for the high indentation speed regime observed in this study, this means that all the collagen molecules in contact with the tip apex during indentation are bent homogeneously. It follows that the measured HRM should be proportional to the molecular density. With this in mind the amplitude of the HRM contrast observed within a D-period (Figure 2.2) is directly related to fluctuations in molecular density. Furthermore, our observation that the HRM of the gap region is 80% of the overlap region supports the quarter-staggered model of collagen fibril axial structure proposed by Hodge and Petruska.[5]

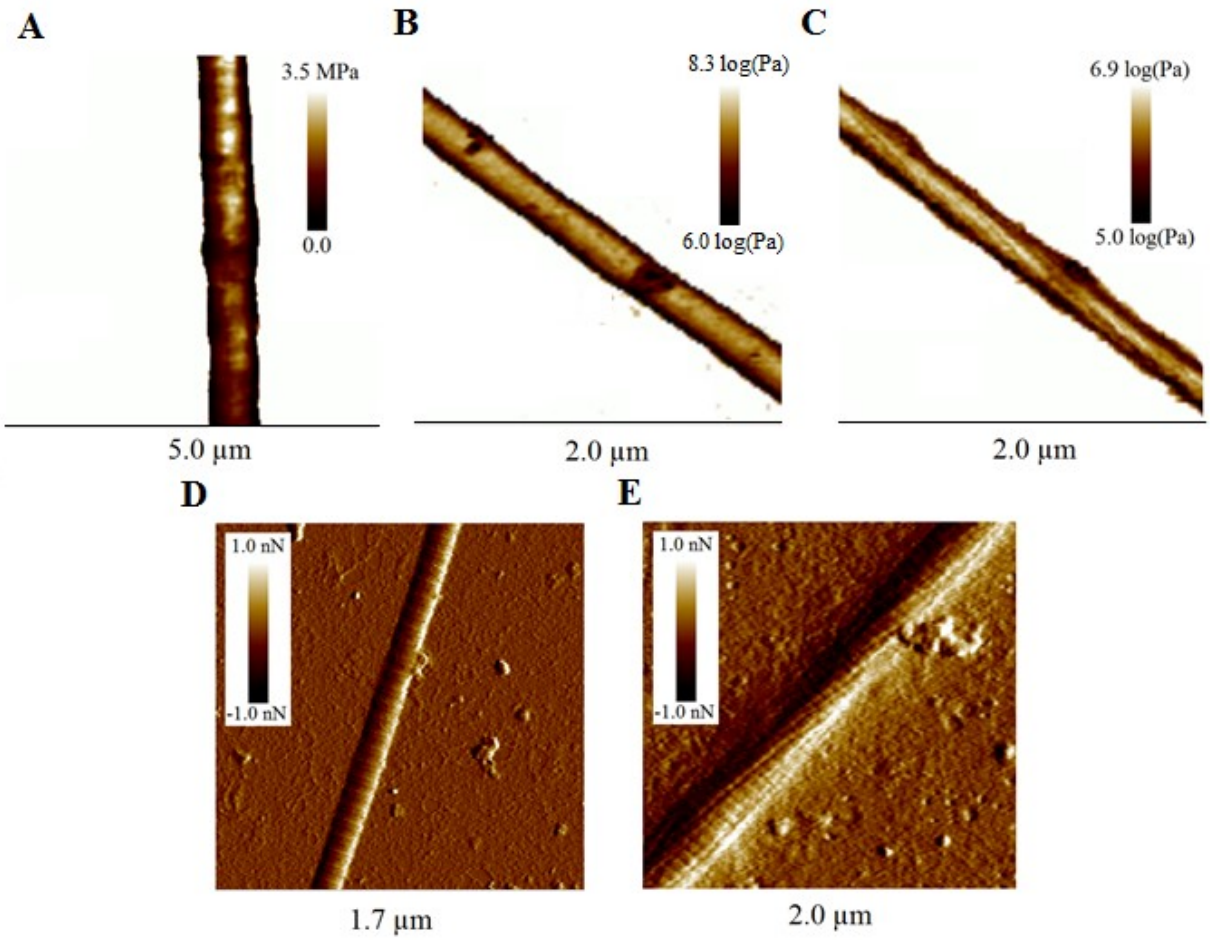

Figure 2.6: *Structural changes in fibrils exposed to high temperatures.* Sneddon modulus and Log Sneddon modulus channels of two collagen fibrils after repeated temperature exposure from 25°-62°C as seen in Figure 2.5 (A), and a fibril before (B) and after (C) 30 min exposure to 62°C. Peak force error channel images of a typical dehydrated collagen fibril (D) and of a fibril exposed to 62°C for 30 min before dehydration (E).

2.5.2 The effects of temperature exposure on collagen fibrils' structure and mechanical properties

The glassy state model discussed in the previous section predicts that collagen fibrils should soften as the temperature is raised towards 65°C. This is confirmed by our temperature exposure experiments with an onset of softening around 50°C and an overall ten-fold decrease in HRM (Figure 2.5). Based on similar results obtained for a model cross-linked polymer network, we expect at most a five-fold decrease in HRM when crossing the glass to rubber transition.[199] The extra two-fold decrease can be attributed to fibril swelling due to water uptake (Figure 2.5). Assuming that the length of the fibril remains constant due to the adsorption to the glass substrate, and that the measured HRM at high indentation speed scales with molecular density as mentioned above, the 30% increase in fibril ZFH (Figure 2.5) should yield a 1.7-fold decrease in HRM due to the shift in molecular density associated with the increase of the fibrils cross-sectional area.

Water uptake by the fibril also has important structural effects beyond radial swelling. The D-period disappears almost completely from the HRM maps in the hydrated state above 50°C (Figure 2.5) but it is visible in the dehydrated state albeit with a reduced height contrasts between gap and overlap regions. A simple explanation for these results is a homogenization of the molecular density along the fibril axis due to water uptake. Details of the homogenization mechanism are difficult to infer from our data. However, it is likely that most of the water uptake is concentrated in the overlap region since it has a higher molecular density than the gap region at room temperature. Still, the situation is complicated by the appearance of twisted subfibrils after temperature exposure (Figure 2.6, C and E) indicating that water may accumulate between these subfibrils rather than

being uniformly distributed in the fibril cross-section. These twisted structures are similar to those seen along *in vitro* fibrils with no temperature exposure (Appendix A, Figure 7)

Finally, our temperature exposure experiments on single fibril are in excellent agreement with second harmonic generation (SHG) measurements of rat tail tendons and pig corneal stroma.[200,202] In both cases the SHG signal intensity decreases with temperature exposure in a similar way as the HRM in our study (Figure 2.5). It has been shown previously that the large SHG signal observed on collagen fibrils is due to the tight packing and alignment of weakly efficient harmonophores.[203] A radial swelling associated with an increase of angular spread of the molecules with respect to the fibril axis, would yield a sharp decrease in SHG signal intensity. Matteini et al. came to the same overall conclusions based on theoretical considerations. [202]

2.5.3 Effect of mechanical deformations

There is mounting evidence that tensile loading can generate plastic deformations called kinks along collagen fibrils.[12] These kinks are short segments of the fibrils, around 200 nm in length, that are characterized by a decreased enthalpy of denaturation and an increased sensitivity to trypsin digestion compared to pristine collagen fibrils .[13,14] In this study, there is no indication that removing the fibrils from their tissue leads to the formation of kinks but we observe two other types of mechanical damage, ruptured ends and sharply bent segments (Figure 2.3). In both cases the HRM decreases by three to fourfold compared to pristine regions of the same fibrils. The surrounding area exhibits a decrease in HRM exhibiting the D-period with the same 20% contrast between gap and overlap regions. The only point where the D-period is not observed is right at the point

where the mechanical deformation took place (Appendix A, Figure 6). Interestingly, the sharply bent segments display a much higher ZFH than the pristine segments of the fibril, while the ruptured end of the fibril has a ZFH consistent with its pristine region. This suggests that the two types of damage are distinct, while having the same effect on the local HRM of the fibril. Since the quarter-staggered organization of the fibrils does not seem affected, we propose that the observed decrease in HRM is due to a loss of mature crosslinks between collagen molecules (ruptured end) and/or the uptake of water in the fibril bend, similar to what is observed with temperature exposure. This loss of the glassy state could be associated with the uptake of water in the fibril bend, similar to fibrils exposed to temperatures higher than 58°C. Alternatively the possibility of the loss of mature crosslinks is strongly supported by HRM data obtained on fibrils assembled *in vitro* from acid solubilized collagen molecules extracted from rat tail tendon. These fibrils have a HRM five times smaller than the *ex vivo* fibrils, which is consistent with an absence of mature crosslinks, and still show the dependency on indentation speed characteristic of a glassy state (Appendix A, Figure 8).[63]

2.6 Conclusion

In this study, we demonstrate that nanomechanical mapping of entire collagen fibrils at indentation speeds around 10^5 nm/s can detect subtle changes in molecular dynamics and fibril architecture due to an external stimulus such as temperature. This is opening the road for the study of mechanical damage at the single fibril and the study of gene mutations that are suggested to impact collagen fibril structure and mechanical properties.

ACKNOWLEDGEMENTS

LK acknowledges support from the Discovery grant program of the National Science and Engineering Research Council (NSERC) and from the Canadian Foundation for Innovation (CFI). SB is the recipient of a PhD scholarship from the NSERC funded CREATE program ASPIRE at Dalhousie University. AQ and CC received undergraduate summer research scholarships from NSERC to participate to this project.

Chapter 3: Characterization via atomic force microscopy of discrete plasticity in collagen fibrils from mechanically overloaded tendons: Nano-scale structural changes mimic rope failure

This chapter has been reproduced from the article “Characterization via atomic force microscopy of discrete plasticity in collagen fibrils from mechanically overloaded tendons: Nano-scale structural changes mimic rope failure”, with permission from the Journal of Mechanical Behaviour of Biomedical Materials (Appendix F). The authors of the article are as follows “Baldwin, S.J., Kreplak, L. and Lee, J.M.”. As First Author I was responsible for experimental design, data acquisition, data analysis, and writing of the first draft of the document and participating in the subsequent edits.

3.1 Motivation and Hypotheses

The study presented in Chapter 2 solidified our understanding of high-speed AFM indentation as a means to quantifying localized structural variations along the axis of a collagen fibril. Furthermore, exposing fibrils to temperatures up to 62°C resulted in an increase in zero force height and a decrease in hydrated radial modulus. Concurrently, colleagues in biomedical engineering were studying the effects of tendon overload on collagen fibrils. In their work they observed a structural phenomenon, discrete plasticity, where localized kink structures were generated along the length of individual collagen fibrils within the overloaded tendon: In this chapter the goal was to use high speed peak-force quantitative nanomechanical mapping to quantify the structural alteration of collagen fibrils displaying discrete plasticity. The hypotheses below were influenced by the observed alteration of heated collagen fibrils discussed in Chapter 2, and structural observations associated with discrete plasticity presented in Chapter 1.

Hypothesis 3.1: Fibrils displaying discrete plasticity will resemble thermally treated collagen fibrils when measured by high speed PF-QNM, with a lower HRM and increased water content compared to unloaded fibrils.

Hypothesis 3.2: HRM and water uptake by fibrils displaying discrete plasticity will, decrease and increase respectively, with the serial kink density of an individual fibril.

Hypothesis 3.3: HRM and water uptake by fibrils displaying discrete plasticity will be heterogeneous due to the localized nature of discrete plasticity and associated fibril shell.

3.2 Introduction

Tendons are tension-bearing tissues that convert muscle contraction into skeletal movement used for every day locomotion. The functional attributes of tendon are the result of a highly organized hierarchical structure of extracellular matrix proteins. The most mechanically structural element is collagen, its most fundamental structural unit being the nano-scaled fibril.[4,204] Injury due to mechanical overload of a tendon results in the disruption of its ordered hierarchical structure, long-term alteration its mechanical properties, and loss of function.[205,206] A structural motif for collagen damage due to tendon overload has recently been identified. It is characterized by a serial disruption (kinking) of collagen fibrils structure along their length.[12] Termed discrete plasticity, such damage is associated with increased enzyme susceptibility, decreased thermal stability and denaturation of collagen, and cellular recognition of locally kinked fibrils.[12-14,153]

The native structure of a collagen fibril (in bovine tendon) consists of collagen molecules, self-assembled into five molecule cross-section microfibrils approximately 4 nm in diameter, these then assembled into subfibrils approximately 10-40 nm in diameter.[28] It has been demonstrated that subfibrils and microfibrils are wound about the axis of the fibril in a manner similar to that in a laid rope strand.[34,38,40,41,207,208] Characteristic, periodic D-banding is observed along the length of native fibrils. This appearance is a result of the non-integer staggering of collagen molecules within microfibrils, resulting in molecular density fluctuations along the fibril's length. A single period of the D-band is ~67 nm in tendon fibrils and consists of a gap and overlap

component where the gap has 4/5's of the molecular density of the overlap region.[5,28,209]

It is now clear that overload damage in a tendon involves alteration to molecular conformation or packing order at the nano-scale within individual collagen fibrils.[12-14,153] In particular, two significant structural alterations to fibril morphology have been reported in association with discrete plasticity under scanning electron microscopy (SEM): (i) the appearance of a shell layer which obscures or replaces D-banding, and (ii) serial kink sites along the fibril's length. These changes appear to relate to radial and longitudinal alterations respectively within the collagen fibril.[12] To this point in time, discrete plasticity has been observed only under SEM, and that after dehydration and sputter coating to achieve nanometer resolution. In the present study, we have sought to circumvent these alterations to collagen fibrils before observation by application of atomic force microscopy (AFM).

We have previously demonstrated acquisition of high-resolution mechanical maps from hydrated collagen fibrils via AFM, using the peak force quantitative nanomechanical mapping (PF-QNM) mode.[210] From the acquired data we are able to calculate the maximum penetration depth of the tip into the collagen fibril, and the fibril's hydrated radial modulus (HRM), all with a spatial resolution of around 10 nm. These mechanical properties were shown to be a measure of the local molecular density of the fibril. By this means, the penetration depth and Sneddon modulus images visualize the interior of the fibril at distinct depths. In the present study, we have used this technique to analyze 25 control and 25 overload-kinked collagen fibrils, seeking to further our understanding of

the molecular alterations in collagen fibrils associated with discrete plasticity damage. Based on the resulting data, and making use of previous description of the collagen fibril as a nanoscale rope and/or as a tube-like structure, we suggest a new model of kink formation which resembles damage motifs found in laid rope strands.[36,38,41]

3.3 Materials and Methods

3.3.1 Sample acquisition

Tissue harvesting and handling were approved by the Health Sciences Research Ethics Board of Dalhousie University (Protocol approvals I-14-20, I-16-20 and I18-15C). Bovine tails were acquired from 18-24-month-old steers immediately after slaughter for meat at a local abattoir. The tails were stored for no more than 2 hours at 4°C, after which the tendons were dissected from the dorsal region of each. In this study tail tendons from 5 animals were used, with a single tendon sourced from each tail.

3.3.2 Tendon preparation

A segment 1 cm in length was cut from each tendon to serve as a control and stored in phosphate-buffered saline solution (PBS) with a pH of 7.4 at 4°C. The remainder of the tendon (5-7 cm) was then clamped into an MTS Series 458 servo-hydraulic testing machine for mechanical loading with an inter-grip sample length of 2-3 cm. Each tendon underwent a pre-loading cycle at 1% strain per second to a maximum strain of 10%. This was followed by 5 overload cycles into the plastic region of the load-deformation curve under computer control at a strain rate of 1%/s as described previously.[13] At the time of this study, this repeated overload regime had been demonstrated to produce the most collagen fibrils displaying discrete plasticity in the tendon collagen while retaining a wide

range of kink density among the individual fibrils.[13] During loading, the tendon samples were kept hydrated by continuous application of PBS with a pipette. At completion of the loading procedure, the overloaded tendon was removed from the apparatus, and the clamped ends were cut away. Both the control tendon sample and the trimmed overload samples were then subjected to a decellularization process (Figure 3.1).

3.3.3 Decellularization

Decellularization was undertaken to allow clear visualization of individual collagen fibrils and has previously been demonstrated to preserve discrete plasticity damage.[153] The process has been fully described previously (Appendix E).[211] It began with treatment in a hypotonic cell-lysing solution lasting 36 hours at 4°C, followed by exposure to a Triton X-100 solution at 4°C for 24 hours, a sterile 3 hour wash in a DNase/RNase solution at 37°C, and finally a sterile 24 hour wash in Triton X-100 solution at room temperature. All solutions were replaced with fresh solution every 12 hours where required. Following the final wash in the Triton X-100 solution, samples were rinsed in sterile PBS, in antifungal/antibiotic solution, and twice in a sterile PBS/antibiotic solution, each wash occurring at room temperature and lasting 30 minutes. A final wash in sterile PBS/antibiotic solution at room temperature lasted 48 hours and occurred before storage in PBS/antibiotic solution at 4°C. The maximum storage time for the now-sterile, decellularized tendon samples never exceeded 3 weeks.

3.3.4 AFM sample preparation

AFM sample preparation followed the method described by Baldwin et al.[210] Decellularized tendon samples were taken from storage and placed on a plastic dissection

dish in 1ml PBS at pH7.4. Collagen fibrils were dissected from the tendons using tweezers and a thin glass needle. After sufficient dissection, the PBS/fibril solution was poured onto a glass-bottomed dish and allowed to settle for a minimum of 45 minutes to facilitate fibril adsorption to the bottom of the dish. These AFM samples were then rinsed 3 times with deionized water and dried under a flow of nitrogen for 10 minutes to completely adhere the fibrils to the glass substrate. At this point the samples were ready for AFM imaging.

3.3.5 AFM imaging

AFM imaging was performed with a Bioscope Catalyst atomic force microscope (Bruker, USA) mounted on an IX71 inverted microscope (Olympus, Japan) equipped with differential interference contrast (DIC) and a 100X, 1.3 NA, oil immersion objective, which allowed optical targeting of single collagen fibrils. ScanAsyst liquid+ cantilevers (Bruker, USA) with a spring constant of ~0.7N/m, resonance frequency of ~150 KHz, tip radius of ~2nm, and cone half-angle of 17.5 degrees, were used in this work. All cantilevers were calibrated using absolute calibration. The deflection sensitivity was measured on fused silica and spring constant was determined using the thermal tune component of the Nanoscope 8.15 software (Bruker) which makes use of the thermal noise method of cantilever calibration.[194] All AFM images were acquired in peak force quantitative nanomechanical mapping mode (PF-QNM) with a tip velocity of 1.2 mm/s and a peak force set point of 10nN, resulting in a 256x256 grid of force displacement curves allowing analysis of the sample areas mechanical properties.[210]

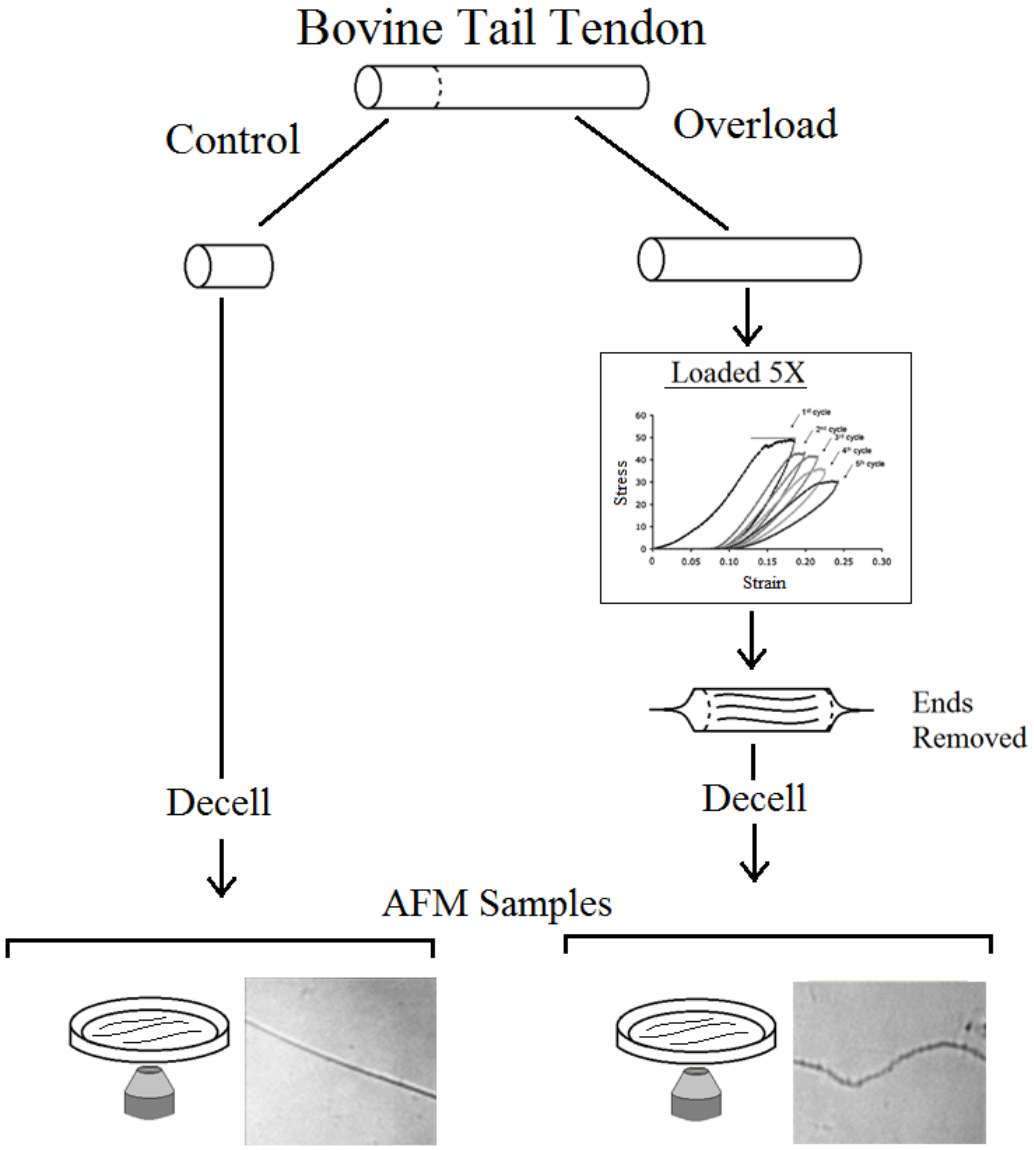

Figure 3.1: Control samples were cut from bovine tail tendons and stored in PBS while the remainder of the tendon was overloaded 5 times as described by Veres et al.[13] After loading, the control and overloaded samples underwent a decellularization process as described by Ariganello et al.[211] At the completion of the decellularization process collagen fibrils were extracted mechanically using tweezers and a glass needle as described in Baldwin et al.[210and dehydrated to encourage adhesion to the bottom of a petri dish. Control and damaged fibrils were identified via DIC optical microscopy.

3.3.6 AFM data acquisition

In this study, ten fibrils from each of 5 tendons were imaged along 10 μm of their length. We selected five fibrils from each control sample and five fibrils from each loaded sample which displayed sites of discrete plasticity that we will subsequently refer to as kinks. In total, we imaged 50 fibrils, 25 control and 25 kinked for a total axial length of 500 μm. Three essential steps were followed in this order for all data acquisition: (i) optical targeting of dehydrated collagen fibrils, (ii) AFM imaging of each dehydrated fibril using PF-QNM with a pixel size of 20 nm, and (iii) AFM imaging of rehydrated fibrils using PF-QNM imaging with a pixel size of 8 nm. Imaging of hydrated collagen fibrils was carried out in PBS with at pH 7.4 and at room temperature. All collagen fibrils were exposed to a single dehydration step during sample preparation and dehydrated imaging, followed by a single hydration step prior to hydrated imaging. Samples were allowed 30 minutes to rehydrate prior to hydrated imaging, and showed no progressive hydration with longer time periods (data not shown). The dehydration process was necessary to ensure that fibrils displaying discrete plasticity were completely adsorbed to the glass AFM substrate. We acknowledge that the dehydration/rehydration process may alter the fibrils, but deemed it to be experimentally necessary.

3.3.7 Data analysis

All data analysis was performed using SPIP 6.3.3 software (Image Metrology). From the acquired data, 6 properties of the collagen fibrils were of interest: the height and deformation of the fibrils in both hydrated and dehydrated states, the HRM, and the mean serial kink density (kinks/μm) along each fibril over a 10 μm length. The deformation of

a fibril at any point was defined from the force/distance data as the distance between the extension curve and maximum indentation at 15% of the peak force (max force) (Figure 3.2). This was used as an estimate of the deformation of the sample by the AFM tip, with the 15% setpoint approximating both the contribution of cantilever compliance associated with its sensitivity measurement and the point of contact between the AFM tip and the collagen fibril. All height and deformation data were extracted from a 20 nm wide strip along the apex of the collagen fibril. The deformations in the hydrated and dehydrated states were summed with the corresponding height measure to provide a value termed the zero-force height (ZFH). This measure represented the corrected height of the fibril in the absence of applied force due to the AFM tip.[210]

Using the means of the hydrated and dehydrated ZFH, a swelling ratio as was calculated for each fibril as shown in Equation 2:

$$\text{Swelling Ratio} = \frac{\text{Hydrated ZFH}}{\text{Dehydrated ZFH}} \qquad (2)$$

This ratio provided insight into the fibril's interaction with the surrounding PBS medium. The HRM of collagen fibrils was calculated by fitting the Sneddon model to the retract curve of the AFM indentation as described in Equation 3:

$$F = \frac{2E}{\pi(1-\nu^2)}(\tan\alpha)(\delta^2) \qquad (3)$$

where F is the applied force, ν is the Poisson ratio, α is the half angle of the cone, δ is the depth of indentation into the sample and E is the elastic modulus (HRM) of the sample.[164,195,196] The Poisson ratio of the fibril was taken to be 0.5, characteristic of incompressibility.[173,210] The retract curve was selected for Sneddon modulus fitting

as the point of contact between the AFM tip and the collagen fibril is poorly defined due to the low radial modulus of the collagen fibril.

The hydrated radial modulus obtained by fitting Equation 3 serves as a probe for the molecular density of the collagen fibril.[210] The Sneddon model was selected for modulus analysis due to the AFM tip geometry and a minimum indentation depth of ~30 nm upon the apex of the control collagen fibrils. The fit range of each force curve was determined using Bueckles' rule, corresponding to a maximum fit range equivalent to 10% of the fibril's ZFH.[197,198] This process produced maps of the HRM of the collagen fibril from which values were extracted along a 20 nm wide strip along the apex of the fibril. Outliers in the HRM of a single fibril were determined using JMP software (version 11.0.0, SAS Institute Inc.) and removed from the data set. The mean HRM and the coefficient of variation of the HRM were calculated for each fibril. The mean HRM was used to quantify the molecular density of the fibrils, as justified previously, while the coefficient of variation of the HRM provided a measure of the heterogeneity of the molecular density for the collagen fibril.[210]

The mean, serial kink density along each fibril was determined by counting the number of kinks along a 10 μm length. This was performed on 10 μm x 10 μm dehydrated height images of kinked fibrils where a kink was classified as a transversal fault line on the fibril (Figure 3.3). Kinked fibrils were split into two separate groups: kinked (mean kink density less than 1.5 kinks/μm), and very kinked (mean kink density greater than 1.5 kinks/μm).

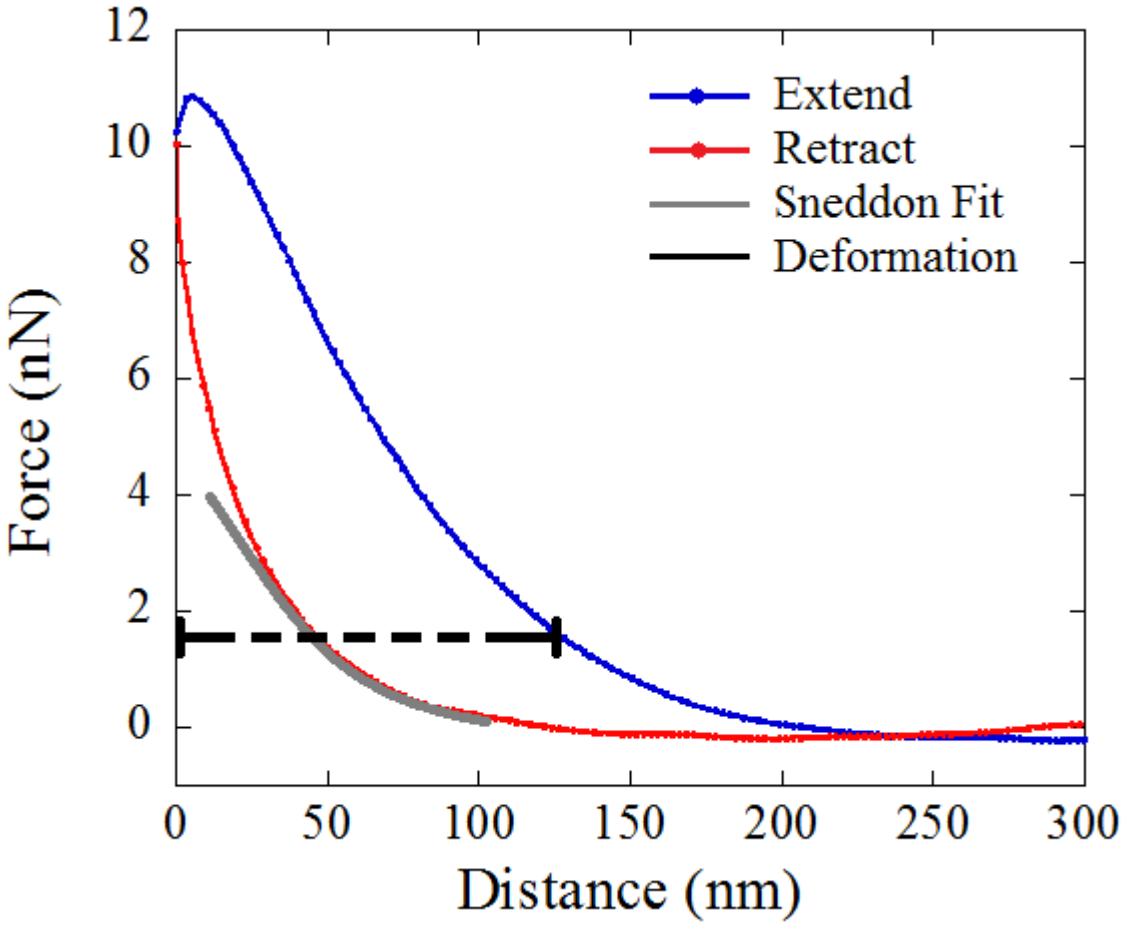

Figure 3.2: An example of a force/distance curve extracted from PF-QNM data with corresponding Sneddon fit and deformation calculation. The extend and retract curves correspond to the indentation and retraction of the AFM tip from the sample surface respectively. Deformation was calculated as the distance from the extend curve at 15% peak force to maximum indentation. The Sneddon modulus was calculated by fitting the Sneddon model to the retract curve within the limits of Bueckles' rule, resulting in the HRM.

3.3.8 Image analysis

To visualize the data, maps of height, deformation, and HRM were extracted using SPIP 6.3.3 and stitched together in Adobe Photoshop. All cross-sectional data presented were extracted along a 20 nm-wide strip along the apex of the corresponding collagen fibril.

3.3.9 Statistical Analysis

Statistical Analysis was performed using JMP software (version 11.0.0, SAS Institute Inc.). A 2-way ANOVA was performed for swelling ratio, HRM, and coefficient of variance data with variables of five animal tails and three kink density groups (control, kinked, very kinked). Where appropriate after the 2-way ANOVA, Bonferroni-corrected post-hoc testing was carried out using Fisher's Least Significant Difference (LSD) test. All parametric data are presented as the mean ± the standard deviation.

3.4 Results

Topographic mapping of dehydrated collagen fibrils extracted from control tendon samples were free of curvature and showed the periodic D-banding pattern indicative of proper, native molecular packing within the fibrils (Figure 3.3, A). By contrast, fibrils extracted from overloaded tendon displaying discrete plasticity damage, following a twisted path with the D-band interrupted at sites of sudden directional changes in the fibril axis (Figure 3.3, B). These sites were consistent with the kink structures previously observed under SEM.[12-14,153] The persistence of the D-banding between kinks suggests retention of ordered molecular packing in these regions (Figure 3.3, B, arrows).

Upon hydration in PBS, both control and damaged fibrils swelled significantly (Figure 3.3). In the hydrated state, D-banding was barely observable for the control fibrils (5-10 nm fluctuation) and not observable for the kinked collagen fibrils (Figure 3.3, C and D). This observation suggests that the gap and overlap regions of the D-band have distinct swelling ratios in PBS, resulting in a nearly constant cross-sectional area along the length of control fibrils. The heterogeneity in swelling does, however, permit observation of D-banding in the HRM maps of collagen fibrils.[210,212] Indeed, in the present study, D-banding of control fibrils was observed in both deformation and Sneddon modulus images (Figure 3.4, A and C). Kinked fibrils, by contrast, often showed no D-banding in either deformation or Sneddon modulus images (Figure 3.4, B and D). Instead, we observed a highly penetrable shell layer enveloping the collagen fibril (Figure 3.4, B, arrow) and a new periodic HRM fluctuation occurring at the kink sites along the collagen fibril (Figure 3.4, D). An inverse relationship is expected between the deformation and HRM values of a collagen fibril. A highly deformed region should have a lower HRM and vice versa. This relationship broke down in the kinked regions of damaged collagen fibrils (Figure 3.4, B and D, rectangles) where a decrease in HRM was observed in the kinked region —without an increase in deformation. This observation is an artifact, due to the indeterminant nature of the point of contact between AFM tip and collagen fibril associated with soft samples, and the method in which the deformation is measured on force curves.

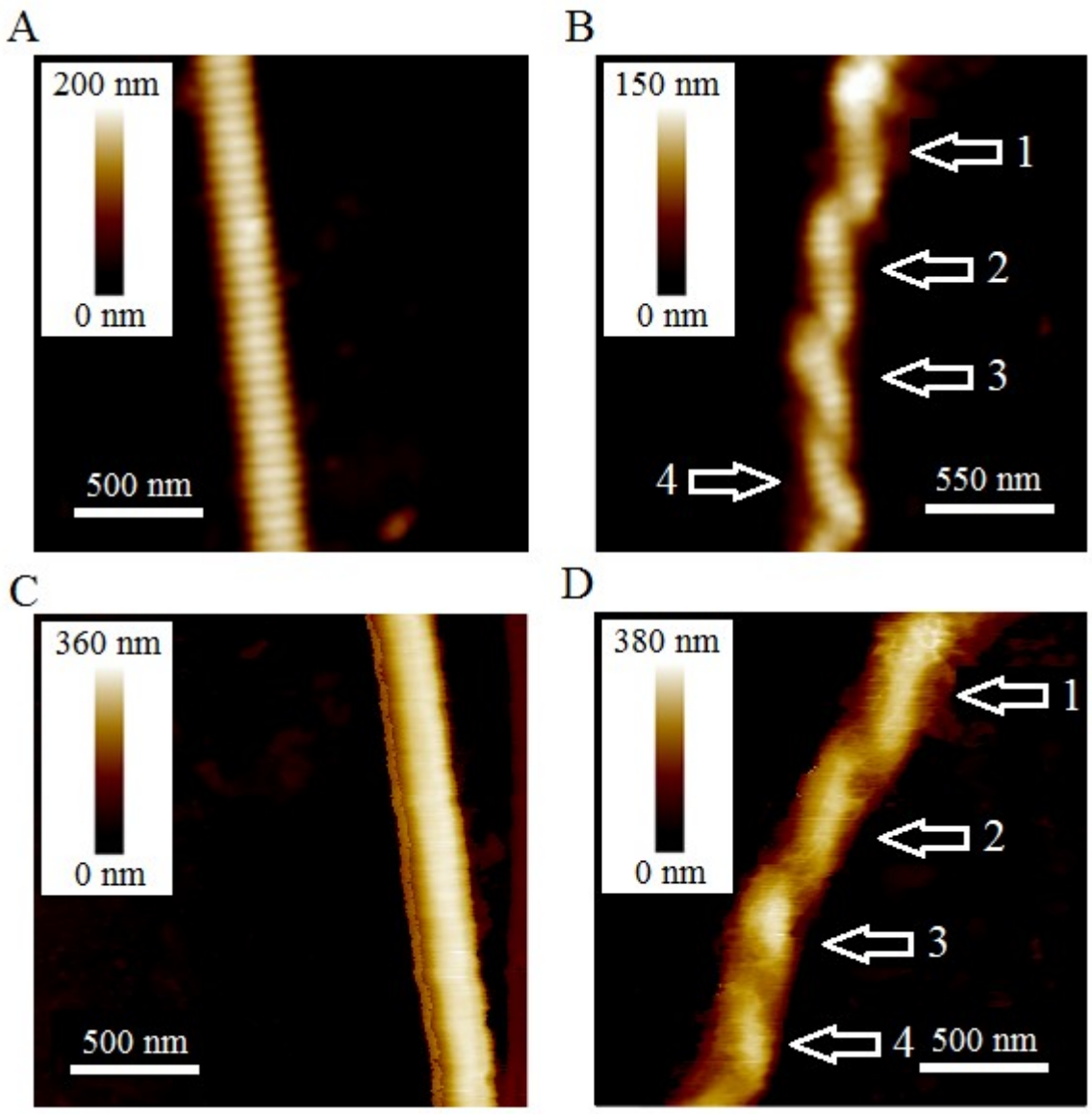

Figure 3.3: Height Images of a native control (A, C) and a kinked damaged (B-D) collagen fibril in the dehydrated (A, B) or hydrated (C, D) state. The arrows in B and D indicate the same sections of the kinked collagen fibril in both images.

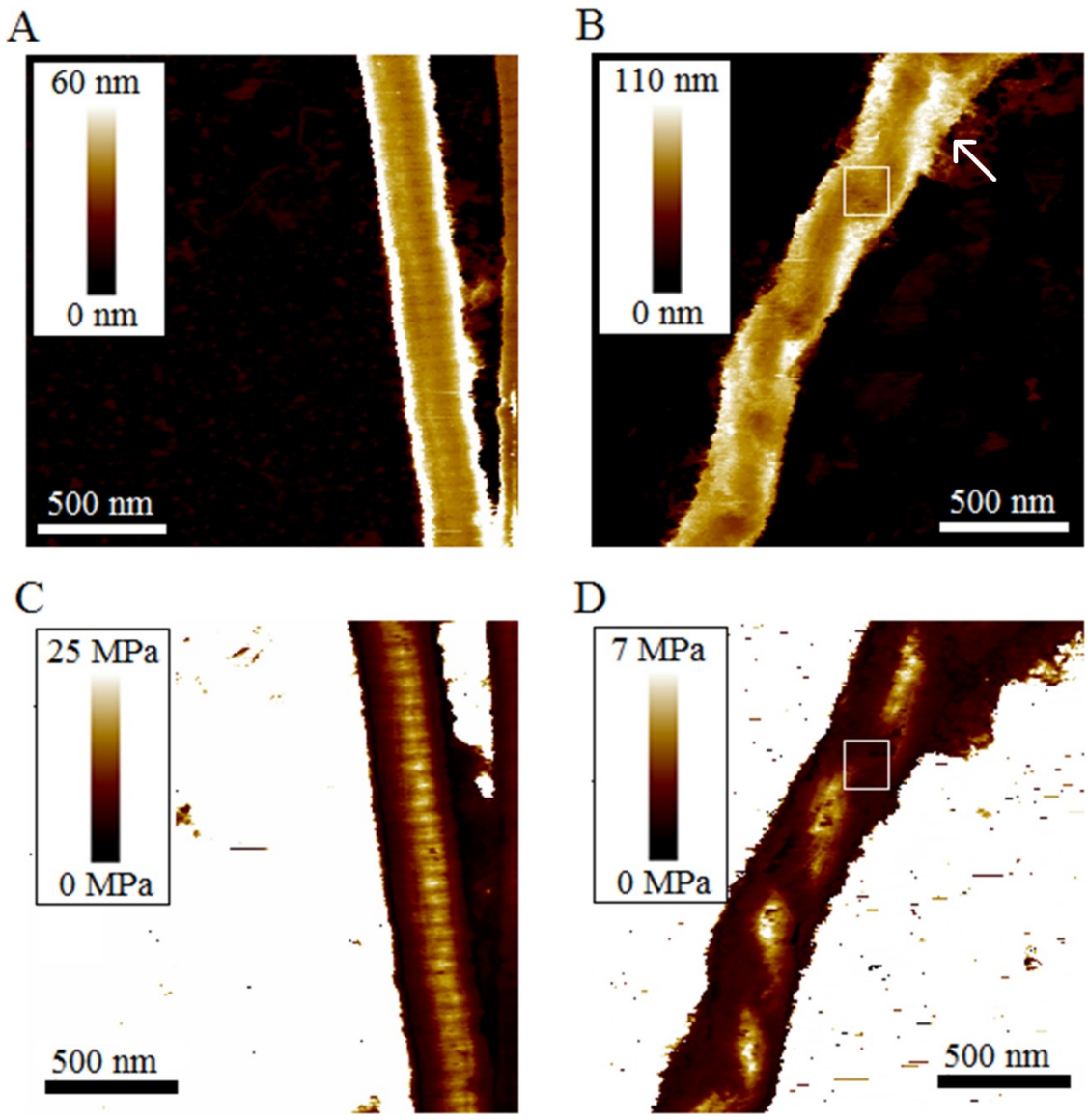

Figure 3.4: Deformation (A, B) and Sneddon modulus (HRM) (C, D) maps of a hydrated native control (A, C) and a kinked damaged (B-D) collagen fibril. The arrow in B points to the highly penetrable shell that surrounds the kinked core of the collagen fibril. The boxes in B and D highlight the discrepancy between the deformation and Sneddon modulus (HRM) of the kink locations. This artifact is due to the manner in which the deformation is calculated.

Comparison of Sneddon modulus (HRM) images from control, kinked, and very kinked collagen fibrils demonstrated the progression of damage as serial kink density increased along collagen fibrils (Figure 3.5). No correlation between tendon source and a region of the kink density range was observed, demonstrating no dependence on kink density and the macroscale loading of the tendons. Again, not all kinked collagen fibrils displayed a complete lack of D-banding when visualized via HRM (Figure 3.5, B and E). Plotting the HRM, coefficient of variation of the HRM, and the swelling ratio of the collagen fibrils against serial kink density revealed an increase in swelling ratio and decrease in HRM with increasing kink density (Figure 3.6, A, C and E). This is consistent with the notion that a decrease in HRM is due to a decrease in molecular density. Comparison of the mean properties from the three fibril groups showed significant, systematic differences between the control, kinked, and very kinked collagen fibrils
(Figure 3.6, B, D and F, Table 3.1). Mean HRM and HRM heterogeneity (coefficient of variation) were distinct between each of the three groups, while the swelling ratio increased significantly between the control and very kinked fibrils (Figure 3.6, B and F). It is striking that the heterogeneity in the HRM changed so greatly with damage: the coefficient of variation of HRM in control fibrils is more than doubled in both kinked and very kinked groups, largely independent of kink density (Figure 3.6, C and Table 3.1).

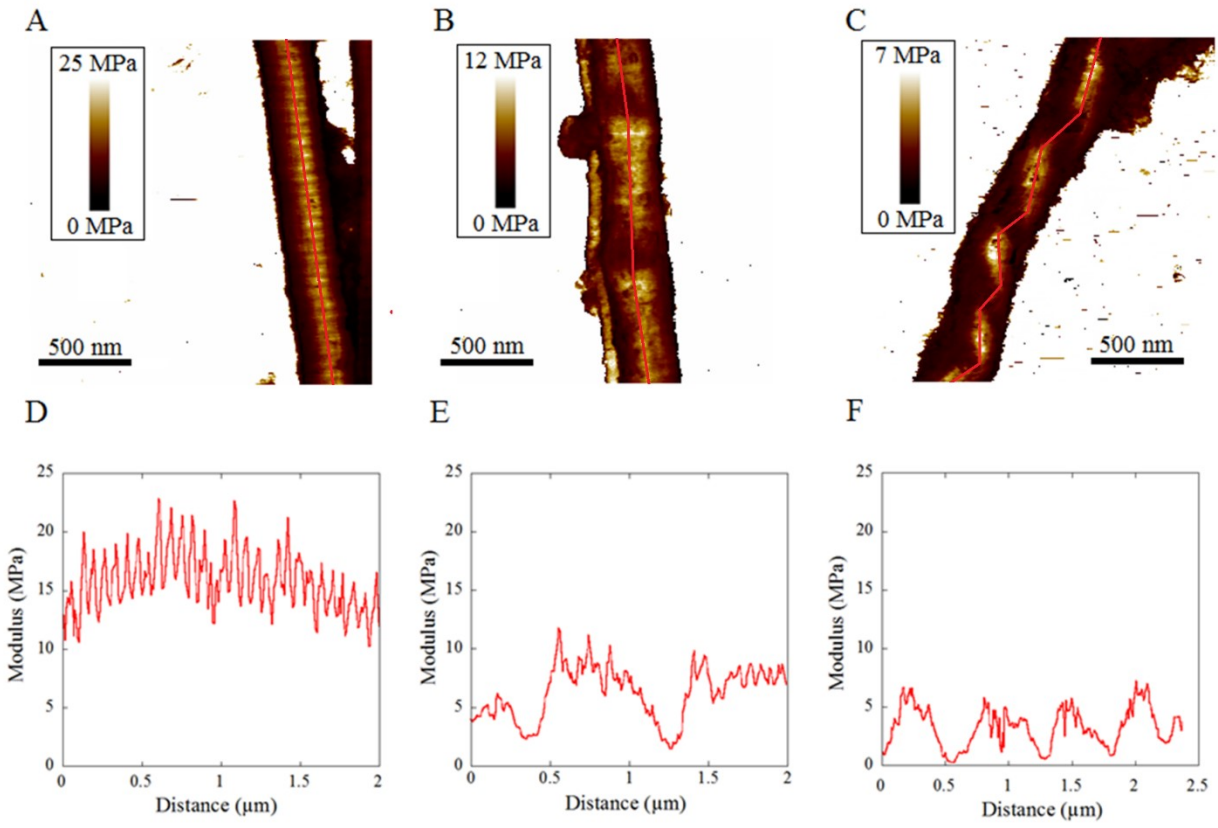

Figure 3.5: Sneddon modulus maps (HRM) (A-C), and Sneddon modulus (HRM) cross-sections (D-F), of control (A, D), kinked (B, E) and very kinked (C, F) collagen fibrils. Kinked collagen fibrils have a kink density less than 1.5 kinks/μm while very kinked collagen fibrils have a kink density greater than 1.5 kinks/μm. HRM cross-sections (D-F) were extracted along the apex of each collagen fibril in (A-C) respectively along the red lines. As shown in the legend for A-C, HRM values strongly decreased with increasing kink density.

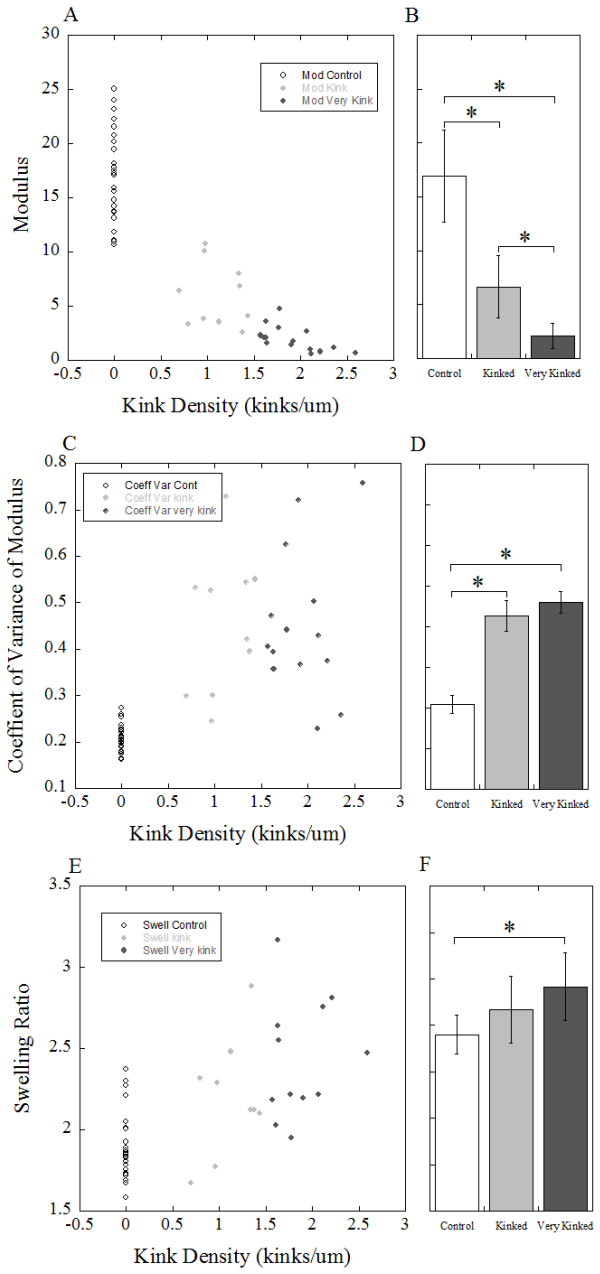

Figure 3.6: The Sneddon modulus (HRM)(A), coefficient of variance of the Sneddon modulus (HRM) (C), and swelling ratio (E) of all collagen fibrils examined are plotted as a function of serial kink density in kinks/µm. The means and standard deviations (error bars) for each parameter are reported for control (n = 25), kinked (n = 10), and very kinked (n = 15) fibril groups respectively in B, D, and F.

Table 3.1: Mean Sneddon modulus (HRM), coefficient of variation of the modulus (HRM), and the swelling ratio for the control, kinked, and very kinked collagen fibril groups. Mean ± standard deviation.

Kink Density	Sneddon Modulus (MPa)	Coefficient of Variation for Modulus	Swelling Ratio
Control	17.3 ± 3.9	0.20 ± 0.02	1.9 ± 0.2
Kinked	6.6 ± 2.1*	0.43 ± 0.04*	2.2 ± 0.4
Very Kinked	2.1 ± 1.2*†	0.46 ± 0.03*	2.4 ± 0.4*

*Difference with value for control fibrils is significant with $p<0.05$, Bonferroni-corrected.
†Difference with value for kinked group is significant with $p<0.05$, Bonferroni-corrected.

3.5 Discussion

Our previous work has addressed two basic questions. First, what does it mean for collagen to be mechanically damaged in an overload event? Second are there identifiable structural motifs, at some characteristic scale, which are associated with damage? These are questions which are important for our understanding of evolutionary "design" in collagen and for biomedical identification and treatment of soft tissue injuries. Examining overload-damaged bovine tail tendons with SEM, we have identified a characteristic, nano-scaled motif for damage in the fundamental collagen fibril: local kinks which increased in serial density under increasing cycles of plastic overloading.[12,13] As well, treatment with the acetyl trypsin, a serine protease, demonstrated that molecular collagen was denatured during this process, gradually obscuring D-banding in SEM images and occurring most intensely at the kink sites.[12-14] Mechanical evidence suggests that these kinks may be part of a structural mechanism which absorbs overload energy via sacrificial destruction of certain subfibrils, toughening collagen at a very basic level. Due to the very local nature of the kink formation, we have termed this damage mechanism "discrete plasticity". Culture of decellularized native and damaged tendons with immortal macrophage-like U937 cells has given the first evidence that inflammatory cells may be able to recognize and respond to discrete plasticity damage.[153]

We recognized that the kink morphology observed by SEM only provides surface characterization of the collagen fibrils following significant alteration due to dehydration and metal sputtering. In the present study, we have sought to remove this barrier and to look at native and damaged fibrils in an unfixed, hydrated state. By comparing features in dehydrated and hydrated specimens, we directly examine the importance of water

solvation in our imaging. Further, by carrying out nano-scaled mechanical examination of fibrils, we are able to probe the interior of damaged fibrils via indentation. In short, AFM offered the opportunity to determine whether the kink morphology of discrete plasticity damage was artifactual to any significant degree, and to greatly expand our structural understanding of accumulating mechanical damage at the fibril level in collagen.

3.5.1 Hydration reveals structural features associated with discrete plasticity

Comparing the dehydrated ZFH, hydrated ZFH, HRM, and deformation of kinked and control collagen fibrils revealed alteration of molecular packing due to tendon overload. Newly-validated structures include a low-density shell which encompassed a higher-density core in the damaged collagen fibril. SEM images after acetyl trypsin digestion suggest that this layer is composed of denatured collagen.[12-14] Along the core of the fibril, the periodic kink structures of discrete plasticity have been confirmed, as have the relatively undamaged inter-kink regions spanning consecutive kinks (Figure 3.4). The kink structures are mechanically characterized by a sharp decrease in HRM compared to the inter-kink regions and an increase in deformation by the tip (Figure 3.4). The alteration in mechanical response of the shell and kink sites is most likely due to uptake of water associated with the loss of native molecular packing and local denaturation of triple-helical collagen. This is supported by the preferential enzymatic digestion of material from the shell and kink structures by trypsin, as well as the decrease in thermal stability of the overloaded tendon.[12,14]

The dramatic increase in the coefficient of variation of the HRM between the control fibrils and discrete plasticity-kinked fibrils (Figure 3.6D) suggests that the kink/inter-kink HRM difference is conserved, independent of kink density—that is, a kink is a local structure which has limited influence on the mechanical behavior of neighboring regions in the fibril. This finding contrasts with the decrease in the mean HRM of damaged fibrils as kink density increases (Figure 3.6A). Fitting the mean HRM versus kink density data with a linear ($r^2 = 0.042$) and an exponential fit ($r^2 = 0.62$), both with p values <0.05, demonstrates the mean HRM is not solely due to an accumulation of discrete kink structures. It follows that, while the kink/inter-kink heterogeneity was captured by the coefficient of variation, the fall in mean HRM with increasing kink density is associated with both the formation of the shell structure and accumulation of kink sites. (Figure 3.7).

The D-banding seen in the HRM maps of control bovine tail collagen fibrils is similar to that seen in rat tail collagen fibrils.[210] Increasing levels of damage in various tendon overload fibrils were associated with an increase in kink density, decreasing mean HRM, and disappearance of the D-banding in Sneddon modulus images (Figure 3.8). The loss of D-banding is tied to increasing thickness of the fibril shell which parallels increasing serial kink density. The swelling ratio in our experiments also increased with greater kink density (Figure 3.6, E). When the sample was dehydrated, though, this shell layer collapsed and the D-band could be seen in the topography of the inter-kinked regions of the kinked collagen fibrils (Figure 3.3, B and D). This suggests that the shell structure consists of a gel-like layer of denatured collagen molecules, highly solvated in water. This denatured collagen is likely not solubilized due to the presence of crosslinking between neighboring alpha chains.[63,214] The similarity in the mean dehydrated ZFH's

of control and kink collagen fibrils suggests that no significant molecular content is lost during kink formation, suggesting retention of the entire shell layer (Appendix B Figure 1).

The higher-density core inside discrete plasticity-damaged fibrils was primarily observed in the deformation maps rather than in the HRM maps. This is due to the difference in depth sensitivity of the two measurements. HRM maps were calculated by fitting the force curves to a maximum depth of 10% of the fibrils ZFH (~40 nm indentation), while the deformation maps are calculated from the maximum indentation depth of the AFM tip into the collagen fibril (~100 nm). Therefore, the deformation maps have increased sensitivity to features buried deep within the core of the fibrils: e.g. the appearance of D-banding in some inter-kink regions of very kinked collagen fibrils (Figure 3.9). The inconsistency of D-band observation in the inter-kink regions may be due to regional variation in the fibril shell thickness.

3.5.2 Laid rope damage motif model of collagen fibrils

It is clear that discrete plasticity damage results from tendon overload, and that the intensity of the associated structural changes increases with repeated loading into the plastic region of the tendon stress-strain curve. Nonetheless, the kinks which we have now observed in dehydrated and hydrated specimens, under both SEM and AFM, are rebound structures which result after unloading of damaged fibrils. We know little about the mechanism via which the local damage occurs and how the kinks form.

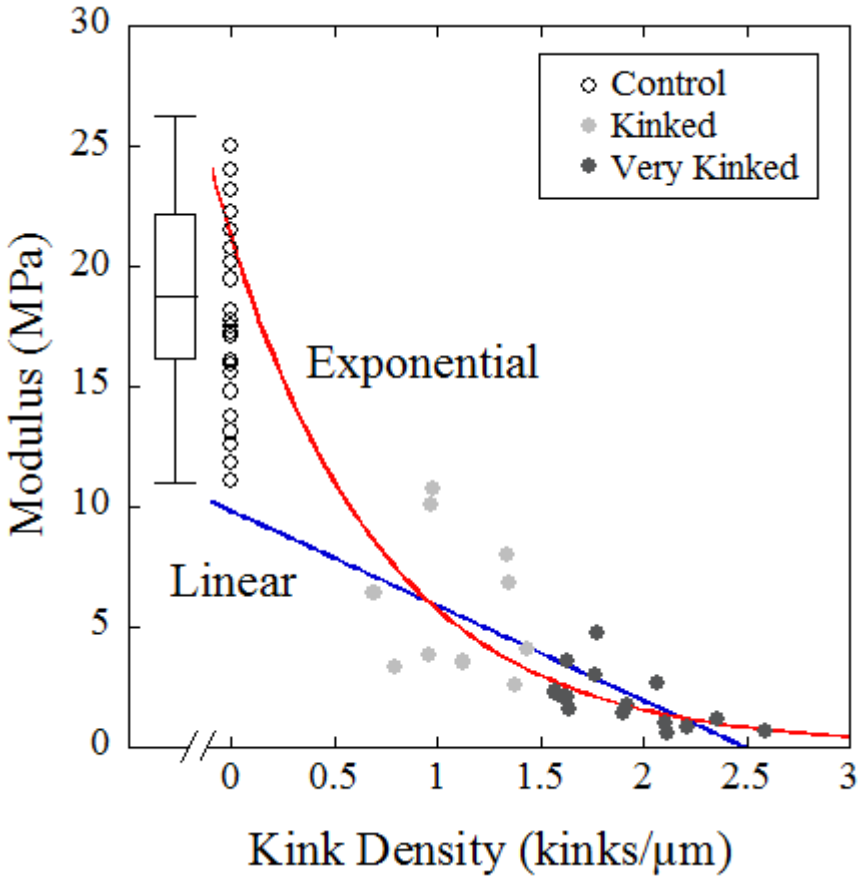

Figure 3.7: The Sneddon modulus (HRM) of all fibrils is plotted as a function of kink density in kinks/µm and fitted with a linear (r^2 = 0.42, *y*-intercept ~10 MPa) and an exponential fit (r^2 = 0.62, *y*-intercept ~ 20 MPa). A box whisker plot displays the distribution of the native fibril group. The exponential fit predicts the HRM of the native, undamaged control fibrils by falling within the range of the box whisker plot. This is the same data as that of Figure 3.6A.

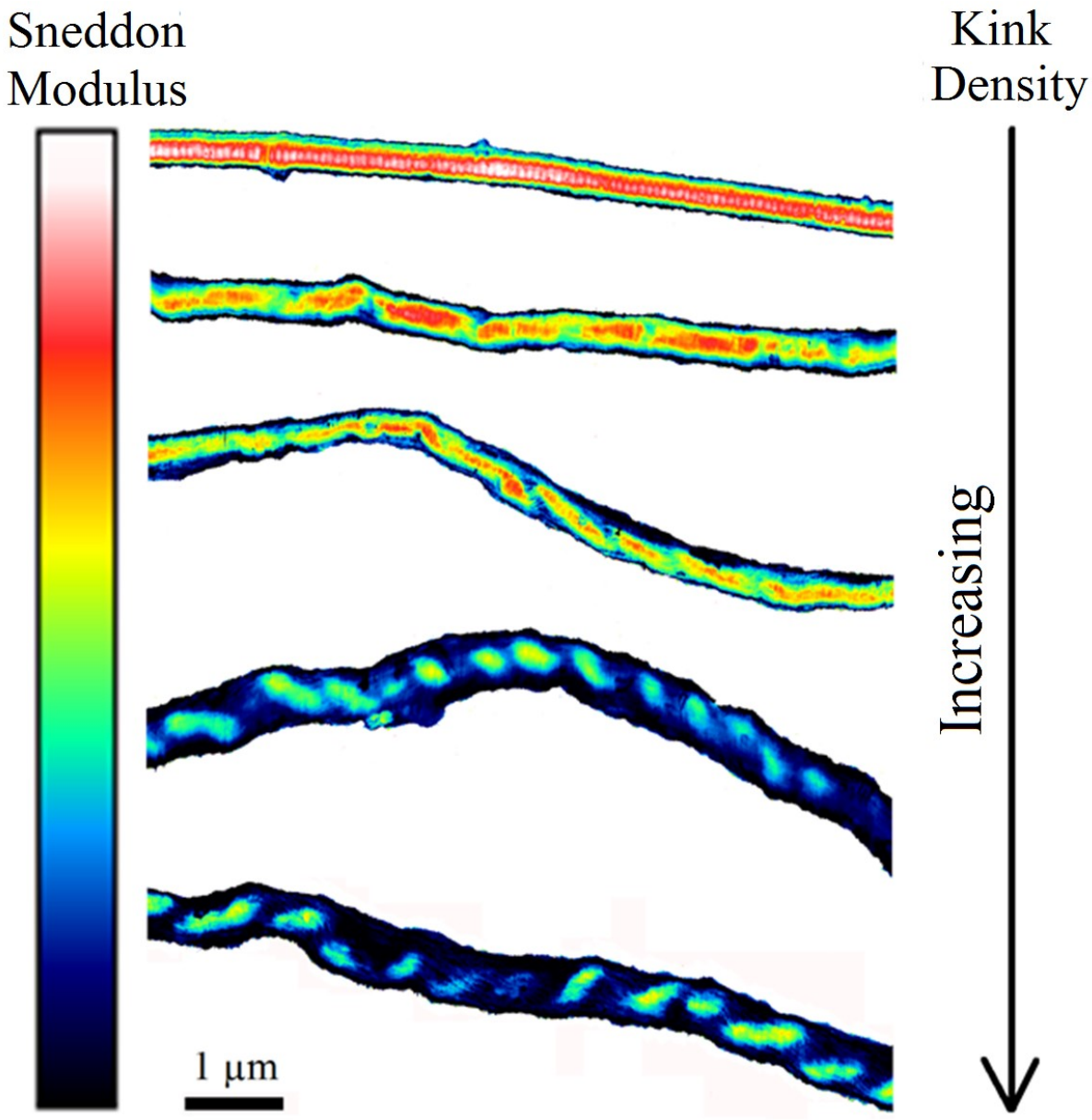

Figure 3.8: Sneddon modulus (HRM) images displayed as the $\log_{10}$ of the HRM value. The five fibrils displayed had increasing levels of damage (top-to-bottom). As serial kink density increased, molecular density decreased with a resulting decrease in typical Sneddon values. There was also an increase in the heterogeneity of the local molecular density and loss of the D-banding structure as displayed in the HRM. HRM Scale Bar: 0-

14 MPa.

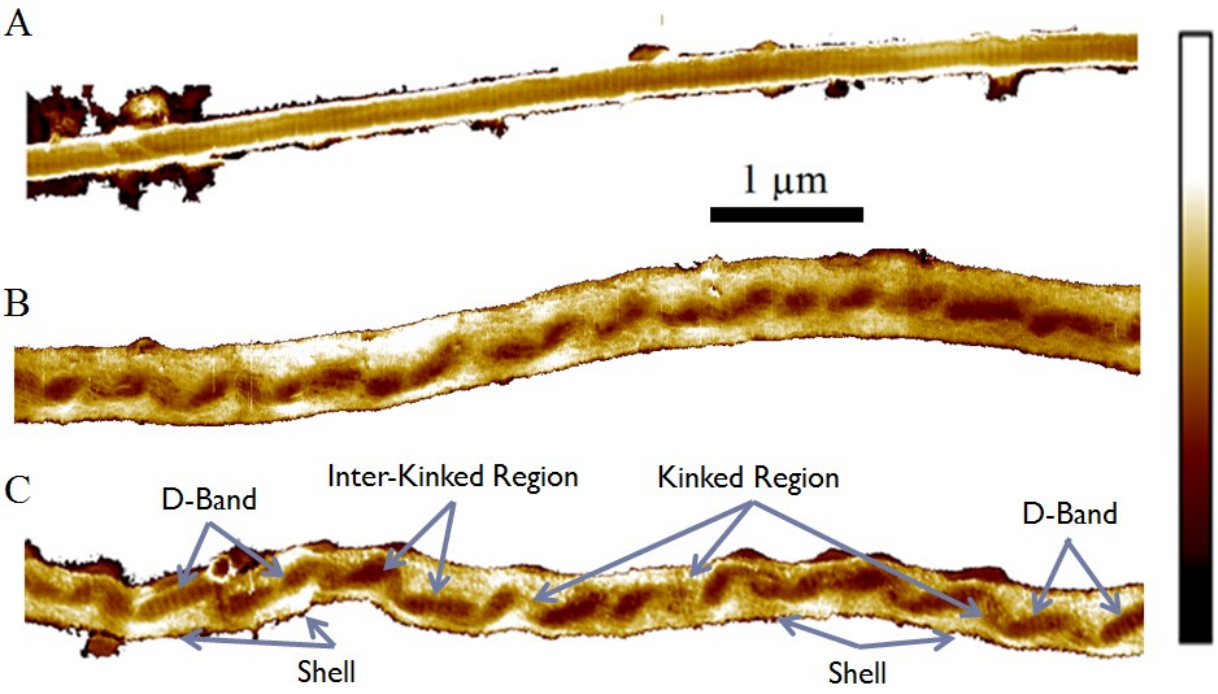

Figure 3.9: Deformation maps of a native collagen fibril (A) and two very kinked collagen fibrils (B, C) are shown. In (C) the deformable shell, D-Banding, inter-kinked regions, and kinked regions are clearly observable at various locations along this 5-times-overloaded fibril. Deformation Scale Bare: A) 0-40 nm, B-C) 0-120 nm.

A collagen fibril consists of helically wound subfibrils and microfibrils composed primarily of crosslinked, triple-helical molecules.[28,34,207,208] The crosslinking of the collagen molecules and the twisted nature of the collagen fibrils sub-components suggest that an apt macroscopic, structural analog of the collagen fibril might be that of a polymerized laid rope strand.[41] While not in the context of understanding damage, models of this sort have been previously proposed. Some investigators have suggested that collagen fibrils are nanoscale ropes, while others have suggested a tube-like organization or a liquid crystalline model for the fibrils structure.[36,38,215] If we consider the collagen fibril as a laid rope strand within a larger rope, it is intriguing to consider whether the shell and kink structures observed in discrete plasticity samples might resemble damage motifs found in laid ropes, associated with internal abrasion and axial compression fatigue.[41,210]

The radial variation of the shell-core structures of kinked, damaged fibrils, coupled with the increases in both swelling coefficient and shell thickness with kink density, offers the possibility that the shell layer may be the result of forces acting directly on the surface of the collagen fibril. There is support in the literature to suggest that shear stress plays a strong role in the behavior of tendons under tension.[216-218] Indeed, inter-fibril shear stress has recently been calculated as being 32kPa.[219] In overload, if shear stress were applied to a particular collagen fibril, we would expect that any shear-induced damage might propagate inwards from the affected surface, Molecular alteration due to interfibrillar shear, would then explain the formation of the denatured shell layer of the damaged collagen fibril. One possible mechanism for such denaturation in the shell might

be inter-strand delamination; a phenomenon wherein α-chains participating in a crosslink are pulled out of their respective collagen molecules, thereby leading to a permanent, stable, denaturation.[14,125,126,220,221] In shear loading of the fibril, such delamination would propagate radially inwards from the surface toward the core of the fibril. This mechanism is similar to internal abrasion within a rope strand, characterized by a low density shell and loss of substructure at the rope surface—features seen in the shell of discrete plasticity damaged collagen fibrils.[41] In considering such a possibility, we must also consider an alternative hypothesis: that there is a pre-existing radial heterogeneity in the fibril structure which preferentially pre-disposes the outermost molecular layers of the fibril to damage: perhaps sacrificial damage which absorbs energy prior to fibril fracture, toughening the fibril. Such a heterogeneity has been proposed in the tube-like model of a collagen fibril.[36] It is not possible at present to differentiate which of these mechanisms may be at play—if not both.

The kink structures observed in association with discrete plasticity are thought to be caused by structural damage which occurred during the overloading of the tendon, but actually formed upon removal of load. Observation of the kink structures, now with both SEM and AFM, confirms their similarity to kink structures seen in laid ropes when their lower hierarchical components experience compression.[12-14,41,153] One experimental difficulty which emerges when intact tendons are mechanically mounted and overloaded is that the resulting damage is heterogeneous: that is, only sub-populations of the collagen fibrils within the tendon display discrete plasticity damage. Some regions appear to have been spared overload and remain entirely intact.[12] Such heterogeneous damage could lead to regions which experience some degree of compression upon removal of external

load, perhaps resulting in kink formation. Should this be the case—and morphological similarity between engineered rope and collagen fibril structure certainly doesn't confirm this mechanism—we might ask whether compressive damage would occur during physiological overloading of a muscle-tendon-bone complex, or whether it is peculiar to a testing machine sample mounted in grips.

One damage motif found in laid ropes, termed axial compression fatigue, is characterized by periodic Z-shaped kink structures along the longitudinal axis of lower hierarchical structures. These structures in some ways resemble the kink structures observed in discrete plasticity. Formation of rope kinks in axial compression fatigue have been shown to be the result of twisting of the hierarchal structures under tension, and a mismatch in component lengths and mechanical properties. Their locations are thought to be determined by regions of low torsional resistance or the non-uniform loading of rope components.[41] We have previously shown micron-scale variation in a collagen fibril's density along its length. This observation suggests weak points may exist along the fibril.[210] Furthermore, there is heterogeneity in fibril diameter in tendon, which may imply accompanying heterogeneity in fibril mechanical properties correlated with diameter.[222] It may be the case that some fibrils or fibril regions are particularly susceptible to the effects of local stress concentration, whether via torsion or other modes. Whether the morphological similarities between laid rope failure motifs and discrete plasticity in tendon collagen fibrils are more than intriguing coincidences remains the subject for further study.

3.6 Conclusions

In this work, we have used AFM in a hydrated environment to quantify the effects of tendon overload on the structure of individual collagen fibrils. We have confirmed the morphology observed under SEM, but have now demonstrated the dependence of water uptake and mean HRM on serial kink density. Further, we have shown that kink and inter-kink regions maintain a constant HRM ratio, independent of kink density, suggesting a truly local mechanism for kink formation. Our data supports the conclusion that the shell and kink structures are associated with molecular denaturation. We have also described a set of interesting resemblances between failures in engineered laid ropes and discrete plasticity kinking seen in tendon collagen. It may follow that discrete plasticity kink formation is an effect of fibril sub-structure and longitudinal, structural heterogeneities which play out under the sort of uneven loading which occurs during *in vitro* testing of tendon samples. It remains to be demonstrated if this is also the case during physiological overloads in high-load bearing tendons as in, for instance, strain injuries. Discrete plasticity in tendon collagen is an important and complex phenomenon, and atomic force microscopy is a particularly valuable tool for its examination.

Acknowledgements

This work was supported by grants to LK and JML from the National Sciences and Engineering Research Council of Canada (NSERC). SJB received salary support from the ASPIRE CREATE program of NSERC. The authors would like to express their thanks to Jasmin Astle for valuable assistance with tissue decellularization and to Dr. Sam Veres for assistance with the mechanical overload protocol. Gratitude is also expressed to Oulton's Meats, Windsor, Nova Scotia for assistance in harvesting tendon samples.

Chapter 4: A new longitudinal variation in the structure of collagen fibrils and its relationship to locations of mechanical damage susceptibility

This chapter has been reproduced from the article “A new longitudinal variation in the structure of collagen fibrils and its relationship to locations of mechanical damage susceptibility” submitted to the Journal of Integrative Biology (Appendix F). The authors of the article are as follows “Baldwin, S.J., Sampson, J., Peacock, C., Martin, M.J., Veres, S.P., Lee, J.M. and Kreplak, L.”. As First Author I was responsible for experimental design, data acquisition, majority of the data analysis of the AFM work, and producing the first draft of the document and participated in the subsequent edits.

4.1 Motivation and Hypotheses

The study presented in this chapter is the result of post hoc analysis of data on unloaded collagen fibrils, sourced from Chapter 3, and scanning electron microscopy images of tendon fibrils displaying discrete plasticity fibrils, acquired by colleagues. Two major questions were to be asked by revisiting these data sets: 1) Were the micron-scale variations observed in Chapter 2 consistent within a fibril population? 2) Could those micron-scale fluctuations in a fibril's HRM locally predispose the fibril to the discrete kink formation associated with discrete plasticity? In this chapter the first question will be answered using a modified analysis of HRM variation as described in Chapter 2, while the second question will be addressed by comparing the length scales of the variation of unloaded collagen fibrils with the kink spacing observed along fibrils displaying discrete plasticity.

Hypothesis 4.1: Native collagen fibrils will display variations in HRM within a 10μm segment of their length which is described by a distinctive distribution.

Hypothesis 4.2: The distribution of kink spacing along fibrils displaying discrete plasticity will resemble the distribution of fluctuations observed in the HRM of unloaded collagen fibrils.

4.2 Introduction

Collagen fibrils are the rope-like supermolecular protein structures which are largely responsible for the tensile strength of tendon and many other connective tissues. The impact of collagen on mechanical properties varies based upon its hierarchical assembly, type, crosslinking, and associated molecules.[17,63,223-225] Due to the pervasive nature of collagen throughout the body and its critical mechanical function, much research has been conducted into the variation of collagen fibrils with respect to anatomical location, loading history, mechanical damage, age, disease and genetic variations of the collagen molecule.[12,39,210,211,226-230]

A common feature of all collagen fibrils is a hierarchical structure consisting of 3 sublevels; the collagen molecule, microfibril and subfibril. These hierarchical components are held together and organized by intermolecular bonding and covalent crosslinks between individual molecules.[21,28,37] A characteristic feature associated with an organized collagen fibril is a periodic molecular density fluctuation termed the D-band which is observed along a fibril's length. This is a result of the non-integer staggering of the individual molecules within the fibril sub-components that persist throughout the hierarchical assembly.[5,32,29,40,231] Each period of the D-band consists of gap and overlap regions where the gap has four-fifths of the molecules compared to the overlap region.[5,231] The periodicity of the D-band has been shown to vary between tissues. In the case of tendon, it has been reported as ~67 nm.[28,37,232,233] Aside from the longitudinally-repeating D-band, collagen fibrils have been taken to be structurally homogenous along their length.

Interestingly, however, assessment of collagen fibrils after tensile overload has shown the development of discrete, repeating sites of plastic deformation, longitudinally separated by hundreds of nanometers: a damage motif termed “discrete plasticity”.[12]

Discrete plasticity is characterized by localized kink structures that form along the length of collagen fibrils in response to mechanical overload.[32] First identified in bovine tail tendon collagen, the phenomenology of discrete plasticity is well-established; however, the mechanism by which each kink forms at a particular location remains uncertain. It is possible that collagen fibrils may possess pre-existing structural variations, not previously identified, which render them locally susceptible to formation of discrete plasticity kinking.[12,210]

Recently, an atomic force microscopy (AFM) based, high resolution, high velocity, hydrated mechanical mapping technique has been applied to single collagen fibrils from tendons. Using this technique, structural variations were resolved that were associated with D-banding, cleaved fibril ends, sharp bends, hydrated temperature rise above 37°C, and the localized plasticity resulting from repetitive mechanical overload: discrete plasticity.[210,226] One structuro-mechanical feature noted in that work—but not attributed to any particular structural motif—was micro-scale variation in the hydrated radial modulus (HRM) along the lengths of unaltered (native) collagen fibrils.[210] Given the localized formation of kinks in overloaded collagen fibrils, we suspect that such pre-existing structural variation could provide an underlying mechanism for the discrete plasticity phenomenon occurring locally along fibrils.[12]

In the present work, we have explored this idea more fully, seeking to link local variation in collagen fibril structure with local susceptibility to plastic kink formation when that fibril is overloaded. To this end, we have expanded the limited sample size of our previous study to demonstrate the prevalence of micro-scale variations among unloaded collagen fibrils. We have mechanically and topographically mapped fibrils from bovine tail tendons—both hydrated and dehydrated—over 10μm segments of their lengths. All fibrils imaged demonstrated micro-scale variation. We have then calculated the distribution of these variations along the fibril length, and compared that distribution with the distribution of discrete plasticity kinks observed in SEM samples from overloaded tail tendons. The two distributions take the same form. We propose from this data that the most likely source of the micro-scale variation in HRM is local differences in the number of collagen molecules per unit length and/or differences in crosslink density as previously observed at this scale by axial mass distribution and urea exposure respectively. We further propose that local structural variation along the length of the collagen fibril predetermines the sites of kink formation in mechanical overload failure via discrete plasticity.[39,227-230]

4.3 Materials and Methods

4.3.1 AFM

Sample source

Whole bovine tails sourced from 18–24-month-old steers were acquired immediately after slaughter for food at a local abattoir and stored for 2 hours at 4°C. Tendons from the dorsal region of each tail were removed and placed in phosphate-buffered saline solution

(PBS), pH 7.4, at 4°C for four hours prior to decellularization. In total, single tendons from five different individuals were used in this study. Tissue harvest was approved by the University Committee on Laboratory Animals at Dalhousie University.

Tendon decellularization

All tendons underwent decellularization, following the protocol established by Ariganello *et al*. (Appendix E). to preserve the tendons, reduce interference of other biomolecules, and sterilize the samples.[211] In brief, the decellularization process consisted of four distinct treatments; a 36 hour bath in a hypotonic lysing solution at 4°C, a 24 hour bath in a Triton X-100 solution at 4°C, a 3 hour sterile bath in a DNase/RNase solution at 37°C, and a 24 hour sterile bath in a Triton X-100 solution at room temperature. Fresh solutions were exchanged every 12 hours. After the final sterile bath in Triton X-100 solution, the samples were rinsed once in sterile PBS, twice in sterile PBS antifungal/antibiotic solution and twice in a sterile PBS antibiotic solution, with each step lasting 30 minutes at room temperature. A final, 48-hour bath in sterile PBS antibiotic solution at 4°C occurred before storage in fresh sterile PBS antibiotic solution at 4°C until use. Sterile, decellularized tendons were stored at 4° C for a maximum of 3 weeks before use.

Sample preparation

Decellularized tendon samples were removed from storage at 4°C and splayed using a glass rod and tweezers into a plastic dissection dish containing 1ml PBS. The splaying of the tendon resulted in the isolation of collagen fibrils from the bulk tendon. After sufficient dissection of fibrils via this method, the PBS/fibril solution was poured onto a glass-bottomed AFM sample dish and allowed to settle for 45 minutes to allow fibril

adsorption to the glass bottom of the dish. The AFM sample was then rinsed 3 times in deionized water and dried under nitrogen flow for 10 minutes. At this stage the AFM samples were ready for imaging.[210]

Imaging

A Bioscope Catalyst atomic force microscope (Bruker, USA) was used for all AFM imaging in this study. The AFM was mounted on an IX71 inverted microscope (Olympus, Japan), which provided optical targeting of individual fibrils. All the imaged fibrils were optically resolved by use of differential interference contrast (DIC) and a 100X, 1.3 NA, oil immersion objective. All the AFM cantilevers used in this study were ScanAsyst liquid+ cantilevers with a spring constant ~0.7 N/m, resonance frequency of ~150 KHz, tip radius of ~2nm, and a cone half-angle of ~18°. Each cantilever was calibrated prior to imaging by measuring a single force/indentation curve upon fused silica from which the deflection sensitivity of the cantilever was determined. Following this process, the thermal noise cantilever calibration method was employed to determine the spring constant of the cantilever.[194] All AFM imaging was performed using peak force quantitative nanomechanical mapping (PF-QNM), with an indentation velocity of 1.2 mm/s and a peak force of 10nN. Each image contained a 256x256 grid of force displacement curves allowing for high resolution mapping (8nm) of the collagen fibril's local mechanical properties.[210]

Data acquisition

Prior to AFM imaging, fibrils were optically targeted with the inverted microscope. Only fibrils displaying linear regions of a minimum length of 40µm were chosen. All AFM

imaging was performed upon the middle of the targeted linear region to avoid sharp bends or cleaved fibril ends (Appendix A, Figure 6). Five fibrils were sourced from each tendon for a total of 25 fibrils spread across five individual animals. Each fibril was sequentially imaged by AFM along 10μm of its length in both the dehydrated and rehydrated states. Dehydrated imaging had a spatial resolution of 20nm. Hydrated imaging was performed after 30 minutes of rehydration in PBS, pH 7.4, at room temperature, and with a spatial resolution of 8nm. Dehydrated imaging consisted of a single 10μm x 10μm image while hydrated imaging consisted of five 2μm x 2μm adjoining regions with each region having 200nm of overlap.

Data extraction

Data extraction from the AFM images was performed using the SPIP 6.3.3 software from Image Metrology (Denmark). All data were extracted from a 20nm wide strip along the top of the collagen fibril. Of interest in this study were the fibrils' dehydrated and hydrated heights, the deformation caused by the AFM tip, and the HRM. The deformation of a fibril at a given point was defined from the force/distance curve as the difference in vertical position between the AFM tip under maximum applied force and under 15% of the maximum applied force. Summing the deformation and height data resulted in the zero-force height (ZFH). The ZFH represents the vertical dimension (height) of the fibril in the absence of applied force by the AFM tip. It is a proxy for the fibril's diameter if it were to have a circular cross-section when adherent to the surface.[210] Using this data, the following characterizing parameters were calculated for each fibril: the period of the D-banding, the gap/overlap ratio of the HRM, the coefficient

of variation of the HRM, the dehydrated ZFH, the hydrated ZFH, and the hydrated/dehydrated ZFH ratio.

Data analysis

By averaging the ZFH measurements for a collagen fibril, a hydrated/dehydrated ZFH ratio was calculated for that fibril to quantify the fibril's ability to take up PBS. The HRM of each fibril was extracted from the force/indentation curves using the Sneddon model which describes the behavior of a conical indenter pushed into an infinite half space. Equation 3 describes this calculation:

$$F = \frac{2E}{\pi(1-\nu^2)}(\tan\alpha)(\delta^2) \quad (4)$$

where ν is the Poisson ratio taken to be 0.5, α is the indenter cone's half angle (18), δ is the depth of indentation into the sample (variable), F is the applied force by the tip (10nN), and E is the elastic modulus of the fibril.[164,195,196] The Poisson ratio was taken as 0.5, representing an isotropic incompressible material, as is standard in the literature.[173,210] The elastic modulus was calculated by fitting Equation 4 to the acquired force curves. The region of fit of the force curves was in accordance with Bueckle's rule which states that regions of fit should not exceed 10% of the overall ZFH of the sample (20-40nm) lest substrate effects begin to contribute to the measurement.[197,198] It was from these calculated HRM maps that the HRM values were extracted along the top 20nm of the collagen fibrils.

The coefficient of variation of the dehydrated ZFH, the hydrated ZFH, the hydrated/dehydrated ZFH ratio and the HRM of each fibril was calculated using Equation 5;

$$Coefficient\ of\ variation = \frac{Standard\ deviation\ of\ parameter}{mean\ of\ parameter} \quad (5)$$

While traditionally used as a statistical value, the coefficient of variation is applied here as a means of quantifying the measured variation of the parameters listed above along the length of individual collagen fibrils. In turn, the calculated coefficient of variation values can capture the ability of each technique to observe structuro-mechanical variability along a single fibril.

The acquired HRM data taken from each 2µm x 2µm image were used to determine the gap/overlap HRM ratio and for FFT analysis as first described in Baldwin et al.[210] The data from each image were treated separately, with the results being averaged together to provide a single, mean, value for each fibril. Moving averages spanning 9 data points (72 nm), corresponding to approximately one D-band, were performed on the raw, extracted data to provide an average local HRM which was nearly devoid of D-band-produced variability. Subtracting the moving averages from the raw data resulted in a plot of fluctuations around the base HRM corresponding to the D-banding. The amplitude of these fluctuations was given by the root mean square (RMS) of their values (Equation 6), where n is the number of HRM data points per fibril and x_i is a single HRM data point. Subtracting the RMS from the mean HRM gave the mean gap HRM value while adding the RMS to the mean HRM provided the mean overlap HRM value (Figure 4.1). Using these two values the gap/overlap HRM ratio was calculated (Equation 7).

$$RMS = \sqrt{\frac{1}{n} * (x_1^2 + x_2^2 + \cdots . + x_n^2)} \quad (6)$$

$$\frac{Gap}{Overlap} = \frac{Mean\ HRM - RMS}{Mean\ HRM + RMS} \quad (7)$$

The fluctuations were discrete fast Fourier transformed, and the signal amplitudes averaged over the images for each fibril. The resulting peak was taken to be the period of D-banding in the HRM.

In addition, we used the acquired 2μm x 2μm images to assemble HRM profiles over a distance of roughly 10 μm for 10 fibrils (2 fibrils per tendon). Moving averages spanning 9 data points (72 nm), corresponding to approximately one D-band, calculated along each of these profiles to qualitatively demonstrate the presence of micro-scale variations. The unadulterated profiles were discrete fast Fourier transformed to compute their autocorrelation function. The raw autocorrelation functions were smoothed using a moving average to remove the maxima associated with the D-band. The micro-scale spacing between successive maxima was obtained using a peak finding algorithm in MATLAB.

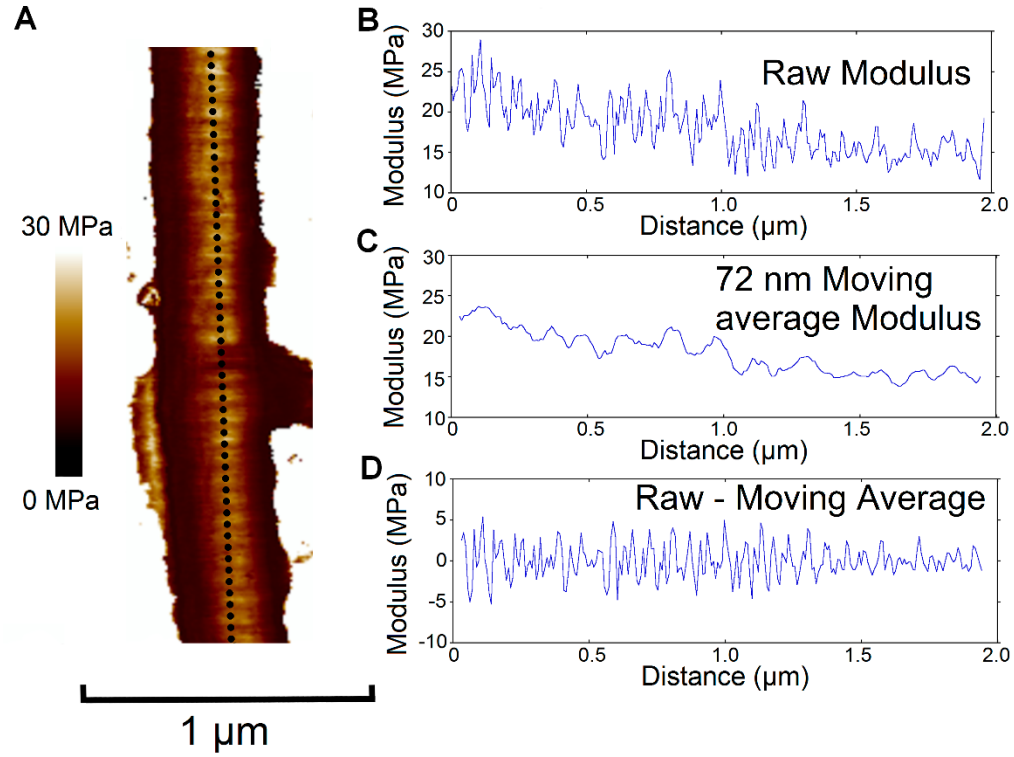

Figure 4.1: The Sneddon modulus (HRM) channel for an AFM image of a single collagen fibril (A). A cross-section along the apex of the fibril in this channel is extracted (B). A nine-pixel (72 nm) moving average is taken (C). Fluctuations in the Sneddon modulus (HRM) corresponding to the D-band are given by the difference between the raw extraction (B) and the moving average (C) to yield the data in (D).

AFM statistics

JMP software (version 11.0.0, SAS Institute Inc.) was used for all statistical analysis. A 1-way ANOVA was performed for the four coefficients of variation reported in Figure 2. Bonferroni-corrected post-hoc testing was carried out using Fisher's Least Significant Difference (LSD) test. All bar-graph data are presented as a mean with error bars representing the standard deviation. The Histogram of peak spacing obtained from the autocorrelation functions of the 10 AFM HRM profiles was analyzed with a Kolmogorov-Smirnov D-test for goodness of fit as per the SEM data.

4.3.2 SEM

Sample source and preparation

As per the AFM samples and under the same ethical approval, tail tendons were harvested from steers aged 24–36 months, slaughtered for food at a local abattoir. Tail tendons were extracted from the dorsal proximal region of each tail and stored at 4°C in Hanks solution with pen/strep antibiotics until use. Sub-samples of each tendon underwent one of two mechanical treatments: (i) simple pull-to-rupture or (ii) 5 cycles of overload into the plastic region of the load-deformation curve without rupture, as previously described.[120,234] Each overloaded sample (from both groups) was then fixed in 2.5% glutaraldehyde, bisected longitudinally so that the inner structure of the tendon was observable, and prepared for scanning electron microscopy as previously described. After examination at up to 100,000X magnification, images were captured of regions which showed significant kinking consistent with the discrete plasticity mechanism.[12,13]

Data acquisition

A total of 38 images at 25,000X magnification were selected from a much larger collection: 20 images came from samples which had been subject to pull-to-rupture, and 18 came from samples which had been subject to 5 cycles of overload without rupture. Criteria for selection of images included having many fibrils with multiple discrete plasticity kinks in them, fibrils lying in the plane of the picture (confirmed by correct spacing of visible D-banding), and the absence of obscuring cellular debris. In each image, 3 fibrils were selected which showed repeated, serial kinks extending across all or most of the image: a total of 114 fibrils. Three adjacent inter-kink segments were then assessed for each fibril, for a total of 342 segments.

Data analysis and statistics

For each inter-kink segment, three independent assessors used Image J software to capture the center of the two kinks forming the boundaries of that segment. The x and y coordinates for these kinks were captured and the inter-kink distances calculated. The population of measured inter-kink distances which occurred was plotted as a histogram and the distribution of data analyzed using JMP software (version 14, SAS Institute). A Kolmogorov-Smirnov D-test for goodness of fit test was performed to determine what distribution type that best-described the data. Analysis of confidence intervals from the best-fit distributions showed that the measurements by the three assessors were indistinguishable, so their measurements were averaged for each inter-kink segment distance value.

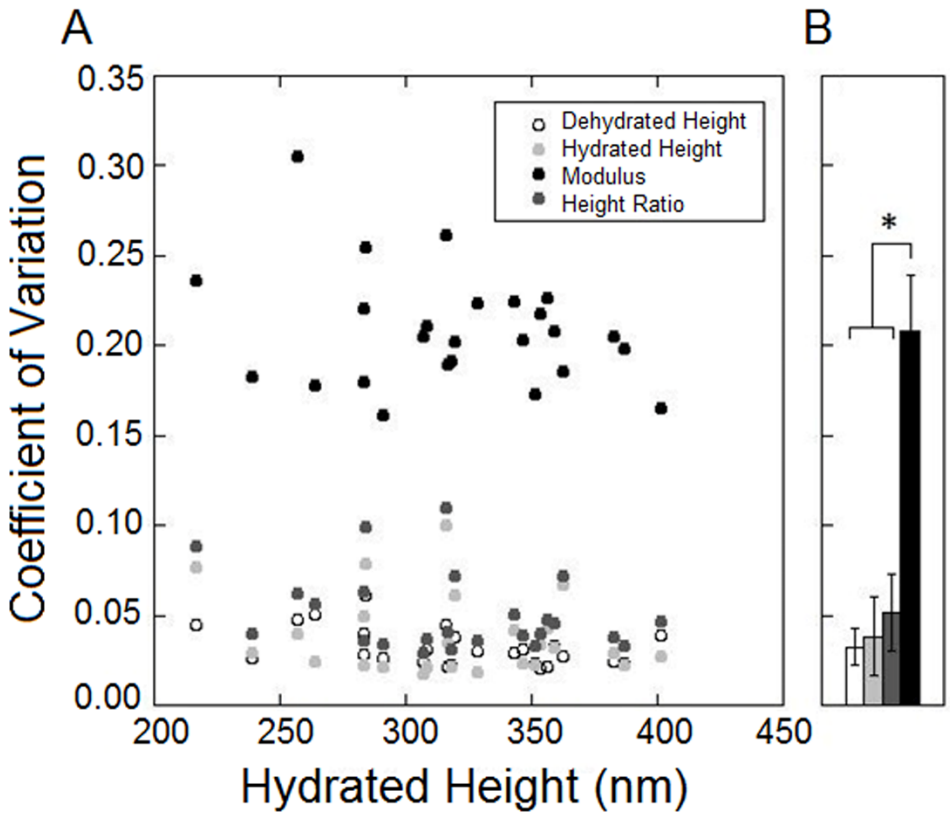

Figure 4.2: The coefficient of variation of the measured dehydrated ZFH, hydrated ZFH, hydrated/dehydrated ZFH ratio and HRM of all collagen fibrils in this study plotted as a function of hydrated ZFH, here a proxy for fibril size (A) and averaged across all fibrils measured (B). The variation seen in the HRM measurements was 4-8 times that observed in the other measurements, demonstrating greater sensitivity of that fibril stiffness to structural fluctuations in the fibrils.

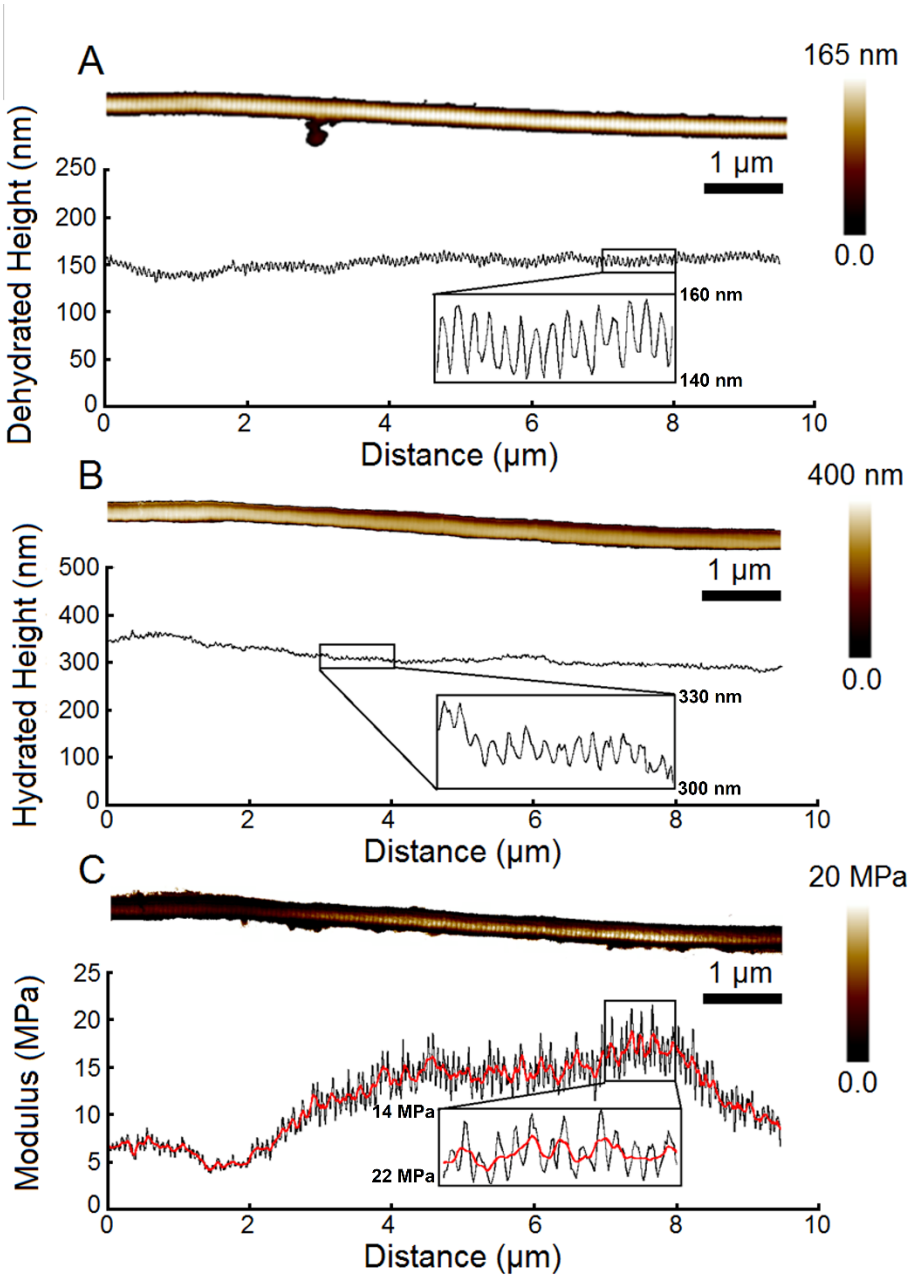

Figure 4.3: Dehydrated ZFH (A), hydrated ZFH (B), and HRM (C) maps shown with cross-sectional profiles of the same region of a collagen fibril. The degree of variation observed in the Sneddon modulus (HRM) channel (C) is not observed in either the dehydrated or hydrated ZFH of the fibril. The red line in (C) represents the 72nm moving average of the HRM, smoothing the D-band-related variation.

4.4 Results and discussion

4.4.1 HRM mapping and ZFH data

In the present study we were able to employ high velocity HRM mapping for detection of structural variations along single (undamaged) collagen fibrils. This technique made possible a 4-8 times increase in structural sensitivity compared to traditional methods of AFM measurement (Figure 4.2). Qualitatively, comparison of the maps of the dehydrated ZFH, hydrated ZFH, and HRM of an individual fibril (Figure 4.3) highlighted this sensitivity.

Of the three separate measures, the hydrated ZFH topographic map demonstrated minimal contrast between the gap and overlap regions of the D-banding (Figure 4.3B). This was due to the gap and overlap having distinct capacities for the absorption of water. The lower molecular density in the gap regions permitted greater water uptake than in the overlap regions, thus minimizing differences in measured hydrated ZFH between them.[210,212] The ratio of the gap to overlap moduli was in close quantitative agreement with the predicted molecular density variation of 0.8 between the two regions (Table 4.1 and Appendix C, Figure 1). This predictable variation in HRM across D-banded regions provided a firm basis upon which to assess superimposed micro-scale variation in structure-mechanical behavior. We used the coefficient of variation of sequential measurements along an individual fibril's length as a measure of spatial variation in properties along the fibril. The coefficient of variation for (i) dehydrated ZFH, (ii) hydrated ZFH, (iii) hydrated/dehydrated ZFH ratio, and (iv) HRM are plotted versus fibril size (Figure 4.2). It is clear from this data that there was much greater

variation in the HRM data along the length of individual fibrils than in the other parameters (Figure 4.2, B). Making use of the viscoelastic dependency of fibril HRM provided a more sensitive window into structural variation than could be captured by assessment of topography.

4.4.2 Micro-scale Variation: observation and function

Along the length of individual fibrils, two types of structural variations were observed, the D-band gap/overlap repeat and a micro-scale variation observed in hydrated nanomechanical mapping. The micro-scale variation (Figure 4.3, C, red profile) was not associated with the topography of the fibril. Plots of 10 moving average HRM profiles (2 fibrils per tendon) illustrates, qualitatively, the presence of non-D-band variations along the length of all the assessed collagen fibrils (Figure 4.4). The autocorrelation function of each raw profile (Figure 4.5, A) showed peaks spaced typically 0.5μm apart that were easily identified after filtering peaks associated with the D-banding (Figure 4.5B). The observed spacing followed an asymmetric distribution with a main peak at 0.5μm and a mean at 1μm (Figure 4.5, C). With all fibrils studied displaying similar structural variation, it is likely that the repeating locations of low HRM are functionally significant. One such function may involve the manner in which collagen fibrils respond to mechanical overload.

Table 4.1: Mean fibril properties of unloaded collagen fibrils.

Fibril properties	Mean Value ± Standard Deviation
Dehydrated ZFH (nm)	169 ± 6
Hydrated ZFH (nm)	320 ± 10
Hydrated/Dehydrated ZFH ratio	1.9 ± 0.2
HRM (MPa)	17.3 ± 3.9
D-period from HRM (nm)	67.5 ± 0.2
Gap/Overlap HRM Ratio	0.813 ± 0.009
Coefficients of Variation	**Mean Value ± Standard Deviation**
Dehydrated ZFH	0.032 ± 0.002
Hydrated ZFH	0.038 ± 0.005
Hydrated/Dehydrated ZFH ratio	0.050 ± 0.004
HRM	0.209 ± 0.005

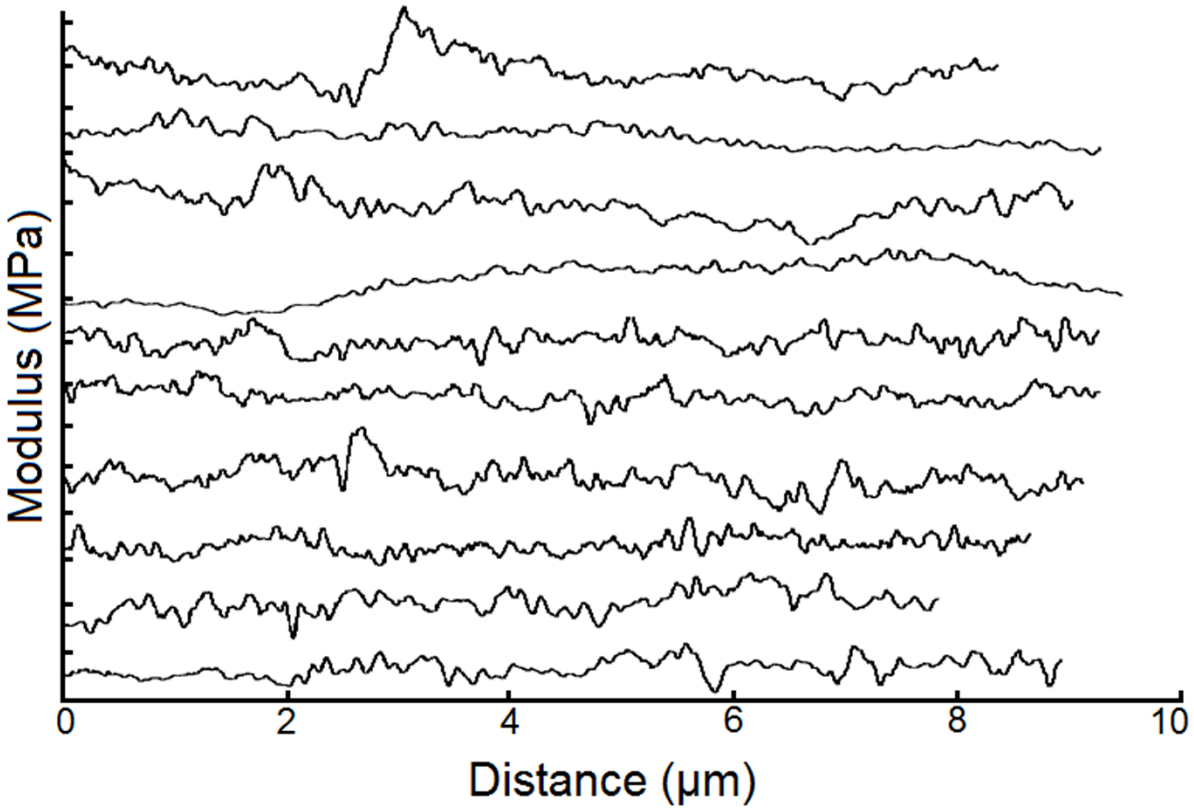

Figure 4.4: A sample of 72nm (9-pixel) moving average HRM profiles of 10 collagen fibrils (2 per tendon). The non-D-band fluctuations in the fibrils' HRM occurred in all the profiles and showed no observable periodicity. Modulus ticks on the y-axis are spaced 10 MPa apart.

When overloaded in tension, the collagen fibrils of bovine tail tendon develop discrete kinks that repeat along a fibril's length. Using scanning electron micrographs from overloaded bovine tail tendons, we measured the distances between successive kinks on individual fibrils. The resulting histograms showed that for the damaged fibrils from both ruptured and cyclically overloaded tendon, inter-kink spacing followed a log-normal distribution (Figure 4.6, B and C): strikingly similar to the distribution of HRM variation found within undamaged fibrils (Figure 4.6, A). Kolmogorov-Smirnov goodness of fit tests for all three log-normal distributions were significant, with D-values greater than 0.15. For the unloaded fibrils the scale parameter μ was 6.65 and the shape parameter σ was 0.66. For the pull-to-rupture samples and the 5-cycle overload samples the μ and σ values were (6.35, 0.44) and (6.02 ,0.50) demonstrating a progressive decrease in μ with an increase in loading history.[13] Earlier data from our group had previously showed the peak of the inter-kink segment distance distribution was lower for 5 cycles of overload than for a simple rupture.[13] That was confirmed here with the peak for the log-normal fit occurring at about 450 nm for the ruptured samples, while it was at about 300 nm for the 5-cycle overload samples.[13] The novel discovery presented here is the parallel observed between the micro-scale variation in HRM of unloaded fibrils and the inter-kink spacing in fibrils damaged by excessive tensile stress. This evidence strongly supports that pre-existing structural variations within unloaded collagen fibrils correspond to locations of increased susceptibility to mechanical damage.[12]

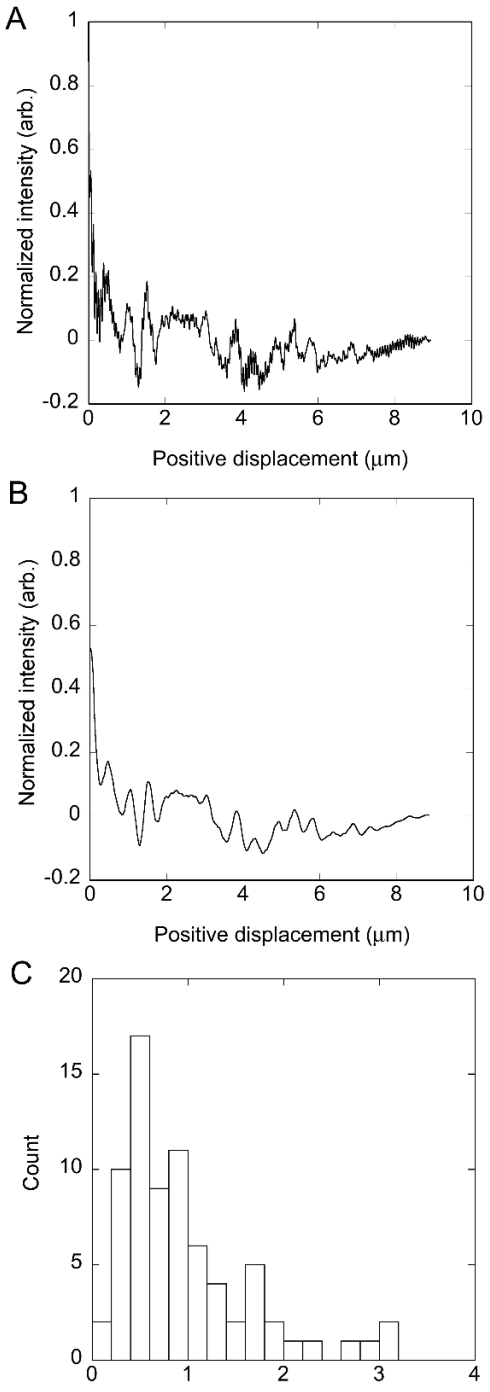

Figure 4.5: (A) Autocorrelation function of one of the HRM profiles in Figure 4.4, before filtering. (B) Same autocorrelation function after filtering of D-band related peaks. (C) Histogram of peak spacing obtained from the autocorrelation functions of the 10 profiles.

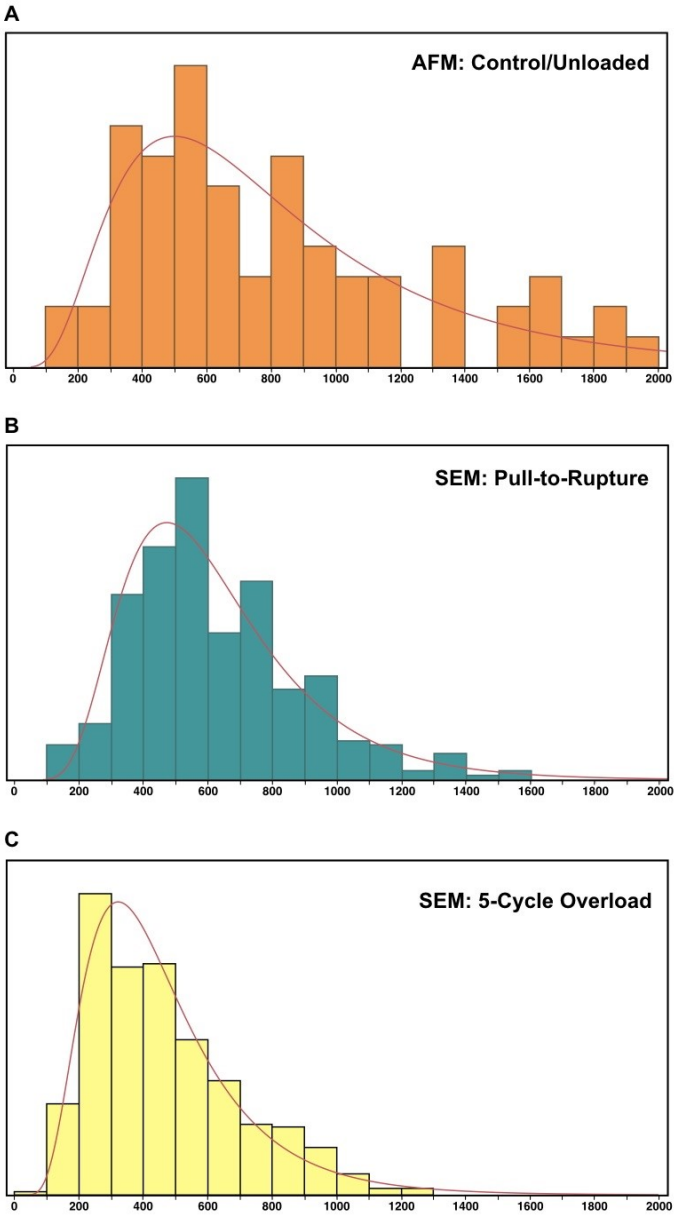

Figure 4.6: The distribution of HRM peak variations along unloaded collagen fibrils HRM profiles (A), inter-kink segment lengths calculated from images of the pull-to-rupture (B) and cyclic overload samples (C) were not normally distributed, but were very well-described by a Lognormal distribution.

Another possible function of the micro-scale variation may be the manner in which collagen fibrils interact with matrix metalloproteinases (MMPs). MMPs are a family of enzymes found in extracellular matrix which, in wound healing, tissue remodeling and cell mobility, are known to be able to cleave various types of collagen.[235-237] In two recent studies, Ditmore and co-workers and Sarkar and co-workers have tracked the binding locations of fluorescently-marked MMP-1 molecules along the length of collagen fibrils.[238,239] MMP-1 is a known collagenase, capable of cleaving native triple-helical collagen molecules in solution. In both studies, they found binding sites to be located at discrete locations spaced approximately 1–2um apart, a similar length-scale to the variation in fibril HRM that we observed in the current study using AFM (Figure 4.5, C). Therefore, the presence of pre-existing sites of mechanical vulnerability along the length of collagen fibrils may be important to biological remodeling of tendon, with mechanically-activated sites having distinct protein binding capabilities and enzyme susceptibility. It would be interesting in the future to apply AFM mapping and MMP localization sequentially on the same fibril to determine if the observed structural variation correlates with the discrete binding sites.

4.4.3 Origin of the micro-scale fluctuation on unloaded fibrils

For the unloaded fibrils measured in this study, the mean coefficient of variation in HRM was about 20% (0.209 +/- 0.005). A variation this large cannot be due to D-banding alone. Considering only the 4/5 gap/overlap ratio known to exist for D-banding, a perfect square wave variation would yield a coefficient of variation of 11%, while a sine wave which took into account convolution with the AFM probe would yield a coefficient of variation of at most 7.8%. The scale of these two values is in good agreement with the

fluctuations in HRM observed at the sub-micron length scale (Figure 4.1, C and 4.3). In other words, the micro-scale variations in the moving average HRM along the fibril axis contribute to at least half of the observed coefficient of variation. We note that it is likely the micro-scale variations are also responsible for the observed slight deviation in the gap/overlap HRM ratio from the expected value of 4/5 (Table 4.1).[5,231]

Interestingly, the observed variations in HRM along single fibrils are in good agreement with previous studies using scanning transmission electron microscopy (STEM) to measure the axial mass distribution of dried fibrils.[227-229] The most detailed study of this type analyzed single collagen fibrils extracted from adult bovine corneal stroma and reported two kinds of variations in mass per length: D-band variations between 3 and 6% superimposed on long range (tens of microns) variation in the mean mass per length of 5 to 11%.[235] More comparable to our data, a mass-per-unit-length profile extracted along a single fibril from a 12d embryonic chick metatarsal tendon showed a coefficient of variation of 7% over a 12 micron length (data digitalized from reference 228).[228] Based on these results, we can hypothesize that part of the micro-scale variation we observe in the HRM is due to variation in the number of collagen molecules present in the local cross-section. This may be due to local, stochastic irregularities in assembly of the collagen fibril from triple-helical molecules leaving solution.

Another factor which likely contributes to the observed micro-scale variation in HRM is variation in crosslink density along the length of collagen fibrils. Periodic micro-scale dissociation of fibril subcomponents was observed by Lille and co-workers in collagen fibrils from the dermis of a 70-year old man in response to incubation with urea, but not for the dermis of a 6-week-old child.[39] This difference in response was attributed to a

higher density in crosslinking associated with the age of the tissue donor. In previous work, we observed a lower HRM along in vitro fibrils than those sourced from 2-year-old rat tail tendon. A possible contributor to this is differences in crosslinking density between the two fibril types (Figure 2.1 and Appendix A Figure 8).[210] Combining the observations of Lille et. al. with ours, we suggest a correlation between the micro-scale variations in HRM (Figure 4.4 and 4.5) and localized crosslinking variations along a collagen fibril's length.

We note that it is difficult to parse out which of the two suggested mechanisms (number of molecules per local cross-section or degree of local covalent crosslinking) contributes most to the observed micro-scale variations. One approach is to consider that local HRM should fall with higher local water content (thus lower molecular collagen content) in a hydrated fibril of a given size as demonstrated previously by thermally driven hydration of collagen fibrils.[28] In the present study, plots of local HRM versus the hydrated/dehydrated ZFH ratio—a proxy for relative content of absorbed water—showed no correlation between the two properties (Appendix C, Figure 1, F). Furthermore, no spatial correlation was observed between local HRM and hydrated/dehydrated ZFH ratio (Data not shown). We therefore propose that the observed micro-scale variations are more likely the result of a variation in the covalent crosslink density along the axis of the collagen fibril.[39,230] Validation of this assertion will require further experimentation which is outside the scope of the present investigation.

Collagen fibril covalent crosslinking consists of two classes: enzymatic crosslinks between lysine/hydroxylysine residues located at the gap-overlap interface, and non-enzymatic advanced glycation end products (AGEs), which have a total of 86 available

sites along the collagen molecule to form both intra- and inter-molecular covalent crosslinks in the presence of glucose.[71] Due to the fixed location of the enzymatic crosslinks, it is unlikely they are responsible for the micro-scale fluctuation observed in the HRM. Alternatively, AGEs have an average spacing between available crosslinking sites of approximately 3.5nm along an individual collagen molecule. This suggests that local accumulation of AGE's could be responsible for the graded micro-scale fluctuation in a collagen fibril HRM. That said, our animals were young, adult male cattle, and have no detectable AGE's. [234]

4.5 Conclusions

Collagen fibrils from bovine tail tendons show structural variation identifiable under AFM using high velocity, hydrated nanomechanical mapping of individual fibrils. This variation occurs over about 500 nm along a fibril's length and, while observable via local HRM, it is not observable via dimensional measurements alone. The distribution of HRM variations identified here using autocorrelation analysis was log-normal—and remarkably similar to the distribution of inter-kink distances observed in SEM of overload-damaged tendon collagen. This strongly suggests that local disruption in mechanically-overloaded collagen fibrils occurs at sites of local mechanical susceptibility. Since the HRM variation appears to be independent of variation in local molecular packing and hydration, we propose that its source lies in a varying crosslinking density along the fibril.

Chapter 5: MMP-9 Selectively Cleaves Non-D-Banded Material on Collagen Fibrils with Discrete Plasticity Damage in Mechanically Overloaded Tendon

This chapter has been reproduced from the article “MMP-9 Selectively Cleaves Non-D-Banded Material on Collagen Fibrils with Discrete Plasticity Damage in Mechanically Overloaded Tendon”, with permission from the Journal of Mechanical Behavior of Biomedical Materials (Appendix F). The authors of the article are as follows “Baldwin, S.J., Kreplak, L. and Lee, J.M.”. As First Author I was responsible for experimental design, data acquisition, data analysis, writing the first draft of the document and participating in the subsequent edits.

5.1 Motivation and Hypotheses

Prior to this study, enzymatic susceptibility of bulk tendon displaying discrete plasticity was assessed using incubation with trypsin, followed by hydroxyproline assay and scanning electron microscopy (SEM). While informative, bulk tendon enzymolysis studies of discrete plasticity using trypsin are not ideal due to: the heterogenous generation of discrete plasticity within a tendon, the dependence on hydroxyproline as a marker for solubilized collagen, and the known ability for trypsin to cleave native collagen molecules. Furthermore, SEM of bulk tendon samples cannot image a single sample both before and after enzyme incubation. In this Chapter we make use of the previously described AFM imaging technique used in the previous chapters and both trypsin and MMP-9 to quantify fibril response to enzyme incubation. MMP-9 was chosen for this study due to its physiological significance: its limited cleavage sites along a native collagen molecule and its upregulation during the initial stages in tendon healing after injury. The following hypotheses for this work are strongly influenced by the literature detailing discrete plasticity response to fibrils, and the progressive nature of fibril damage associated with increased kink density, as described in Chapter 3.

Hypothesis 5.1: Regions devoid of D-banding structure will be the primary substrate for collagen enzymolysis.

Hypothesis 5.2: Trypsin will solubilize more material than MMP-9 from isolated native collagen fibrils and those displaying discrete plasticity.

Hypothesis 5.3: Fibril enzymolysis by trypsin and MMP-9 will be dependent on serial kink density in collagen fibrils displaying discrete plasticity.

5.2 Introduction

Within the body, forces are transmitted between muscle and bone by tendons. Tendon's ability to carry high tensile loads is due to its hierarchical structure, built from bundled collagen fibrils through multiple levels of organization.[4] The collagen fibril itself is a rope-like supermolecular aggregate of collagen molecules, typically 50–500nm in diameter and up to several millimeters in length.[38] It too is a hierarchical structure composed of subfibrils, approximately 20nm in diameter, whose internal molecular packing is semi-crystalline in nature and consists of 5nm microfibril structures.[28,40,225,232] The molecular organization within individual collagen fibrils results in a periodic (67nm) molecular density fluctuation, termed D-banding. The D-band consists of alternating gap and overlap regions where the gap has 4/5 of the collagen density of the overlap.[5,231] The D-band is inherent in the assembly of the collagen microfibril, persisting through the hierarchical structure of the fibril. In microscopy, the loss of D-banding indicates the loss of native molecular packing and damage to the collagen fibril.

When a tendon is damaged *in vivo*, via chronic overuse or sudden rupture, there is an associated decrease or loss of mechanical function indicating changes in the collagen support. It is of considerable interest to determine just what the structural motifs are for damage in tendon collagen and thereafter the relevance of such motifs to cellular action at the damage site. Recently, a novel damage motif has been discovered in some tendons after mechanical overload.[12] This motif, termed discrete plasticity, is characterized by serial kink structures along the length of a collagen fibril and a disorganized shell on the fibril's surface. Both structures are associated with the loss of characteristic D-

banding.[12] Work to date has focused on understanding the degree of molecular damage associated with discrete plasticity and the inflammatory cell response to it. Damaged fibrils have been incubated with the serine protease trypsin, a widely-used probe for denatured collagen molecules. It preferentially removed non-D-banded material from fibrils displaying discrete plasticity and revealing D-banded sections along the collagen fibril which spanned the kink structures. These results suggested that denatured collagen molecules are present in both kinks and shell.[12,14] A follow-up study using macrophage-like U937 cells cultured for 3 days on discrete plasticity-damaged fibrils demonstrated a distinctive spread morphology to the cells, with increased contact area between cells and collagen. After 3 days of incubation, the discrete plasticity-damaged fibrils were altered, suggesting that cells had begun to enzymatically degrade the damaged fibrils. Undamaged fibrils were not degraded.[153]

The remodeling of extracellular matrix (ECM) components such as collagen is accomplished via matrix metalloproteinases (MMPs).[145-151,240] Altered expression of these enzymes by the U937 cells incubated on discrete plasticity damage suggests a role for the MMPs in degrading damaged collagen.[153] The MMP family encompasses 28 zinc-dependent enzymes known for facilitating cell mobility and participating in wound healing through selective cleavage of ECM proteins.[151,240] Within the MMP family there are six sub-groups based upon their active substrates: collagenases, gelatinases, stromelysins, matrilysins, membrane type MMP's and others.[240] The molecular structure of this protein family consists of a Pro domain which inhibits the activity of the enzyme while attached, a catalytic domain which contains the active zinc-dependent cleavage site, a hinge region allowing flexibility, and a hemopexin domain

which assists in substrate binding.[151,240] Multiple studies have revealed that collagenases MMP-1 and -13, as well as the gelatinases MMP-2 and -9 are key components in the collagen remodeling process.[145-151,240] Following a tendon injury, these MMPs are up-regulated for periods of time that correlate with specific sequences in the wound healing process.[145,146] Along the length of a collagen fibril displaying discrete plasticity damage, the sections spanning the kink sites have been shown to retain native D-banding underneath the shell layer of the fibrils.[12,226] Therefore, those fibril regions displaying the D-band are not damaged. This makes a case for the selective removal *in vivo* of the damaged, non-D-banded sections of a fibril displaying discrete plasticity. The gelatinases MMP-2 and MMP-9 are naturally prime candidates for this selective degradation. Of these, MMP-9 is of particular interest. It is active on fewer collagen types than MMP-2, and is specifically up-regulated during debridement of damaged collagen matrix within the tendon, and down-regulated during the subsequent deposition of new matrix in an *in vivo* tendon injury model.[145-148,151,240]

In the present work, we explore the ability of MMP-9 to selectively remove material from collagen taken from: (i) control tendons, (ii) partially heat-denatured tendon, and (iii) mechanically-damaged tendons whose fibrils display discrete plasticity damage. Atomic force microscopy (AFM) was used to image *individual* collagen fibrils in both dehydrated and hydrated states, before and after incubation with the enzyme. Our AFM technique has previously been used to visualize the internal and external structure of discrete plasticity-damaged fibrils, and allows for sequential imaging of the effects of enzyme action.[226] We show that non-D-banded material was the only active substrate for MMP-9. In contrast, both non-D-banded and D-banded collagen fibrils were (to

varying degrees) active substrates for trypsin. The identical action of MMP-9 on non-D-banded material generated by thermal denaturation or by mechanical overload supports the conclusion that the two types of non-D-banded, damaged collagen are indistinguishable to MMP-9.

5.3 Materials and Methods

5.3.1 Tendon source, treatments, and AFM sample preparation

Bovine tails were acquired from steers aged 18–24 months, slaughtered for food. Tissue harvest was approved by the Dalhousie University Committee on Laboratory Animals (protocol number: I16-20). The tails were kept at 4°C for 2 hours until tendons were dissected from the proximal dorsal region of the tail. Extracted Tendons were stored at 4°C in phosphate-buffered saline (PBS) for less than 2 hours as paired control and overloaded sub-samples were processed for each tendon as described below. To generate discrete plasticity along collagen fibrils, a tendon piece 5-7 cm in length, hydrated with PBS by dropper, was clamped into an MTS series 458 servo-hydraulic testing machine, with inter-grip length of 2-3 cm, and pre-stretched 5 times to 10% strain at a strain rate of 1%/s and then overloaded 5 times into the plastic deformation region of the force-strain curve at a strain rate of $1\%s^{-1}$. Each individual tensile overload was until the stress-strain curve had reached zero slope, a measure provided as a feed-back parameter during the loading procedure.[13] This loading procedure was selected to generate discrete plasticity damage along individual fibrils that spanned the entire range of kink densities previously observed.[13] After the loading protocol all samples (control and overloaded) underwent a decellularization process spanning 7 days (Appendix E).[211] Decellularized tendon

samples were then stored in sterile conditions in an antibiotic-PBS solution at 4°C until AFM sample preparation (no longer than 4 weeks). AFM sample preparation has been described in detail previously.[226] Briefly, the process involved splaying apart each tendon sample using tweezers and a thin glass rod within a plastic dish containing 1ml 0.1M Tris-HCl buffer with 20mM $CaCl_2$. Each tendon was splayed until sufficient collagen fibrils were released into the 1ml solution. The fibril solution was poured into a glass-bottomed AFM dish and left undisturbed for 45 minutes as collagen fibrils adsorbed to the bottom of the dish. The samples were then rinsed 3x with 5ml nanopure water, dehydrated under nitrogen at room temperature for 10 minutes, and stored with desiccant until use but no longer than 2 days.

5.3.2 AFM imaging

AFM imaging was performed according to the method described previously.[226] All imaging was performed with ScanAsyst liquid+ cantilevers (Bruker, USA). ScanAsyst liquid+ cantilever nominal properties are: a spring constant of 0.7 N/m, resonance frequency of 150KHz, tip radius of 2 nm and cone half-angle of 17.5 degrees. Cantilever spring constant was determined prior to measurements via the thermal noise method.[194] Hydrated images were acquired with peak force set points (PFSP) of 1nN and 10nN consecutively, while dehydrated images were acquired with tip velocity of 0.6mm/s with a PFSP of 10nN on a 10µm by 10µm area with a resolution of 20nm, followed by a 3.33µm by 3.33µm area with a resolution of 6nm.

5.3.3 Enzyme treatment and AFM data acquisition

A total of 20 collagen fibrils were imaged in dehydrated and hydrated states, before and after incubation with an enzyme. The 20 fibrils consisted of 2 groups. Half (10) were sourced from unloaded tendon samples and the other half (10) were sourced from overloaded tendon samples which displayed discrete plasticity damage. Five fibrils from each group were incubated for 24hours with either 0.1 mg acetylated trypsin (Bovine Pancreas, Catalog #T8003) in 3ml 0.1M Tris-HCl buffer pH7.6 with 20mM $CaCl_2$ at room temperature or with 10µg recombinant human MMP-9 (Catalog #SRP6271), 1µg Trypsin, and 3µg serine protease inhibitor (Catalog #T9003) in 3ml 0.1M Tris-HCl buffer pH 7.6 with 20mM $CaCl_2$ at 37°C. The MMP-9 protocol also required activation of the enzyme (see below). All enzymes and inhibitors were purchased from Sigma-Aldrich.

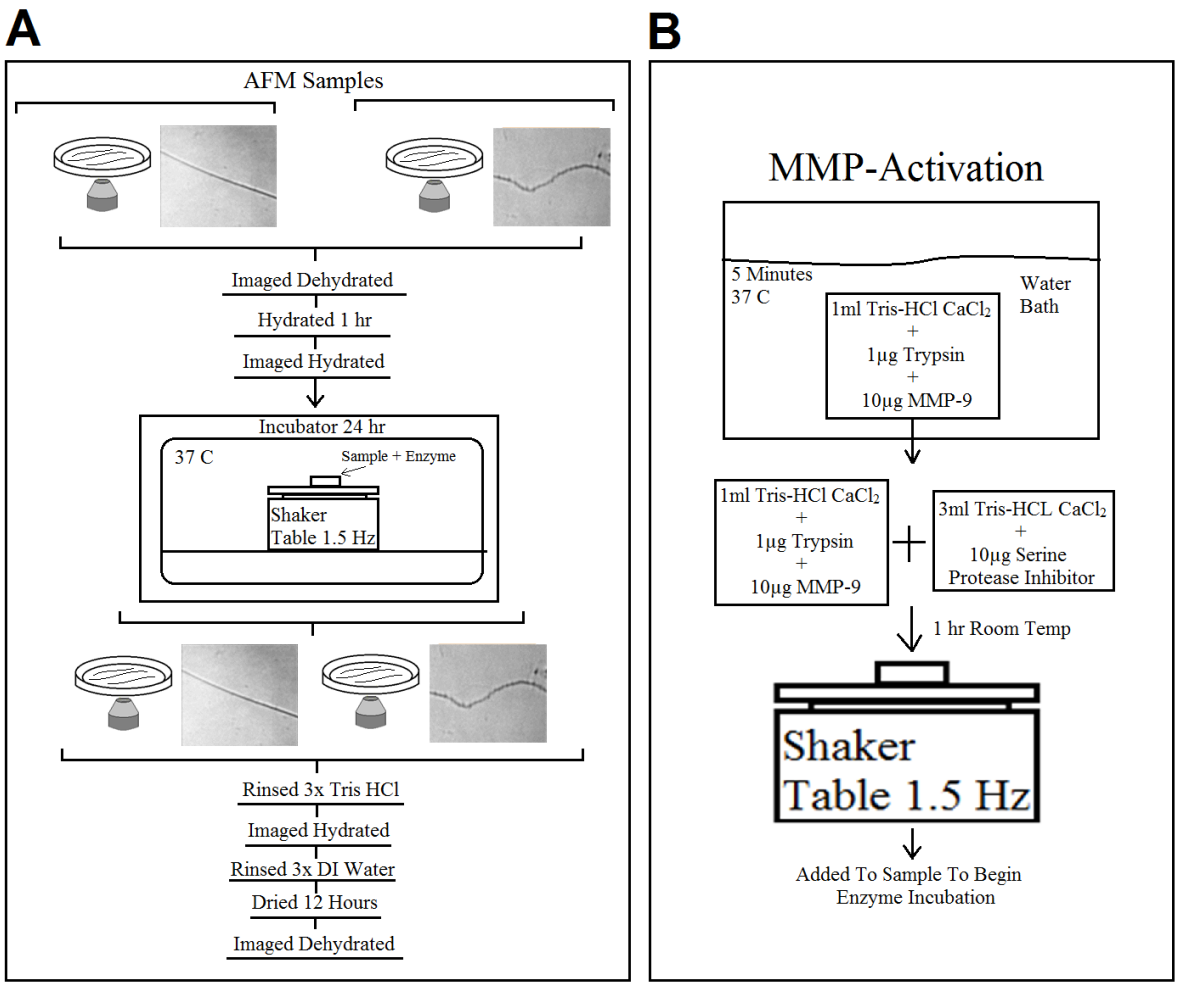

Figure 5.1: Schematic of procedure for performing enzyme incubation and AFM data analysis (A). Schematic detailing the procedure for activating MMP-9 with trypsin and the following inhibition of trypsin by serine protease (B).

Data acquisition involved six steps: (i) optical targeting of dehydrated collagen fibrils, (ii) dehydrated AFM imaging of 10 μm along each fibril with 20nm pixel size, followed by a 3.33μm zoom in with a 6nm pixel size, (iii) rehydration of the fibrils for 30 minutes prior to hydrated AFM imaging of 5μm along each fibril with 1nN and 10nN PFSPs with a pixel size of 8nm, (iv) 24 hour incubation with an enzyme solution, (v) repetitive rinsing of the sample with 0.1M Tris-HCl buffer pH 7.6 with 20mM CaCl2 prior to repetition of step (iii), (vi) repetitive rinsing with nanopore water followed by dehydration of the AFM sample under nitrogen flow and then repetition of step (ii) (Figure 5.1, A). Hydrated imaging was performed in 3ml of 0.1M Tris-HCl buffer pH 7.6 with 20mM $CaCl_2$ at room temperature. Prior to hydrated imaging, all samples were allowed 30 minutes to rehydrate. Enzyme incubation took place on a linear shaker table set to 1.5 Hz. Following enzyme incubation and sequential hydrated imaging, the sample was rinsed three times with 5ml of the Tris-HCl $CaCl_2$ solution and nanopure water respectively. All dehydrated imaging was performed after 10 minutes of drying under nitrogen gas and a minimum of 12 hours stored with desiccant to control the samples' exposure to a humid atmosphere. All imaging from step (i) to (vi) was performed at the same location along the collagen fibril in all steps.

5.3.4 MMP-9 activation

Human MMP-9 was purchased in the inactivated pro-MMP state. Activation of proMMP-9 was achieved by incubation with trypsin, followed by a serine protease inhibitor to cease trypsin activity.[241] Initially a 5-minute incubation at 37°C of 10μg of ProMMP-9 and 1μg trypsin in 1ml 0.1M Tris-HCl buffer with 20mM $CaCl_2$ at pH 7.6 was used to activate the ProMMP-9. To deactivate the trypsin, the solution was then added to 2ml

0.1M Tris-HCl buffer pH 7.6 with 20mM $CaCl_2$ containing 10µg serine protease inhibitor sourced from soybean. The combined solution was incubated at room temperature for 1 hour under constant agitation. At this point, the solution (3ml Tris-HCl buffer pH 7.6 with 20mM $CaCl_2$, 10 µg MMP-9, 10 µg serine protease inhibitor and 1 µg trypsin) was ready for incubation with the AFM samples—with the MMP-9 active and the trypsin inactive (Figure 5.1, B).

5.3.5 Confirmation of enzyme activity

Partially heat-denatured collagen fibrils were used to test enzyme activity. The preparation of these samples involved heating covered AFM samples of unloaded collagen fibrils to 62°C for 45 minutes in 3ml of nanopure water using a Bioscope Catalyst AFM heating stage.[210] The samples were allowed to cool to room temperature after heating, rinsed three times with 5ml nano-pure water, dehydrated 10 minutes under nitrogen flow, and then sealed with desiccant for a minimum of 12 hours. Three separate solutions; (i) 3ml 0.1M Tris-HCl buffer-20mM $CaCl_2$ at pH 7.6 with 1mg serine protease inhibitor and 0.3mg trypsin, (ii) 3ml 0.1M Tris-HCl buffer with 20mM $CaCl_2$ at pH 7.6 with 0.3mg trypsin, and (iii) the activated MMP-9 solution, were incubated with the thermally denatured fibrils for 24 hours. The first and second solutions were incubated in sequence on the same collagen fibrils (Appendix D, Figure 1), while the third solution was tested on a separate sample. Dehydrated images along 10µm of the same collagen fibrils were acquired after incubation with every solution. These experiments tested the following: (i) that the serine protease inhibitor could prevent trypsin from cleaving denatured collagen, (ii) that incubation of the same denatured collagen with active trypsin would result in cleavage and removal of denatured collagen, (iii) that the MMP-9

solution contained active MMP-9 despite inactivation of trypsin with the serine protease inhibitor. Taken together, these tests demonstrated that MMP-9 was the only active enzyme in the third solution.

5.3.6 Data analysis

The bulk of the data analysis was performed using the methods described previously.[226] Briefly, using SPIP 6.3.3 software (Image Metrology), structural properties were extracted from the AFM images of the collagen fibrils: the hydrated and dehydrated heights and deformation of each collagen fibril, as well as the mean kink density (kinks/μm) along 10μm of each collagen fibril imaged in the dehydrated state. The kink density provides measurement for the degree of discrete plasticity damage in each fibril. The hydrated 1nN PFSP images were used to calculate the hydrated height and deformation. The corresponding height and deformation images were added together to provide the zero-force height (ZFH) of each fibril, which functions as a measure of the fibril's dimension in the absence of the AFM tip. Cross-sectional data were extracted along the apex of collagen fibrils as described previously.[226] The 10nN PFS images were used to visualize the fibril structures while hydrated.

Using Gwyiddion image analysis software, the mean cross-sectional area of each fibril in the dehydrated state was extracted. A zero-basis filter of 5nm was applied, selecting the entire collagen fibril. Summing the volume of each pixel in the selected area and dividing this volume by the length of the collagen fibril in the image yielded the mean cross-sectional area. Cross-sectional area measurements were taken on hydrated fibrils but discarded due to AFM imaging artifacts and the exceedingly low hydrated radial modulus

(HRM) shell structure, both before and after enzyme incubation.[226] Due to this fact the measure of ZFH was employed both as a metric of fibril dimension in the hydrated state, and in water uptake by taking the ratio of the hydrated/dehydrated ZFH's. The percent changes of each fibril's dehydrated ZFH, hydrated ZFH, ZFH ratio, and mean dehydrated cross-sectional area were calculated from data taken before and after enzyme incubation and served as a quantitative measure of fibril alteration associated with each enzyme. The resulting percent change data were then grouped by fibril type and enzyme exposure, or plotted as a function of kink density for each enzyme.

5.3.7 Statistical analysis

Statistical analysis was performed using JMP software (version 11.0.0, SAS Institute Inc.). A one-way ANOVA was performed with Bonferroni correction for post-hoc t-testing for four groups. Least squares regression analysis was performed to obtain best linear fits to scatter plot data.

5.4 Results

Dehydrated AFM imaging showed that control (unload), heated, and discrete plasticity-damaged fibrils were affected in different ways by enzyme incubation for 24 hours. The D-band structure of unloaded fibrils was not altered following incubation with either enzyme (Figure 5.2, A and B). In contrast, both enzymes solubilized regions of non-D-banded material on heated collagen fibrils (Figure 5.2, C and D). This confirmed that both enzymes were active, and that thermally-generated, non-D-banded material is susceptible to MMP-9 and trypsin. A large portion of the shell structure was solubilized from collagen fibrils displaying discrete plasticity damage, while the core of the fibrils

remained nearly unaltered (Figure 5.2, E and F). A key distinction between these two structures is the lack of D-band on the shell and the presence of the D-band in the core of the fibrils. The selective ability of both enzymes to solubilize material lacking the D-band structure, independent of damage type (thermal or mechanical), suggests the loss of the D-band coincides with the formation of active binding sites for both MMP-9 and trypsin: that is, binding sites associated with collagen denaturation.

Grouping fibrils by damage condition (unloaded, discrete plasticity) and incubation enzyme (trypsin, MMP-9) demonstrated how the enzymes differentially affected fibril dimension (Figure 5.3, Table 5.1). The reductions in dehydrated ZFH and dehydrated cross-section area seen after MMP-9 and trypsin exposure varied significantly with damage level. If the samples were undamaged, MMP-9 did not change dimensions. By contrast, trypsin produced a significant decrease in unloaded fibril dimensions, either compared to the effects of MMP-9 or to fibrils not incubated with enzyme (Figure 5.3, A and D). This indicates that unloaded, individual fibrils, fully D-banded, can be active substrates for trypsin, but not for MMP-9. If discrete plasticity damage was present, the effects of MMP-9 and trypsin were equivalent (Figure 5.3, A and D). When the same fibrils were examined in the hydrated state, the results indicated that solubilized material was replaced by water absorption, restoring the fibril height. A positive change in ZFH ratio (hydrated height: dehydrated height) after enzymatic incubation was correlated with loss of dehydrated ZFH (Figure 5.3, A and C). That is, the enzyme treatment solubilized collagen but increased the ability of the remaining collagen to absorb water in the hydrated state.

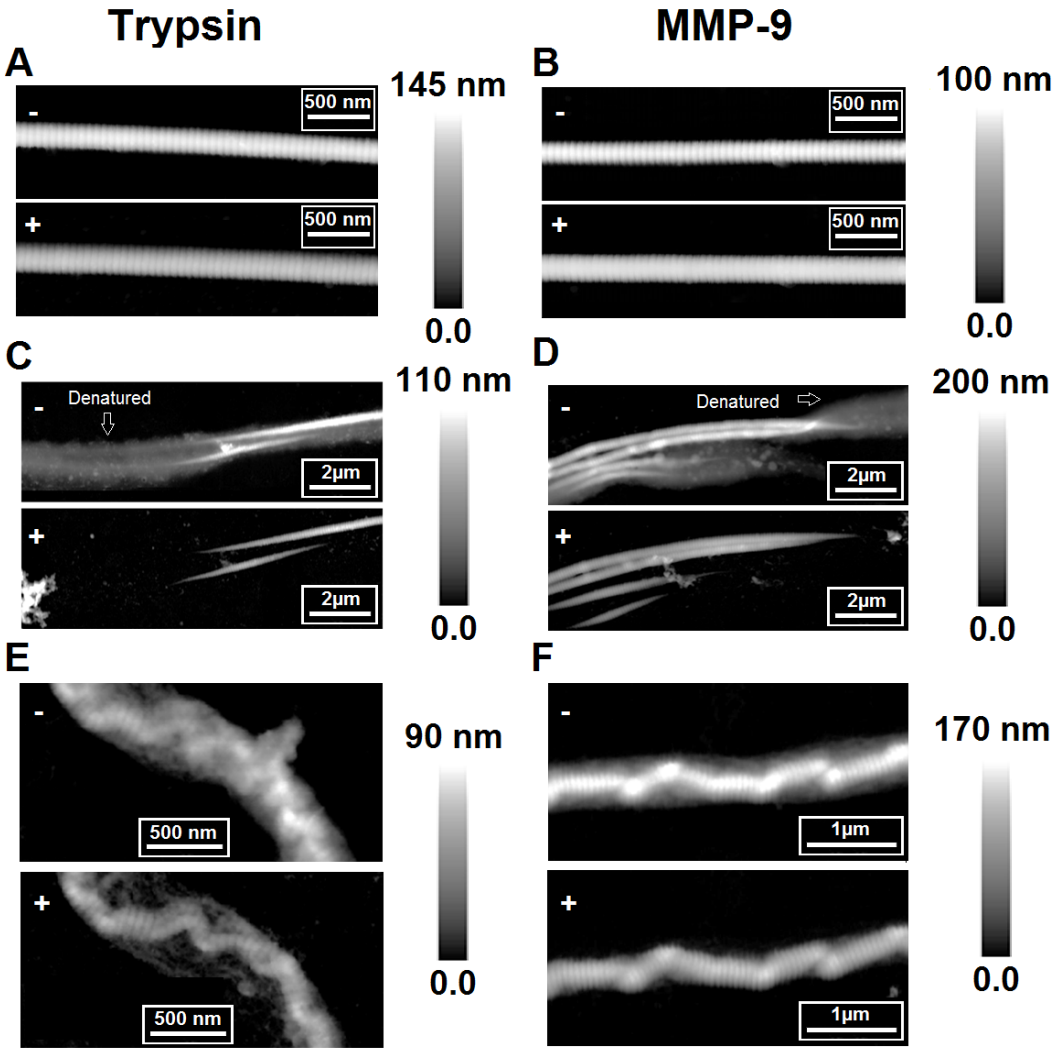

Figure 5.2: Dehydrated height images before (-) and after (+) incubation with trypsin (A,C,E) or human MMP-9 (B,D,F) for 24h. Shown are native (control) collagen fibrils (A,B), heated collagen fibrils (C,D), and collagen fibrils displaying discrete plasticity (E,F). The denatured material from the heated samples was completely removed by both enzymes (C,D, arrows) as well as most of the shell material from the fibrils displaying discrete plasticity (E,F, arrows). Alteration to the native fibrils, D-banded regions of heated fibrils, and the D-banded core of the collagen fibrils was limited, demonstrating a selective action of the enzymes on structurally-altered regions of collagen fibrils.

Table 5.1: Percent change in: dehydrated ZFH, hydrated ZFH, hydrated/dehydrated ZFH ratio, and dehydrated cross-sectional area of loaded and collagen fibrils displaying discrete plasticity following incubation with trypsin, MMP-9, or no enzyme.

Measurement	Fibril Type	Trypsin	MMP-9	No
Dehydrated ZFH	Unloaded	-15 ± 6	0 ± 9	5 ± 1
	Discrete	-4 ± 5	-17 ± 12	
Hydrated ZFH	Unloaded	7 ± 7	1 ± 3	2 ± 2
	Discrete	-3 ± 9	2 ± 4	
Hydrated/Dehydrated ZFH Ratio	Unloaded	27 ± 15	2 ± 6	-4 ± 2
	Discrete	0 ± 4	19 ± 13	
Mean Dehydrated Cross-Sectional Area	Unloaded	-2 ± 8	29 ± 5	32 ± 8
	Discrete	-20 ± 18	-14 ± 15	

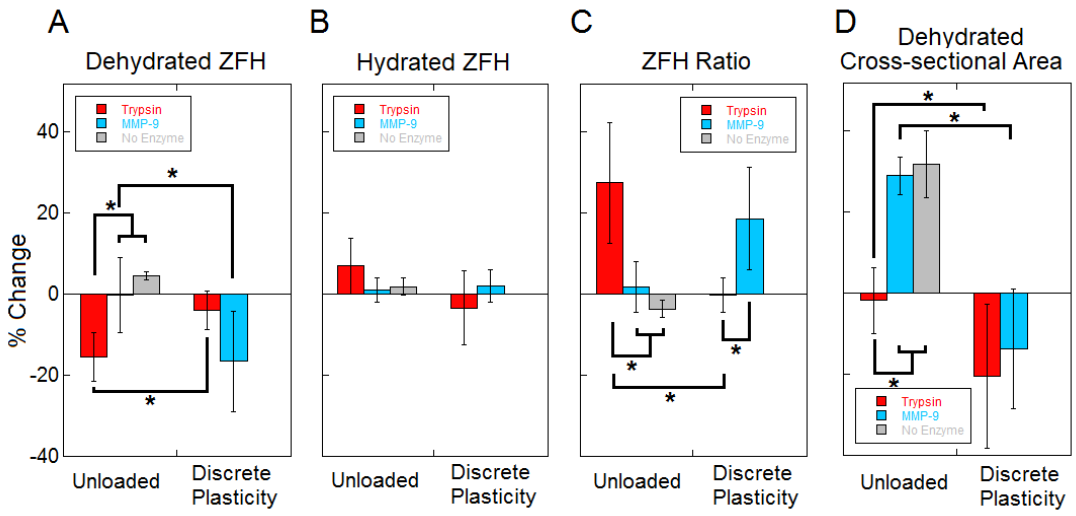

Figure 5.3: The mean percent change in dehydrated ZFH of collagen fibrils (A), hydrated ZFH (B), hydrated/dehydrated ZFH ratio (C), and mean dehydrated cross-sectional area (D), following 24h enzyme incubation. Significant differences (asterisks) were found between native fibrils and those displaying discrete plasticity following incubation with trypsin (A,C,D) and MMP-9 (A,D) demonstrating the increased interaction between the enzymes and mechanically damaged collagen fibrils. Significant differences were also found when comparing the interaction of trypsin with native collagen fibrils to that with MMP-9 or with no enzyme (A,C,D). This indicates unloaded fibrils are active substrate for trypsin treatment but not for MMP-9. Error bars represent standard deviation.

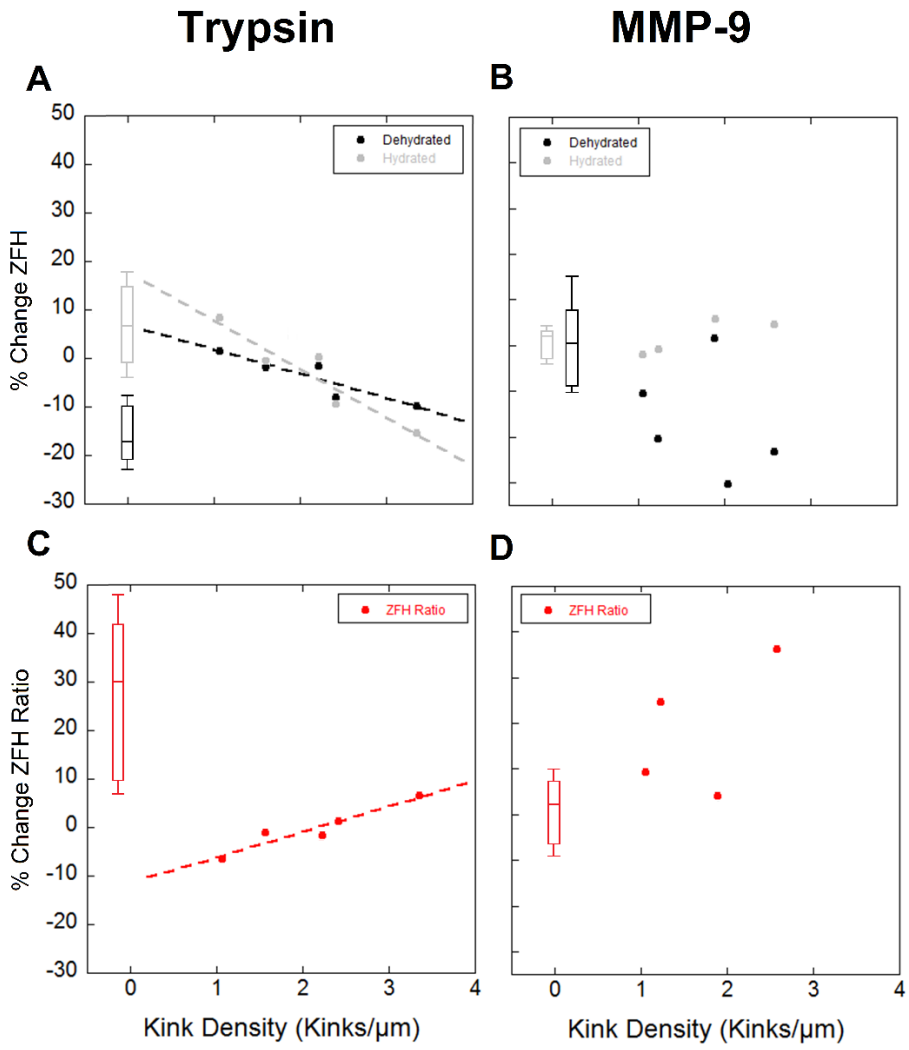

Figure 5.4: The percent change in dehydrated and hydrated ZFH (A,B), and hydrated/dehydrated ZFH ratio (C,D) as a function of kink density following incubation with trypsin (A,C) and MMP-9 (B,D). Significant relationship between the kink density and the three measures was found with trypsin incubation (A,C, Dashed Lines) while no such relationship was observed with MMP-9. The box-whisker plots representing the range of native fibril alteration with enzyme incubation clearly shows MMP-9 does not alternative collagen fibrils while trypsin does. As such, zero kink density fibrils are an active substrate for trypsin (A,C) while it is not for MMP-9.

To examine the effect of discrete plasticity damage level on enzyme susceptibility, changes in the dimensions of each fibril were plotted as a function of serial kink density. Here, as previously demonstrated, serial kink density is an excellent proxy for damage.[226] These plots revealed negative linear correlation between dehydrated or hydrated ZFH and kink density, as well as a positive linear correlation between ZFH ratio and kink density (Figure 5.4, A and Table 5.2) for fibrils incubated with trypsin. These significant relationships allow us to use kink density measured by other techniques (SEM) as a metric for the amount of denatured material.[12-14,153] No correlation between kink density and ZFH changes in fibrils following MMP-9 incubation was found (Figure 5.4 B, and D). Plotting the mean dehydrated cross-sectional area as a function of kink density for fibrils incubated with MMP-9 showed a significant decrease in the cross-sectional area with an increase in kink density ($p < 0.02$, $r^2 = 0.75$, Figure 5.5).

Much of the structural response in the collagen fibrils to enzymatic incubation was observed as alteration to the shell component of discrete plasticity damage. Prior to enzyme incubation, the shell of the fibrils displaying discrete plasticity was comprised of a mesh of collagenous components (Figure 5.6, A-D). Following incubation, the shell lost this cohesion, separating into individual strands of material (Figure 5.6, E-H). Shell fragments following MMP-9 incubation exhibited D-banding (Figure 5.7, B and D, Arrows, inset) while shell fragments following trypsin incubation continued to be mesh-like (Figure 5.7, A and C). This further exemplifies MMP-9's selective cleavage of non-D-banded material.

Table 5.2: Equations for the significant linear correlations between kink density and percent change in dehydrated ZFH, hydrated ZFH, hydrated/dehydrated ZFH ratio, and cross-sectional area (%change = mx+b), and their corresponding r^2 values, following incubation with trypsin and MMP-9.

Percent Change Trypsin	m	b	r^2	p <
Dehydrated ZFH	-5.03	6.82	0.83	0.05
Hydrated ZFH	-10.01	17.91	0.89	0.05
Hydrated/Dehydrated ZFH Ratio	5.21	-11.25	0.89	0.05
Percent Change MMP-9	m	b	r^2	
Cross-section area	-22.21	32.78	0.75	0.02

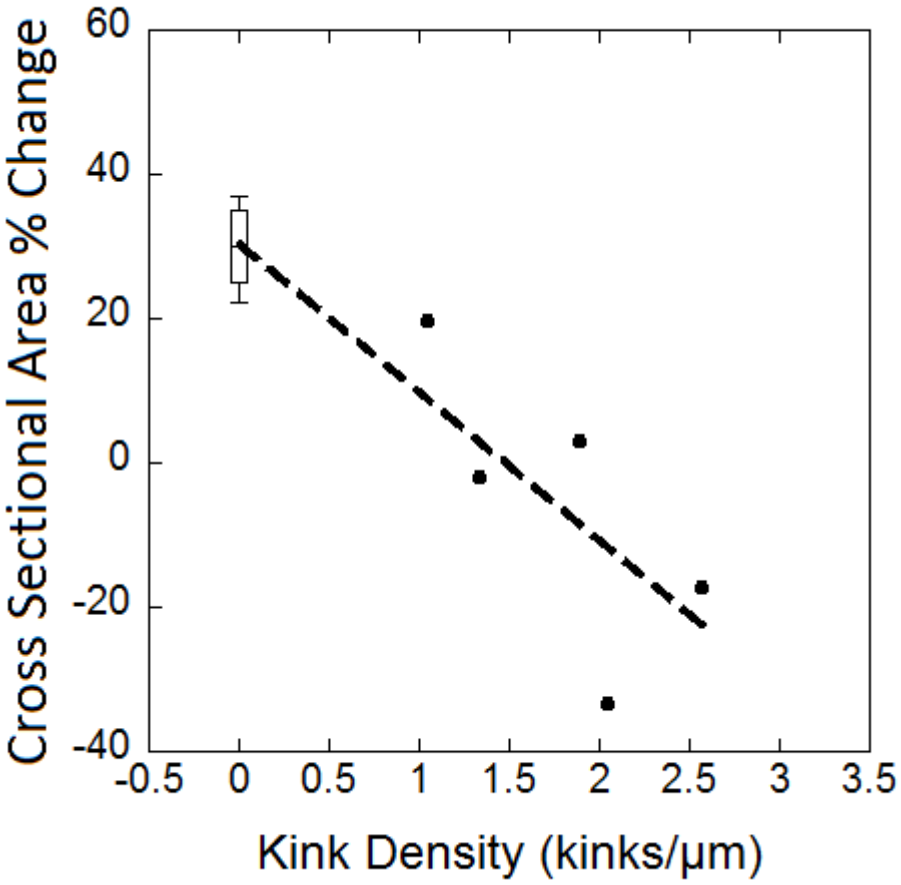

Figure 5.5: The percent change of the cross-sectional area of dehydrated fibrils incubated with MMP-9 displayed as a function of kink density. Higher kink density, correlated with a decrease in the percent change. This indicates an increasing loss of volume upon exposure to MMP-9 with progressive damage to the collagen fibril. Linear regression line significant with $p<0.02$ and $r^2=0.75$.

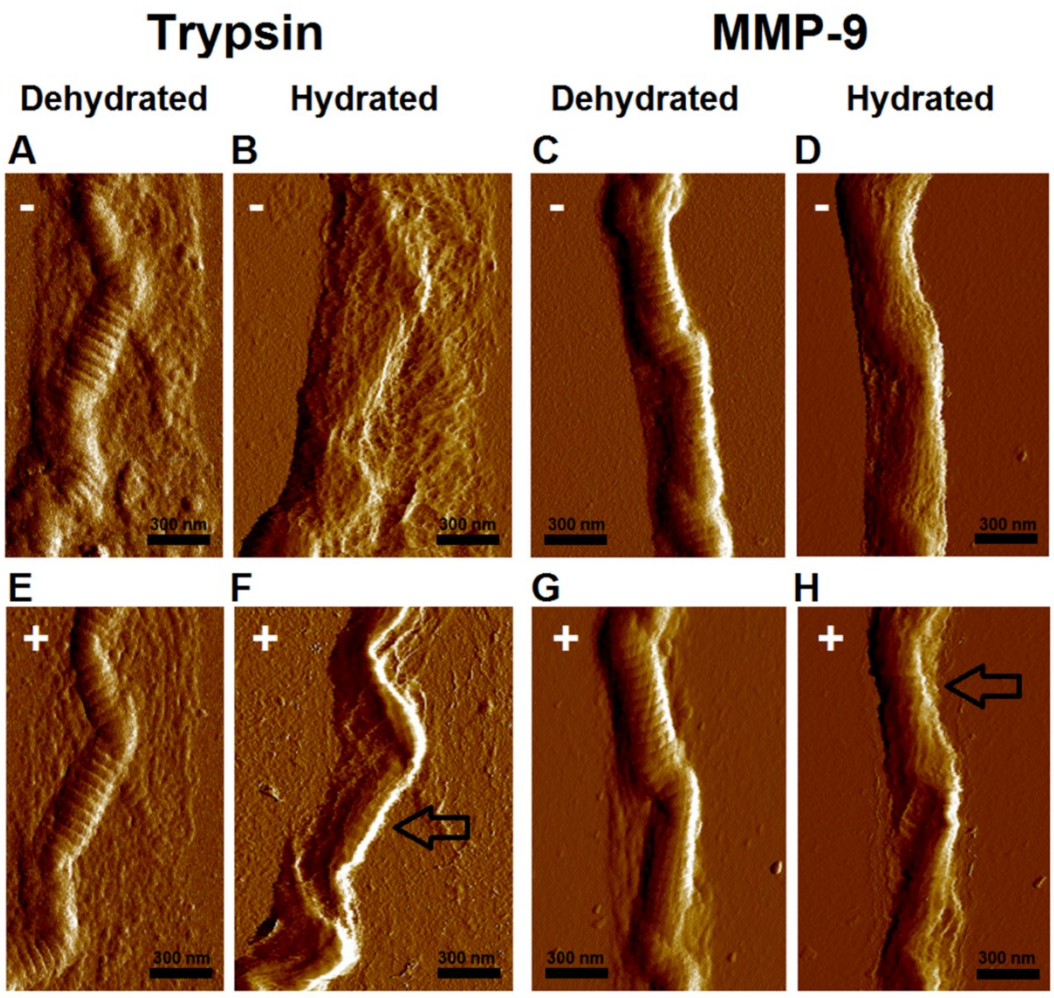

Figure 5.6: Peak force error images of fibrils displaying discrete plasticity before (A-D, -) and after (E-H, +) Trypsin (A,B,E,F) and MMP-9 (C,D,G,H) in dehydrated (A,C,E,G) and hydrated (B,D,F,H) states. Before enzyme incubation hydration of the fibrils hid the D-band structure along the core of the fibril due to the swelling of the shell (A-D). Hydration of the fibril reveals the cohesive mesh structure of the shell (A-D). Following enzyme incubation, the D-band structure is observable along the core of the fibrils in a hydrated state (Arrows F,H) and the shell is reduced to loosely connected strands of collagen (E-H).

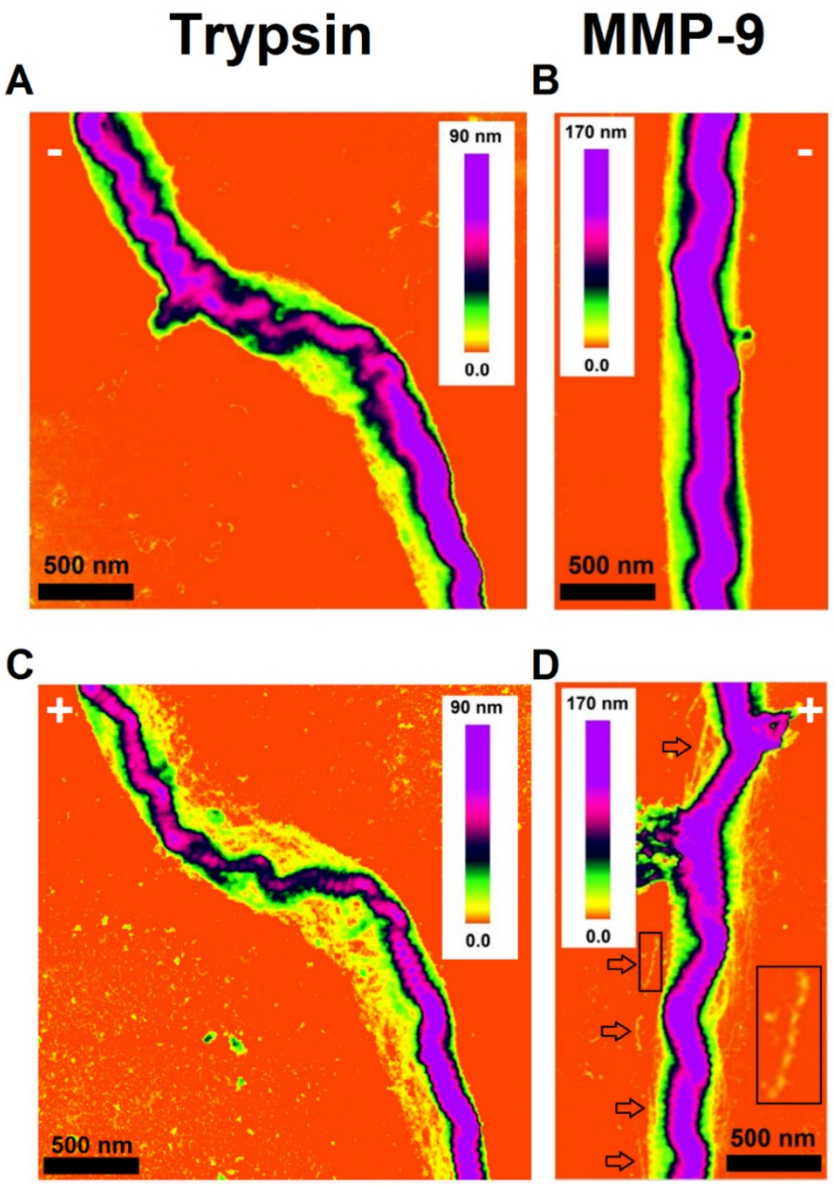

Figure 5.7: Dehydrated height images of two fibrils displaying discrete plasticity before (A,B,-) and after (C,D,+) incubation with trypsin (C) or MMP-9 (D). The color scale has been selected to emphasize the condition of the shell after enzymatic incubation. Both MMP-9 and trypsin removed material from the shell of the respective fibrils but only MMP-9 left shell components clearly displaying periodic banding indicative of molecular organization (D, Arrows and inset).

5.5 Discussion

5.5.1 MMP-9

Following tendon damage, an inflammatory response is initiated which results in cell migration and MMP synthesis.[145-150] Many MMP's have been shown to be up-regulated at the site of damage at specific time points during the healing process.[145,146] Work which tracked the expression of MMP-2 and MMP-9 mRNA at the site of surgically-induced tendon ruptures revealed that MMP-9 expression was specifically associated with the degradation of collagen hierarchical structure at the wound site, but not with the following deposition of new matrix.[148] This selective up-regulation *in vivo* supports the view of MMP-9 as being essential to "debriding" of damaged tendon in preparation for the deposition of new matrix.

In this study, we incubated individual unloaded, partially heat-denatured, and discrete plasticity-damaged fibrils for 24 hours with either the serine protease trypsin, or with the human gelatinase MMP-9. Discrete plasticity is a newly discovered characteristic motif of damage in certain tendons following mechanical overload.[12] Discrete plasticity damage is characterized by a serially kinked fibril core, with D-banded inter-kink regions, and a disorganized shell. It also results in decreased thermal stability of collagen, an increased susceptibility to enzymatic cleavage by trypsin, a negative correlation between fibril HRM and kink density, as well as recognition and degradation of damaged zones by macrophage-like U937 cells .[12-14,153,226] Since MMP-9 has been shown to be up regulated during the initial stage of tendon repair, it was important to determine if discrete plasticity-damaged fibrils were an active substrate for MMP-9. Our results

confirmed that idea. MMP-9 removed more material from discrete plasticity-damaged fibrils than from unloaded fibrils (Figure 5.3, A and D), with greater removal correlated with increasing damage (Figure 5.5 and Table 5.2) and, further, with selective removal of non-D-banded material (Figure 5.7, A and C). Partially heat-denatured fibrils also displayed degradation with incubation MMP-9 (Figure 5.2), suggesting that the non-D-banded material on fibrils displaying discrete plasticity damage is denatured collagen, similar to that generated by heat denaturation.

The shell of fibrils displaying discrete plasticity is a mesh-like structure in the hydrated state (Figure 5.6, B and D).[226] Following incubation with MMP-9, the shell structure was greatly solubilized, leaving thin strands of material which lacked the cohesion observed before incubation (Figure 5.6, F and H). The loose network of remaining material in the shell following enzyme incubation prevented the acquisition of mechanical data following enzyme incubation. The shell remnants consisted of subfibril and microfibril fragments exhibiting D-banding (Figure 5.7, D), coupled with the appearance of subfibril components along the core of the fibril (Figure 5.6, G). This appearance was similar to that revealed by macrophage U937 activity.[153] Previously, it was shown that collagen I molecules in solution contained a single active cleavage site for MMP-9, with cleavage producing two fragments of ¼ and ¾ the length of the molecule.[180] We observed a lack of activity of MMP-9 on undamaged collagen fibrils (Figure 5.3). The microfibril fragments observed following MMP-9 incubation herein demonstrate that collagen aggregates displaying the characteristic D-band structure can prevent MMP-9 from accessing the ¼ ¾ cleavage site.

5.5.2 Trypsin

Trypsin is commonly used as a probe for denatured collagen, and is known to cleave collagen molecules in solution.[12,14,120,153,180,242] Its use as a probe has been justified by the long-standing notion that collagen aggregates inhibit the 90 possible active trypsin cleavage sites along a collagen molecule at room temperature. This has led to the development of a fibril extraction technique based on tissue incubation with trypsin.[15,243] Our findings indicate that trypsin is capable of cleaving fibrillar collagen in isolated fibrils well below the denaturation temperature of collagen molecules in solution.[56] Therefore, one or more of these active sites must be available along the fibril. The availability of active sites is likely due to micro unfolding events resulting from thermally-driven structural fluctuations.[134,244]

It is interesting that we found that trypsin and MMP-9 equally removed material from fibrils displaying discrete plasticity damage, although only trypsin was capable of cleaving molecules in D-banded collagen aggregates. This indicates that the rate of cleavage of fibrillar collagen by trypsin is far slower than its cleavage of non-D-banded, disorganized material, or that the resulting cleavage products could not be solubilized from the fibril due to the presence of crosslinks. This observation has implications for trypsin's use as a tool for isolating collagen fibrils for study and its application as a probe for denatured collagen.[243] It is important to note that, in this study, both native and damaged fibrils were obtained from tendons which had first been decellularized and then adhered to glass by dehydration. This processing may have enhanced susceptibility of D-banded collagen fibrils to trypsin, although apparently not to MMP-9.

Shell remnants following trypsin incubation were disorganized and exhibited no D-banding (Figure 5.7, C). The lack of D-banded material in discrete plasticity shell remnants, coupled with trypsin's ability to alter unloaded fibrils, demonstrates that even properly-packed collagen aggregates are active substrates for trypsin (Figure 5.7, C and 5.3, A, C and D). Interestingly, the ZFH ratio of unloaded collagen fibrils significantly increased following trypsin incubation (Figure 5.3, C) while the dehydrated ZFH and mean cross section area decreased (Figure 5.3, A and D). This indicates that the loss of collagen from the unloaded fibrils is coupled with an increase in water uptake per molecule. We propose two possible scenarios that would result in this behavior, either: (i) the selective cleavage of a population of fibril sub-components which allowed for water uptake, (ii) retention of cleaved but still-bound molecules on the fibril, with an increased affinity of those fragments for water. In the present study, we did not assay for solubilized collagen since we were examining single isolate fibrils only. Such an assay might determine which of the two proposed scenarios is more likely.

Plotting the percent change in dehydrated and hydrated ZFH versus serial kink density (a measure of damage level) revealed a significant negative correlation in both cases. This indicated that enzyme susceptibility increased with more discrete plasticity-type damage to the fibrils (Figure 5.4, A and C). The opposite was true for the ZFH ratio (wet/dry): a significant positive correlation was observed with kink density, showing an increase in water uptake per molecule following enzymatic incubation. It is possible that any partially-cleaved but non-solubilized material is highly hydrophilic. An example of such material can be found in the non-D-banded shell remnants seen on the side of the fibril core after trypsin incubation (Figure 5.7, C, yellow and green colored regions). By

contrast, ZFH and ZFH ratio were not correlated with kink density following MMP-9 incubation (Figure 5.4, B and D). The appearance of D-banded shell fragments following MMP-9 incubation demonstrated that, in addition to non-D-banded (denatured) material in the shell, D-banded material was present there prior to incubation (Figure 5.7, D). Of the two enzymes tested only MMP-9 was sensitive to this distinction, preferentially solubilizing the non-D-banded components of the shell, and having no effect on unloaded/undamaged fibrils (Figure 5.3).

5.5.3 Fibril level enzymatic assay

The decision to use AFM as the primary measurement tool in this study was due to its ability to perform sequential imaging upon the same collagen fibril in dehydrated and hydrated states and following enzymatic incubations.[226] Therefore, differences in response to a given enzyme were minimally affected by natural variations within the sample group. The sequential studies here were made possible by optical targeting of collagen fibrils with an inverted optical microscope and required no chemical alteration to the collagen fibrils to image them. This opens the door for fibril-level enzymatic assays capable of visualizing cleavage heterogeneities along the fibril structure.

Treating the dehydrated ZFH as the diameter of the fibril, or using the difference in percent change between trypsin incubated and no enzyme unloaded fibrils showed that unloaded *isolated* fibrils incubated with trypsin had 36-53% of their collagen mass solubilized (dehydrated ZFH as diameter, mean cross section area). By comparison, trypsin incubation of bulk tendon at room temperature only solubilized 2.5% of the tendon. (See Table 5.1).[14] This suggests that fibril packing and fibre assembly in the

intact tissue is an important modulator of solubilization of degradation products, although not necessarily an inhibitor of degradation per se. Our technique directly measured changes in the dehydrated volume of a fibril, which is directly correlated to the amount of material solubilized. Even further, our technique can determine if an enzyme is capable of cleaving fibrillar collagen without solubilizing it, as observed by the change in the ZFH ratio as described above.[120,210,245] This proved vital in concluding that MMP-9 is incapable of cleaving fibrillar collagen, rather than just solubilizing collagen. Finally, the technique permitted the use of small amounts of enzyme per incubation, making the work economically feasible.

We recognize that in an *in vivo* injury, overload damage might affect not only the collagen per se, but also its interactions with other important extracellular matrix molecules such as glycosaminoglycans, proteoglycans, fibrillin, elastin, and so on. The present experiments cannot address how disruption of those interactions might affect susceptibility of damaged collagen to metalloproteinases. However, perhaps due to the action of the tendon decellularization applied here, there was no evidence of other molecular structures adhering to the isolated collagen fibrils examined. Therefore, our data is informative on how metalloproteinases like MMP-9 would interact with that collagen which is available to it as a substrate, damaged or undamaged, and which is not screened by other adherent molecular species.

5.6 Conclusion

We have demonstrated the selective cleavage of non-D-banded material along collagen fibrils by MMP-9. MMP-9's known participation in collagen degradation *in vivo*

following tendon rupture, as well as its selective cleavage of damaged collagen molecules found in this work strongly suggests that it is an active—and selective—participant in the healing/repair process of discrete plasticity and other fibril-scale mechanical damage *in vivo*. The comparison of MMP-9's ability to solubilize non-D-banded material to that of trypsin revealed the same action upon fibrils displaying discrete plasticity damage. This indicates that the non-D-banded material, mainly found in the shell of the damaged fibrils, is primarily composed of significantly-denatured molecules. An unexpected result of this work was that unloaded *isolated* fibrils were active substrates for trypsin. This has implications for the use of the enzyme for fibril extraction and as a probe for denatured collagen. In the future, we envision to applying this novel, fibril-level, enzymatic assay to the activity of MMPs-1, -2, and -13 on discrete plasticity-damaged fibrils, as well as enzymatic response to other damage motifs (mechanical, thermal, genetic) found in collagenous tissues.

Chapter 6: Discussion

6.1 Discussion

This thesis represents the first in-depth, sequential, study of molecular and fibril level damage on isolated collagen fibrils from overloaded tendon, facilitated by high indentation speed HRM mapping, providing increased structural sensitivity. The technique is capable of quantifying fibril level damage in both a dehydrated and a hydrated environment before and after collagen fibril alteration. Applying the technique to isolated fibrils displaying discrete plasticity resulted in: the first study to mechanically quantify longitudinal and radial fibril damage motifs associated with tendon overload, the discovery of micron-scale variation of unloaded fibril possibly predetermining the sites of kink formation, and the first study of enzymatic susceptibility on isolated, mechanically damaged, collagen fibrils. Rather than repeating the individual findings of each individual chapter, this section will focus on broader considerations encompassing the entire body of work.

6.1.1 Discerning between fibril level and molecular level alteration and variation

Within this thesis, hydrated radial modulus (HRM), hydrated indentation depth, zero force height (ZFH) ratio and fibril enzymolysis functioned as novel measures of structural variations along isolated native fibrils and those displaying discrete plasticity. Truly decoupling fibril level and molecular level damage with these measures remains impossible, but arguments can be made as to whether fibril level or molecular level damage functions as a more prominent signal in each of the measures. The most

successful isolation of molecular level damage associated with discrete plasticity was achieved by measuring fibril enzymolysis by MMP-9. The inability of MMP-9 to solubilize material from native collagen fibrils strongly suggests that the disruption of fibril structure into D-banded subfibril and microfibril components would not result in an active substrate for MMP-9 as demonstrated in Chapter 5 (Figures 5.3 and 5.7 B, D).

MMP-9 has long been known as a gelatinase and was only recently shown to cleave soluble collagen.[146-150,180] This suggests two possible options which would result in collagen molecular aggregates becoming an active substrate for MMP-9: increased molecular gyration exposing the ¾ - ¼ cleavage site characteristic of MMP collagenases and gelatinases, or the denaturation of the collagen molecules.[146-150,179]

In this thesis, the loss of the characteristic D-band structure of a collagen fibril was associated with increased water uptake, resulting in increased molecular gyration, independent of the origin of damage (Figures 2.5.6, 3.8, 3.9, 5.6 and 5.7).[54-56,58] This permanent mechanical alteration to fibril structure is unlikely to be independent of molecular denaturation due to the, interlinked, cohesive nature of fibrillar collagen facilitated by covalent crosslinks. Evidence of D-banded segments of the shell structure persisting through MMP-9 incubation supports molecular denaturation as the avenue in which MMP-9 solubilizes collagen from discrete plasticity fibrils (Figures 5.7 B, D). It is likely that the molecular denaturation is associated with stress localization at inter-fibril crosslink sites and that increases in molecular gyration only play a minor roll in collagen solubilization by MMP-9.[146-150, 180]

6.1.2 Trypsin digestion of isolated fibrils and bulk tendon, improvements by a single fibril assay

The results presented in Chapter 5 clearly demonstrate that trypsin does not function as a probe of molecular denaturation on collagen fibrils (Figure 5.2, 5.3 and 5.4). However, trypsin did function as a probe of progressive fibril damage as measured by serial kink density and amount of solubilized collagen. (Figure 5.4 and Table 5.2). A similar trend is observed in bulk tissue studies, demonstrating a 2.2-2.6% solubilization of unloaded bulk tendon by trypsin at temperatures ranging from 4-30°C, and with progressive cyclic overload.[14] The ability of trypsin to cleave native collagen fibrils in this thesis could be associated with the decellularization technique employed. Recent work has shown increased binding of a collagen hybridizing peptide (CHP), which functions as a probe for molecular denaturation, following the use of 3% Triton-x100 during a 24h decellularization process of porcine ligament.[246] Within the same cited paper, porcine ligaments decellularized with sodium dodecyl sulfate (SDS) demonstrated a significant decrease in CHP binding as a function of SDS concentration.[246] The decellularization protocol used in this thesis, includes a 24h incubation with Triton x-100 at a concentration of 0.01% (Appendix E). This is 1/300th of the concentration used in the CHP porcine ligament study.[246] Considering the difference in concentrations of Triton x-100 in the cited study and that used within this thesis, coupled with decreased CHP binding with decreased SDS concentration, it is unlikely that the concentration of Triton x-100 significantly contributes to the digestion of collagen fibrils by trypsin in Chapter 5.

Comparison between trypsin digestion of isolated collagen fibrils and bulk tissue demonstrates the sensitivity of the isolated fibril enzymolysis assay presented in this

thesis.[14] Solubilization of bulk overloaded tendon containing discrete plasticity by trypsin was ~4% greater than unloaded bulk tendon.[14] In contrast, solubilization differences between isolated unloaded fibrils and those displaying discrete plasticity are 20% (Figure 5.3, D). The difference in collagen solubilization by trypsin between isolated fibrils and bulk tendon is likely due to the non-uniform generation of discrete plasticity in bulk tendon due to heterogenous loading.[12] Compounding the discrepancy between bulk tendon and isolated fibril enzymolysis are differences in the method of measurement of solubilized material. The hydroxyproline assay for solubilized collagen employed in the bulk tendon study is likely an under estimation of solubilized material. The molecular regions of fibrillar collagen most likely to be cleaved by trypsin are the thermally labile regions due to micro-unfolding events.[51,55,242] By definition, these regions are devoid of hydroxyproline and would go undetected by this assay.[25,51,54,55,245]. The isolated fibril assay used in this thesis directly measures the change in fibril dimension following enzyme incubation, and as such is not limited by the amino acid content of the solubilized material for detection.

6.1.3 HRM as a local measure of collagen thermal stability

The thermal stability of a collagen molecule within a fibril is adequately described by the polymer-in-a-box model.[58] The foundation of this model is based upon minimization of molecular conformational entropy associated with confinement by neighboring molecules (molecular density), and crosslinking (crosslink density).[58,59] In Chapter 2, it was demonstrated that the HRM of isolated collagen fibrils is inversely correlated to water content of the fibril, and as such, molecular density (Figure 2.5). The 4/5's variation in HRM associated with the D-band of a hydrated collagen fibril (Figure 2.2) coupled with

the minimal variation in the longitudinal ZFH (Figures 4.2, 4.3 and Table 4.1) supports the HRM as a relative measure of localized variations in fibril hydration per molecule, and molecular density.[5]

Data presented in Chapters 2 and 4 support the notion that HRM is also sensitive to localize fluctuations in crosslink density. In Chapter 2, the HRM of *in vitro* reconstituted collagen fibrils, containing no mature crosslinks, (Appendix A, Figure 8) is an order of magnitude less than that of fibrils sourced from 2-year-old rat tail tendon which are heavily crosslinked (Figure 2.1, Table 2.1). While the presence of crosslinks is not directly measured in this study, it is possible that the discrepancy in HRM between the two fibril types is partially dependent on the known discrepancy in crosslinking between them. The notion that HRM is sensitive to crosslink density within a fibril is further supported by the micron-scale variations in HRM along individual collagen fibrils as discussed in Chapter 4 (Figure 4.4).

The dependence of the HRM of collagen fibrils displaying discrete plasticity on serial kink density, presented in Chapter 3, allows the comparison between the HRM of isolated fibrils displaying discrete plasticity with the thermal characterization of bulk overloaded tendon displaying discrete plasticity. DSC endotherms of overloaded tendons displaying discrete plasticity demonstrate a decrease in onset and peak denaturation temperatures as well as total enthalpy of denaturation (Figure 1.8). The total enthalpy of denaturation has been demonstrated to be inversely correlated to the number of overload cycles performed on a tendon.[14] in turn, the number of overload cycles performed on a tendon are positively correlated to mean serial kink density on fibrils displaying discrete plasticity.[14] The result is a negative correlation between kink density and total enthalpy

of denaturation.[14] Data presented in Chapter 3 presents a similar negative correlation between mean serial kink density and HRM (Figure 3.6). As such, both the HRM of collagen fibrils displaying discrete plasticity and total enthalpy of denaturation of overloaded tendon displaying discrete plasticity are inversely correlated to serial kink density. This similar trend of HRM and total enthalpy of denaturation on kink density further supports the hypothesis that HRM is a measure of local molecular stability along a collagen fibril.[14]

6.1.4 Novel longitudinal heterogeneities of collagen fibrils

The four studies presented in this thesis (Chapters 2-5) follow a common pattern: (i) isolate fibrils from unloaded or overloaded samples, (ii) expose them to some alteration via hydration, temperature exposure, enzyme incubation or combinations there of, and (iii) quantify their response via novel AFM methodologies. A common outcome of the studies are various heterogeneous radial and longitudinal responses of the collagen fibrils to whichever combination of treatments they were exposed.

Longitudinal heterogeneities in fibril structure are presented throughout chapters 2-4. They included: the 4/5's molecular density D-band fluctuation in the HRM (Figure 2.2 and Table 2.1), a decrease in HRM due to structural irregularities (Figure 2.3), serial kink and inter-kink regions of isolated fibrils displaying discrete plasticity (Figures 3.5 and 3.9), and micron-scale variations observed in the HRM of unloaded fibrils (Figure 4.4). The most relevant of these discoveries is longitudinal heterogeneities of collagen fibrils is the pre-existing, micron-scale variation in unloaded collagen fibrils. This longitudinal heterogeneity occurs at a similar length scale as kinks along fibrils displaying discrete

plasticity (Figure 4.6). This finding is suggestive of a cause-effect relationship between the two structures.

6.1.5 Discrete Plasticity suggests a novel collagen fibril model

Fibril damage motifs have commonly been used as an investigative tool into native fibril structure.[36,38-40] The previously presented models of fibril structure, the tube-like and rope-like models, were both proposed following AFM investigations of structural irregularities (damage) along collagen fibrils and a known molecular pitch within collagen fibrils.[36,38] The AFM investigations performed in this thesis on thermally damaged fibrils and those displaying discrete plasticity revealed a pitched subfibril structure (Figure 2.6, E) and sequential kink structures (Figures 3.8 and 3.9) reminiscent of the laid rope damage motif termed “axial compression fatigue”. Axial compression fatigue in laid ropes is characterized by serial Z-shaped kink structures along the length of the substructures within a laid rope, similar to the kink structures observed in discrete plasticity. In this model, the radially dependent strain response of a laid rope results in a localized, compressional force at the center of the rope upon relaxation of the applied strain, resulting in kink structures.[41]

Within the laid rope strand model, the location of the axial compression fatigue kinks is thought to be predetermined by regions of low torsional resistance.[41] The local minima in the HRM associated with micron-scale variations along unloaded collagen fibrils could function as regions of low torsional resistance, predetermining the location of kinks in fibrils displaying discrete plasticity. Support for this hypothesis is found in Chapter 4, where both kink spacing and micron-scale variation HRM distributions have a log-normal

distribution and similar scale and shape parameters (6.65, 0.66), (6.35, 0.44). Taken together the: micron-scale fluctuations in a fibril's HRM (Figure 4.4), similarity between discrete plasticity and axial fatigue compression kink structures, and the structural evidence of a radially dependent rope-like collagen fibril (Figure 2.6 D) strongly suggests a collagen fibril is adequately modeled as a laid rope strand and that discrete plasticity is formed in the same manner as axial compression fatigue.[38,39,41]

6.1.6 Comparison of mechanical and thermal damage on isolated collagen fibrils

In this thesis, mechanical overload and thermal damage motifs were studied at the isolated fibril level. Mechanical overload of bulk tendon resulted in discrete plasticity, a damage motif characterized by longitudinal heterogeneous kink damage and a radially dependent shell layer along individual fibrils within the tendon (Figure 3.9). Heating isolated fibrils in deionized water resulted in the loss of fibrillar D-band (Figures 2.6, and 5.2, C and D). The qualitative observations of the thermal damage suggest that alterations in fibril structure progressed from the ends of the fibrils on the AFM sample plate with a radial dependence, resulting in a conical D-banded interface between damaged and native regions reminiscent of the conical tips observed during fibrillogenesis (Figure 5.2, C and D).[29] Observed minima in local HRM at fibril ends coincide with increased molecular gyration and decreased thermal stability, supporting this hypothesis (Fig. 2.3 and Appendix A, Figure 6).

Incubation with trypsin or MMP-9 removes all thermally damaged, non-D-banded material (Figure 5.2 C and D). The complete removal of thermal damage by both

enzymes demonstrates the uniform alteration of the collagen molecules in the non-D-banded regions of the thermally damaged fibrils. In contrast, both trypsin and MMP-9 did not fully remove the shell layers associated with discrete plasticity, demonstrating a non-uniform radial damage associated with the shell layer (Figures 5.6 and 5.7). As such, the outer layers of bovine tail tendon collagen fibrils are more damaged by thermal exposure than bulk tendon mechanical overload. Whether this is a result of the uniformity of either treatment (inhomogeneous, longitudinal loading vs. homogeneous temperature exposure) or the source of damage (mechanical or thermal) is uncertain.

The evidence provided in the previous paragraph supports the notion that thermal damage and mechanical damage are different at the fibril level. As such, the damage incurred at the fibril level from the treatments must be fundamentally distinct. Thermal denaturation is initiated at the thermally labile regions of the collagen molecule and progresses over the length of the fibril.[51,55] The denaturation process affects all three α-chains, resulting in molecular melting into a semi-random-coil structure without breaking any covalent bonds.[47-59] Alternatively, collagen denaturation from mechanical overload favors local denaturation associated with tensile forces transmitted through intermolecular covalent crosslinks as demonstrated by molecular simulation.[121,125,126,221] This would result in a partially denatured stable state of collagen molecules following mechanical overload. The complete solubilization of non-D-banded regions on thermally damaged collagen fibrils and partially solubilization of fibrils displaying discrete plasticity, coupled with DSC and enzymolysis studies in the literature, support the hypothesis of a partially denatured molecular state in fibrils displaying discrete plasticity.[12-14]

6.1.7 Cellular response to denatured collagen and collagen fibrils

The ability of macrophages to recognize collagen conformation and aggregation is well documented, but only recently has been observed following mechanical overload of tendon.[153,250,251] RAW 264.7 murine macrophages demonstrated an 8-10 fold increase in adhered cell count to monomeric collagen, thermally denatured fibrillar collagen and fibrillar collagen treated with Clostridium hystolytical collagenase, when compared to native fibrillar collagen (an increase from ~7% to ~70% in all cases).[250] Similarly, Macrophage-like U937 cells demonstrated a two fold increase in cell adhesion count (26% to 48%) between acid solubilized bovine type I collagen and its denatured counterpart, achieved by a 100°C temperature bath for 3 minutes.[251] These cells were differentiated into macrophages via PMA prior to adhesion testing, the same as the U937 cells cultured on overloaded tendons displaying discrete plasticity.[153,251]

The ability of macrophage-like U937 cells to recognize discrete plasticity damage was quantified by measuring an increase in MMP-1 and decrease in MMP-9 in cellular releasate from cells cultured on overloaded tendon displaying discrete plasticity when compared to cells cultured on unloaded tendon. While the differences between cellular adhesion tests and changes in cellular releasate are inadequate for direct comparison, both studies report high levels of cell clustering on unloaded tendon and native collagen I when compared to either thermally denatured or mechanically overloaded substrates.[130,251] The similar morphological behaviour, coupled with the quantifiable change in cellular adhesion or releasate of macrophage-like U937 cells to heat denatured collagen I or discrete plasticity suggests that macrophage-like U937 cells are responding

to mechanically denatured molecules present in fibrils displaying discrete plasticity in a similar manner to thermally denatured molecules.[130,251]

Substrate stiffness and architecture are known influencers on macrophage behaviour, with substrate stiffness being positively correlated with macrophage activation.[252-254] The data presented in this thesis conclusively demonstrates that discrete plasticity results in a decrease in substrate stiffness (Figures 3.6) and is thus unlikely to result in increased macrophage activation. Macrophage response to substrate architecture involves cellular alignment on linear architectures (grooves or fibers) and increased inflammatory response upon rough substrates.[254] It has been shown that discrete plasticity is associated with increased linearity of collagen fibrils, providing a favorable environment for macrophage alignment and activation.[113,254] It could be argued that kink formation results in an increase in substrate roughness, but whether or not this is visible to macrophages is uncertain. A specific study isolating substrate roughness at the scale of discrete plasticity from molecular denaturation is required to determine the impact of both increases in fibril linearity and substrate roughness within discrete plasticity.

6.2 Conclusion

This section will discuss the outcomes of each chapter in reference to the hypotheses posed prior to each study. The ability for the resultant data to confirm or disprove each hypothesis will be discussed.

6.2.1 Sensitivity of isolated fibril measurement

Hypothesis 2.1: The HRM of collagen fibrils will increase with increasing AFM tip indentation speeds used in mechanical measurements.

Hypothesis 2.2: Increases in fibril radius associated with water uptake following thermal treatments of collagen fibrils will decrease as fibril HRM increases.

Hypothesis 2.3: High-speed indentation HRM of collagen fibrils is increased with higher molecular density and decreased with lower molecular density.

The novel application of PF-QNM based analysis to collagen fibrils is a powerful tool for quantifying structural variation along individual fibrils and within the large fibril population of a tissue. Hypothesis 2.1 is confirmed by HRM measurements taken at AFM indentation speeds spanning 5 orders of magnitude (Figure 2.1 and Appendix A, Figure 8). The relationship between the indentation speed and HRM was found to be logarithmic in nature, mirroring the relationship between indenter speed and indentation modulus of polymer networks below the glass transition temperature.[199] The intersecting point of the two regions of logarithmic behaviour were used to calculate a characteristic molecular relaxation time of 0.1 ms

The thermal treatment of isolated collagen fibrils results in increases in fibril ZFH (Figure 2.5) resulting in decreases in the molecular density of collagen fibrils. An inverse relationship is observed between HRM and thermal treatments, linking decreases in fibril density with decreased HRM, confirming Hypothesis 2.2. Confirmation of Hypothesis 2.2 and the agreement between the 4/5's molecular density relationship between the gap and overlap of the D-band as measured by X-ray diffraction and the 4/5's gap/overlap ratio found in a fibrils HRM (Figure 2.2 and Table 2.1) provides strong evidence supporting the confirmation of Hypothesis 2.3.[5] Confirmation of Hypothesis 2.3 allows for structural observations beyond the initial scope of the hypotheses such as: decreases in HRM due to structural irregularities along native collagen fibrils (Figure 2.3), the

observation of a micron-scale structural variation reported in Chapters 2 and 4 (Figure 4.4), and the loss of the D-band in HRM following heat treatments (Figure 2.5 C and F). The observed micron-scale variation in fibril HRM was not correlated with a change in fibril dimension as observed in the case of heated fibrils. This led to a new, post hoc hypothesis which includes crosslink density as a contributing factor to HRM sensitivity (Chapter 4) culminating in a new hypothesis, stating that HRM is a measure of localized molecular thermal stability associated with the fibril structure as discussed in section 6.1.2.[58,59]

6.2.2 Quantification of heterogeneous damage associated with discrete plasticity

Hypothesis 3.1: Fibrils displaying discrete plasticity will resemble thermally treated collagen fibrils when measured by high speed PF-QNM, with a lower HRM and increased water content compared to unloaded fibrils.

Hypothesis 3.2: HRM and water uptake by fibrils displaying discrete plasticity will, decrease and increase respectively, with the serial kink density of an individual fibril.

Hypothesis 3.3: HRM and water uptake by fibrils displaying discrete plasticity will be heterogeneous due to the localized nature of discrete plasticity and associated fibril shell.

Findings from the first study presented in this thesis (Chapter 2) greatly influenced the Hypotheses 3.1-3.3 All hypotheses presented in Chapter 3 are confirmed by the data presented in chapter 3. Fibrils displaying discrete plasticity have both: a lower HRM than

unloaded fibrils (Figure 3.6, A and B) and have increased water content (Figure 3.6, E and F), as a function of kink density (Hypothesis 3.1. and 3.2). Hypothesis 3.1 was a direct result of findings presented in Chapter 2, and confirms that fibril response to thermal and mechanical damage follow similar motifs concerning fibril molecular density.

Hypotheses 3.2 and 3.3 combine the previous observations in Chapter 2 with knowledge of the longitudinal heterogeneities along fibrils displaying discrete plasticity (kink and inter-kink sites) and loss of surface D-band (Shell) found within the literature.[12-14] The data presented in chapter 3 clearly demonstrated a progressive decrease in fibril HRM with serial kink density (Figure 3.6, A and B and Table 3.1) and corresponding increase in HRM heterogeneity associated with variations between kink and inter-kink regions (Figure 3.6, A-D, 3.5 and Table 3.1) (Hypothesis 3.2). While direct measurement of fibril shell thickness was not performed, its contribution to decreases in HRM and increases in water uptake were qualitatively demonstrated (Figure 3.8 and 3.9) (Hypothesis 3.3).

6.2.3 Implications for collagen fibril structure

Hypothesis 4.1: Native collagen fibrils will display variations in HRM within a 10μm segment of their length which is described by a distinctive distribution.

Hypothesis 4.2: The distribution of kink spacing along fibrils displaying discrete plasticity will resemble the distribution of fluctuations observed in the HRM of unloaded collagen fibrils.

The observation of a novel micron-scale variation in native collagen fibril structure observed in the HRM of collagen fibrils in Chapter 2 (Figures 2.3 and 2.4) coupled with

kink spacing distributions along fibrils displaying discrete plasticity in the literature lead to Hypotheses 4.1 and 4.2 and the study presented in Chapter 4. Hypothesis 4.1 is confirmed for the tendon model used in this thesis due to the consistent coefficient of variation of the HRM (Figure 4.2 and Table 4.1) and the variation observed along HRM fibril maps (Figure 4.4). Hypothesis 4.2 was not confirmed, but the acquired data strongly supports it. Comparison of the distribution of HRM peak variations along unloaded collagen fibrils and the distribution of inter-kink segment lengths along fibrils displaying discrete plasticity, sourced from tendon pulled to rupture, demonstrate both distributions are described by lognormal distributions with similar scale and shape parameters (Figure 4.6). The difficulty in confirmation lies in the variability in the spacing of the HRM variation along unloaded fibrils (Figure 4.4). As such confirmation of the hypothesis may be beyond the reach of this method.

6.2.4 Quantification of fibril enzymolysis by trypsin and MMP-9

Hypothesis 5.1: Regions devoid of D-banding structure will be the primary substrate for collagen enzymolysis.

Hypothesis 5.2: Trypsin will solubilize more material than MMP-9 from isolated native collagen fibrils and those displaying discrete plasticity.

Hypothesis 5.3: Fibril enzymolysis by trypsin and MMP-9 will be dependent on serial kink density in collagen fibrils displaying discrete plasticity.

Hypothesis 5.1 proposes that fibril enzymolysis will primarily occur in regions devoid of D-banding, due to the availability of more cleavage sites for both enzymes following disruption in the molecular packing of a fibril and accompanying denaturation.

Confirmation of hypothesis 5.1 was not quantifiably achieved but qualitative evidence presented throughout chapter 5 (Figures 5.6 and 5.7) strongly supports the hypothesis.

Confirmation of hypothesis 3.2 implied a similar correlation between serial kink density and enzymolysis was likely, as stated in Hypothesis 5.3. Confirmation of Hypotheses 5.3 is achieved in Chapter 5 by the statistically significant linear correlation between changes in fibril dimension following enzyme incubation and fibril kink density (Figures 5.4, 5.5 and Table 5.2). While the correlation between kink density and enzymolysis is confirmed, there is no definitive confirmation of increased solubilization of fibrils displaying discrete plasticity by trypsin compared to MMP-9 as proposed by Hypothesis 5.2 (Figure 5.3). Instead the fundamental difference between trypsin and MMP-9 is in their respective ability to solubilize unloaded collagen fibrils (Figure 5.3 and Table 5.1). The fundamental concept that led to Hypothesis 5.2 was the larger number of active cleavage sites for trypsin along the collagen molecule than MMP-9. This concept still appears to be the case, but no fibril damage is necessary for a fibril to be partially solubilized by trypsin. Instead, trypsin has more than one active cleavage site along a molecule in an unloaded fibril, allowing solubilization of collagen, while MMP-9 has one or less, preventing solubilization.

Important unpredicted takeaways from this chapter are the selective solubilization of non-D-banded material by MMP-9 and the non-selective solubilization of D-banded material by trypsin (Figures 5.1, 5.3 and Table 5.1). The former has significant implications for the use of MMP-9 as a selective debriding agent, as well as understanding its role in wound healing.[146-148]

6.3 Recommendations

6.3.1 Confirming HRM is sensitive to crosslinking density and a measure of thermal stability

Initially, the HRM was described as a probe of molecular density (Chapter 2). The 4/5's ratio of the gap/overlap structure of the D-band (Figure 2.2 and Table 2.1) and inverse relationship between ZFH ratio and HRM (Figures 2.5 and 3.6) definitively support this approach. The appearance of the micron-scale fluctuation on native collagen fibrils, only observed in the HRM (Figures 2.4 and 4.4), is what first suggested that the HRM was sensitive to more than just molecular density. The presentation of the HRM as a measure of thermal stability in this thesis is a hypothesis which needs validation. To confirm that the HRM is sensitive to crosslink density, a direct study must be performed which directly compares changes in crosslink density of individual fibrils with HRM. This study would ideally combine the application of zero-length crosslinkers, bulk tissue thermal analysis, and single fibril thermal and mechanical analysis as presented in this thesis (Chapter 2).[58-60 247-249] The use of a zero-length crosslinkers, such as EDC, rather than glutaraldehyde would be beneficial as the crosslinking of dense collagenous tissues by glutaraldehyde has been shown to be limited to the surface of collagen fibers.[255] Furthermore, the initial collagen-glutaraldehyde complexes function as nucleation sites for glutaraldehyde-glutaraldehyde interactions resulting in a polymerized shell of glutaraldehyde about individual collagen fibers.[256] The use of glutaraldehyde in the initial study of crosslinking effect on thermal stability in the polymer-in-a-box model, is also called into question due to the previously mentioned limitations of glutaraldehyde-

collagen interaction.[59] This novel study would not only result in determining HRM's sensitivity to crosslink density but clarify the role of crosslinking in the polymer-in-a-box model.

6.3.2 Applications of the single fibril enzymatic assay

This thesis was designed with the goal of quantifying and delineating between molecular and fibril level damage following the mechanical overload of tendon. The development of the single fibril enzymatic assay in chapter 5 proved to be the sharpest scalpel for separating these two levels of damage, depending on the enzyme used. While MMP-9 served excellently as a probe for molecular denaturation, it also answered a physiological question by demonstrating a key aspect of its function *in vivo*, the selective cleavage of denatured molecules from collagen fibrils during tendon debridement.[148] There are two different, yet related, research directions for this technique. The first is the use of other physiological enzymes as probes for molecular denaturation and the construction of a comprehensive library of fibril-enzyme interactions relevant to the *in vivo* response to discrete plasticity. The second is the application of the single fibril enzymatic assay to various tissue models, damage motifs, and genetic alterations either as a probe for molecular structure or for physiological responses.[146-148,151,152] This methodology may also prove useful for non-collagenous structures.

6.3.3 Comprehensive examination of molecular and structural heterogeneities within a collagen fibril

Throughout this thesis, the appearance of radially dependent and sub-structure-dependent heterogeneities within unloaded fibrils and those displaying discrete plasticity is evident.

Using the indentation depth measurement of the AFM revealed a radially dependent shell layer and a D-banded core in fibrils displaying discrete plasticity (Figure 3.9). Additionally, this shell layer is likely more susceptible to solubilization by enzyme incubation (Figure 5.6 and 5.7). These results are supported in the literature following the incubation of bulk overloaded tendon with trypsin.[12]

Both thermal damage of unloaded rat tail collagen fibrils (Figure 2.6, E) and the incubation of isolated fibrils displaying discrete plasticity with MMP-9 (Figure 5.6, G) revealed pitched subfibrillar structures. Subfibrillar structures were also revealed following trypsin incubation of overloaded bulk tendon in the literature (Figure 1.7, D).[12,13] The appearance of subfibrils following both mechanical and thermal damage suggests bulk heterogeneities within the fibril, resulting in some material being more susceptible to thermal and mechanical damage. If this were not the case the response of fibrils to thermal and mechanical alteration would be uniform, and no substructure would appear.

The heterogeneity within a cross-section of the collagen fibril is further supported by the partial enzymolysis of native collagen fibrils by trypsin in chapter 5 (Figures 5.2A, 5.3, 5.4 and Table 5.1). Both the α1 and α2 chains in acid extracted collagen I from rat skin have single active cleavage sites for trypsin 15 and 14 amino acids from the N-terminus respectively. This cleavage site is the only active substrate for trypsin held at 20°C and requires the absence of the enzymatic crosslink typically found at the N-terminus of the α-chains.[242] Taking the thermal, mechanical and enzymatic heterogeneous responses of collagen fibrils into consideration simultaneously, an argument can be made for a subset of molecules existing within the fibril that are more susceptible to thermal and

mechanical damage. With the appearance of subfibrils following thermal or mechanical damage it is likely these molecules exist outside of subfibrillar structures.

Targeted studies incorporating the techniques in this thesis are needed to refine the statement above. Incorporating collagen fibrils sourced from: varying tissue types, animals of different age, genetic knockouts, and in vitro preparations would be essential for parsing out structural heterogeneities in a fibril as a response to known variations within fibril associated with its origin.

Appendix A

Modulus distribution

A simple methodology to extract radial modulus distributions over an entire segment of a fibril that takes into account the effect of the underlying substrate and the shape of the fibril was developed. Fitting different regions of the FD curves has a dramatic impact on the obtained radial modulus distribution. As an example, we extract the radial modulus distribution of a collagen fibril using two different methods. We either fit the upper part of the FD curves between 30 and 90% of the applied peak force (Figure S1, A) or we fit the lower part of the FD curves up to an indentation depth corresponding to 10% of the mean ZFH of the fibril (Figure S1, B) in accordance with Bueckle's rule.(1, 2) The corresponding images and histograms are very different with a mean indentation modulus of 63.5±0.3 and 15.5±0.1 MPa, respectively (Figure S2, A-D). This fourfold overestimation of the indentation modulus in the first method is attributable to the presence of the glass substrate underneath the fibril and highlights the importance of only fitting the FD curves according to Bueckle's rule.(1, 2)However, it is noticeable that in both methods the indentation modulus distribution has a tail on the left side of the main peak (Figure S2, C and D).

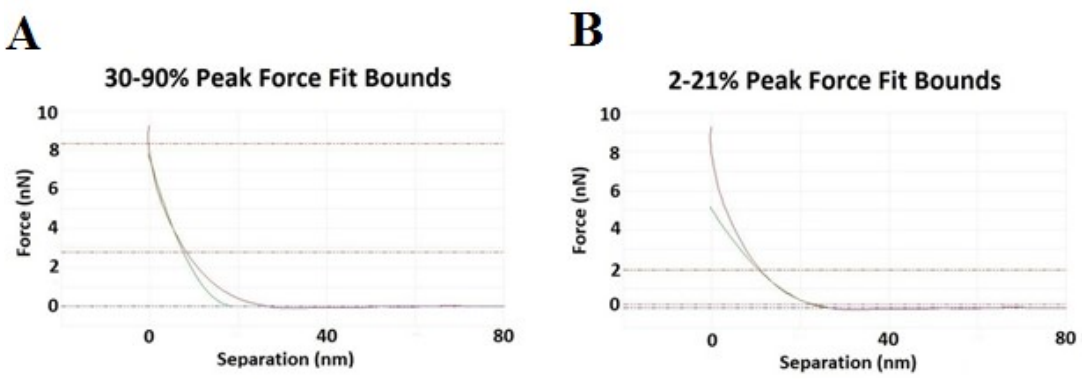

Figure S1: *Regions of fit.* Two different Sneddon modulus fits of a force-separation curve acquired from the apex of a collagen fibril. A) 30-90% peak force fit bounds. B) 2-21% peak force fit bounds corresponding to an indentation depth of 10% of the mean ZFH of the fibril.

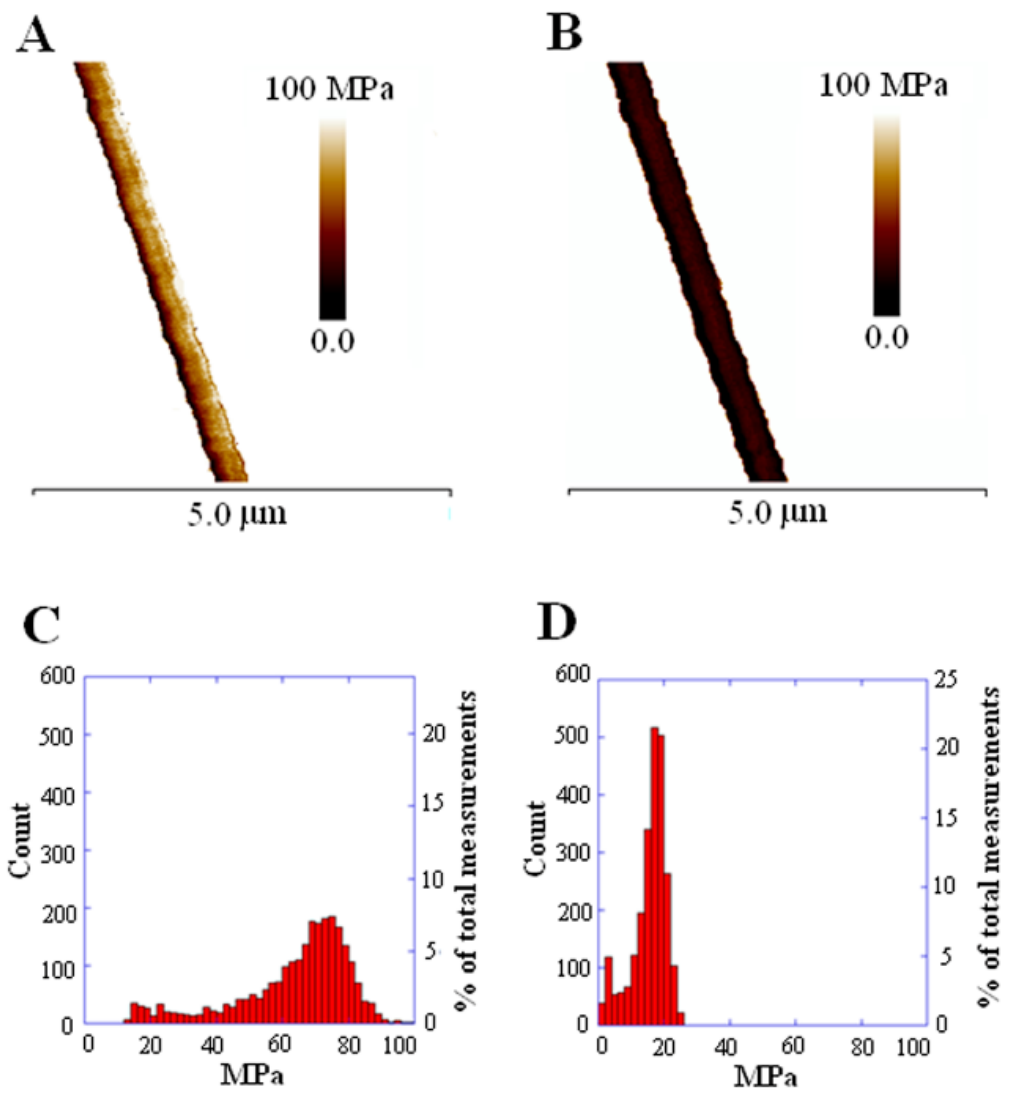

Figure S2: *Effect of the substrate on the modulus (HRM) distribution*. Sneddon modulus (HRM) maps of a collagen fibril. A) Fitting the FD curves in the region between 30 and 90% of the applied peak force. B) Fitting the FD curves up to an indentation depth corresponding to 10% of the mean ZFH of the fibril, 20 nm in this case. C) (n = 2508) and D) (n = 2387) Corresponding histograms of modulus (HRM) distribution. Notice that the first method provides a fourfold overestimate of the modulus (HRM) compared to the second method.

To understand the origin of this tail we look at the systematic variations in peak force associated with the response time of the feedback loop observed in AFM tapping modes (1.7) (Figure S3). The image obtained from the peak force error channel always shows a dark and a bright edge on each side of the fibril (Figure S3 A). Inverting the scanning direction exchanges the bright and dark edges. One possible explanation is that the response time of the feedback loop is too long to accommodate the rapid change in topography on the sides of the fibril. Another explanation is that the bright edge occurs due to coupled cantilever torsion and deflection away from the fibril. This results in an applied force in excess of the set point visible as a spike on the right side of the peak force error profile across the fibril (Figure S3, C). As the tip scans across the fibril the peak force error first (1.7) goes through zero as it passes the apex and then spikes negatively as it slips of the side of the fibril (Figure S3, C), giving rise to a dark edge on the image (Figure S3, B).

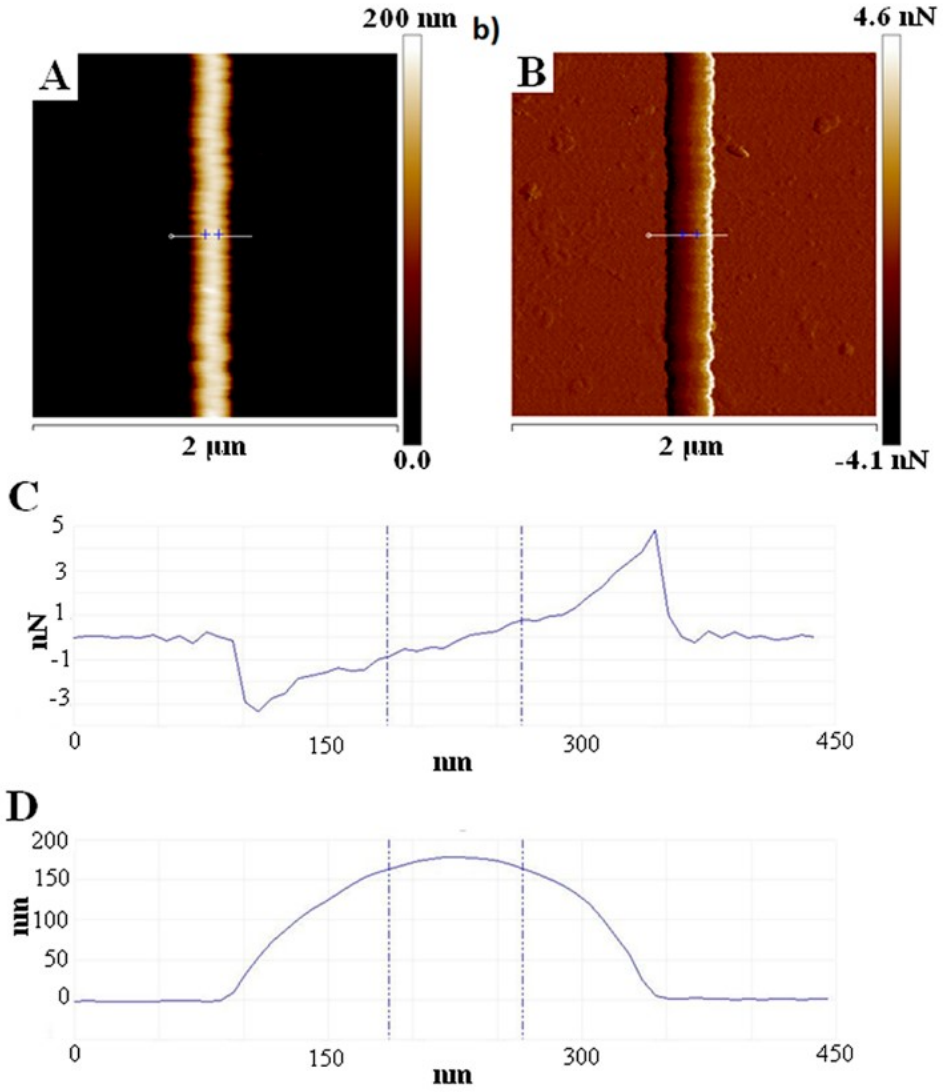

Figure S3: *Variations in applied peak force correlate with sample topography*. Height and peak force error images of a collagen fibril, A) and B), respectively. The peak force set point was 10 nN and the scanning direction was right to left. C) and D) are corresponding line profiles across the fibril. The region where the peak force error is ±10% of the peak force set point (broken lines) corresponds to the apex of the fibril.

Due to the systematic nature of the peak force error profile across a fibril, it is possible to select different regions across the fibril by selecting different ranges of peak force error

(see Supplement S5). Force curves were sorted into 0.1 nN bins to allow accurate fitting parameters to be applied to the sorted force curves due to the uniformity of the applied force within each sorted bin. This becomes relevant when considering the fitting parameters within the analysis software are based on percent peak force per curve and not on specific force values.

The modulus (HRM) distributions extracted from a 5 by 5 μm image are shown for an entire fibril (Figure S4, A), the left side corresponding to negative peak force error (Figure S4, B), the right side corresponding to positive peak force error (Figure S4, C), and the apex corresponding to minimal peak force error (Figure S4, D). The tail in the distribution obtained for the full fibril is associated only with the left side of the collagen fibril (Figure S4, B) whereas the positive peak force error on first contact is responsible for a broadening of the main peak (Figure S4, C). The distribution obtained from the apex of the fibril is Gaussian with a standard deviation of 2.5 MPa giving rise to an estimate of the modulus (HRM) with an accuracy better than 1% at 18.63±0.07 MPa (Figure S4, D). This is not the absolute accuracy of the measurement since the cantilever spring constant calibration is only 10% accurate, but it shows the potential of the approach to detect fluctuations in HRM along the length of a fibril or before and after modifications of a fibril by an external factor such as temperature or pH.

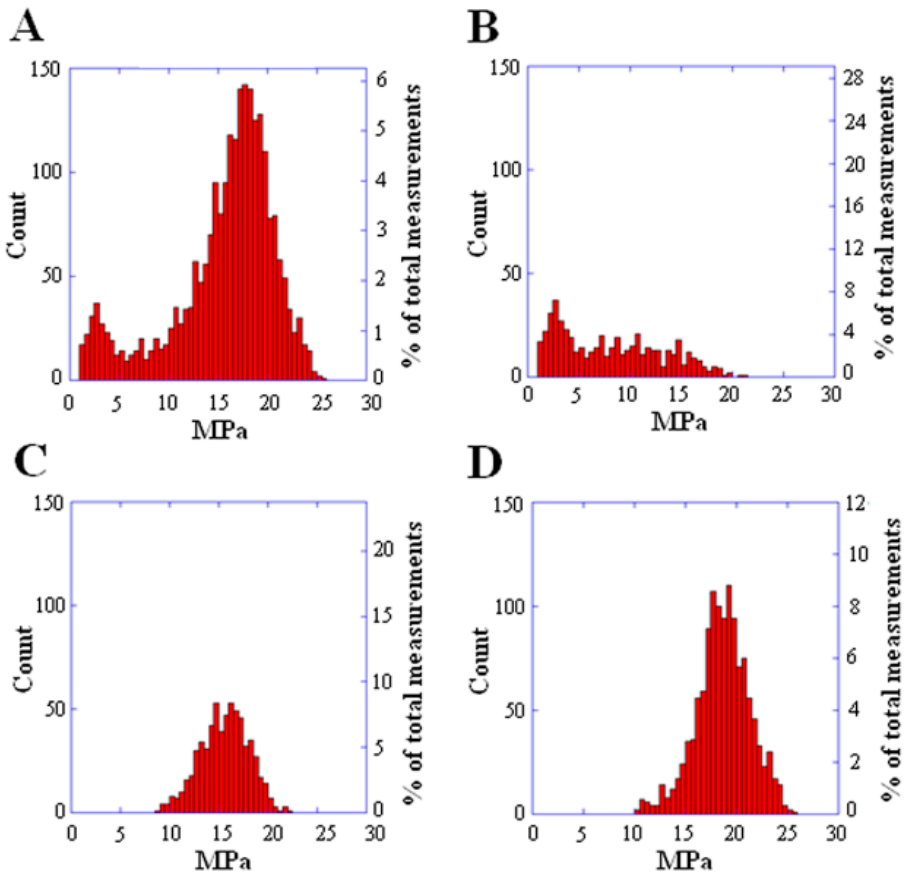

Figure S4: *Selecting the apex of the fibril using the peak force error*. Modulus (HRM) distributions extracted from a 5 by 5 μm image of a collagen fibril according to Bueckle's rule (ref). A) Entire fibril, peak force error ranging from -5 nN to +5 nN. B) Region where the tip slip on the fibril side, peak force error ranging from -5 nN to -1 nN. C) Region where the tip first contacts the fibril, peak force error ranging from +1 nN to +5 nN. D) Apex of the fibril, peak force error ranging from -1 nN to +1 nN. The peak force setpoint was 10 nN as in figure 2. The total number of force curves (n) of each region, a-d, are 2297,515, 632, and 1250 respectively.

Supplement S5

Sorting Algorithm (MATLAB v7.10.0)

```
DataSourceFolder =('C:\Users\Sam\Desktop\before\');%make sure it ends with a \
DataSortedFolder =('C:\Users\Sam\Desktop\after\'); %make sure it ends with a \


LowBound =(0)
HighBound = (22)
SEnN = (.1)  %Sorting by this many nN  MAKE SURE THAT FOLDERS
GENERATED ARE ALWAYS A FACTOR OF AN INTEGER.
SD = (1/SEnN)  %Sorting Denominator



LowerBound= (LowBound);
UpperBound= (HighBound*SD);
BoundRange=[LowerBound:UpperBound];


%Making Destination Folders


mkdir(DataSortedFolder)
for x=(BoundRange)
    str = num2str(x/SD);
    MakeFolders = strcat(DataSortedFolder,str);
    mkdir(MakeFolders)
```

```
end
UBoundFolder=strcat(DataSortedFolder,'Above Upper Bound');
mkdir(UBoundFolder)
LBoundFolder=strcat(DataSortedFolder,'Below Lower Bound');
mkdir(LBoundFolder)

%Defining Nanoscope utilities
NS = NSMatlabUtilities();

F = dir(DataSourceFolder);
F = F(~[F.isdir]);
NumberOfFiles = length(F);

%CHECK TO SEE I AF NEEDS TO UPDATE WITH EACH LOOP AKA IT LOOKS
FOR (1,1)
%and its GONE after first go
for p=[1:NumberOfFiles]
   FN = {F.name}; %FileNames=FN
   AF = FN(1,p); %ActiveFile=AF
   AF = AF{1};  %Reads Cell element as a string
   TAF = strcat(DataSourceFolder,AF);%TAF= total active file path
   NS.Open(TAF)
```

```
    [xTrace, xRetrace, yTrace, yRetrace, xLabel, yLabel] = NS.CreateForceZPlot(1,
NS.FORCE, 0);
    PF = max(yTrace);
    for x=(BoundRange);
        if ((x/SD)> PF+SEnN)
            break;
        end
        if ((x/SD)>PF)
            XS=num2str(x/SD);
            TargetFolder = strcat(DataSortedFolder,XS);
            movefile(TAF,TargetFolder)% EX if moved to folder 9 the PF is between 8 and 9
            %WHEN USEING FITTING SOFTWARE USE %BOUNDS AJUSTED FOR
THE
            %MIDDLE OF THE RANGE EX 6-7 BOUNDS ARE AT 6.5nN
        elseif (PF>UpperBound)
            movefile(UBoundFolder)

        elseif (PF<LowerBound)
            movefile(LBoundFolder)
        end

    end
end
```

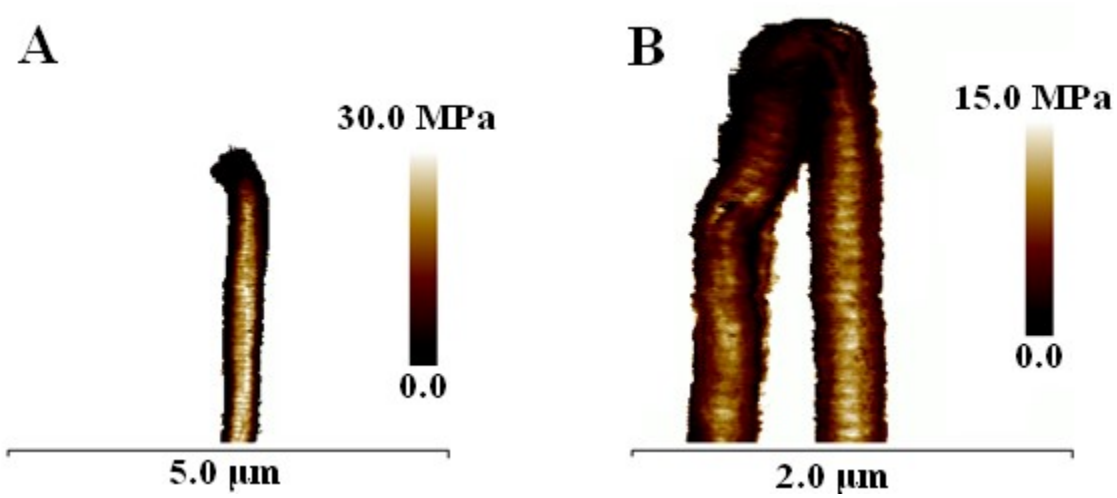

Figure S6: *Modulus (HRM) maps of mechanical alterations*. A cleaved collagen fibril (a) and a sharp bend (b). The D-period is observed in the surrounding regions demonstrating a decrease in mean HRM, but not at the localized site of alteration.

Collagen assembly *in vitro*.

In vitro collagen fibrils were synthesized from rat tail collagen I purchased from (Sigma, St. Louis, MO). The collagen molecules were diluted in PBS to a concentration of .2mg/ml. Such solutions were incubated ate 37°C for 1 hour after which 0.5 ml of solution was deposited onto a glass bottom dish. After 1 hour the samples were trice rinsed with deionized water to remove residual salts. During the washing process careful technique ensured the sample remained hydrated. The hydrated sample underwent mechanical measurement as previously described or was stored at 4°C until use. The fibrils formed were polydisperse in their dimensions, while only those with a greater than 200nm were used for the acquisition of figure S8. The fibrils displayed no D-period when hydrated, but it appeared upon dehydration. Interestingly the *in vitro* fibrils displayed a twisting structure in the Sneddon modulus channel similar to that of *ex vivo* fibrils after temperature exposure.

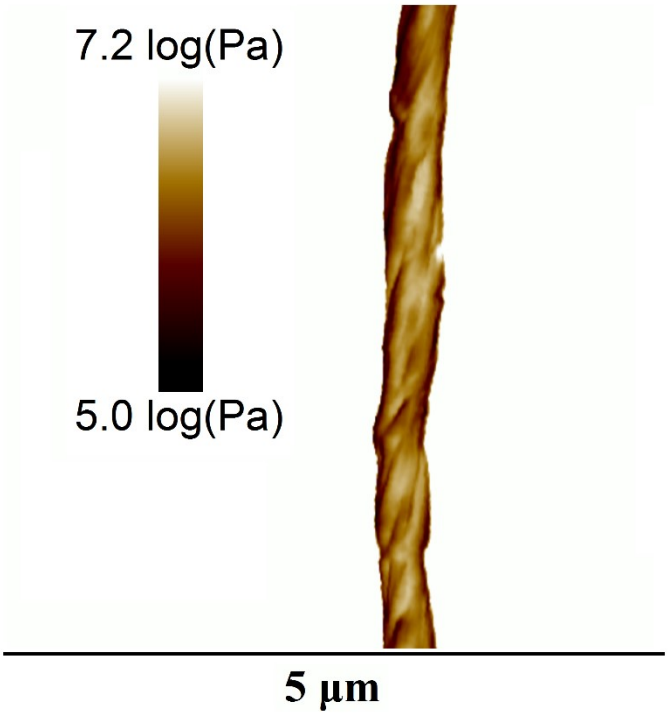

Figure S7: *Twisted structure of in vitro fibrils in Sneddon modulus.* The log Sneddon modulus (HRM) map of an *in vitro* fibril acquired at 1200 µm/s.

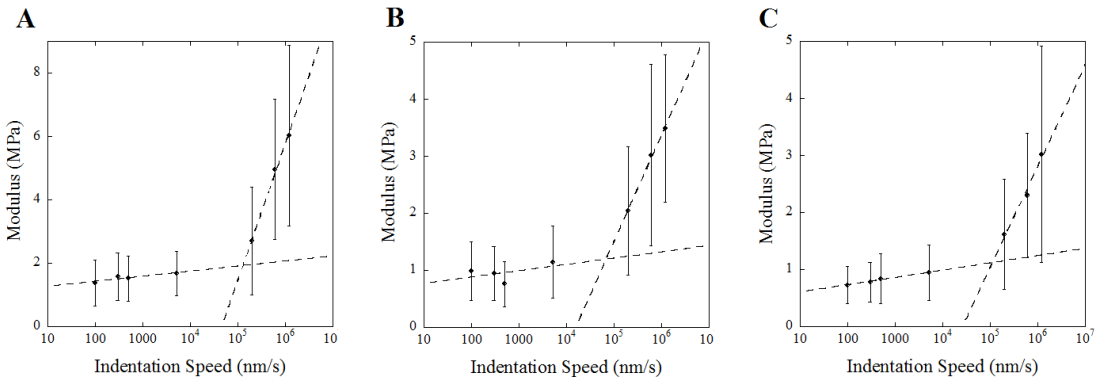

Figure S8: *Dependence of the HRM of in vitro fibrils with indentation speed*. The HRM of three, 5µm segments of different *in vitro* assembled collagen fibrils as a function of indentation speed. Logarithmic least square fits of the data highlight the presence of two distinct regimes.

Supporting references

1. Persch, G., C. Born, and B. Utesch. 1994. Nano-Hardness Investigations of Thin-Films by an Atomic-Force Microscope. Microelectronic Engineering 24:113-121.
2. Bueckle, H. 1973. The Science of Hardness Testing and its Research Applications. American Society for Metals, Ohio.

Appendix B

Figure 1: The mean dehydrated and hydrated ZFH's of the control and overloaded fibrils. From this we observe that it is likely that overloading does not result in the removal of material from fibrils, but only alters the molecules, changing their fundamental interaction with water.

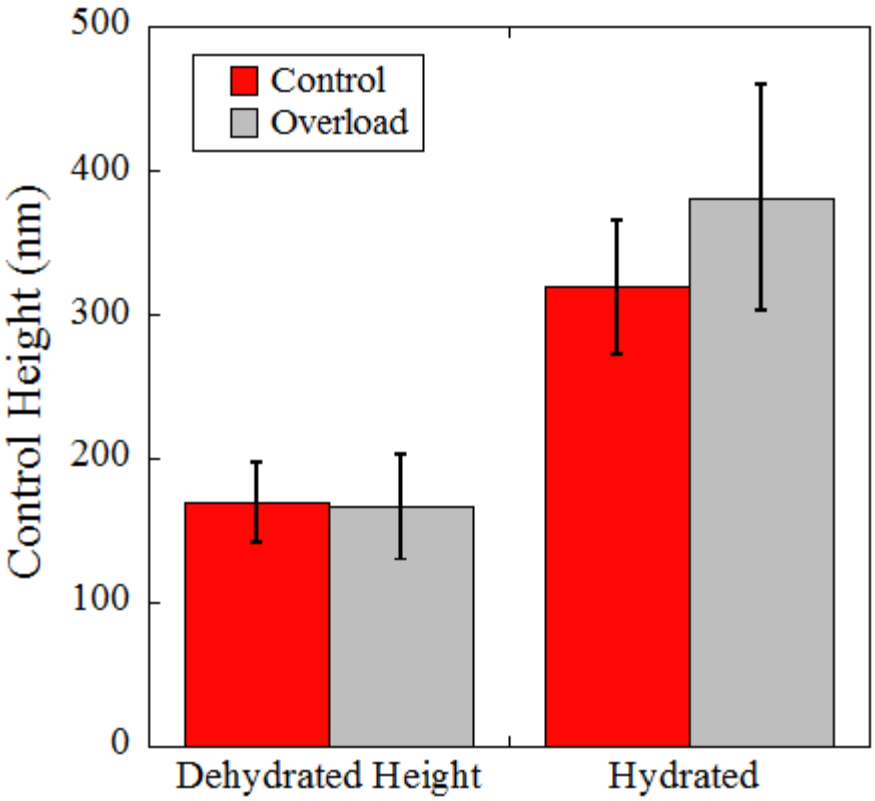

Appendix C

JMP software (version 11.0.0, SAS Institute Inc.) was used for all statistical analysis. A 1-way ANOVA was performed for dehydrated ZFH, hydrated ZFH, swelling ratio, HRM, coefficient of variance of the HRM, gap/overlap HRM ratio, and the D-band period, with the variable of five animal individuals. Scatter plot data were examined for correlation via least squares regression fit.

Table S1: Mean values of measured fibril properties by individual animal.

Animal	Hydrated ZFH (nm)	Dehydrated ZFH (nm)	Hydrated/ Dehydrated ZFH Ratio	HRM (MPa)	HRM D-Period (nm)	Gap/Overlap HRM Ratio
A	339±51	168±30	2.24±0.12	19.7±3.4	66.6±1	0.86±0.02
B	320±49	152±12	1.91±0.09	14.6±1.8	67.2±0.3	0.76±0.01
C	300±35	177±20	1.70±0.07	17.8±4.2	67.7±0.1	0.77±0.04
D	350±23	188±16	1.86±0.04	17.3±3.2	68.0±0.6	0.82±0.01
E	287±55	162±37	1.78±0.13	17.2±5.7	67.7±0.7	0.85±0.03
Mean	320±10	169±6	1.9±0.2	17.3±3.9	67.5±0.2	0.813±0.009

Table S2: Coefficient of variation data by individual animal and measured property.

Animal	Dehydrated ZFH (nm)	Hydrated ZFH (nm)	Hydrated/Dehydrated ZFH Ratio	HRM (MPa)
A	0.029±0.005	0.022±0.003	0.036±0.006	0.22±0.02
B	0.030±.008	0.05±0.03	0.06±0.03	0.19±0.03
C	0.04±0.01	0.04±0.02	0.06±0.02	0.21±0.03
D	0.029±0.005	0.04±0.01	0.05±0.01	0.20±0.01
E	0.035±0.009	0.04±0.02	0.05±0.02	0.21±0.05
Mean	0.032±0.002	0.038±0.005	0.05±0.004	0.209±0.005

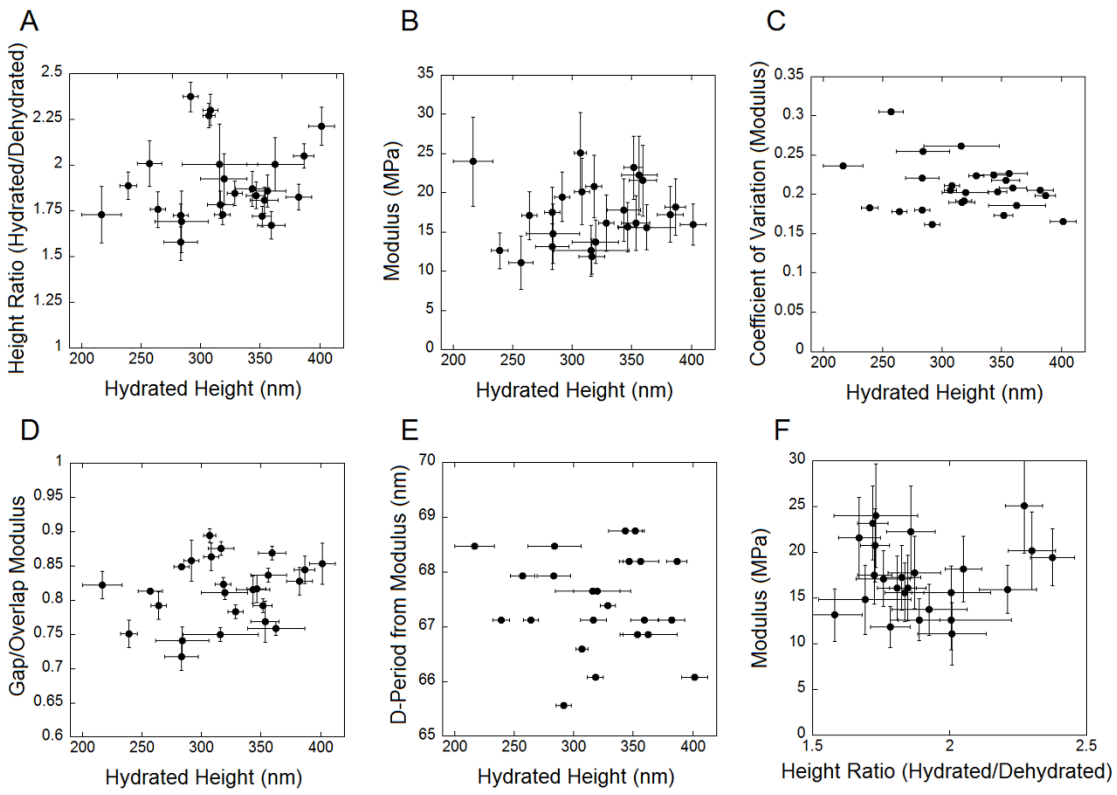

Figure S1: Dimensional dependence of collagen fibril properties. Scatter plots of the: hydrated/dehydrated ZFH ratio (A), modulus (HRM) (B), coefficient of variation of the modulus (HRM) (C), gap/overlap modulus (HRM) ratio (D) and modulus (HRM) channel D-period (E) as functions of hydrated ZFH which serves as a proxy for fibril diameter. No correlation was found between any of the five properties and fibril size. The HRM of each fibril is also plotted as a function of its hydrated/dehydrated ZFH ratio (F). Again, no significant correlation was observed, suggesting that water uptake is not a determinant of the mean HRM for the fibrils. Each point is the x-y mean ± SD.

Appendix D

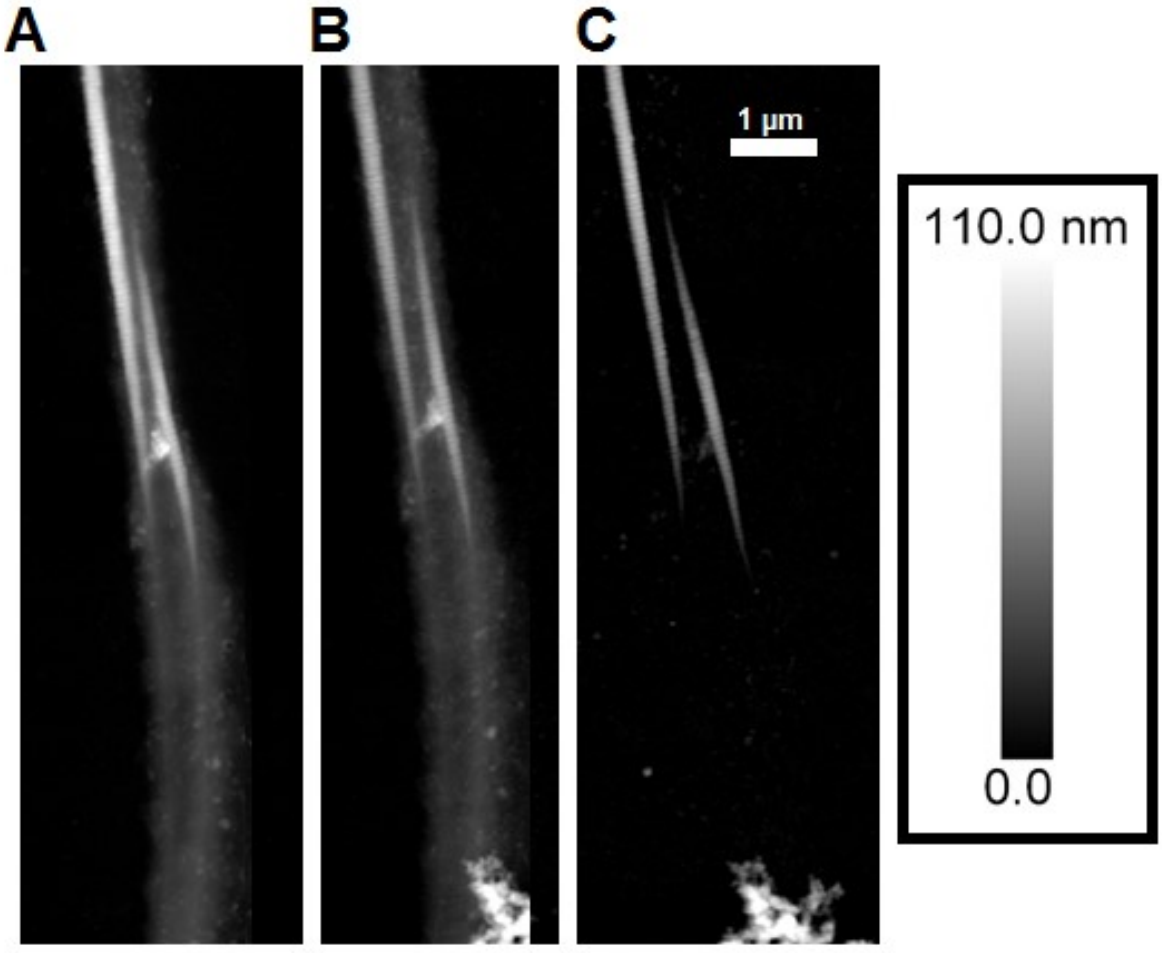

Figure S1: Sequential dehydrated imaging of heated collagen fibrils. (A) before incubation with solution 1 (containing trypsin and serine protease inhibitor). (B) after incubation with solution I., (C) after incubation with solution 2 (trypsin, no inhibitor) (C). The images were taken in the above sequence. No enzymolysis occurred in the presence of the serine protease inhibitor (Solution 1), (B), but did occur following incubation with trypsin in the absence of the serine protease inhibitor (C). This demonstrates the full inhibition of trypsin to cleave heated collagen fibrils in the presence of the serine protease inhibitor.

Appendix E

Adapted Lab Resource from M.J. Lee Biomechanics Lab, Dalhousie University

Day before Abattoir:

Determine the number of Tails you will need and the amount of tissue you will be harvesting, then determine the volume of solutions required. Autoclave appropriate glass containers with stir bars:

For solutions: 2 L beakers, 1.5 L beakers

For pouring: 150 mL beakers (1 for each solution change)

For water: Glass bottles (will fill with sterile water from the 4th floor)

For dissecting: 2 tweezers, 1 metal spatula, 1 scalpel

Make PBS (add fungizone and P/S right before using)

Make Solution A (without P/S or PMSF)

Day 1:

Collect whole, skinned, tails from abattoir. Place in bags, then coolers of ice.

Return to the lab (~1h) and remove proximal dorsal tail tendons from each tail.

Place tendons into PBS (~50 ml per tail) until all desired tendons have been removed. This serves to keep the tissue hydrated at physiological pH.

Split tendons into 50mL Falcon Tubes labeled with Animal identification. Fill with PBS solution plus 1 % Amphotericin B and 1% Pen/Strep (~30 mL).

Using a cutting board cut each tendon into 2 pieces, (1 cm in length and ~5-6 cm in length). The 1cm piece will serve as a paired control to the overloaded 5-6 cm section of tendon (The long blades work better than surgical blades). Place paired tendon samples into 20ml Falcon Tubes, labeled with animal identification and tendon number.

Store at 4°C until overload procedure (~1-3h)

Overload 5-6 cm section of tendon, cut clamped ends at 45° from tendon axis to differentiate from control sample. Return overloaded tendon to 20ml Falcon Tube containing paired sample.

Replace old PBS with new PBS and wash on shaker table for 30 minutes (120 rpms)

Replace PBS again with new PBS (containing 1% inoculants) (~20 mL).

Wash on shaker table for 30 minutes. Repeat one last time using only 20 mL.

Make sure Solution A contains PEN/STREP and PMSF

Replace PBS with 50 mL of Solution A.

Day 2

Total Solution A rinse should be ~ 30 hrs at 4 C, replace Solution A every 12 hours (The final rinse of Solution A is more important to finish at a decent time in the Morning so that the rest of the process is not completed in the wee hours of the night).

Make sure Solution B contains PEN/STREP and PMSF

Day 3:

Exchange Solution A for equal amounts of Solution B (20 mL), then place on a shaker at 4 C for 24 hours, replace Solution B every 12 hours with equal volumes (20 mL).

Day 4:

Turn on water bath to 37 C

Get ice for DNase and RNase

Thaw appropriate aliquots of DNase and RNase solutions at room temperature (once thawed keep on ice)

Rinse all tubes with 50 mL of prepared water for approximately 30 min at room temperature.

Rinse all containers with equal amounts of Hanks/Hepes Solution (50 mL) for approximately 30 minutes at room temp. (Try to keep Hanks as sterile as possible, e.g. pour in flow hood, keep covered, etc. but don't filter, use sterile water)

Everything in flow hood so the tissue is never exposed to tainted air.

While tissue are rinsing with Hanks, label new tubes, fill with 25 mL of Hanks, add enzymes to these filled tubes. 166.67 ⌈L of each enzyme/ 25 mL of Hanks (for a tissue that is ~ 3.7 cm x 3.7 cm or ~ 1369 mm^2). **Do this in the flow hood.**

In flow hood, transfer the pieces into the enzyme cocktails. Place in water bath and shake for 1 hr at 37 C.

In flow hood, rinse enzyme cocktails with new Hanks/HEPES (50 mL), then in the order you rinsed, replace with Solution C. (Try to keep solution C as sterile as possible).

Shake containers for 24 hours at room temperature. Replace Solution C every 12 hours.

<u>Day 5:</u>

Replace Solution C with sterile PBS (50 mL) with PEN/STREP and Fungizone cocktail (1%)

Rinse at room temperature for 30 minutes.

Replace with sterile PBS with PEN/STREP (1 %), without Fungizone. Rinse for 30 min at room temperature. Repeat once (50 mL).

Replace with sterile PBS with PEN/STREP (1%) and wash at room temperature for ~ 46 hours.

NOTE: If using pH 9.0 wash, replace Solution C with pH 9.0 solution then rinse for 24 hrs with an exchange every 12 hours. On Day 6 do PBS rinsings

Day 6: Do nothing

Day 7:

Label sterilized glass bottles. Place sterile tissue into bottles, try not to touch the edges of the lid. Using sterile PBS and PEN/STREP (1%), pour ~ 30 - 40 mL of cocktail into bottles. Wipe tops of bottles with ethanol wipe to remove any droplets before tightening lid.

Store in Refrigerator Indefinitely.

Solutions

PMSF Stock

- Measure 100 mL ethanol
- 5 g PMSF as delivered
    - © add enough ethanol to dissolve PMSF in original container
    - © transfer by pipette to an amber bottle
    - © add remaining ethanol up to 100 mL
- seal amber bottle, wrap in tinfoil, label and leave in hood

DNase Stock

- prepare culture hood
- dissolve 0.175g NaCl in 10 mL sterile water
    - © adjust pH to 7.3 (0.01M stocks)
- add 10 mL glycerol and mix

- IN HOOD: dissolve 200, 000 units DNase in **15 mL** NaCl/glycerol solution

    - © Pipette 900□L aliquots into 1.5 mL cryovials
    - © Label, store in deep freeze (-80 °C)

    - © THAW FOR USE AND DO NOT REFREEZE

RNase Stock

- prepare culture hood
- weigh out: - 0.03 g Tris Base
  - 0.22 g NaCl

- In Hood: add to 25 mL sterile water
  - © Allow to dissolve without agitation
  - © Adjust to pH 7.5 using 0.01 M stocks NaOH/Hcl

  - © Mix **20 mL** Tris Base/NaCl and 250 mg Rnase protein
    - Allow to dissolve without agitation

  - © Transfer 900 □L aliquots to cryovials
    - Label and store in deep freeze (-80°C)

  - © THAW FOR USE AND DO NOT REFREEZE

Solution A

- Autoclave 2 L beaker, stir bar, water, storage bottle

- For 2 L solution of A:

  - © In ~1900 mL sterile water, dissolve:
    - 2.41 g Tris Base (10 mM)
    - 2.92 g EDTA (5 mM)

    - adjust to pH 8.0 using 0.1 NaOH/Hcl stocks

  - © top off to 2 L

- STORE INDEFINITELY IN THE FRIDGE

- Before Use: add 10 mL PEN/STREP per 2 L
  add 700 □L PMSF stock per 2 L

- Do not keep > 24 hr after adding P/S, PMSF

Solution B: (Cannot be stored > 24 hr)

- Autoclave 2 L beaker, stir bar, water, storage bottle
- For 2 L solution B:
    - © In ~ 1800 mL sterile water, dissolve:
        - 12.12 g Tris Base (50 mM)
        - 223.66 g KCl (1.5 M)
        - 2.92 g EDTA
        - 20 mL Triton X –100 (1%)
        - adjust to pH 8.0 using 0.1 M NaOH/Hcl stocks
        - add 10 mL PEN/STREP per 2 L
        - add 700 □L PMSF stock per 2 L
    - top up to 2L
- store in fridge up to 24 hr

HANKS'S HEPES PHYSIOLOGICAL BUFFER:

Can be stored, but remember no antibiotics are added.

∴ store < 72 hrs

- Autoclave 2 L beaker, stir bar, water, storage container
- For 2 L Hanks/HEPES:
    - In ~1900 mL sterile water, dissolve:

- 16.00 g NaCl
- 0.80 g KCl
- 0.074 g Na_2HPO_4 (anhydrous, dibasic)
- 0.12 g KH_2PO_4
- 0.70 g $NaHCO_3$
- 5.20 g HEPES
- 2.44 g $CaCl_2$ (dihydrate)
- 0.10 g $MgSO_4$ (heptahydrate)
- 0.10 g $MgCl_2$ (hexahydrate)

- Adjust to pH 7.35 using 0.1 M NaOH/HCl stock
- Top to 2 L

- Store in fridge because no antibiotics

Solution C: Cannot be stored > 24 hr

- Autoclave 2 L beaker, stir bar, water, storage bottle

- For 2 L solution of C

  - In ~ 1900 mL of sterile water, dissolve:

    - 12.12 g Tris Base
    - 20 mL Triton-X (1%)

  - adjust to pH 9.0 using 0.1 M NaOH/HCl stocks
  - top to 2 L

- Store in fridge up to 24 hr

PBS (Phosphate Buffered Saline)

- Autoclave 2 L beaker, stir bar, water, storage bottle

- For 2 L PBS:
    - In ~ 1900 mL sterile water, dissolve:
        - 16.0 g NaCl
        - 0.40 g KCl
        - 1.84 g Na_2HPO_4
        - 0.40 g KH_2PO_4
    - adjust to pH 7.4 using 0.1 M NaOH/HCl stock
    - top to 2L
- store indefinitely in fridge

Appendix E

ELSEVIER LICENSE
TERMS AND CONDITIONS

Jan 08, 2019

This Agreement between Dalhousie University -- Samuel Baldwin ("You") and Elsevier ("Elsevier") consists of your license details and the terms and conditions provided by Elsevier and Copyright Clearance Center.

License Number	4504370912494
License date	Jan 08, 2019
Licensed Content Publisher	Elsevier
Licensed Content Publication	Structure
Licensed Content Title	The In Situ Supermolecular Structure of Type I Collagen
Licensed Content Author	Joseph P.R.O Orgel,Andrew Miller,Thomas C Irving,Robert F Fischetti,Andrew P Hammersley,Tim J Wess
Licensed Content Date	Nov 1, 2001
Licensed Content Volume	9
Licensed Content Issue	11
Licensed Content Pages	9
Start Page	1061
End Page	1069
Type of Use	reuse in a thesis/dissertation
Portion	figures/tables/illustrations
Number of figures/tables/illustrations	1
Format	both print and electronic
Are you the author of this Elsevier article?	No
Will you be translating?	No
Original figure numbers	Figure 1
Title of your thesis/dissertation	STRUCTURAL VARIATION AND ENZYMATIC SUSCEPTIBILITY OF COLLAGEN FIBRILS EXTRACTED FROM NATIVE AND OVERLOADED TAIL TENDONS
Expected completion date	May 2019
Estimated size (number of pages)	200
Requestor Location	Dalhousie University 6310 Coburg road halifax, NS b3h4r2 Canada Attn: Samuel Baldwin
Publisher Tax ID	GB 494 6272 12
Total	0.00 CAD
Terms and Conditions	

ELSEVIER LICENSE
TERMS AND CONDITIONS

Jan 08, 2019

This Agreement between Dalhousie University -- Samuel Baldwin ("You") and Elsevier ("Elsevier") consists of your license details and the terms and conditions provided by Elsevier and Copyright Clearance Center.

License Number	4504371405250
License date	Jan 08, 2019
Licensed Content Publisher	Elsevier
Licensed Content Publication	Biophysical Journal
Licensed Content Title	Collagen Fibrils: Nanoscale Ropes
Licensed Content Author	Laurent Bozec,Gert van der Heijden,Michael Horton
Licensed Content Date	Jan 1, 2007
Licensed Content Volume	92
Licensed Content Issue	1
Licensed Content Pages	6
Start Page	70
End Page	75
Type of Use	reuse in a thesis/dissertation
Intended publisher of new work	other
Portion	figures/tables/illustrations
Number of figures/tables/illustrations	1
Format	both print and electronic
Are you the author of this Elsevier article?	No
Will you be translating?	No
Original figure numbers	Figure 3
Title of your thesis/dissertation	STRUCTURAL VARIATION AND ENZYMATIC SUSCEPTIBILITY OF COLLAGEN FIBRILS EXTRACTED FROM NATIVE AND OVERLOADED TAIL TENDONS
Expected completion date	May 2019
Estimated size (number of pages)	200
Requestor Location	Dalhousie University 6310 Coburg road halifax, NS b3h4r2 Canada Attn: Samuel Baldwin
Publisher Tax ID	GB 494 6272 12
Total	0.00 CAD

ELSEVIER LICENSE
TERMS AND CONDITIONS

Jan 08, 2019

This Agreement between Dalhousie University -- Samuel Baldwin ("You") and Elsevier ("Elsevier") consists of your license details and the terms and conditions provided by Elsevier and Copyright Clearance Center.

License Number	4504371297153
License date	Jan 08, 2019
Licensed Content Publisher	Elsevier
Licensed Content Publication	Biophysical Journal
Licensed Content Title	Evidence that Collagen Fibrils in Tendons Are Inhomogeneously Structured in a Tubelike Manner
Licensed Content Author	Thomas Gutsmann,Georg E. Fantner,Manuela Venturoni,Axel Ekani-Nkodo,James B. Thompson,Johannes H. Kindt,Daniel E. Morse,Deborah Kuchnir Fygenson,Paul K. Hansma
Licensed Content Date	Apr 1, 2003
Licensed Content Volume	84
Licensed Content Issue	4
Licensed Content Pages	6
Start Page	2593
End Page	2598
Type of Use	reuse in a thesis/dissertation
Intended publisher of new work	other
Portion	figures/tables/illustrations
Number of figures/tables/illustrations	1
Format	both print and electronic
Are you the author of this Elsevier article?	No
Will you be translating?	No
Original figure numbers	Figure 2A
Title of your thesis/dissertation	STRUCTURAL VARIATION AND ENZYMATIC SUSCEPTIBILITY OF COLLAGEN FIBRILS EXTRACTED FROM NATIVE AND OVERLOADED TAIL TENDONS
Expected completion date	May 2019
Estimated size (number of pages)	200
Requestor Location	Dalhousie University 6310 Coburg road halifax, NS b3h4r2 Canada Attn: Samuel Baldwin

ELSEVIER LICENSE
TERMS AND CONDITIONS

Jan 08, 2019

This Agreement between Dalhousie University -- Samuel Baldwin ("You") and Elsevier ("Elsevier") consists of your license details and the terms and conditions provided by Elsevier and Copyright Clearance Center.

License Number	4504381114832
License date	Jan 08, 2019
Licensed Content Publisher	Elsevier
Licensed Content Publication	Journal of Ultrastructure Research
Licensed Content Title	Collagen structure: Evidence for a helical organization of the collagen fibril
Licensed Content Author	John H. Lillie,Donald K. MacCallum,Lawrence J. Scaletta,Joseph C. Occhino
Licensed Content Date	Feb 1, 1977
Licensed Content Volume	58
Licensed Content Issue	2
Licensed Content Pages	10
Start Page	134
End Page	143
Type of Use	reuse in a thesis/dissertation
Intended publisher of new work	other
Portion	figures/tables/illustrations
Number of figures/tables/illustrations	1
Format	both print and electronic
Are you the author of this Elsevier article?	No
Will you be translating?	No
Original figure numbers	Figure 3
Title of your thesis/dissertation	STRUCTURAL VARIATION AND ENZYMATIC SUSCEPTIBILITY OF COLLAGEN FIBRILS EXTRACTED FROM NATIVE AND OVERLOADED TAIL TENDONS
Expected completion date	May 2019
Estimated size (number of pages)	200
Requestor Location	Dalhousie University 6310 Coburg road halifax, NS b3h4r2 Canada Attn: Samuel Baldwin

OXFORD UNIVERSITY PRESS LICENSE TERMS AND CONDITIONS

Jan 08, 2019

This Agreement between Dalhousie University -- Samuel Baldwin ("You") and Oxford University Press ("Oxford University Press") consists of your license details and the terms and conditions provided by Oxford University Press and Copyright Clearance Center.

License Number	4504380249482
License date	Jan 08, 2019
Licensed content publisher	Oxford University Press
Licensed content publication	Microscopy
Licensed content title	Some observations on the subfibrillar structure of collagen fibrils as noted during treatment with NKISK and cathepsin G with mechanical agitation
Licensed content author	Zhao, Tailun; Weinhold, Paul S.
Licensed content date	Feb 22, 2011
Type of Use	Thesis/Dissertation
Institution name	
Title of your work	STRUCTURAL VARIATION AND ENZYMATIC SUSCEPTIBILITY OF COLLAGEN FIBRILS EXTRACTED FROM NATIVE AND OVERLOADED TAIL TENDONS
Publisher of your work	n/a
Expected publication date	May 2019
Permissions cost	0.00 CAD
Value added tax	0.00 CAD
Total	0.00 CAD
Title	STRUCTURAL VARIATION AND ENZYMATIC SUSCEPTIBILITY OF COLLAGEN FIBRILS EXTRACTED FROM NATIVE AND OVERLOADED TAIL TENDONS
Institution name	n/a
Expected presentation date	May 2019
Portions	Figure 5
Requestor Location	Dalhousie University 6310 Coburg road halifax, NS b3h4r2 Canada Attn: Samuel Baldwin
Publisher Tax ID	GB125506730
Billing Type	Invoice
Billing Address	Dalhousie University 6310 Coburg road halifax, NS b3h4r2

ELSEVIER LICENSE
TERMS AND CONDITIONS

Feb 14, 2019

This Agreement between Dalhousie University -- Samuel Baldwin ("You") and Elsevier ("Elsevier") consists of your license details and the terms and conditions provided by Elsevier and Copyright Clearance Center.

License Number	4527670570089
License date	Feb 14, 2019
Licensed Content Publisher	Elsevier
Licensed Content Publication	Journal of Biomechanics
Licensed Content Title	Nomenclature of the tendon hierarchy: An overview of inconsistent terminology and a proposed size-based naming scheme with terminology for multi-muscle tendons
Licensed Content Author	Geoffrey G. Handsfield,Laura C. Slane,Hazel R.C. Screen
Licensed Content Date	Sep 6, 2016
Licensed Content Volume	49
Licensed Content Issue	13
Licensed Content Pages	3
Start Page	3122
End Page	3124
Type of Use	reuse in a thesis/dissertation
Portion	figures/tables/illustrations
Number of figures/tables/illustrations	1
Format	both print and electronic
Are you the author of this Elsevier article?	No
Will you be translating?	No
Original figure numbers	Figure 2
Title of your thesis/dissertation	STRUCTURAL VARIATION AND ENZYMATIC SUSCEPTIBILITY OF COLLAGEN FIBRILS EXTRACTED FROM NATIVE AND OVERLOADED TAIL TENDONS
Expected completion date	May 2019
Estimated size (number of pages)	200
Requestor Location	Dalhousie University 6310 Coburg road halifax, NS b3h4r2 Canada Attn: Samuel Baldwin
Publisher Tax ID	GB 494 6272 12
Total	0.00 CAD

ELSEVIER LICENSE
TERMS AND CONDITIONS

Jan 08, 2019

This Agreement between Dalhousie University -- Samuel Baldwin ("You") and Elsevier ("Elsevier") consists of your license details and the terms and conditions provided by Elsevier and Copyright Clearance Center.

License Number	4504380368978
License date	Jan 08, 2019
Licensed Content Publisher	Elsevier
Licensed Content Publication	Journal of Structural Biology
Licensed Content Title	Fibrillar Structure and Mechanical Properties of Collagen
Licensed Content Author	Peter Fratzl,Klaus Misof,Ivo Zizak,Gert Rapp,Heinz Amenitsch,Sigrid Bernstorff
Licensed Content Date	Jan 1, 1998
Licensed Content Volume	122
Licensed Content Issue	1-2
Licensed Content Pages	4
Start Page	119
End Page	122
Type of Use	reuse in a thesis/dissertation
Intended publisher of new work	other
Portion	figures/tables/illustrations
Number of figures/tables/illustrations	2
Format	both print and electronic
Are you the author of this Elsevier article?	No
Will you be translating?	No
Original figure numbers	Figures 1 and 3
Title of your thesis/dissertation	STRUCTURAL VARIATION AND ENZYMATIC SUSCEPTIBILITY OF COLLAGEN FIBRILS EXTRACTED FROM NATIVE AND OVERLOADED TAIL TENDONS
Expected completion date	May 2019
Estimated size (number of pages)	200
Requestor Location	Dalhousie University 6310 Coburg road halifax, NS b3h4r2 Canada Attn: Samuel Baldwin
Publisher Tax ID	GB 494 6272 12

ELSEVIER LICENSE
TERMS AND CONDITIONS

Jan 08, 2019

This Agreement between Dalhousie University -- Samuel Baldwin ("You") and Elsevier ("Elsevier") consists of your license details and the terms and conditions provided by Elsevier and Copyright Clearance Center.

License Number	4504380849748
License date	Jan 08, 2019
Licensed Content Publisher	Elsevier
Licensed Content Publication	Biophysical Journal
Licensed Content Title	Fracture Mechanics of Collagen Fibrils: Influence of Natural Cross-Links
Licensed Content Author	Rene B. Svensson,Hindrik Mulder,Vuokko Kovanen,S. Peter Magnusson
Licensed Content Date	Jun 4, 2013
Licensed Content Volume	104
Licensed Content Issue	11
Licensed Content Pages	9
Start Page	2476
End Page	2484
Type of Use	reuse in a thesis/dissertation
Intended publisher of new work	other
Portion	figures/tables/illustrations
Number of figures/tables/illustrations	2
Format	both print and electronic
Are you the author of this Elsevier article?	No
Will you be translating?	No
Original figure numbers	Figures 3 and 4B
Title of your thesis/dissertation	STRUCTURAL VARIATION AND ENZYMATIC SUSCEPTIBILITY OF COLLAGEN FIBRILS EXTRACTED FROM NATIVE AND OVERLOADED TAIL TENDONS
Expected completion date	May 2019
Estimated size (number of pages)	200
Requestor Location	Dalhousie University 6310 Coburg road halifax, NS b3h4r2 Canada Attn: Samuel Baldwin

ELSEVIER LICENSE
TERMS AND CONDITIONS

Jan 08, 2019

This Agreement between Dalhousie University -- Samuel Baldwin ("You") and Elsevier ("Elsevier") consists of your license details and the terms and conditions provided by Elsevier and Copyright Clearance Center.

License Number	4504380976351
License date	Jan 08, 2019
Licensed Content Publisher	Elsevier
Licensed Content Publication	Biophysical Journal
Licensed Content Title	Designed to Fail: A Novel Mode of Collagen Fibril Disruption and Its Relevance to Tissue Toughness
Licensed Content Author	Samuel P. Veres,J. Michael Lee
Licensed Content Date	Jun 20, 2012
Licensed Content Volume	102
Licensed Content Issue	12
Licensed Content Pages	9
Start Page	2876
End Page	2884
Type of Use	reuse in a thesis/dissertation
Intended publisher of new work	other
Portion	figures/tables/illustrations
Number of figures/tables/illustrations	1
Format	both print and electronic
Are you the author of this Elsevier article?	No
Will you be translating?	No
Original figure numbers	Figure 3
Title of your thesis/dissertation	STRUCTURAL VARIATION AND ENZYMATIC SUSCEPTIBILITY OF COLLAGEN FIBRILS EXTRACTED FROM NATIVE AND OVERLOADED TAIL TENDONS
Expected completion date	May 2019
Estimated size (number of pages)	200
Requestor Location	Dalhousie University 6310 Coburg road halifax, NS b3h4r2 Canada Attn: Samuel Baldwin
Publisher Tax ID	GB 494 6272 12

References

1. Shoulders, M.D., Raines, R.T., 2009. Collagen structure and stability. Annu. Rev. Biochem. 78, 929-958.
2. Fratzl, P., 2008. Collagen structure and mechanics. Springer.
3. Kirkendall, D.T., Garrett, W.E., 1997. Function and Biomechanics of tendons. Scand. J. Med. Sci. Sports 7, 62-66.
4. Kannus, P., 2000. Structure of the tendon connective tissue. Scand. J. Med. Sci. Sports 10, 312-320.
5. Hodge, A.J., Schmitt, F.O., 1960. The charge profile of the tropocollagen macromolecule and the packing arrangement in native-type collagen fibrils. Biochemistry 46, 186-197.
6. Riley, G., 2008. Tendinopathy--- from basic science to treatment. Nat. Clin. Pract. Rheum. 4(2),82-89.
7. Liu, C.F., Aschbacher-Smith, L., Barthelery, N.J., Dyment, N., Butler, D., Wylie, C., 2011. What we should know before using tissue engineering techniques to repair injured tendons: a developmental biology perspective. Tiss. Eng. Part B 17(3), 165-176.
8. Snedeker, J.G., Foolen, J., 2017. Tendon injury and repair – a perspective on the basic mechanisms of tendon disease and future clinical therapy. Acta. Biomat. http://dx.doi.org/10.1016/j.actbio.2017.08.032
9. Glazebrook, M.A., Wright, J.R. Jr., Langman, M., Stanish, W.D., Lee, J.M., 2007. Histological analysis of Achilles tendons in an overuse rat model. J. Orthop. Res. 26(6), 840-846.
10. Jones, M.E., Mudera, V., Brown, R.A., Cambrey, A.D., Grobbelaar, A.O., McGrouther, D.A., 2003, The early surface cell response to flexor tendon injury. J. Hand Surg. Am. 28(2), 221-230.
11. Astrom, M., Rausing, A., 1995. Chronic Achilles tendinopathy. A survey of surgical and histopathologic findings. Clin. Orthop. Relat. Res. 316, 151-164.
12. Veres, S.P., Lee, J.M., 2012. Designed to fail: a novel mode of collagen fibril disruption and its relevance to tissue toughness. Biophys. J. 102, 2876-2884.
13. Veres, S.p., Harrison, J.M., Lee, J.M., 2013. Repeated subrupture overload causes progression of nanoscaled discrete plasticity damage in tendon collagen fibrils. J. ortho. Res. 31, 731-737.
14. Veres, S.P., Harrison, J.M., Lee, J.M., 2014. Mechanically overloading collagen fibrils uncoils collagen molecules, placing them in a stable, denatured state. Matrix Bio. 33, 54-59.

15. Exposito, J.Y., Valcourt, U., Cluzel, C., Lethias, C., 2010. The fibrillar collagen family. Int. J. Mol. Sci. 11, 407-426.

16. Soderhall, C., et. Al. 2007. Variants in a novel epidermal collagen gene (COL29A1) are associated with atopic dermatitis. PLoS Bio. 5(9), 1952-1961.

17. Birk, D.E., Mayne, R., 1997. Localization of collagen types I, III and V during tendon development. Changes in collagen types I and III are correlated with changes in fibril diameter. Eur. J. Cell Biol. 72(4), 352-361.

18. Birk, D.E., 2001. Type V collagen: heterotypic type I/V collagen interactions in the regulation of fibril assembly. Micron. 32, 223-237.

19. Kjear, M., 2004. Role of extracellular matrix in adaptation of tendon and skeletal muscle to mechanical loading. 84, 649-698.

20. Kirkendall, D.T., Garrett, W.E., 1997. Function and Biomechanics of tendons. Scand. J. Med. Sci. Sports 7, 62-66.

21. Ramachandran, G.N., Kartha, G., 1955. Structure of collagen. Nature. 176, 593-595.

22. Rich, A., Crick, F.H.C., 1961. The molecular structure of collagen. J. Mol. Biol. 3(5), 483-506.

23. Rich, A., Crick, F.H., 1955. The structure of collagen. Nature. 176, 915-916.

24. Cowan, P.M., McGavin, S., North, A.C.T., 1955. The polypeptide chain configuration of collagen. Nature. 176, 1062-1064.

25. Brodsky, B., Thiagarajan, G., Madhan, B., Kar, K., 2008. Triple-helical peptides: an approach to collagen conformation, stability, and self-association. Biopolymers, 89(5), 345-353.

26. Smith, J.W., 1968. Molecular pattern in native collagen. Nature. 219, 157-158.

27. Trelstad, R.L., Hayashi, K., Gross, J., 1976. Collagen fibrillogenesis: intermediate aggregates and suprafibrillar order. Proc. Natl. Acad. Sci. 73(11), 4027-4031.

28. Wess, T.J., 2005, Collagen fibril form and function. Adv Protein Chem. 70, 341-374.

29. Kadler, K.E., Holmes, D.F., Trotter, J.A., Chapman, J.A., 1996. Collagen fibril formation. Biochem. J. 316, 1-11.

30. Orgel, J.P.R.O, Miller, A., Irving, T.C., Fischetti, R.F., Hammersley, A.P., Wess, T.J., 2001, The *in situ* supermolecular structure of type I collagen. Structure. 9, 1061-1069.

31. Orgel, J.P.R.O., Irving, T.C., Miller, A., Wess, T.J., 2006, Microfibrillar structure of type I collagen *in situ*. PNAS. 103(24), 9001-9005.

32. Christiansen, D.L., Huang, E.K., Silver, F.H., 2000, Assembly of type I collagen: fusion of fibril subunits and the influence of fibril diameter on mechanical properties. Matrix Biol. 19, 409-420.

33. Hulmes, D.J.S., 1979. Quasi-hexagonal molecular packing in collagen fibrils. Nature. 282, 878-880.

34. Hulmes, D.J.S., Wess, T.J., Prockop, D.J., Fratzl, P., 1995, Radial packing, order, and disorder in collagen fibrils. Biophys. J. 68, 1661-1670.

35. Prockop, D.J., Fertala, A., 1998, The collagen fibril: the almost crystalline structure. J. Struct. Bio. 122, 111-118.

36. Gutsmann, T., Fantner, G.E., Venturoni, M., Ekani-Nkodo, A., Thompson, J.B., Kindt, J.H., Morse, D.E., Fygneson, D.K., Hansma, P.K. 2003. Evidence that collagen fibrils in tendons are inhomogeneously structured in a tube-like manner. Biophys. J. 84, 2593-2598.

37. Raspanti, M., Reguzzoni, M., Protasoni, M., Martini, D., 2011. Evidence of a discrete axial structure in unimodal collagen fibrils. Biomacromolecules. 12, 4344-4347.

38. Bozec, L., Van der Heijden, G., Horton, M., 2007. Collagen Fibrils: Nanoscale Ropes. Biophys. J. 92, 70-75.

39. Lillie, J.H., MacCallum, D.K. Scaletta, L.J., Occhino, J.C., 1977. Collagen structure: evidence for a helical organization of the collagen fibril. J. Ultrastruct Res. 58, 134-143.

40. Zhao, T., Weinhold, P.S., Lee, N.Y., Dahners, L.E., 2011. Some observation on the subfibrillar structure of collagen fibrils as noted during treatment with NKISK and cathepsin G with mechanical agitation. J. Elect. Micro. 60(2), 177-182.

41. McKenna, H.A., Hearle, J.W.S., O'Hear, N., 2004. Handbook of Fibre Rope Technology. Woodhead Publishing LTD, Cambridge (UK).

42. Ottani, V., Raspanti, M., Ruggeri, A., 2001, Collagen structure and function implications. Micron. 32, 251-260.

43. Zanaboni, G., Rossi, A., Onana, A.M.T., Tenni, R., 2000, Stability and networks of hydrogen bonds of the collagen triple helical structure: influence of pH and chaotropic nature of three anions. Matrix Biol. 19, 511-520.

44. Ripamonti, A., Roveri, N., Braga, D., Hulmes, D.J.S., Miller, A., Timmins, P.A., 1980. Effects of pH and ionic strength on the structure of collagen fibrils. Biopolymers. 19(5), 969-975.

45. Komsa-Penkova, R., Koynova, R., Kostov, G., Tenchov, B.G., Thermal stability of calf skin collagen type I in salt solutions. Biochimica Biophysica Acta 1297, 171-181.

46. Russell, A.E., 1972. Effect of alcohols and neutral salt on the thermal stability of soluble and precipitated acid-soluble collagen. Biochem. J. 131, 335-342.

47. Hall, D.A., Reed, R., 1957. Hydroxyproline and thermal stability of collagen. Nature. 180, 243.

48. Ramachandran, G.X., Chandrasekharan, R., 1968. Interchain hydrogen bonds via bound water molecules in the collagen triple helix. Biopolymers. 6(11), 1649-1658.

49. Kramer, R.Z., Venugopal, M.G., Bella, J., Mayville, P., Brodsky, B., Berman, H.M., 2000. Staggered molecular packing in crystals of collagen-like peptide with a single charged pair. J.Mol. Biol. 301, 1191-1205.

50. Bella, J., Berman, H.M., 1996. Crystallographic evidence of C^{α}-H ⋯O=C hydrogen bonds in a collagen triple helix. J. Mol. Biol. 264, 734-742.

51. Miles, C.A., Bailey, A.J., 1999, Thermal denaturation of collagen revisited. Proc. Indian. Acad. Sci. 111(1), 71-80.

52. Sun, Y.L., Luo, Z.P., Fertala, A., An, K.N., 2002. Direct quantification of the flexibility of type I collagen monomer. Biochem. Biophys. Res. Commun. 295(2), 382-386.

53. McClain, P.E., Wiley, E.R., 1972. Differential scanning calorimeter studies of the thermal transitions of collagen. Implications on structure and stability. J. Biol. Chem. 247(3), 692-7.

54. Miles, C.A., Burjanadze, T.V., Bailey, A.J., 1995. The kinetics of the thermal denaturation of collagen in unrestrained rat tail tendon determined by differential scanning calorimetry. J. Mol. Biol. 245, 437-446.

55. Miles, C.A., Bailey, A.J., 2001. Thermally labile domains in the collagen molecule. Micron. 32, 325-332.

56. Leikina, E., Mertts, M.V., Kuznetsova, N., Leikin, S., 2002. Type I collagen is thermally unstable at body temperature. PNAS. 99(3), 1314-1318.

57. Tiktopulo, E.I., Kajava, A.V., 1998. Denaturation of type I collagen fibrils is an endothermic process accompanied by a noticeable change in the partial heat capacity. Biochemistry. 37, 8147-8152.

58. Miles, C.A., Ghelashvili, M., 1999. Polymer-in-a-Box mechanism for the thermal stabilization of collagen molecules in fibres. Biophys. J. 76, 3243-3252.

59. Miles, C.A., Avery., N.C., Rodin, V.V., Bailey, A.J., 2005. The increase in denaturation temperature following cross-linking of collagen is caused by dehydration of fibres. J. Mol. Biol. 346, 551-556.

60. Herod, T.W., Chambers, N.C., Veres, S.P., 2016, Collagen fibrils in functionally distinct tendons have differing structural responses to tendon rupture and fatigue loading. Acta. Biomat. 42, 296-307.

61. Bozec, L., Odlyha, M., 2011. Thermal denaturation studies of collagen by microthermal analysis and atomic force microscopy. Biophys. J. 101, 228-236.

62. Lin, S.J., Lo, W., Tan, H.Y., Chan, J.Y., Chen., W.L., Wang, S.H., Lin, W.C., Chen, J.S., Hsu, C.J., Tjiu, J.W., Yu, H.S., Jee, S.H., Dong C.Y., 2006. Prediction of heat-induced collagen shrinkage by use of second harmonic generation microscopy.

63. Eyre, D.R., Wu, J.J. 2005. Collagen cross-links. Top. Curr. Chem. 247, 207-229.

64. Bailey, A.J., Paul, R.G., Knott, L., 1998, Mechanisms of maturation and ageing of collagen. Mech. Age. Develop. 106, 1-56.

65. Paul, R.G., Bailey, A.J., 1996. Glycation of collagen: the basis of its central role in the late complications of ageing and diabetes. Cell Biol. 28(12), 1297-1310.

66. Piez, K., 1968, Cross-linking of collagen and elastin. Ann. Rev. Biochem. 37, 547-570.

67. Bailey, A.J., Robins, S.P., Balian, G. 1974. Biological significance of the intermolecular crosslinks of collagen. Nature. 251, 105-109.

68. Andreassen, T.T., Seyer-Hansen, K., Bailey, A.J., 1981. Thermal stability, mechanical properties and reducible crosslinks of rat tail tendon in experimental diabetes. Biochimica Biophysica Acta. 677(2) 313-317.

69. Monnier, V.M., Mustata, G.T., Biemel, K.L., Reihl, O., Lederer, M.O., Zhenyou, D., Sell, D.R., 2005. Cross-linking of the extracellular matrix by the maillard reaction in aging and diabetes. Ann. N.Y. Acad. Sci. 1043, 533-544.

70. Gorisse, L., Pietrement, C., Vuiblet, V., Schmelzer, C.E.H., Kohler, M., Duca, L., Debelle, L., Fornes, P., Jaisson, S., Gillery., P., 2016. Protein carbamylation is a hallmark of aging. PNAS. 113(5), 1191-1196.

71. Gautieri, A., Redaelli, A., Buehler, M.J., Vesentini, S., 2014., Age- and diabetes-related nonenzymatic crosslinks in collagen fibrils: candidate amino acids involved in advanced glycation end-products. Matrix Biol. 34, 89-95.

72. Sasaki, N., Odajima, S., 1996. Elongation mechanism of collagen fibrils and force-strain relations of tendon at each level of structural hierarchy. J. Biomechanics. 29(9), 1131-1136.

73. Fratzl, P., Misof, K., Zizak, I. 1997. Fibrillar structure and mechanical properties of collagen. J. Struct. Bio. 122, 119-122.

74. Abrahams, M. 1967. Mechanical behaviour of tendon *in vitro*. Med. & Biol. Eng. 5, 433-443

75. Handsfield, G.G., Slane, L.C., Screen H.R.C. 2016. Nomenclature of the tendon hierarchy: An overview of inconsistent terminology and proposed size-based naming scheme with terminology for multi-muscle tendons. J. Biomech. 49(13), 3122-3124.

76. Diamant, J., Keller, A., Baer, E., Litt, M., Arridge, R.G.C., 1972. Collagen; ultrastructure and its relation to mechanical properties as a function of ageing. Proc. B. Soc. Lond. B. 180, 293-315.

77. Misof, K., Rapp, G., Fratzl, P., 1997. A new molecular model for collagen elasticity based on synchrotron S-ray scattering evidence. Biophys. J. 72, 1376-1381.

78. Fraser, R.D.B., Trus, B.L., 1986. Molecular mobility in the gap regions of type 1 collagen fibrils. Bioscience Rep. 6(2), 221-6.

79. Sasaki, N., Odajima, S., 1996. Stress-strain curve and young's modulus of a collagen molecule as determined by the x-ray diffraction technique. J. Biomechanics. 29(5), 655-658.

80. Folkhard, W., Mosler, E., Geercken, W., Knorzer, E., Nemetschek-Gansler, H., Nemetschek, Th., Koch, M.H.J., 1987. Quantitative analysis of the molecular sliding mechanisms in native tendon collagen --- time-resolved dynamic studies using synchrotron radiation. Int. J. Bio. Macromole. 9(3) 169-175.

81. Mosler, E., Folkhard, W., Knorzer, E., Nemetschek-Gansler, H., Nemetschek, Th., Koch, M.H.J., 1985. Stress-induced molecular rearrangement in tendon collagen. 182(4), 589-596.

82. Chang, S.W., Buehler, M., 2014. Molecular biomechanics of collagen molecules. 17(2), 70-76.

83. Shayegan, M., Rezaei, N., Lam, N.H., Altindal, T., Wieczorek, A., Forde, N.R., 2013. Probing multiscale mechanics of collagen with optical tweezers. Proc SPIE.

84. Svensson, R.B., Hansen, P., Hassenkam, T., Haraldsson., B.T., Aagaard, P., Kovanen, V., Krogsgaard, M., Kjaer, M., Magnusson, S.P., 2012. Mechanical properties of human patellar tendon at the hierarchical levels of tendon and fibril. J. Appl. Physiol. 112, 419-426.

85. Shen, Z.L., Dodge, M.R., Kahn, H., Ballarini, R., Eppell, S.J., 2008. Stress-strain experiments on individual collagen fibrils. Biophys. J. 95, 3956-3963.

86. Shen, Z.L., Dodge, M.R., Kahn, H., Ballarini, R., Eppell, S.J., 2010. *In vitro* fracture testing of submicron diameter collagen fibril specimens. Biophys. J. 99, 1986-1995.

87. Yang, L., van der Werf, K.O., Dijkstra, P.J., Feijen, J., Bennink, M.L., 2012, Micromechanical analysis of native and cross-linked collagen type I fibrils supports the existence of microfibrils. J. Mech. Behav. Biomed. Mat. 6, 148-158.

88. Ng, B.H., Chou, S.M., Lim, B.H., Chong, A., 2004. Strain rate effect on the failure properties of tendons. Proc. Inst. Mech. Eng. H. 218(3), 203-206.

89. Wren, T.A.L., Yerby, S.A., Beaupre, G.S., Carter, D.R., 2001, Mechanical properties of the human Achilles tendon. Clin. Biomech. 16, 245-251.

90. Peltonen, J., Cronin, N.J., Stenroth, L., Finni, T., Avela, J., 2013, Viscoelastic properties of the Achilles tendon *in vivo*. SpringerPlus. 2(1), 212.

91. Haut, R.C., 1983. Age-dependent influence of strain rate on the tensile failure of rat-tail tendon. J. Biomech. Eng. 105, 296-299.

92. Karunaratne, A., Li, S., Bull, A.M.J., 2018. Nano-scale mechanisms explain the stiffening and strengthening of ligament tissue with increasing strain rate. Scientific Reports. 8, 3707.

93. Svensson, R.B., Hassenkam, T., Hansen, P., Magnusson, S.P., 2010. Viscoelastic behavior of discrete human collagen fibrils. J. Mech. Behav. Biomed. Mat. 3, 112-115.

94. Shen, Z.L., Kahn, H., Ballarini, R., Eppell, S.J., 2011. Viscoelastic properties of isolated collagen fibrils. Biophys. J. 100, 3008-3015.

95. Gautieri, A., Vesentini, S., Redaelli, A., Buehler, M.J., 2012. Viscoelastic properties of model segments of collagen molecules. Matrix. Biol. 31, 141-149.

96. Yoon, Y.J., Cho, K.H., Han, S.Y., 2014. Viscoelastic behavior of a single collagen molecule. Int. J. Prec. Eng. Man. 15(4), 783-786.

97. Gupta, H.S., Seto, J., Krauss, S., Boesecke, p., Screen, H.R.C., 2010, *In situ* multi-level analysis of viscoelastic deformation mechanisms in tendon collagen. J. Struct. Biol. 169, 183-191.

98. Robinson, P.S., Lin, T.W., Reynolds, P.R., Derwin, K.A., Iozzo, R.V., Soslowsky, L.J., 2004. Strain-Rate sensitive mechanical properties of tendon fascicles from mice with genetically engineered alterations in collagen and decorin. J. Biomech. Eng. 126(2), 252-257.

99. Puxkandl, R., Zizak, I., Paris, O., Keckes, J., Tesch, W., Bernstorff, S., Purslow, P., Fratzl, P., 2002. Viscoelastic properties of collagen: synchrotron radiation investigations and structural model. Phil. Trans. R. Soc. Lond. B. 357, 191-197.

100. Szczesny, S.E., Elliott, D.M., 2014. Incorporating plasticity of the interfibrillar matrix in shear lag models is necessary to replicate the multiscale mechanics of tendon fascicles. J. Mech. Behav. Mat. 40, 325-338.

101. Baer, E., Hiltner, A., Friedman, B., 1975. Relationship of the ultrastructure and mechanical properties in tendinous collagen, a highly ordered macromolecular composite. Polymer Mech. 11(6), 896-904.

102. Fratzl, P., 2008. Collagen structure and mechanics. Tendons and ligaments: structure, mechanical behavior and biological function. Springer. 269-284.

103. Shadwick, R.E., 1985. Elastic energy storage in tendons: mechanical differences related to function and age. J. Appl. Physiol. 68(3), 1033-1040.

104. Parry, D.A.D., Craig, A.S., Barnes, G.R.G., 1978. Tendon and ligament from the horse: an ultrastructural study of collagen fibrils and elastic fibres as a function of age. Proc. R. Soc. Lond. B. 203, 193-303.

105. Parry, D.A.D., Barnes, G.R.G., Craig, A.S., 1978. A comparison of the size distribution of collagen fibrils in connective tissues as a function of age and a possible relation between fibril size distribution and mechanical properties. Proc. R. Soc. Lond. B. 203, 305-321.

106. Rumian, A.P. Wallace, A.L., Birch, H.L., 2006. Tendons and ligaments are anatomically distinct but overlap in molecular and morphological features—A comparative study in an ovine model. J. Ortho. Res. 25(4), 458-464.

107. Goh, K.L., Holmes, D.F., Lu, Y., Purslow, P.P., Kadler, K.E., Bechet, D., Wess, T.J., 2012. Bimodal collagen fibril diameter distributions direct age-related variations in tendon resilience and resistance to rupture. J. Appl. Physiol. 113, 878-888.

108. Magnusson, S.P., Qvortrup, K., Larsen, J.O., Rosager, S., Hanson, P., Aagaard, P., Krogsgaard, M., Kjaer, M., 2002. Collagen fibril size and crimp morphology in ruptured and intact Achilles tendons. Matrix Biol. 21, 369-377.

109. Strocchi, R., Pasquale, V.D., Guizzardi, S., Govoni, P., Facchini, A., Raspanti, M., Girolami, M., Giannini, S., 1991. Human Achilles tendon: morphological and morphometric variations as a function of age. Foot & Ankle. 12(2), 100-104.

110. Avery, N.C., Bailey, A.J., 2005. Enzymic and non-enzymic cross-linking mechanisms in relation to turnover of collagen: relevance to aging and exercise. Scand. J. Med. Sci. Sports. 15, 231-240.

111. Couppe, C., Hansen, P., Konsgaard, M., Kovanen, V., Suetta, C., Aagaard, P., Kjaer, M., Magnusson, S.P., 2009. Mechanical properties and collagen cross-linking of the patellar tendon in old and young men. J. Appl. Physiol. 107, 880-886.

112. Gillis, C., Pool R.R., Meagher, D.M., Stover, S.M., Reiser, K., Willits, N., 1997. Effect of maturation and aging on the histomorphometric and biochemical characteristics of equine superficial digital flexor tendon. Amer. J. Vet. Res. 58(4), 425-430.

113. Birch, H.L., Bailey, J.V.B., Bailey, A.J., Goodship, A.E., 1999. Age-related changes to the molecular and cellular components of equine flexor tendons. Equine Vet. J. 31(5), 391-396.

114. O'Brien, T.D., Reeves, N.D., Baltzopoulos, V. Jones, D.A., Maganaris C.N., 2010. Mechanical properties of the patellar tendon in adults and children. J. Biomech. 43, 1190-1195.

115. Svensson, R.B., Mulder, H., Kovanen, V., Magnusson, S.P., 2013. Fracture mechanics of collagen fibrils: influence of natural cross-links. Biophys. J. 104, 2476-2484.

116. Svensson, R.B., Smith, S.T., Moyer, P.J., Magnusson, S.P., 2018. Effects of maturation and advanced glycation on tensile mechanics of collagen fibrils from rat tail and Achilles tendons. Acta Biomat. 70, 270-280.

117. Wiens, R., Findlay, C.R., Baldwin, S.J., Kreplak, L., Lee, J.M., Veres, S.P., Gough, K.M., 2016. High spatial resolution (1.1μm and 20nm) FTIR polarization contrast imaging reveals pre-rupture disorder in damaged tendon. Faraday Dicuss. 187, 555-573.

118. Knorzer, E., Folkhard, W., Geerchen, W., Boschert, C., Koch, M.H.J., Hilbert, B., Krahl, H., Mosler, E., Neinetschek0Gansler, H., Nemetschek, T., 1986. New aspects of the etiology of tendon rupture. Arch. Orthop. Trauma Surg. 105, 113-120.

119. Minns, R.J., Steven, F.S., 1980. Local denaturation of collagen fibres during the mechanical rupture of collagenous fibrous tissue. Annals Rheum. Disease. 39, 164-167.

120. Willett, T.L., Labow, R.S., Avery, N.C., Lee, J.M., 2007. Increased Proteolysis of collagen in an *in vitro* tensile overload tendon model. Annals Biomed. Eng. 35(11), 1961-1972.

121. Zitnay, J.L., LI, Y., Qin, Z., San, B.H., Depalle, B., Reese, S.P., Buehler, M.J., Yu, S.M., Weiss, J.A., 2017. Molecular level detection and localization of mechanical damage in collagen enabled by collagen hybridizing peptides. Nat. Comm. 8, 14913.

122. Bruckner, P., Prockop, D.J., 1981. Proteolytic enzymes as probes for the triple-helical conformation of procollagen. Analy. Biochem. 110(2), 360-368.

123. Willett, T.L. Labow, R.S., Lee, J.M., 2008. Mechanical overload decreases the thermal stability of collagen in an *in vitro* tensile overload tendon model. J. Orthop. Res. 26(12), 1605-1610.

124. Li, Y., Foss, C.A., Summerfield, D.D., Doyle, J.J., Torok, C.M., Dietz. H.C., Pomper, M.G., Yu, S.M., 2012. Targeting collagen strands by photo-triggered triple-helix hybridization. PNAS. 109(37), 14767-14772.

125. Marino, M., 2016, Molecular and intermolecular effects in collagen fibril mechanics: a multiscale analytical model compared with atomistic and experimental studies. Biomech. Model. Mechanobiol. 15, 133-154.

126. Bourne, J.W., Torzilli, P.A., 2011, Molecular simulations predict novel collagen conformations during cross-link loading. Matrix Biol. 30, 356-360.

127. Gautieri, A., Buehler, M.J., Redaelli, A., 2009, Deformation rate controls elasticity and unfolding pathway of single tropocollagen molecules. J. Mech. Behav. Biomed. Mat. 2, 130-137.

128. Kwansa, A.L., Vita., R.D., Freeman, F.W., 2014, Mechanical recruitment of N- and C-crosslinks in collagen type I. Matix Biol. 34, 161-169.

129. Collier, T.A., Nash, A., birch, H.L., De Leeuw, N.H., 2018. Effect on the mechanical properties of type I collagen of intra-molecular lysine-arginine derived advanced glycation end-product cross-linking. J. Biomech. 67, 55-61.

130. Chambers, N.C., Herod, T.W., Veres, S.P., 2018. Ultrastructure of tendon rupture depends on strain rate and tendon type. J. Orthop. Res. Epub.

131. Quigley, A. S., Bancelin, S., Deska-Gauthier, D., Legare, F., Kreplak, L., Veres, S. P., 2018. In tendons, differing physiological requirements lead to functionally distinct nanostructures. *Sci. Rep.* 8, 4409.

132. Lee, J.M., Pereira, C.A., Abdulla, D, Naimark, W.A., Crawford, I., 1995. A multi-sample denaturation temperature tester for collagenous biomaterials. Med. Eng. Phys. 17(2), 115-121.

133. Bruckner, P., Prockop, D.J., 1981. Proteolytic enzymes as probes for the triple-helical conformation of procollagen. Analyt. Biochem. 110(2), 360-368.

134. Kadler, K.E., Hojima, Y., Prockop, D.J. 1988. Assembly of type I collagen fibrils *de novo* between 37 and 41°C the process is limited by micro-unfolding of monomers. J. Biol. Chem. 263(21), 10517-10523.

135. Ryhanen, L., Zaragoza, E.J., Uitto, J., 1983. Conformational stability of type I collagen triple helix: Evidence for temporary and local relaxation of the protein conformation using a proteolytic probe. Arch. Biochem. Biophys. 223(2), 562-571.

136. Olsen, J.V., Ong., S.E., Mann, M., 2004. Trypsin cleaves exclusively C-terminal to arginine and lysine residues. Mol & Cell Proteomics. 3(6), 608-614.

137. Bank., R.A., Krikken, M., Beekman, B., Stoop, R., Maroudas, A., Lafebers, F.P.J.G., Te Koppele, J.M., 1997. A simplified measurement of degraded collagen in tissues: application in healthy, fibrillated and osteoarthritic cartilage. Matrix Biol. 16, 233-243.

138. Egger, A.C., Berkowitz, M.J., 2017. Achilles tendon injuries. Curr. Rev. Musculoskelet. Med. 10, 72-80.

139. Snedeker, J.G., Foolen, J., 2017. Tendon injury and repair – a perspective on the basic mechanisms of tendon disease and future clinical therapy. Acta Biomaterialia. 63, 18-36.

140. Herod, T.W., Veres, S.P., 2018. Development of overuse tendinopathy: A new descriptive model for initiation of tendon damage during cyclic loading. J. Orthop. Res. 36(1), 467-476.

141. Wu, F., Nerlich, M., Docheva, D., 2017. Tendon injuries: basic science and new repair proposals. EFFORT Open Rev. 2(7), 332-342.

142. Heinemeier K.M., Schjerling, P., Heinemeier, J., Magnusson, S.P., Kjaer, M., 2013. Lack of issue renewal in human adult Achilles tendon is revealed by nuclear bomb ^{14}C. FASEB J. 27(5), 2074-2079.

143. Wang, T., Chen, P., Zheng, M., Wang, A., Lloyd, D., Leys, T., Zheng, Q., Zheng, M.H., 2017. *In vitro* loading models for tendon mechanobiology. J. Orthop. Res. 36(2), 566-575.

144. Jones, M.E., Mudera, V., Brown, R.A., Cambrey, A.D., Grobbelaar, A.O., McGrouther, D.A., 2003. The early surface cell response to flexor tendon injury. J. Hand. Surg. Am. 28(2), 221-30.

145. Oshiro, W., Lou, J., Xing, X., Tu, Y., Manske, P.R., 2003. Flexor tendon healing in the rat: a histologic and gene expression study. J. Hand Surg. 28A(5), 814-823.

146. Gong, F., Dui, L., Zhang, X., Zhan, X., Gong, X., Wen, Y., 2017. Piperine ameliorates collagenase-induced Achilles tendon injury in the rat. Con. Tiss. Res. 59(1), 21-29.

147. Jones, G.C., Corps, A.N., Pennington, C.J., Clark, I.M., Edwards, D.R., Bradley, M.M., Hazleman, B.L., Riley, G.P., 2006. Expression profiling of metalloproteinases and tissue inhibitors of metalloproteinases in normal and degenerate human Achilles tendon. Arthritis Rheumatism. 54(3), 832-842.

148. Karousou, E., Ronga, M., Vigetti, D., Passi, A., Maffulli, N., 2008. Collagens, proteoglycans, MMP-2, MMP-9 and TIMPS in human Achilles tendon rupture. Clin. Orthop. Relat. Res. 466, 1577-1582.

149. Riley, G.P., Curry, V., DeGroot, J., van El, B., Verzijl, N., Hazleman, B.L., Bank, R.A., 2002, Matrix metalloproteinase activities and their relationship with collagen remodelling in tendon pathology. Matrix Bio. 21, 185-195.

150. Tsai, W.C., Hsu, C.C., Chang, H.N., Lin, Y.C., Lin, M.S., Pang, J.H., 2010. Ibuprofen upregulates expressions of matrix metalloproteinase-1,-8,-9, and -13 without affecting expressions of types I and III collagen in tendon cells. J. Orthop. Res.

151. Nagase, H., Visse, R., Murphy, G., 2006. Structure and function of matrix metalloproteinases and TIMPS. Cardiovascular Res. 69, 562-573.

152. Metalloproteinases and Tissue Inhibitors of metalloproteinases structure, function and biochemistry. Circ. Res. 2003, 827-839.

153. Veres, S.P., Brennan-Pierce, E.P., Lee, J.M., 2015. Macrophage-like U937 cells recognize collagen fibrils with strain-induced discrete plasticity damage. J. Biomed. Mater. Res. Part A. 103(A) 397-408.

154. Binnig, G., Quate, C.F., Gerber, C.H., 1986. Atomic Force Microscope. Phys. Rev. Let. 56(9), 930-934.

155. Jalili, N., Laxminarayana, K., 2004, A review of atomic force microscopy imaging systems: application to molecular metrology and biological sciences. Mechatronics. 14, 907-945.

156. Chang, K.C., Chiang, Y.W., Yang, C.H., Liou, J.W., 2012. Atomic force microscopy in biology and biomedicine. Tzu Chi Med. J. 24, 162-169.

157. Maver, U., Velnar, T., Gaberscek, M., Planinsek, O., Finsgar, M., 2016, Recent progressive use of atomic force microscopy in biomedical applications. Trends. Anal. Chem. 80, 96-111.

158. Kranz, C., Kueng, A., Lugstein, A., Bertagnolli, E., Mizaikoff, B., 2003. Mapping of enzyme activity by detection of enzymatic products during AFM imaging with integrated SECM-AFM probes. Ultramicro. 100, 127-134.

159. Li, Q.S., Lee, G.Y.H., Ong, C.N., Lim, C.T., 2008, AFM indentation study of breast cancer cells. Biochem. Biophys. Res. Comm. 374, 609-613.

160. Putman, C.A.J., van der Werf, K.O., de Grooth, B.G., van Hulst, N.F., Greve, J, 1994, Viscoelasticity of living cells allows high resolution imaging by tapping mode atomic force microscopy. Biophys. J. 67, 17-49-1753.

161. Wojcikiewicz, E.P., Zhang, X., Moy, V.T., 2004, Force and compliance measurements on living cells using atomic force microscopy (AFM). Biol. Proced. 6(1), 1-9.

162. Ohnesorge, F.M., Horber, K.H., Haberle, W., Czerny, C.P., Smith, P.E., Binnig, G., 1997. AFM review study on pox viruses and living cells. Biophys. J. 73, 2183-2194.

163. Heinz, W.F., Hoh, J.H., 1990. Spatially resolved force spectroscopy of biological surfaces using the atomic force microscope. Tibtech. 17, 143-150.

164. Sneddon, I., 1965. The relation between load and penetration in the axisymmetric boussinesq problem for a punch of arbitrary profile.

165. Cisneros, D.A., Hung, C., Franz, C.M., Muller, D.J., 2006, Observing growth steps of collagen self-assembly by time-lapse high-resolution atomic force microscopy. J. Struct. Biol. 154, 232-245.

166. Stamov, D.R., Muller, A., Wegrowski, Y., Brezillon, S., Franzy, C.M., 2013. Quantitative analysis of type I collagen fibril regulation by lumican and decorin using AFM. J. Struct. Biol. 183(3), 394-403. μ

167. Paige, M.F., Lin, A.C., Goh, C., 2002. Real-time enzymatic biodegradation of collagen fibrils monitored by atomic force microscopy. Inter. Biodeter. & Biodegrad. 50(1), 1-10.

168. Androitis, O.G., Manuyakorn, W., Zekonyte, J., Katsamenis, O.L., Fabri, S., Howarth, P.H., Davies, D.E., Thurner, P.J., 2014. Nanomechanical assessment of human and murine collagen fibrils via atomic force microscopy cantilever-based nanoindentation. J. Mech. Behav. Biomed. Mat. 39, 9-26.

169. Wenger, M.P.E., Bozec, L., Horton, M.A., Mesquida, P., 2007. Mechanical properties of collagen fibrils. Biophys J., 93, 1255-1263.

170. Grant, C.A., Phillips, M.A., Thomson, N.H., 2012. Dynamic mechanical analysis of collagen fibrils at the nanoscale. J. Mech. Behav. Biomed. Mat. 5, 165-170.

171. Minary-Jolandan, M., Yu, M.F., 2009. Nanomechanical heterogeneity in the gap and overlap regions of type I collagen fibrils with implications for bone heterogeneity. Biomacromol. 10, 2565-2570.

172. Grant, C.A., Brockwell, D.J., Radford, S.E., Thomson, N.H., 2008. Effects of hydration on the mechanical response of individual collagen fibrils. Appl. Phys. Lett. 92, 233902.

173. Grant, C.A., Brockwell, D.J., Radford, S.E., Thomson, N.H., 2009. Tuning the elastic modulus of hydrated collagen fibrils. Biophys. J. 97(11), 2985-2992.

174. Doren, S.R.V., 2015. Matrix metalloproteinase interactions with collagen and elastin. Matrix. Biol. 0, 224-231.

175. Bhole, A.P., Flynn, B.P., Liles, M., Saeidi, N., Dimarzio, C.A., Ruberti, J.W., 2009. Mechanical strain enhances survivability of collagen micronetworks in the presence of collagenase: implications for load-bearing matrix growth and stability. Phil. Trans. R. Soc. A. 367, 3339-3362.

176. Flynn, B.P. Bhole, A.P., Saeldi, N., Liles, M., DiMarzio, C.A., Ruberti, J.W. 2010. Mechanical strain stabilizes reconstituted collagen fibrils against enzymatic degradation by mammalian collagenase matrix metalloproteinase 8 (MMP-8). Plos ONE. 5(8), e12337.

177. Chang, S.W., Flynn, B.P., Ruberti, J.W., Buehler, M.J. 2012. Molecular mechanism of force induced stabilization of collagen against breakdown. Biomaterials. 33, 3852-3859.

178. Aimes, R.T., Quigley, J.P. 1995. Matrix metalloproteinase-2 is an interstitial collagenase. J. Biol. Chem. 270(11), 5872-5876.

179. Patterson, M.L., Atkinson, S.J., Knauper, V., Murphy, G., 2001. Specific collagenolysis by gelatinase A, MMP-2, is determined by the hemopexin domain and not the fibronectin-like domain. FEBS Let. 503, 158-162.

180. Bigg, H.F., Rowan, A.D., Barker, M.D., Cawston, T.E., 2007. Activity of matrix metalloproteinase-9 against native collagen types I and III. FEBS J. 274, 1246-1255.

181. Gautieri, A., S. Vesentini, A. Redaelli, and M. J. Buehler. 2011. Hierarchical structure and nanomechanics of collagen microfibrils from the atomistic scale up. Nano Lett 11:757-766.

182. Woo, S. L., R. E. Debski, J. Zeminski, S. D. Abramowitch, S. S. Saw, and J. A. Fenwick. 2000. Injury and repair of ligaments and tendons. Annu Rev Biomed Eng 2:83-118.

183. Camacho, N. P., L. Hou, T. R. Toledano, W. A. Ilg, C. F. Brayton, C. L. Raggio, L. Root, and A. L. Boskey. 1999. The material basis for reduced mechanical properties in oim mice bones. J Bone Miner Res 14:264-272.

184. Abramowitch, S. D., M. Yagi, E. Tsuda, and S. L. Woo. 2003. The healing medial collateral ligament following a combined anterior cruciate and medial collateral ligament injury--a biomechanical study in a goat model. J Orthop Res 21:1124-1130.

185. Lavagnino, M., S. P. Arnoczky, K. Frank, and T. Tian. 2005. Collagen fibril diameter distribution does not reflect changes in the mechanical properties of *in vitro* stress-deprived tendons. Journal of biomechanics 38:69-75.

186. Magnusson, S. P., P. Hansen, and M. Kjaer. 2003. Tendon properties in relation to muscular activity and physical training. Scand J Med Sci Sports 13:211-223.

187. Misof, K., W. J. Landis, K. Klaushofer, and P. Fratzl. 1997. Collagen from the osteogenesis imperfecta mouse model (oim) shows reduced resistance against tensile stress. The Journal of clinical investigation 100:40-45

188. Screen, H. R., S. Toorani, and J. C. Shelton. 2013. Microstructural stress relaxation mechanics in functionally different tendons. Med Eng Phys 35:96-102.

189. Eppell, S. J., B. N. Smith, H. Kahn, and R. Ballarini. 2006. Nano measurements with micro-devices: mechanical properties of hydrated collagen fibrils. J R Soc Interface 3:117-121.

190. van der Rijt, J. A., K. O. van der Werf, M. L. Bennink, P. J. Dijkstra, and J. Feijen. 2006. Micromechanical testing of individual collagen fibrils. Macromol Biosci 6:697-702.

191. Graham, J. S., A. N. Vomund, C. L. Phillips, and M. Grandbois. 2004. Structural changes in human type I collagen fibrils investigated by force spectroscopy. Exp Cell Res 299:335-342.

192. Yang, L., K. O. van der Werf, C. F. Fitie, M. L. Bennink, P. J. Dijkstra, and J. Feijen. 2008. Mechanical properties of native and cross-linked type I collagen fibrils. Biophysical journal 94:2204-2211.

193. Dufrene, Y. F., D. Martinez-Martin, I. Medalsy, D. Alsteens, and D. J. Muller. 2013. Multiparametric imaging of biological systems by force-distance curve-based AFM. Nat Methods 10:847-854.

194. Sader, J. E., I. Larson, P. Mulvaney, and L. R. White. 1995. Method for the Calibration of Atomic-Force Microscope Cantilevers. Review of Scientific Instruments 66:3789-3798.

195. Maugis, D., and M. Barquins. 1978. Fracture Mechanics and Adherence of Viscoelastic Bodies. Journal of Physics D-Appalied Physics 11(14):1989.

196. Stolz, M., R. Raiteri, A. U. Daniels, M. R. VanLandingham, W. Baschong, and U. Aebi. 2004. Dynamic elastic modulus of porcine articular cartilage determined at two different levels of tissue organization by indentation-type atomic force microscopy. Biophysical journal 86:3269-3283.

197. Persch, G., C. Born, and B. Utesch. 1994. Nano-Hardness Investigations of Thin-Films by an Atomic-Force Microscope. Microelectronic Engineering 24:113-121.

198. Bueckle, H. 1973. The Science of Hardness Testing and its Research Applications. American Society for Metals, Ohio.

199. Tranchida, D., Z. Kiflie, S. Acierno, and S. Piccarolo. 2009. Nanoscale mechanical characterization of polymers by atomic force microscopy (AFM) nanoindentations: viscoelastic characterization of a model material. Measurement Science & Technology 20.

200. Ricci, D., and P. C. Braga. 2004. Recognizing and avoiding artifacts in AFM imaging. Methods Mol Biol 242:25-37.

201. Lin, S. J., C. Y. Hsiao, Y. Sun, W. Lo, W. C. Lin, G. J. Jan, S. H. Jee, and C. Y. Dong. 2005. Monitoring the thermally induced structural transitions of collagen by use of second-harmonic generation microscopy. Opt Lett 30:622-624.

202. Matteini, P., R. Cicchi, F. Ratto, D. Kapsokalyvas, F. Rossi, M. de Angelis, F. S. Pavone, and R. Pini. 2012. Thermal transitions of fibrillar collagen unveiled by second-harmonic generation microscopy of corneal stroma. Biophysical journal 103:1179-1187.

203. Deniset-Besseau, A., J. Duboisset, E. Benichou, F. Hache, P. F. Brevet, and M. C. Schanne-Klein. 2009. Measurement of the Second-Order Hyperpolarizability of the Collagen Triple Helix and Determination of Its Physical Origin. J Phys Chem B 113:13437-13445.

204. Benjamin, M., Kaiser, E., & Milz, S. (2008). Structure-function relationships in tendons: a review. J. Anat. 212, 211-228.

205. Spiesz, E.M., Thorpe, C.T., Chaudhry, S., Riley, G.P., Birch, H.L., Clegg P.D., & Screen, H.R.C. (2015). Tendon extracellular matrix damage, degradation and inflammation in response to *in vitro* overload exercise. J. Ortho. Res. 33(6), 889-97.

206. Sharma, P., & Maffulli, N. (2005). Tendon Injury and Tendinopathy: Healing and Repair. J. Bone Joint Surg. Am. 87(1), 187-202.

207. Ottani, V., Martini, D., Franchi, M., Ruggeri, A., & Raspanti, M. (2002). Hierarchical structures in fibrillary collagens. Micron. 33:587-596.

208. Silver, D., Miller, J., Harrison, R., & Prockop, D.J. (1992). Helical model of nucleation and propagation to account for the growth of type I collagen fibrils from the symmetrical pointed tips: a special example of self-assembly of rod-like monomers. Proc. Natl. Acad. Sci. USA. 89, 9860-9864.

209. Orgel, J. P., Miller, A., & Wess, T. J. (2001). The *in situ* supermolecular structure of type I collagen. Structure. 9, 1061-1069.

210. Baldwin, S.J., Quigley, A.S., Clegg, C., & Kreplak, L. (2014). Nanomechanical mapping of hydrated rat tail tendon collagen I fibrils. Biophys. J. 107(8), 1794-801.

211. Ariganello, M.B., Labow, R.S., & Lee, J.M. (2009). Response of macrophage-like U937 cells to decellularized tissue heart valve materials. J. Heart Valve Dis. 18, 187-197.

212. Spitzner, E.C., Roper, S., Zerson, M., Bernstein, A., & Magerle, R. (2015). Nanoscale swelling heterogeneities in type I collagen fibrils. ACS Nano. 9(6), 5683-5694.

213. Fawzy, A.S., Beng, L.T., & Lee, N. (2012). Characterization of the structural/properties correlation of crosslinked dentin collagen fibrils: AFM study. Curr. Micro. Cont. 1 533-539.

214. Hormann, H., & Schlebusch, H. (1971). Reversible and Irreversible Denaturation of Collagen Fibers. Biochem. 10(6), 932-937

215. Brown, A.I., Kreplak, L., & Rutenberg, A.D. (2014). An equilibrium double-twist model for the radial structure of collagen fibrils. Soft. Mat. 10, 8500-8511.

216. Szczesny, S. E. & Elliott, D. M. (2014). Interfibrillar shear stress is the loading mechanism of collagen fibrils in tendon. Acta Biomater. 10, 2582–2590.

217. Screen, H. R. C., Lee, D. A., Bader, D. L. & Shelton, J. C. (2004). An investigation into the effects of the hierarchical structure of tendon fascicles on micromechanical properties. Proc. Inst. Mech. Eng. 218, 109–119.

218. Bruehlmann, S. B., Matyas, J. R. & Duncan, N. A. (2004). ISSLS prize winner: Collagen fibril sliding governs cell mechanics in the annulus fibrosus: an *in situ* confocal microscopy study of bovine discs. Spine 29, 2612–2620.

219. Szczesny, S.E., Caplan, J.L., Pedersen, P. & Elliott D.M. (2015). Quantification of interfibrillar shear stress in aligned soft collagenous tissues via notch tension testing. Sci. Rep. 5:14649.

220. Svensson, R.B, Mulder, H., Kovanen, V., & Magnusson, S.P. (2013). Fracture mechanics of collagen fibrils: influence of natural cross-links. Biophys. J. 104(11), 2476-2484.

221. Uzel, S.G.M., & Beuhler, M.J. (2011). Molecular structure, mechanical behavior and failure mechanism of the C-terminal cross-link domain in type I collagen. J. Mech. Behav. Biomed. Mater. 4, 153-161.

222. Moeller, H.D., Bosch, U. & Decker, B. (1995). Collagen fibril diameter distribution in patellar tendon autografts after posterior cruciate ligament reconstruction in sheep: changes over time. J. Anat. 187(1), 161-167.

223. Bai, P., Phua, K., Hardt, T., Cernadas, M., Brodsky, B., 1992. Glycation alters collagen fibirl organization. Connect. Tiss. Res. 28, 1-12.

224. Danielson, K.G., Baribault, H., Holmes, D.F., Graham, H., Kadler, K.E., Iozzo, R.V., 1997. Targeted disruption of decorin leads to abnormal collagen fibril morphology and skin

225. Scott, J.E., 1990. Proteoglycan:collagen interactions and subfibrillar structure in collagen fibrils. Implications in the development and ageing of connective tissues. J.Anat. 169, 23-35.

226. Baldwin, S.J., Kreplak, L., Lee, J. M., 2016. Characterizaion via atomic force microscopy of discrete plasticity in collagen fibrils from mechanically overloaded tendons: Nano-scale structural changes mimic rope failure. J. Mech. Behav. Biomed. Mater. 60, 356-366.

227. Holmes, D.F., 1995. Mass mapping of extracellular matrix assemblies. Biochem. Soc. Trans. 23, 720-725.

228. Holmes D.F., Graham, H.K., Trotter, J.A., Kadler, K.E., 2001. STEM/TEM studies of collagen fibril assembly. Micron. 32(3), 273-285

229. Holmes, D.F., Kadler, K.E., 2005. The precision of lateral size control in the assembly of corneal collagen fibrils. J. Mole. Bio. 345(4), 773-784.

230. Kopp, J., Bonnet, M., Renou, J.P., 1989. Effect of collagen crosslinking on collagen-water interactions (a DSC investigation). Matrix. 9(6), 443-450.

231. A. J. Hodge and J. A. Petruska, in Aspects of Protein Chemistry, ed. G. N. Ramachandran, Academic Press, London, 1963, pp. 289-300.

232. Fank, M., Holl, M.M., 2013. Variation in type I collagen fibril nanomorphology: the significance and origin. Bonekey Rep. 2, 394.

233. Marchini, M., Morocutti, M., Ruggeri, A., Koch, M.H.J., Bigi, A, Roveri, N., 1985. Differences in the ibril structure of corneal and tendon collagen. An electron microscopy and X-ray diffraction investigation. Connect. Tiss. Res. 15, 269-281.

234. Willet, T.L., Labow, R.S., Aldous, I.G., Avery, N.C., Lee, J.M., 2010. Changes in collagen with aging maintain molecular stability after overload: evidence from an initro tendon model. J. Biomech. Eng. 132(3), 031002

235. Bonnans, C., Chou, J., Werb, Z., 2014.Remodelling the extracellular matrix in development and disease. Nat. Rev. Mol. Cell. Biol. 15(12), 786-801.

236. Humphrey, J.D., Dufresne, E.R., Schwartz, M.A., 2014. Mechanotransduction and extracellular matrix homeostasis. Nat. Rev. Mol. Cell. Biol. 15(12), 802-812.

237. Page-McCaw, A., Ewald, A.J., Werb, Z., 2007. Matrix metalloproteinases and the regulation of tissue remodelling. Nat. Rev. Mol. Cell. Biol. 8(3), 221-233.

238. Dittmore, A., Silver, J., Sarkar, S.K., Marmer, B., Goldberg, G.I,, Neuman, K.C., 2016. Internal strain drives spontaneous periodic buckling in collagen and regulates remodeling. PNAS. 113, 8436-8441.

239. Sarkar, S.K., Marmer, B., Goldberg, G., Neuman, K.C., 2012. Single-molecule tracking of collagenase on native type I collagen fibrils reveals degradation mechanism. Current Biol. 22(12), 1047-1056.

240. Visse, R., Nagase., H., 2003. Matrix metalloproteinases and tissue inhibitors of metalloproteinases structure, function, and biochemistry. Circulation Res. 92, 827-839.

241. Cawston, T.E., Koshy, P., Rowan, A.D., Assay of matrix metalloproteinases against matrix substrates. In: Matrix Metalloprteinase Protocol, Humana Press Inc, Totowa, New Jersey, 2001, pp 389-398.

242. Bornstein, P., Kang, A.H., Piez, K.A., 1966. The limited cleavage of native collagen with chymotrypsin, trypsin, and cyanogen bromide. Biochemistry 5: 3803-3812.

243. Liu, Y., Andarawis-Puri, N., Eppell, S.J., 2016. Method to extract minimally damaged collagen fibrils from tendon. J Biological Methods 3: e54.

244. Kuznetsova, N.V., McBride, D.J.Jr., Leikin, S., 2003. Changes in thermal stability and microunfolding pattern of collagen helix resulting from the loss of α2(I) chain in osteogenesis imperfecta murine. J Mol Bio 331: 191-200.

245. Woessner, J.F.Jr. Determination of hydroxyproline in connective tissues. In: The Methodology of Connective Tissue Research, Hall D (ed), Joynson-Bruvvers Ltd Oxford, 1976, pp 227-223.

246. Hwang, J., San, B.H., Turner, N.J., White, L.J., Faulk, D.M., Badylak, S.F., Li, Y., Yu, S.M., 2017. Molecular assessment of collagen denaturation in decellularized tissues using a collagen hybridizing peptide. Acta Biomater. 53, 268-278.

247. Lee, J.M., Edwards, H.H.L., Pereira, C.A., Samii, S.I., 1996. Crosslinking of tissue-derived biomaterials in 1-ethyl-3-(3-dimethylaminopropyl)-carbodiimide (EDC). J. Mater. Sci-Mater. M. 7, 531-541.

248. Shepherd, D.V., Shepherd, J.H., Ghose, S., Kew, S.J., Cameron, R.E., Best, S.M., 2014. The process of EDC-NHS cross-linking of reconstituted collagen fibres increases collagen fibrillar order and alignment. Apl. Materials. 3, 014902.

249. Ahmad, Z., Shepherd, J.H., Shepherd, D.V., Ghose, S., Kew, S.J., Cameron, R.E., Best, S.M., Brooks, R.A., Wardale, J., Rushton, N., 2015. Effect of 1-ethyl-3-(3-dimethylaminopropyl) carbodiimide and N-hydroxysuccinimide concentrations on the mechanical and biological characteristics of cross-linked collagen fibres for tendon repair. Regen. Biomater. 2(2), 77-85.

250. Gowen, B.B., Borg, T.K., Ghaffar, A., Mayer, E.P., 2000. Selective adhesion of macrophages to denatured forms of type I collagen is mediated by scavenger receptors. Matrix Biol. 19, 61-71.

251. Koyama, Y.I, Norose-Toyoda, K., Hirano, S., Kobayashi, M., Ebihara, T., Someki, I., Fujisaki, H., Irie, S., 2000. Type I collagen is a non-adhesive extracellular matrix for macrophages. Arch. Histol. Cytol. 63(1), 71-79.

252. Blakney, A.K., Swartzlander, M.D., Bryant, S.J., 2012, The effects of substrate stiffness on the in vitro activation of macrophages and in vivo host response to poly)ethylene glycol)-based hydrogels. J. Biomed. Mater. Res. A. 100(6), 1375-1386.

253. Adherz, K.M., Aranada-Espinoza, H., Hayenga, H.N., 2016. Substrate elasticity regulates the behavior of human monocyte-derived macrophages. Eur. Biophys. J. 45, 201-309.

254. McWhorter, F.Y., Davis, C.T., Liu, W.F., 2015. Physical and mechanical regulation of macrophage phenotype and function. Cell Mol. Life Sci. 72(7), 1303-1316.

255. Cheung, D.T., Perelman, N., Ko, E.C., Nimni, M.E., 1985. Mechanism of crosslinking of proteins by glutaraldehyde III. Reaction with collagen in tissues. Connect. Tissue. Res. 13(2), 109-115.

256. Cheung, D.T., Nimni, M.E., 1982. Mechanism of crosslinking of proteins by glutaraldehyde II. Reaction with monomeric and polymeric collagen. Connect. Tissue. Res. 10(2), 201-216.